Modelling Quantum Well Lasers

by

Philip Weetman

A thesis
presented to the University of Waterloo
in fulfillment of the
thesis requirement for the degree of
Doctor of Philosophy
in
Physics

Waterloo, Ontario, Canada 2002

I hereby declare that I am the sole author of this thesis. This is a true copy of the thesis, including any required final revisions, as accepted by my examiners.

I understand that my thesis may be made electronically available to the public.

Acknowledgements

I would like to thank my supervisor, Dr. Marek Wartak, for his knowledge, generosity, patience over the last several years of this program. It has been a great help.

Others who have been very helpful to me are Richard Voino and Dan Nedelko for their computer expertise friendship and great support staff at UW and WLU, especially Margaret Gaber and Judy McDonnell.

A special thanks to Rebecca Tiessen for being my inspiration.

Abstract

In this thesis, two methods to model quantum well lasers will be examined. The first model is based on well-known techniques to determine some of the spectral and dynamical properties of the laser. For the spectral properties, an expression for TE and TM modal amplitude gain is derived. For the dynamical properties, the rate equations are shown. The spectral and dynamical properties can be examined separately for specific operating characteristics or used in conjunction with each other for a complete description of the laser. Examples will be shown to demonstrate some of the analysis and results that can be obtained.

The second model used is based on Wigner functions and the quantum Boltzmann equation. It is derived from general non-equilibrium Greens functions with the application of the Kadanoff-Baym ansatz. This model is less phenomenological than the previous model and does not require the separation of physical processes such as the former spectral and dynamical properties. It therefore has improved predictive power for the performance of novel laser designs. To the Author's knowledge, this is the first time such a model has been formulated. The quantum Boltzmann equations will be derived and some calculations will be performed for a simplified system in order to illustrate some calculation techniques as well as results that can be obtained.

Contents

List of Figures

Chapter 1

Introduction

1.1 Semiconductor Lasers

Since their advent in 1962, semiconductor lasers have become very important in the field of opto-electronics. They have a wide range of uses from CD player components to optical communications. Future applications will likely include optical memory storage and optical computing. The laser's small size, high efficiency, long life-time and ease of integrability into electronic circuits means they can be a very cost effective solution for many applications. Additionally, there is also the beneficial property that the device can be designed to operate over a wide range of optical wavelengths. This is good for optical communications as the important fiber wavelengths of 1.5 μm (minimum optical loss) and 1.3 μm (minimum optical dispersion) are within the laser's effective wavelength range.

The semiconductor laser is used for generating a modulated signal as an input to an optical fiber. It is now possible to obtain gigahertz transmission rates [1, 2, 3, 4]. Similar devices known as semiconductor optical amplifiers (SOA's) are being developed as an alternative to electronic based optical amplifiers. SOA's have no mirrors to set up a resonant cavity and are therefore only single pass devices. In all other aspects however, their design is similar to the lasers and so can be simulated with some of (but not all) the tools developed in this thesis. Many researchers obtain SOA's by simply applying an anti-reflection coating to the mirrors of semiconductor lasers.

The first semiconductor lasers were essentially one semiconductor slab with an applied

potential across it [5, 6, 7]. They were not practical to use as they required large input currents and had to be cooled to cryogenic ($\sim 5K$) temperatures. Over the years, more complicated structures have been developed (which require advanced fabrication techniques) in order to decrease the current required and the need for such cooling [8, 9]. There is still much research to be done in this field for additional improvements. Since the late 80's researchers have been studying the "Quantum Well (QW) Laser" [10, 11].

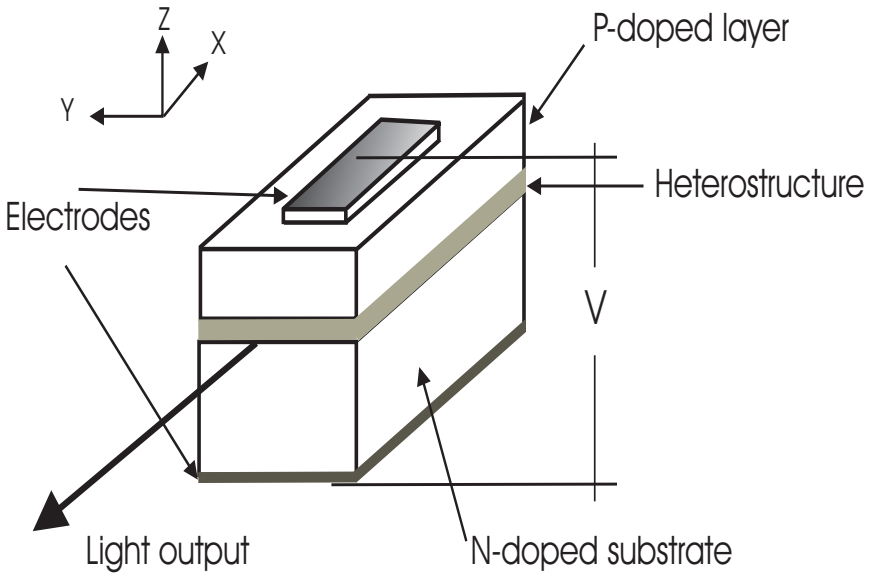

Figure 1.1: Schematic of a Quantum Well Laser

A schematic representation of a QW laser is shown in figure 1.1. A semiconductor structure is grown in the z-direction on top of a base material known as the substrate. A potential bias is applied in this direction which, with the doping of various layers, causes a current flow into the shaded region of figure 1.1 labeled the "heterostructure". In this region, electrons and holes recombine due to the interaction with an electromagnetic field. The EM field propagating in the x-direction is selected and mirrors may be placed perpendicular to this direction to set up the resonant cavity.

The heterostructure region is expanded in figure 1.2. Layers of various materials and compositions are placed together to make up this structure. In this case, the so-called separate confinement regions are constructed from InP. The well and barrier are both

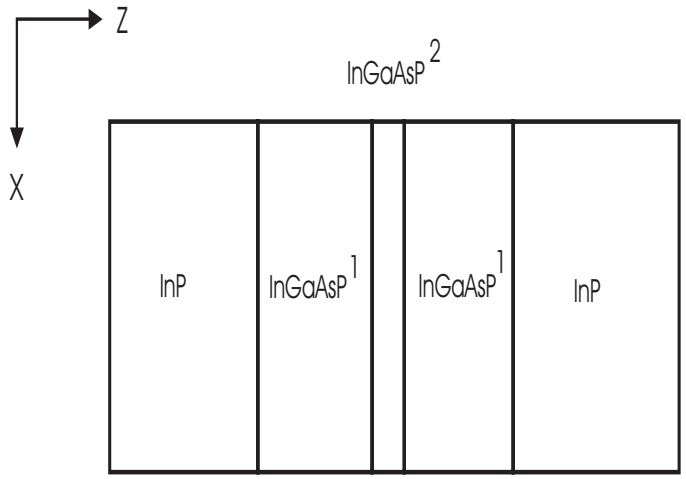

Figure 1.2: The Heterostructure Region of the QW Laser in fig 1.1

made from InGaAsP, those with superscript 1 have a composition $In_{1-x_1}Ga_{x_1}As_{y_1}P_{1-y_1}$ and the layers with superscript 2 have composition $In_{1-x_2}Ga_{x_2}As_{y_2}P_{1-y_2}$. These subscripts are used to denote the fractions of the various compounds in the layer. Since each different layer has a different band-gap (the energy difference between the conduction and valence band-edge), the potential profile shown in the energy representation of this structure in figure 1.3 will be created.

The variation in potential energy creates wells and barriers. The carriers (electrons or holes) localize around the wells. In addition to this, the layers are designed in such a way that the dielectric constants vary and also cause the electromagnetic field to be confined (although not as strongly) in this region. The favorable overlap between the carriers and the field in the active region (area where lasing mostly occurs) gives a higher probability of interaction than the original single layer devices. Less current is therefore required for lasing and they therefore produce less heat. This type of laser is called a quantum well laser because the wells are on the quantum scale ($\sim 5nm$).

There are additional improvements that can be made. It is common now to add more than one well to the structure [1, 2, 3, 4], this is referred to as a multiple quantum well (MQW). MQW lasers have the benefit of a lower threshold current and higher modulation response than a single QW because a higher proportion of the carriers are captured into

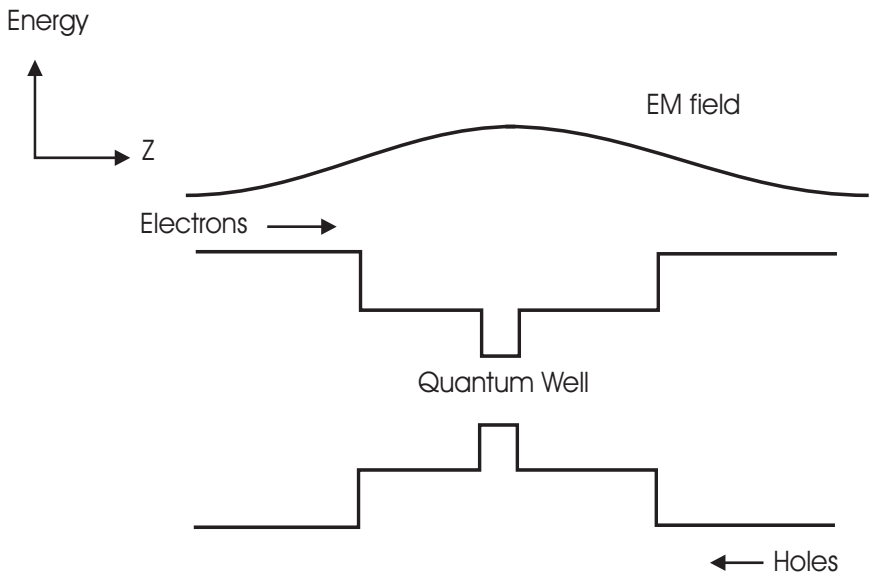

Figure 1.3: Energy Representation and Electric Field Envelope Over the Heterostructure Region of the QW Laser

active wells. Other developments include introducing strain into the system by lattice mismatch between various layers [12]. This modifies the band-structure which can have the effect of lowering Auger recombination and reducing differences in gain due to different light polarizations, a very beneficial property for SOA's [13, 14, 15, 16].

1.2 Purpose

The purpose of this thesis is to develop a physical model of the quantum well laser that will be able to simulate many of the operating characteristics. It is costly and time consuming to fabricate and test new laser designs and so it is desirable to simulate new designs on a computer. Even if it is not possible to predict the exact operating characteristics of a design, it can still be beneficial to come up with some "quality factor" to weed out less promising designs. These devices are complicated by various interactions which include photon, phonon, coulombic and other many-body interactions. A number of simplifications and approximations have to be made for any model to be computationally practical. Here, two

models will be developed to describe the QW lasers and some of their important operating characteristics. Each of these have their strengths and weaknesses. The first model will be referred to as the conventional model. It is based on some standard techniques and combines two commonly used models that describe different aspects of the laser [12, 16, 17, 18, 19, 20, 21, 22, 23, 24, 25, 26]. The next model will be referred to as the Wigner function model. It is derived from general non-equilibrium Greens functions [27, 28, 29, 30, 31, 32, 33, 34]. The models to be constructed in this thesis will focus on the area around the heterostructure region where the quantum effects are most significant.

1.2.1 Conventional Model

The main attractions of the conventional model are the speed of calculation and the simplicity of incorporating physical effects. It is a good model for an engineer who needs to get a quick estimate of the characteristics of a design that is not too dissimilar to current designs. In this approach the properties of the laser are roughly divided into two parts, the spectral and dynamical properties. The physical basis for this is that the two parts operate on different time scales, the dynamical being slower (on the scale of picoseconds to nanoseconds, 10^{-12}s - 10^{-9}s) and the spectral faster (on the scale of femtoseconds, 10^{-15}s). The spectral properties include gain, refractive index change and line-width of the laser. Here, an expression for the amplitude gain will be derived. This equation is slightly different than current expressions used as it does not require one to define explicitly the active region [17, 18, 19]. This is beneficial when barriers separating QW's are so small that coupling effects occur and a significant portion of the carrier wave-functions are not within the wells. The dynamical properties are the transport of the carriers as they interact with each other, phonons, and the electromagnetic field. Rate equations are used in this part [22, 23]. The spectral and dynamical parts are linked together because the rate equations require the spectral properties as input.

There are a number of drawbacks with this model. Physical distinctions between various effects have to be made. One distinction already discussed is the separation of spectral and dynamical properties. Another is the designation of "2D" and "3D" carriers in the rate equations [22, 23]. This is a delineation between carriers that are low enough in energy to be within the well and those at energies too high to be in the well. This is a semi-classical

approximation to a complicated quantum mechanical situation. There is also the logical inconsistency that the spectral properties assume the carriers are in equilibrium (which is certainly not the case or there would be no transport) and that there is spin-orbit coupling while the dynamical part assumes the carriers are not in equilibrium and ignores spin-orbit coupling. The potential profile of the heterostructure is also not correct which will become apparent when comparisons are made between the heterostructures calculated by the two different methods.

In addition to these logical inconsistencies, a major problem is that the physical effects are incorporated in a simplistic and phenomenological manner. The biggest culprit of this is the rate equations. In this case physical interactions are incorporated via effective time constants. These time constants have to be calculated from other microscopic theories, taken from experimental results, or curve-fitted. This is a major hindrance if one is interested in designing a novel device where it is not possible to estimate the parameters from previous similar designs and so reduces the stand-alone predictive power of this model.

1.2.2 Wigner Function Model

The second model used in this thesis is based on non-equilibrium one-particle Greens functions with their evolution described by Dyson's equations [27, 28, 32]. It is intended to make up for the shortcomings of the conventional model by treating all physical interactions in a consistent manner via their self-energies. In this model, there are no distinctions between spectral and dynamical properties or 2D and 3D carriers and the various transport processes between them. Since interactions are treated more rigorously, there is less of a reliance on phenomenological parameters and thus has enhanced predictive power.

The whole laser structure is too time consuming to model with Greens functions. One therefore focuses on the heterostructure region in detail and models the outer regions as blackbody reservoirs (particles that enter the heterostructure will come from a constant equilibrium distribution, particles that leave the heterostructure region will be completely absorbed by the reservoirs). By virtue of these boundary conditions, this is an open and irreversible system (regardless of the types of interactions that occur within the heterostructure region). A more convenient method to model open system boundaries in this case is to replace the Greens functions with Wigner functions by performing the Wigner-

Weyl transformation [27, 32, 34] (and later a Markovian approximation). The evolution equations for the Wigner functions are derived from Dyson's equations using this transformation and are commonly referred to as the quantum Boltzmann equations (QBE). They are referred to this way because in the limit of classical interactions, they reduce to the classical Boltzmann equation (BE). This also means that in the classical limit, the coordinates used for the Wigner functions become the classical phase space variables. The classical limit of phase space is a tremendous advantage for formulating the open system boundary conditions in this problem. If the boundaries are taken far enough away from the most significant quantum effects, then it can be assumed that classical boundary conditions are approximately valid [29, 31]. A common form for the BE boundary conditions is in terms of in-going and out-going particles and this will be adopted here.

There are other benefits to the Wigner function formulation. Although care must be taken not to think of the Wigner functions as a pure distribution function in phase-space (due to Heisenberg uncertainty which manifests itself in the lack of positive definiteness [29]), they are much more intuitive than the Greens functions. As Kadanoff states [35, 36] "the most important consequence is the natural manner in which self-consistent field theories appear in the simplest approximation such as Hartree-Fock and random-phase." Another benefit of the Wigner functions is, due to their BE form at the boundaries, it is an easier matter to couple these to classical models such as drift-diffusion if it is desired to model a larger system. This will not be done here as the focus is on the active region. Other areas where Wigner functions have been used include nuclear reaction modeling [37, 38] and expressions of potential scattering cross-sections[39, 40].

The model to be derived is an extension of the Wigner function model of the resonant tunneling diode[29, 31, 32, 41] which has also been used to describe some properties of the QW laser[33, 42]. This is extended by adding interband coupling via the electromagnetic interaction. As well, coulombic interactions and phonon interactions are incorporated generally. There are other Greens function models[42] but they are often too complicated to be practical for calculation. Other classes of models known as the Maxwell Bloch and Semiconductor Bloch Equations incorporate some of these effects and they can be derived by simplifying the QBE [43, 44, 45]. This model has a good physical foundation to incorporate additional effects or to examine particular effects in more detail.

The drawback of this model is the increase in computation time. Therefore, for practical calculations, some interactions have to be simplified and dimensionality (we effectively average out x-y dependence) reduced. This is done in a physically reasonable way so that the specific details of the interactions that are deemed most important are kept.

1.3 Outline of Thesis

Chapter 2 summarizes some background theory in semiconductors and basic techniques that are common to both methods. The thesis is then divided into two main parts. Part I is a grouping of chapters that describe the conventional model. Chapter 3 describes the calculation of the spectral property of amplitude gain. Chapter 4 describes the dynamical properties and the basic model of the rate equations. Chapter 5 shows some results of the spectral and dynamical properties calculated individually and together for consistency. Part II is a grouping of chapters that describe the Wigner function model. Chapter 6 derives the model starting with the non-equilibrium Greens functions and Dyson's equations. Chapter 7 describes numerical implementation and presents some results. Chapter 8 concludes and discusses future work.

Chapter 2

Basic Semiconductor Theory

The technique of designing a heterostructure to meet desired requirements is known as band-structure engineering [10, 11, 46]. Of importance to semiconductor lasers is the confinement of carriers and electromagnetic fields, the light output wavelength and polarization sensitivity. This chapter will discuss how to choose the compositions of semiconductor layers such as in figure 1.2 to arrive at the desired profile of figure 1.3. Band-structure engineering cannot tell exactly what the profile should be to obtain the desired output characteristics. However, it can be used to obtain a good first guess on such properties as the energy of maximum laser gain and carrier confinement. Given enough simulations and experience, researchers can estimate quite well some of the operating characteristics with just band-profile information. It is also fundamental to have this information for the later detailed calculations.

In order to understand the principles behind band-structure engineering, it is necessary to understand some basic theory of semiconductors. This chapter will summarize the semiconductor theory required. The first section will discuss the carrier properties and the second section will discuss the electromagnetic properties.

2.1 Dispersion Relations, Band Structure

The dispersion (energy-momentum) relationships will be analyzed by finding the eigensolutions for carriers in the structures.

2.1.1 Bulk Materials

A single, large layer is referred to as a bulk material. This will first be analyzed before the heterostructures are developed.

The general Hamiltonian that incorporates the spin-orbit interaction is[12]

$$H = \frac{p^2}{2m_o} + U(\mathbf{r}) + \frac{\hbar}{4m_o^2c^2}\boldsymbol{\sigma} \cdot \nabla U(\mathbf{r}) \times \mathbf{p} \tag{2.1}$$

where $U(\mathbf{r})$ is the periodic potential due to the positive ion core background. It is assumed to be static. The last term represents the spin-orbit interaction, $\boldsymbol{\sigma}$ are the Pauli spin matrices.

It is desired to find the eigen-solutions of equation (2.1). The n^{th} eigen-vector is assumed to be of the form

$$\psi_{n,\mathbf{k}}(\mathbf{r}) = \frac{e^{i\mathbf{k}\cdot\mathbf{r}}}{\sqrt{V}} u_{n,\mathbf{k}}(\mathbf{r}) \tag{2.2}$$

where $u_{n,\mathbf{k}}(\mathbf{r})$ is the Bloch function, a normalized function periodic in the unit cell defined by the periodicity of $U(\mathbf{r})$. The subscript n represents the band index and includes spin. Thus the solution is a plane-wave in box-normalization modulated by a periodic function. Using this, the eigen solution to equation (2.1) can be written as

$$\left[\frac{p^2 + k^2}{2m_o} + U(\mathbf{r}) + \frac{\hbar}{m_o}\mathbf{k} \cdot \mathbf{p} + \frac{\hbar}{4m_o^2c^2}\boldsymbol{\sigma} \cdot \nabla U(\mathbf{r}) \times [\mathbf{p} + \mathbf{k}]\right] u_{n,\mathbf{k}}(\mathbf{r}) = E_n(\mathbf{k}) u_{n,\mathbf{k}}(\mathbf{r}) \tag{2.3}$$

This equation is difficult to solve exactly so generally simplifications and perturbative solutions are applied. The perturbation expansions are around band extremums ($\mathbf{k}_o$) and are referred to as the $\mathbf{k} \cdot \mathbf{p}$ method [47, 48].

The term $E_n(0)$ is the band-edge energy and is the eigenvalue solution $Hu_{n,0}(r) = E_n(0)u_{n,0}(r)$. The Hamiltonian can be difficult to diagonalize as $U(\mathbf{r})$ in equation (2.1) can be complicated depending on the molecular model used. In practice, researchers do not calculate this, but use commonly accepted values (deduced from experiment or previous detailed calculations) of the band-gap. $E_g = E_c(0) - E_v(0)$ is the difference between the band-edge energy of the first conduction and valence bands, . This is sufficient here because for laser calculations of a single layer, only the difference between band-edges is important, not the actual value of the band-edge.

Parabolic Approximation

The first approximation to make is to ignore the spin-orbit interaction and to apply the $\mathbf{k}\cdot\mathbf{p}$ expansion. To first order the periodic function is

$$u_{n,\mathbf{k}}(\mathbf{r}) = u_{n,o}(\mathbf{r}) + \sum_{n'\neq n}\left[\frac{\hbar\mathbf{k}\cdot\mathbf{p}_{n,n'}}{m_o\left(E_n(0)-E_{n'}(0)\right)}\right] \tag{2.4}$$

where $u_{n,o}$ is the $\mathbf{k}=0$ solution which can be found by standard methods, $\mathbf{p}_{n,n'} = \int_\Omega u^*_{n,o}(\mathbf{r})\mathbf{p}u_{n',o}(\mathbf{r})d^3\mathbf{r}$ and Ω is the unit cell.

The energy must be expanded to second order (the first order does not exist)

$$E_n(\mathbf{k}) = E_n(0) + \frac{\hbar^2}{2}\sum_{\alpha,\beta}\left(\frac{1}{m^*}\right)_{\alpha\beta}k_\alpha k_\beta \tag{2.5}$$

where α,β range over the x,y,z directions and

$$\left(\frac{1}{m^*}\right)_{\alpha,\beta} = \frac{1}{m_o}\left[\delta_{\alpha,\beta} + \sum_{n'\neq n}\frac{p^\alpha_{n,n'}p^\beta_{n',n} + p^\beta_{n,n'}p^\alpha_{n',n}}{E_n(0)-E_{n'}(0)}\right]$$

The inverse effective mass tensor $\left(\frac{1}{m^*}\right)_{\alpha\beta}$ is diagonal ($\alpha=\beta$) in the principal axis for an isotropic approximation. The diagonal term is defined as

$$\left(\frac{1}{m^*}\right)_{\alpha,\alpha} \equiv \frac{1}{m^*_\alpha}$$

and called the effective mass. It is now apparent why this is referred to as the parabolic solution, the energy dispersion is parabolic in the momentum. An example of this dispersion is graphed in figure 2.1.

The Luttinger Kohn (LK) Hamiltonian

In this case, the spin-orbit terms are included in the Hamiltonian. A $\mathbf{k}\cdot\mathbf{p}$ expansion is once again used [12, 49]. Upon examination of equation (2.3) it can seen that at the band extremum, the solutions are of the Hydrogen Atom form. For that reason, a basis of s orbitals near the bottom of the conduction band and p orbitals near the top of the valence band are chosen :

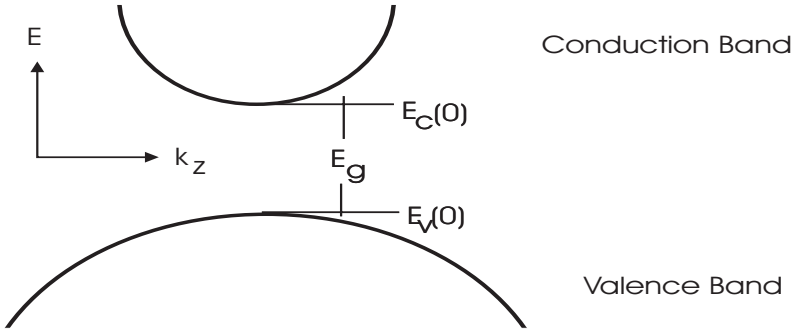

Figure 2.1: The Band Dispersions for the First Conduction and Valence Bands in the Parabolic Model

s orbitals:

$$\{|iS\downarrow> \;\; |iS\uparrow>\} \tag{2.6}$$

which is the spherical harmonic for total angular momentum = 0. The symbol i in this case is $\sqrt{-1}$.

p orbitals:

$$\left\{ \begin{array}{c} \left|\frac{3}{2},\frac{3}{2}\right\rangle \equiv \frac{-1}{\sqrt{2}}\left|(X+iY)\uparrow\right\rangle \\ \left|\frac{3}{2},\frac{1}{2}\right\rangle \equiv \frac{-1}{\sqrt{6}}\left|(X+iY)\downarrow\right\rangle + \sqrt{\frac{2}{3}}\left|(Z)\uparrow\right\rangle \\ \left|\frac{3}{2},\frac{-1}{2}\right\rangle \equiv \frac{1}{\sqrt{6}}\left|(X-iY)\downarrow\right\rangle + \sqrt{\frac{2}{3}}\left|(Z)\downarrow\right\rangle \\ \left|\frac{3}{2},\frac{-3}{2}\right\rangle \equiv \frac{1}{\sqrt{2}}\left|(X-iY)\uparrow\right\rangle \end{array} \right\} \tag{2.7}$$

which are the spherical harmonics for total angular momentum = 1.

The s and p orbitals shown here are degenerate in energy. The two other p orbitals will be ignored because their $k = 0$ energy is offset from the other p orbitals by such a value so that they are assumed to be uncoupled from the rest of the orbitals in a first approximation. This is known as the 4x4 LK approximation.

It is assumed that the energy gap between the s and p orbitals is large enough that any coupling between them is negligible. Therefore, the conduction band electrons are completely described by the s-orbitals and can once again be modeled with the parabolic approximation and have solutions using equations (2.4) and (2.5). The $\mathbf{k} \cdot \mathbf{p}$ expansion of the 4x4 LK Hamiltonian for the valence bands under consideration is

$$\begin{bmatrix} P+Q & -S & R & 0 \\ -S^{+} & P-Q & 0 & R \\ R^{+} & 0 & P-Q & S \\ 0 & R^{+} & S^{+} & P+Q \end{bmatrix} \tag{2.8}$$

where

$$P = \frac{\hbar^2 \gamma_1}{2m_o}\left(k_x^2 + k_y^2 + k_z^2\right)$$

$$Q = \frac{\hbar^2 \gamma_2}{2m_o}\left(k_x^2 + k_y^2 - 2k_z^2\right)$$

$$R = \frac{\hbar^2}{2m_o}\left[-\sqrt{(}3)\gamma_2\left(k_x^2 - k_y^2\right) + i2\sqrt{3}\gamma_3 k_x k_y\right]$$

$$S = \frac{\hbar^2 \gamma_3}{m_o}\sqrt{3}\left(k_x - ik_y\right)k_z \tag{2.9}$$

The Luttinger coefficients ($\gamma_{1,2,3}$) can be determined from expressions similar to that of the effective mass, but there are standard well documented experimental values that are normally used. These are listed in Appendix A.

An example of energy dispersion for this case is shown in figure 2.2. The different bands are labeled by their properties. The bands $|3/2, \pm 3/2>$ are called heavy-holes (HH) and $|3/2, \pm 1/2>$ are the light holes (LH) because in the case when $k_x = k_y = 0$ (momentum transverse to the growth direction) the Hamiltonian is parabolic and the HH effective mass (deduced from the band's curvature) is greater than the LH effective mass.

Mixed Compounds

The eigen-solutions above apply to any semiconductor material. Normally however, the parameters such as effective mass and Luttinger coefficients are only given for "pure com-

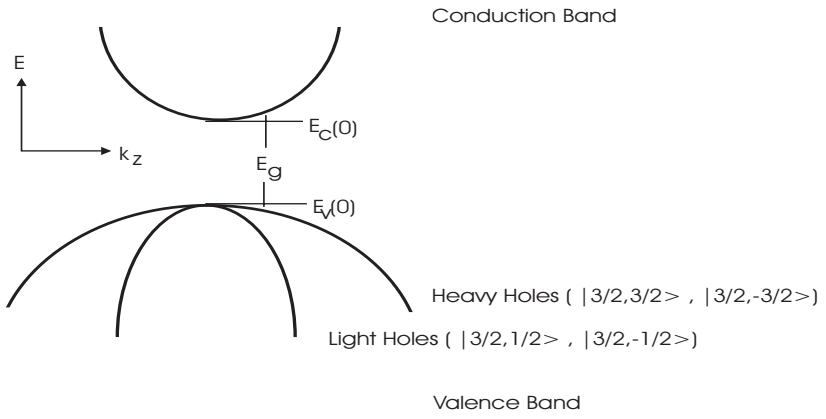

Figure 2.2: Band Dispersions for the First Conduction Band in the Parabolic Model and the First Four Valence Bands in the LK Model

pounds". That is GaAs, InP, GaP and InAs in the cases required here. For mixed compounds such as InGaAsP, which is shorthand for $\mathrm{In}_x\ \mathrm{Ga}_{1-x}\ \mathrm{As}_y\ \mathrm{P}_{1-y}$, the common practice is to interpolate all parameters except for band-gap by the formula

$$\begin{aligned} P(A_xB_{1-x}C_yD_{1-y}) &= xyP(AC) + (1-x)(1-y)P(BD) \\ &+ (1-x)yP(BC) + x(1-y)P(AD) \end{aligned} \tag{2.10}$$

where P represents some physical property other than band-gap. For the band-gap, this interpolation is not sufficient, what is required is to actually solve equations (2.5) and (2.8) for the compound of interest. This has been done and phenomenological curve-fitted expressions of these are commonly used [25, 46]. For InGaAsP the band-gap energy is often given by [25]

$$\begin{aligned} E_g(x,y) &= 1.35 + 0.642x - 1.101y + 0.758x^2 + 0.101y^2 \\ &- 0.159xy - 0.28x^2y + 0.109xy^2 eV \end{aligned} \tag{2.11}$$

2.1.2 Heterostructures

The previous section discussed the eigenvalue problem of a single layer. The actual devices however, have a heterostructure with multiple layers. It is necessary to determine the eigen-solutions of the heterostructure. A simple schematic of some layers of a heterostructure with the pertinent parameters is shown in figure 2.3.

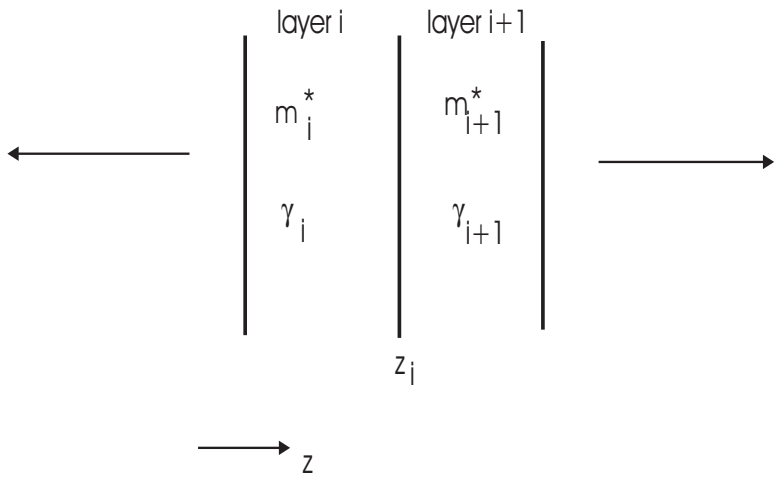

Figure 2.3: Schematic of two Layers of the Heterostructure

Effective Mass Theory

Parabolic

Effective mass theory [12], neglecting spin-orbit interactions, shows that the eigenfunction of the Hamiltonian for a heterostructure is no longer given by equation (2.2) for a single layer, but can be replaced by

$$\psi_n(\mathbf{r}) = F_n(z)\frac{e^{i\mathbf{k}_\perp\cdot\mathbf{x}_\perp}}{\sqrt{S}}u_{n,o}(\mathbf{r}) \tag{2.12}$$

where $F_n(z)$ is the envelope function and is the solution of

$$\left[-\frac{\hbar^2}{2m_n^*(z)}\frac{d^2}{dz^2} + V(z)\right]F_n(z) = E_nF_n(z) \tag{2.13}$$

where $V(z) = E_n(0;z)$, the band-edge potential of each layer. The effective mass and band-edge potential have been given a z-dependence for future convenience. If z is within the position of layer i in figure 2.3, then $m_n^*(z) = m_{n,i}^*$ and $V(z) = E_{n,i}(0)$.

LK

When the spin-orbit interaction is included, a similar procedure to the parabolic method can be employed. The effective mass theory in this case gives the eigenfunction solution

$$\psi_n(\mathbf{r}) = \sum_\alpha F_\alpha(z) \frac{e^{i\mathbf{k}_\perp \cdot \mathbf{x}_\perp}}{\sqrt{A}} u_{\alpha,o}(\mathbf{r}) \tag{2.14}$$

where the envelope functions are the solutions of

$$\begin{bmatrix} P+Q+V & -S & R & 0 \\ -S^+ & P-Q+V & 0 & R \\ R^+ & 0 & P-Q+V & S \\ 0 & R^+ & S^+ & P+Q+V \end{bmatrix} \begin{bmatrix} F_{3/2} \\ F_{1/2} \\ F_{-1/2} \\ F_{-3/2} \end{bmatrix} = E \begin{bmatrix} F_{3/2} \\ F_{1/2} \\ F_{-1/2} \\ F_{-3/2} \end{bmatrix} \tag{2.15}$$

Each of the terms has a z dependence. Similarly to the parabolic case of the position dependent effective mass. The P, Q, S, and R terms incorporate now position dependent Luttinger coefficients. The total spin index of 3/2 has been dropped for simplicity as all these subbands have it.

Band offsets

Effective mass theory requires knowledge of the portions of the bandgap energies given to the conduction and valence bands. Unfortunately data provided is only for the total (conduction plus hole) band-gap. For a single layer this was not a problem. For the heterostructure however, it can make a large difference to the structure's potential profile as shown in figure 2.4. How a layer's bandgap is positioned with respect to the other layers is given by their band offsets which is labeled by $\Delta_{i,n}$ for each layer in figure 2.4[12, 25]. It is therefore required too have a theory to determine these offsets.

A common approximation for the offsets is $\Delta_c/E_g \approx 0.7$ for AlGaAs materials and $\Delta_c/E_g \approx 0.4$ for InGaAsP materials. There are also complicated semi-empirical formulas

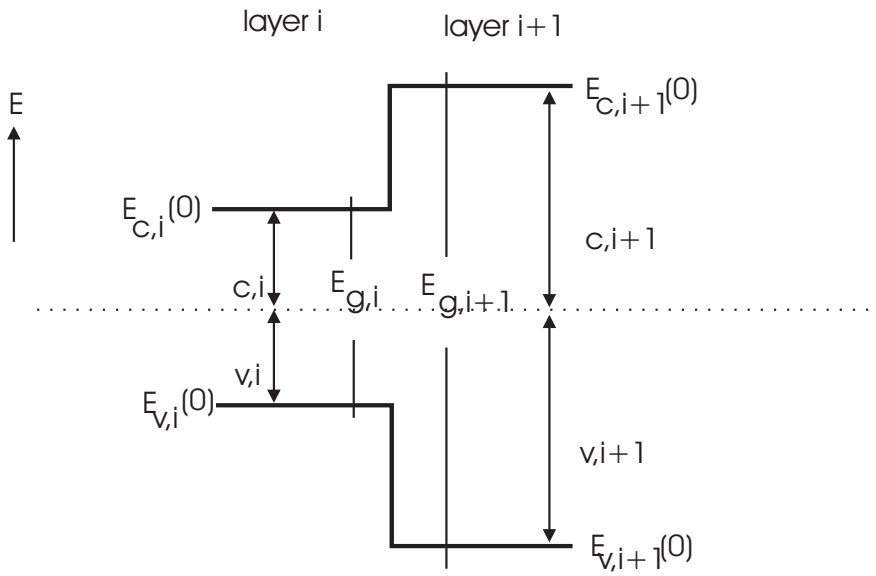

Figure 2.4: Potential Profile for two Layers of the Heterostructure of Figure 2.3

employed such as model-solid theory[12, 50] and Harrison's model[51, 25]. Often tables are simply referenced from data generated for these models[25].

Strain

A technique that is very important in band-structure engineering is the introduction of strain. This is caused by placing a semiconductor layer next to another layer with a different lattice constant. Assuming the lattice mismatch is not large enough to cause dislocations, an extra stress will be introduced in the system given by the Coulomb relations between strain and perpendicular stress. This is incorporated into the model by adding a stress-energy tensor to the Hamiltonian. For uniaxial strain this results in a modification of the Hamiltonian for the conduction band as[12]

$$H \to H + \delta E_c \ , \ \delta E_c = a_c(\varepsilon_{xx} + \varepsilon_{yy} + \varepsilon_{zz}) \tag{2.16}$$

and for the valence bands this is accomplished by replacing the terms in the Hamiltonian

$$P \to P + P_\varepsilon \ , \ Q \to Q + Q_\varepsilon \tag{2.17}$$

$$P_\varepsilon = -a_v(\varepsilon_{xx} + \varepsilon_{yy} + \varepsilon_{zz}) \ , \ Q_\varepsilon = -\frac{b}{2}(\varepsilon_{xx} + \varepsilon_{yy} - 2\varepsilon_{zz})$$

where

$$\varepsilon_{xx} = \varepsilon_{yy} = \frac{(a - a_o)}{a} \ , \ \varepsilon_{zz} = -2\frac{C_{12}}{C_{11}}\varepsilon_{xx} \tag{2.18}$$

a_o is the lattice constant of the substrate (size of the unit cell, data shown in Appendix A) and a is the lattice constant of the layer. C_{12}, C_{11} are the coulomb coefficients. Figures 2.5 a-c show how the strain changes the band dispersion. Looking at the band-edge LK Hamiltonian, that the band-gaps will be different for the light holes and heavy holes.

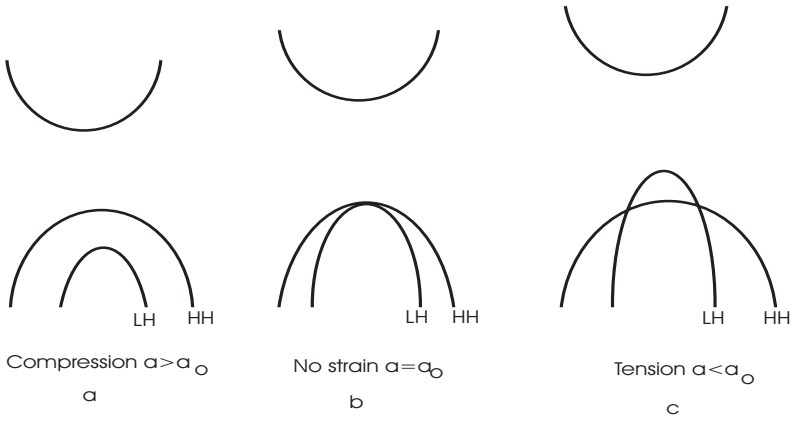

Figure 2.5: The Sketch of Conduction and Valence Band Dispersions for Three Different Strains

$$E_{c-HH}(x, y) = E_g(x, y) + \delta E_c(x, y) - \delta E_{HH}(x, y) \tag{2.19}$$

and

$$E_{c-LH}(x, y) = E_g(x, y) + \delta E_c(x, y) - \delta E_{LH}(x, y) \tag{2.20}$$

where δE_c is the modification in equation (2.16) and

$$\delta E_{HH} = -P_\varepsilon - Q_\varepsilon \ , \ \delta E_{LH} = -P_\varepsilon + Q_\varepsilon$$

2.1.3 Numerical Methods for Eigen-solutions

This section will discuss the numerical methods used to solve equations (2.13) and (2.15).

Parabolic

This is handled by a simple finite difference method and then solved with matrix methods. It is assumed the wave-functions have periodic boundary conditions. The Hamiltonian of equation (2.13) will not be Hermitian in the finite difference approximation. In order to ensure the Hermicity of the Hamiltonian which must be the case [52] and therefore the realness of the eigen-values some of the terms must be modified so that they will retain their Hermicity in the numerical formulation. This is accomplished by making the following replacements [53]:

$$A(z)\frac{\partial^2}{\partial z^2} \rightarrow \frac{\partial}{\partial z}A(z)\frac{\partial}{\partial z}\ ,\ A(z)\frac{\partial}{\partial z} \rightarrow \frac{1}{2}\left[A(z)\frac{\partial}{\partial z} + \frac{\partial}{\partial z}A(z)\right]$$

LK

This can also be done by finite difference methods, but it was found to be more convenient and less time consuming to solve using a plane-wave expansion[53]. To begin, expand the following variables in a Fourier series

$$F_\alpha(z) = \sum_{n=-N}^{n=N} f_{\alpha,n}\frac{e^{iK_n z}}{\sqrt{L}}\ ,\ V_\nu(z) = \sum_{n=-2N}^{n=2N} V_{\nu,n}\frac{e^{iK_n z}}{\sqrt{L}}\ ,\ \gamma_i(z) = \sum_{n=-2N}^{n=2N} \gamma_{i,n}\frac{e^{iK_n z}}{\sqrt{L}} \tag{2.21}$$

where $K_n = \frac{2\pi n}{L}$ and $\alpha = \{3/2, 1/2, -1/2, -3/2\}$ Substituting this into equation (2.15), multiplying by $\int_0^L \frac{e^{-iK_{n'}z}}{\sqrt{L}}$ and using orthogonality relations gives

$$\begin{bmatrix} \left[E^{3/2}_{n'n}\right] & [-S_{n'n}] & [R_{n'n}] & [0] \\ \left[-S^{+}_{n'n}\right] & \left[E^{1/2}_{n'n}\right] & [0] & [R_{n'n}] \\ \left[R^{+}_{n'n}\right] & [0] & \left[E^{1/2}_{n'n}\right] & [S_{n'n}] \\ [0] & \left[R^{+}_{n'n}\right] & \left[S^{+}_{n'n}\right] & \left[E^{3/2}_{n'n}\right] \end{bmatrix} \begin{bmatrix} \left[f_{3/2,n}\right] \\ \left[f_{1/2,n}\right] \\ \left[f_{-1/2,n}\right] \\ \left[f_{-3/2,n}\right] \end{bmatrix} = (E - E_o) \begin{bmatrix} \left[f_{3/2,n}\right] \\ \left[f_{1/2,n}\right] \\ \left[f_{-1/2,n}\right] \\ \left[f_{-3/2,n}\right] \end{bmatrix} \tag{2.22}$$

where

$$E^{3/2}_{n'n} = P_{n'n} + Q_{n'n} + V_{n'n} \ , \ E^{1/2}_{n'n} = P_{n'n} - Q_{n'n} + V_{n'n}$$

The brackets around each term in the plane wave expanded LK Hamiltonian indicate that each is a matrix in n, n'. These have elements

$$P_{n'n} = \gamma_{1,n'-n}(k_x^2 + k_y^2 + K_{n'}K_n) + P_\varepsilon$$

$$Q_{n'n} = \gamma_{2,n'-n}(k_x^2 + k_k^2 - 2K_{n'}K_n) + Q_\varepsilon$$

$$S_{n'n} = \sqrt{3}\gamma_{3,n'-n}(k_x - ik_y)(K_{n'} + K_n)$$

$$R_{n'n} = -\sqrt{3}\gamma_{2,n'-n}(k_x^2 - k_y^2) + i2\sqrt{3}\gamma_{3,n'-n}k_xk_y$$

$$V_{\nu,n'n} = V_{\nu,n-n'} \ , \ \gamma_{j,n'n} = \gamma_{j,n-n'}$$

The terms $[f_{\alpha,n}]$ are column vectors of the components of the envelope functions and $n,\ n'$ go from $-N \rightarrow N$, the smallest number that will give accurate results. To find the total eigen-functions, diagonalize equation (2.22) to get the m^{th} envelope eigen-function $\left[f_{\alpha,n,(m)}\right]$. The complete eigen-function is then

$$\psi_m(\mathbf{k}_\perp, \mathbf{r}) = \sum_{n,\alpha} f_{n,\alpha,(m)} e^{iK_n z} u_\alpha(\mathbf{r}) e^{i\mathbf{k}_\perp \cdot \mathbf{x}_\perp} \tag{2.23}$$

2.2 Electromagnetic Waveguides

In addition to the carrier confining properties, the structures also have wave-guiding properties due to the different refractive indices of each layer. These are an important component of the semiconductor laser as it is necessary for mode stability and improves the overlap with the carrier wave-functions. The electric and magnetic fields will be derived here from the source-free Maxwell's equations. The laser is not source-free, but this makes a very convenient basis to expand the later Maxwell's equations with sources.

Maxwell's equations for source free time-harmonic equations are[12, 54]

$$\nabla \times \mathbf{E}^o = -i\omega\mu_o \mathbf{H}^o \tag{2.24}$$

$$\nabla \times \mathbf{H}^o = i\omega\varepsilon_o\varepsilon \mathbf{E}^o \tag{2.25}$$

where ω is the radian frequency, $\varepsilon = n^2$ is the relative permitivity. The superscript o denotes these as source-free (homogeneous) solutions. In general, the electric and magnetic fields will be of the form

$$E^{\alpha o}(\mathbf{r},t) = \sum_{\omega,\beta} E^{\alpha o}_{\omega\beta}(\mathbf{r},t) \ , \ H^{\alpha o}(\mathbf{r},t) = \sum_{\omega,\beta} H^{\alpha o}_{\omega\beta}(\mathbf{r},t)$$

$$E^{\alpha o}_{\omega\beta}(\mathbf{r},t) = e^{\alpha o}_{\omega\beta} F_{\omega\beta}(z) \frac{e^{i\beta x + i\omega t}}{\sqrt{ST}} \tag{2.26}$$

$$H^{\alpha o}_{\omega\beta}(\mathbf{r},t) = h^{\alpha o}_{\omega\beta} G_{\omega\beta}(z) \frac{e^{i\beta x + i\omega t}}{\sqrt{ST}} \tag{2.27}$$

where α denotes the coordinate directions, β is the propagation constant, S is the area normal to the z direction and T is a large length of time (for normalization purposes). For the structures of interest, y dependence can be neglected. The functions $F_{\omega\beta}(z)$ and $G_{\omega\beta}(z)$ are normalized functions to describe the dependence in the transverse direction. It is the purpose of this section to derive these functions as well as determine the propagation constant. This will be accomplished by using a propagation matrix method for the TE and TM modes (to be defined).

2.2.1 TE Modes

In the TE mode, $E^{xo} = E^{zo} = H^{yo} = 0$. Substituting equations (2.26) and (2.27) into (2.24) and (2.25) then multiplying by $\int dxdydt \frac{e^{-i\beta' x + i\omega' t}}{\sqrt{ST}}$ gives

$$\frac{\partial}{\partial z} e^{yo}_{\omega\beta} F_{\omega\beta}(z) = -i\omega\mu_o h^{xo}_{\omega\beta} G_{\omega\beta}(z) \tag{2.28}$$

$$\omega\mu_o \frac{\partial}{\partial z} h^{xo}_{\omega\beta} G_{\omega\beta}(z) = i\left[\beta^2 - \omega^2\mu_o\varepsilon_o\varepsilon\right] e^{yo}_{\omega\beta} F_{\omega\beta}(z) \tag{2.29}$$

There are many ways to solve this, the method used here is based on [55]. Define two new functions $U(z) = e^{yo}_{\omega\beta} F_{\omega\beta}(z)$ and $V(z) = \omega\mu_o h^{xo}_{\omega\beta} G_{\omega\beta}(z)$ then equations (2.28) and (2.29) can be rewritten as

$$\frac{d}{dz} U(z) = -iV(z) \tag{2.30}$$

$$\frac{d}{dz}V(z) = -i\kappa^2 U(z) \tag{2.31}$$

where $\kappa^2 = \omega^2\mu_o\varepsilon_o\varepsilon - \beta^2$ The solutions of this are of the form

$$U(z) = Ae^{-i\kappa(z-z_o)} + Be^{i\kappa(z-z_o)} \tag{2.32}$$

$$V(z) = Ce^{-i\kappa(z-z_o)} + De^{i\kappa(z-z_o)} \tag{2.33}$$

They are written in this form because it is assumed the values at $z = z_o$ are known. The solution will be written in reference to this. Substitute equations (2.32) and (2.33) into equations (2.30) and (2.31) so that equation (2.33) can be written as

$$V(z) = \kappa Ae^{-i\kappa(z-z_o)} - \kappa Be^{i\kappa(z-z_o)} \tag{2.34}$$

The value at z_o is then

$$U(z_o) = A + B \ , \ V(z_o) = \kappa A - \kappa B \tag{2.35}$$

Equations (2.32) and (2.34) are rearranged to solve for A and B. In matrix form this is

$$\begin{bmatrix} U(z_o) \\ V(z_o) \end{bmatrix} = \begin{bmatrix} \cos[\kappa(z-z_o)] & \frac{i}{\kappa}\sin[\kappa(z-z_o)] \\ i\kappa\sin[\kappa(z-z_o)] & \cos[\kappa(z-z_o)] \end{bmatrix} \begin{bmatrix} U(z) \\ V(z) \end{bmatrix} \tag{2.36}$$

or inverting,

$$\begin{bmatrix} U(z) \\ V(z) \end{bmatrix} = \begin{bmatrix} \cos[\kappa(z-z_o)] & -\frac{i}{\kappa}\sin[\kappa(z-z_o)] \\ -i\kappa\sin[\kappa(z-z_o)] & \cos[\kappa(z-z_o)] \end{bmatrix} \begin{bmatrix} U(z_o) \\ V(z_o) \end{bmatrix} \tag{2.37}$$

Equation (2.37) is the propagation matrix solution.

The above work is for a single type of material and must be generalized to a multi-layer structure as shown on figure 2.6. Make the replacements

$$U(z) \to U_i(z) \ , \ V(z) \to V_i(z)$$

$$\kappa^2 \to \kappa_i^2 = \omega^2\mu_o\varepsilon_o\varepsilon_i - \gamma^2$$

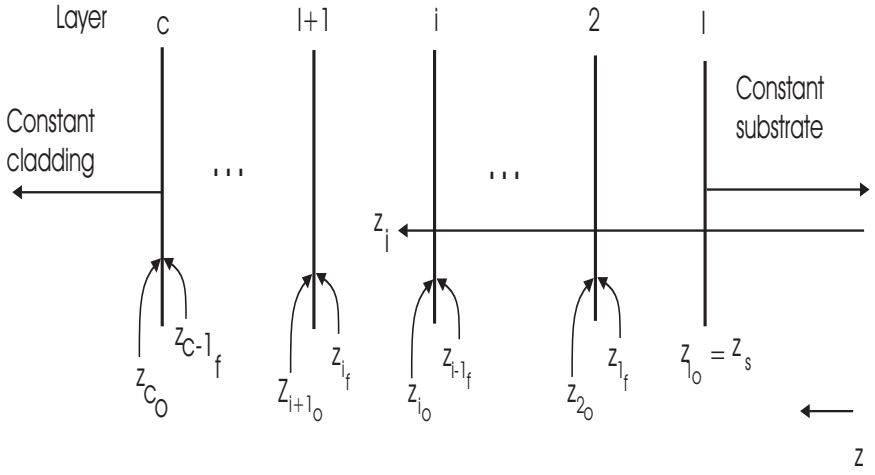

Figure 2.6: A Schematic Representation of a Multi-Layer Dielectric Structure

where the subscript i denotes each layer. Using equation (2.37) in this generalization, with known values at z_{1_o}, values of the fields up to position z_{1_f} can be determined. Since the transverse components of the electric and magnetic fields are continuous across boundary at z_{1_f},

$$\begin{bmatrix} U_2(z_{2_o}) \\ V_2(z_{2_o}) \end{bmatrix} = \begin{bmatrix} U_1(z_{1_f}) \\ V_1(z_{1_f}) \end{bmatrix} = \begin{bmatrix} \cos[\kappa_1(z_{1_f} - z_{1_o})] & -\frac{i}{\kappa_1}\sin[\kappa_1(z_{1_f} - z_{1_o})] \\ -i\kappa_1 \sin[\kappa_1(z_{1_f} - z_{1_o})] & \cos[(\kappa_1(z_{1_f} - z_{1_o})] \end{bmatrix} \begin{bmatrix} U_1(z_{1_o}) \\ V_1(z_{1_o}) \end{bmatrix}$$

This can then be applied to find the values in the next layer. In general, U and V at a position z_i in layer i are given by

$$\begin{bmatrix} U_i(z_i) \\ V_i(z_i) \end{bmatrix} = \prod_{j=1}^{i} M_j \begin{bmatrix} U_1(z_{1_o}) \\ V_1(z_{1_o}) \end{bmatrix} = \begin{bmatrix} m_{11} & m_{12} \\ m_{21} & m_{22} \end{bmatrix} \begin{bmatrix} U_1(z_{1_o}) \\ V_1(z_{1_o}) \end{bmatrix} \tag{2.38}$$

where

$$M_j = \begin{bmatrix} \cos[\kappa_j(z_j - z_{j_o})] & -\frac{i}{\kappa_j}\sin[\kappa_j(z_j - z_{j_o})] \\ -i\kappa_j \sin[\kappa_j(z_j - z_{j_o})] & \cos[(\kappa_j(z_j - z_{j_o})] \end{bmatrix} \begin{bmatrix} U_j(z_{j_o}) \\ V_j(z_{j_o}) \end{bmatrix} \tag{2.39}$$

and for $j < i$, use $z_j = z_{j_f}$.

The first and last layers are known as the substrate and cladding. For a waveguide, these layers are chosen such that there are guided modes (the dielectric constant in these

layers is greater). Therefore, the electric field decays exponentially out of the boundaries of these layers. Let $z_1 = 0$ and z_c is at the interface between the cladding and the second last layer. The wave-functions will then behave as

$$U_s(z) = A_s e^{\alpha_s z} \ , \ V_s(z) = i\alpha_s A_s e^{\alpha_s z} \quad z < 0 \tag{2.40}$$

$$U_c(z) = A_c e^{-\alpha_c(z-z_c)} \ , \ V_c(z) = i\alpha_c A_c e^{-\alpha_c(z-z_c)} \quad z > z_c \tag{2.41}$$

where $\alpha_i = \sqrt{|\kappa_i^2|}$. The second terms in these equations comes from using equation (2.32). By equation (2.38) the relation between the cladding and substrate fields is

$$A_c = m_{11} A_s e^{-\alpha_s(z_1 - z_{1_o})} + m_{12}\alpha_s A_s e^{-\alpha_s(z_1 - z_{1_o})} \tag{2.42}$$

$$-i\alpha_c A_c = m_{21} A_s e^{-\alpha_s(z_1 - z_{1_o})} + m_{22}\alpha_s A_s e^{-\alpha_s(z_1 - z_{1_o})} \tag{2.43}$$

With the appropriate values of m_{ij}. Combining these two equations and eliminating the common factors gives the relation

$$i\alpha_c m_{11} + \alpha_c\alpha_s m_{12} - m_{21} + i\alpha_s m_{22} = 0 \tag{2.44}$$

The only unknown in this equation is the propagation constant. Once the propagation constant has been found, the fields can be determined. For convenience, start with the assumption that $A_s = 1$. It doesn't matter what value is chosen as the fields will be normalized in the end. With the knowledge of propagation constant, all that is necessary now is to apply the propagation matrix of equation (2.38) to find $U(z)$ and $V(z)$. Finally, substitute these back into the relations for the electric and magnetic fields. Normalizing will then give $F_{\omega\beta}(z)$ and $G_{\omega\beta}(z)$.

2.2.2 TM modes

These are very similar to the TE modes. In this case, the components of the field that are zero are H^{xo} , H^{zo} and E^{yo}. Define the functions

$$U(z) = h^{yo}_{\omega\beta} G_{\omega\beta}(z) \ , \ V(z) = \omega\varepsilon_o e^{xo}_{\omega\beta} F_{\omega\beta}(z) \tag{2.45}$$

all equations will then be the same as for the TE modes if the replacement $\kappa \to -\frac{\kappa}{\varepsilon}$ is made.

2.3 Summary

This chapter describes some standard basic theory used in later chapters for both the conventional and Wigner model. The major points covered are the calculation of the band dispersion relations and eigenfunctions from band-gap properties and the electromagnetic envelope functions from the dielectric properties of various structures.

Part I

Conventional

The conventional model refers to methods that are often used to describe the characteristics of lasers and SOA's. In this part, aspects of the conventional models will be discussed. These break down into two main areas. The first is known as the spectral properties. This deals with calculations of properties that are approximated as equilibrium functionals of the carrier density such as gain, spectral line-width and spontaneous emission. In actuality, the system is not in equilibrium, but it is assumed that these functions will not be greatly affected by this. The spectral property of interest in the work is the amplitude gain. The second main area is referred to as the dynamical properties. These are assumed not to be in equilibrium and will describe how the carriers vary as a function of injected current. This area will also calculate the light output of the laser.

These two areas can be used in conjunction with each other because the major input required for the dynamical model is the gain as a function of carrier density. Often however, the dynamical model will just use a simple approximation of the gain to speed calculations. In chapter 5, both cases will be shown.

Chapter 3

Gain

The gain describes how the amplitude of the power changes as a function of time. It is the term g_α in the formula

$$P_\alpha = P_{\alpha o} e^{g_\alpha t} \tag{3.1}$$

Where α refers to the laser mode and $P_{\alpha o}$ is the power's initial value which can also be determined with the gain and some other key parameters (discussed in chapter 4). This will be derived for the TE and TM modes of a QW laser or SOA and is calculated by finding the first-order perturbation of the electric and magnetic fields due to the interactions with the electrons and holes. It will be required to solve Maxwell's equations to determine the models of the laser and the Heisenberg's equation for the density matrix to first order for the perturbing interaction of carriers and the light field.

The derivation here differs from most in that it does not require a definition of an active layer, a region where all lasing interaction occurs[17, 18, 19]. It is roughly the size of the QW but corrections must be be added to take into account the incomplete confinement of carriers to the well. The freedom not to define an active layer is important for coupled quantum wells where the exact active regions are difficult to determine because of carrier leakage into the barriers. This model is a generalization of Aversa and Iizuka's model for QW lasers in the parabolic approximation[17].

3.1 Maxwell's Equations for Active Modes

Maxwell's Equations for a system that is not source-free are

$$\nabla^2\mathbf{E}(\mathbf{r},t) = \mu_o\varepsilon(z)\frac{\partial^2\mathbf{E}(\mathbf{r},t)}{\partial t^2} + \mu_o\sigma\frac{\partial\mathbf{E}(\mathbf{r},t)}{\partial t} + \mu_o\frac{\partial^2\mathbf{P}(\mathbf{r},t)}{\partial t^2} \tag{3.2}$$

$$\nabla^2\mathbf{H}(\mathbf{r},t) = \mu_o\varepsilon(z)\frac{\partial^2\mathbf{H}(\mathbf{r},t)}{\partial t^2} + \mu_o\sigma\frac{\partial\mathbf{H}(\mathbf{r},t)}{\partial t} - \nabla\times\frac{\partial\mathbf{P}(\mathbf{r},t)}{\partial t} \tag{3.3}$$

where $\mathbf{P}$ is the polarization. For a TE field, $\nabla\cdot\mathbf{P} = 0$ exactly and for a TM field, the approximation $\nabla\cdot\mathbf{P}\approx 0$ is commonly used [17]. The term σ accounts for the losses. The interaction with the carriers is incorporated by the polarization which is calculated below.

3.2 Polarization

The polarization density is related to the macroscopic current density by

$$\frac{\partial\mathbf{P}(\mathbf{r},t)}{\partial t} = \mathbf{J}(\mathbf{r},t) \tag{3.4}$$

There are other methods that can be used to define the polarization, but this method will prove to be useful here because it will enable a definition of the polarization in terms of the momentum matrix elements which are well-defined for the various LK bands.

3.2.1 Current Density

The macroscopic current density can be related to the microscopic expectation value by

$$\mathbf{J}(\mathbf{r},t) =< \mathbf{j}(\mathbf{r},t) >= \sum_{\alpha,\beta} < \alpha|\rho(t)|\beta >< \beta|\mathbf{j}(\mathbf{r})|\alpha >= \sum_{\alpha,\beta}\rho_{\alpha,\beta}(t)\mathbf{j}_{\beta,\alpha}(\mathbf{r}) \tag{3.5}$$

where α and β represent states in the system, $\rho(t)$ is the density matrix operator. To first order, the microscopic current operator $\mathbf{j}(\mathbf{r})$ is[52]

$$\mathbf{j}(\mathbf{r}) = \frac{q}{2m_o}\left[\mathbf{p}|\mathbf{r}><\mathbf{r}| + |\mathbf{r}><\mathbf{r}|\mathbf{p}\right] \tag{3.6}$$

where $\mathbf{p} = i\hbar\nabla$ is the momentum operator.

Optical polarization is due to the transitions between bands, specifically between conduction and valence bands the intra-band transitions are not of interest because they are not close in energy to the laser light output. Therefore, the only components of the macroscopic current required are the off-diagonal components

$$\mathbf{J}(\mathbf{r},t) = \sum_{c,v} \left(\rho_{c,v}(t)\mathbf{j}_{v,c}(\mathbf{r}) + \rho_{v,c}(t)\mathbf{j}_{c,v}(\mathbf{r})\right) \tag{3.7}$$

where $c,\ v$ denote the states in the conduction and valence bands. In this case, these can be simplified to (Appendix C)

$$\mathbf{j}_{v,c}(\mathbf{r}) = \frac{q}{m_o} < v|\mathbf{p}|\mathbf{r} >< \mathbf{r}|c > \ ,\ \mathbf{j}_{c,v}(\mathbf{r}) = \frac{q}{m_o} < c|\mathbf{r} >< \mathbf{r}|\mathbf{p}|v > \tag{3.8}$$

3.2.2 Density Matrix Evolution

The general equation for the evolution of the density matrix from Heisenberg's equation of motion is[52]

$$\frac{\partial \rho}{\partial t} = -\frac{i}{\hbar}\left[\rho, H\right] \tag{3.9}$$

From equation (3.7), the required off-diagonal components are to first order[12, 15]

$$\frac{\partial \rho_{\alpha,\beta}(t)}{\partial t} = \frac{i}{\hbar}(E_\beta - E_\alpha)\rho_{\alpha,\beta}(t) + \frac{i}{\hbar}\left(\rho^o_{\alpha,\alpha} - \rho^o_{\beta,\beta}\right) H^{'}_{\alpha,\beta}(t) - \frac{1}{\tau}\rho_{\alpha,\beta}(t)\ ,\ \alpha \neq \beta \tag{3.10}$$

The diagonal elements are assumed to be close to equilibrium and therefore do not need to be solved by this equation. They are modeled by the equilibrium Fermi distribution $\rho^o_{\alpha,\alpha} = f_\alpha = \frac{1}{1+e^{(E_\alpha - E_f)/k_B T}}$, E_f is the Fermi energy. The perturbed part of the Hamiltonian is the electromagnetic interaction in the Coulomb gauge ($\nabla \cdot \mathbf{A} = 0$)

$$H^{'}_{\alpha,\beta}(t) =< \alpha|H^{'}|\beta >= -\frac{q}{m_o}\int d^3\mathbf{r}\mathbf{A}(\mathbf{r},t)\cdot < \alpha|\mathbf{p}|\mathbf{r} >< \mathbf{r}|\beta > \tag{3.11}$$

where $\mathbf{A}(\mathbf{r})$ is the vector potential.

A common technique that will be used throughout the chapter as well as in later chapters is to expand time-dependent variables into the relatively few modes of interest.

$$X(\mathbf{r},t) \approx \sum_\omega x_\omega(\mathbf{r},t)\frac{e^{i\omega t}}{\sqrt{T}} \tag{3.12}$$

where $X(\mathbf{r},t)$ is some time-dependent function. This is not a complete Fourier expansion so that there will still be some time dependence of the coefficients $x_\omega(\mathbf{r},t)$ however, this time dependence is assumed to be slow compared to the time variation of the exponential term in equation (3.12). This technique will be referred to as *expanding in the slowly varying components*. T is some time that is large compared to $2\pi/\omega$ but $x_\omega(\mathbf{r},t)$ is approximately constant over this time[15].

The vector potential $\mathbf{A}(\mathbf{r},t)$ is expanded into slowly varying components, i.e. $\mathbf{A}(\mathbf{r},t) \approx \sum_{\omega'} \mathbf{a}_{\omega'}(\mathbf{r},t)\frac{e^{i\omega' t}}{\sqrt{T}}$. If the off-diagonal densities used in equation (3.10) are also expanded into slowly varying components, then substituting equation (3.11) into (3.10) and multiplying by $\int_{t-T/2}^{t+T/2} dt \frac{e^{-i\omega t}}{\sqrt{T}}$ will give the approximate relation

$$\rho_{\alpha,\beta,\omega}(t) \approx \frac{(E_\alpha - E_\beta + \hbar\omega + i\hbar/\tau)(f_\alpha - f_\beta)}{(E_\alpha - E_\beta + \hbar\omega)^2 + \hbar^2/\tau^2} H'_{\alpha,\beta,\omega}(t) \tag{3.13}$$

between the slowly-varying quantities

$$H'_{\alpha,\beta,\omega}(t) = -\frac{q}{m_o}\int d^3\mathbf{r}\mathbf{a}_\omega(\mathbf{r},t) < \alpha|\mathbf{p}|\mathbf{r} >< \mathbf{r}|\beta > \quad , \quad \rho_{\alpha,\beta,\omega}(t) = \int \frac{e^{i\omega t}}{\sqrt{T}}\rho_{\alpha,\beta}(t)dt$$

The optical transitions of interest will have an energy close to the band-gap energy ($\hbar\omega \approx E_c - E_v$) so that, the only non-negligible terms for the density matrix are

$$\rho_{c,v}(t) = \sum_{\omega>0} \frac{(E_c - E_v - \hbar\omega + i\hbar/\tau)(f_c - f_v)}{(E_c - E_v - \hbar\omega)^2 + \hbar^2/\tau^2} H'_{c,v,-\omega}(t)\frac{e^{-i\omega t}}{\sqrt{T}} \tag{3.14}$$

$$\rho_{v,c}(t) = \sum_{\omega>0} \frac{(E_v - E_c - \hbar\omega - i\hbar/\tau)(f_v - f_c)}{(E_c - E_v - \hbar\omega)^2 + \hbar^2/\tau^2} H'_{v,c,\omega}(t)\frac{e^{i\omega t}}{\sqrt{T}} \tag{3.15}$$

The gain of equation (3.1) will eventually have real and imaginary components. The real part will determine the change in the amplitude of the power and this is the term of primary concern here. For this part of the gain, it can be shown that only the terms with $i\hbar/\tau$ will survive (all that is required is to keep all terms throughout the derivation to see this). For convenience then, all the other terms will be ignored.

Substituting equations (3.14) and (3.15) into equation (3.7) gives the current

$$\begin{aligned}
\mathbf{J}(\mathbf{r},t) &= \sum_{c,v,\omega>0} \frac{i\hbar(f_c - f_v)/\tau}{(E_c - E_v - \hbar\omega)^2 + \hbar^2/\tau^2} \left[H'_{c,v,-\omega}(t) \frac{e^{-i\omega t}}{\sqrt{T}} \mathbf{j}_{v,c} - H'_{v,c,\omega}(t) \frac{e^{i\omega t}}{\sqrt{T}} \mathbf{j}_{c,v} \right] \\
&= \sum_{c,v,\omega>0} \frac{i\hbar(f_c - f_v)/\tau}{(E_c - E_v - \hbar\omega)^2 + \hbar^2/\tau^2} \frac{q^2}{m_o^2\sqrt{T}} \\
&\times \left\{ \begin{array}{l} -\left[\int d^3\mathbf{r}' \mathbf{a}_{-\omega}(\mathbf{r}',t) \cdot < c|\mathbf{r}' >< \mathbf{r}'|\mathbf{p}|v > \right] < v|\mathbf{p}|\mathbf{r} >< \mathbf{r}|c > e^{-i\omega t} \\ -\left[\int d^3\mathbf{r}' \mathbf{a}_{\omega}(\mathbf{r}',t) \cdot < v|\mathbf{p}|\mathbf{r}' >< \mathbf{r}'|c > \right] < c|\mathbf{r} >< \mathbf{r}|\mathbf{p}|v > e^{i\omega t} \end{array} \right\} \quad (3.16)
\end{aligned}$$

3.2.3 Polarization Component

Recall that the polarization is related to the current by equation (3.4). It will be required in the following section to find the slowly varying component of the polarization $\mathbf{p}_\omega(\mathbf{r}) = \int_{t-T/2}^{t+T/2} \frac{e^{-i\omega t}}{\sqrt{T}} \mathbf{P}(\mathbf{r},t)$. Multiplying equations (3.4) and (3.16) by $\int_{t-T/2}^{t+T/2} dt \frac{e^{-i\omega t}}{\sqrt{T}}$ and equating them gives a relation for the slowly varying components of the polarization

$$\begin{aligned}
\mathbf{p}_\omega(\mathbf{r},t) &= \frac{i}{\omega} \sum_{c,v,\omega>0} \frac{i\hbar(f_c - f_v)/\tau}{(E_c - E_v - \hbar\omega)^2 + \hbar^2/\tau^2} \frac{q^2}{m_o^2\sqrt{T}} \\
&\times \int d^3\mathbf{r}' \mathbf{a}_\omega(\mathbf{r}',t) \cdot \left\{ \begin{array}{l} [< c|\mathbf{r}' >< \mathbf{r}'|\mathbf{p}|v >] < v|\mathbf{p}|\mathbf{r} >< \mathbf{r}|c > \\ +[< v|\mathbf{p}|\mathbf{r}' >< \mathbf{r}'|c >] < c|\mathbf{r} >< \mathbf{r}|\mathbf{p}|v > \end{array} \right\} \quad (3.17)
\end{aligned}$$

3.3 TE, TM modes and Power

The gain will be more precisely defined shortly. For now, an argument based on the power from the Poynting vector is used[12, 54] to simplify the analysis by reducing the number of equations from (3.2) and (3.3) that are necessary to solve. The power intensity of the laser is determined by using the complex Poynting vector

$$\mathbf{S}(\mathbf{r},t) = \mathbf{E}(\mathbf{r},t) \times \mathbf{H}^*(\mathbf{r},t) \quad (3.18)$$

Of interest here is the x component as this is the direction of output from the laser facets.

$$S^x(\mathbf{r},t) = E^y(\mathbf{r},t) H^{z*}(\mathbf{r},t) - E^z(\mathbf{r},t) H^{y*}(\mathbf{r},t) \quad (3.19)$$

For the TE modes only the $E^y H^{z*}$ term is non-zero because $E^z = 0$. The Maxwell equation

$$\nabla \times \mathbf{E} = -\frac{\partial}{\partial t}\mathbf{B} \tag{3.20}$$

and the assumption of negligible variation in the y direction gives the relation

$$\frac{\partial}{\partial x}E^y \approx -\mu\frac{\partial}{\partial t}H^z \;\; \rightarrow H^z \propto E^y \tag{3.21}$$

Therefore it is only necessary to solve for the gain of the E^y component to describe the power output of the TE mode. Similarly, for the TM mode, the power is $-E^z H^{y*}$ and by the relation

$$\nabla \times \mathbf{H} = \frac{\partial}{\partial t}\mathbf{D} \tag{3.22}$$

again with no variation in the y direction,

$$\frac{\partial}{\partial x}H^y = \frac{\partial}{\partial t}(\varepsilon E^z) \;\; \rightarrow E^z \propto H^y \tag{3.23}$$

Therefore it is only necessary to solve for the gain of the H^y component to describe power output of the TM mode.

3.4 TE Modes

To solve for the y component of equation (3.2) the field is expanded in the orthonormal basis of the passive modes of equation (2.26)

$$E^y(\mathbf{r},t) = \sum_{\omega\beta} e^y_{\omega\beta}(t)F_{\omega\beta}(z)\frac{e^{i\beta x + i\omega t}}{\sqrt{ST}} \tag{3.24}$$

where β is the propagation constant of the passive modes described in section 2.2. The term $e^y_{\omega\beta}(t)$ is the slowly varying component of the TE field in the passive modes of equation (2.26). The y component of the polarization will also be expanded in these modes

$$P^y(\mathbf{r},t) = \sum_{\omega\beta} p^y_{\omega\beta}(t)F_{\omega\beta}(z)\frac{e^{i\beta x + i\omega t}}{\sqrt{ST}} \tag{3.25}$$

Since $e^y_{\omega\beta}(t)$ and $p^y_{\omega\beta}(t)$ are slowly varying, only terms up to the first derivative will be kept. Actually, only the zeroth order component of $p^y_{\omega\beta}(t)$ will be kept because the polarization

is already assumed to be small. Substituting these into equation (3.2) and performing the derivatives gives

$$\sum_{\omega\beta}\left[\ddot{F}_{\omega\beta}(z)-\left(\beta^2+\mu_o\varepsilon(z)\omega^2\right)F_{\omega\beta}(z)\right]\frac{e^{i\beta x+i\omega t}}{\sqrt{ST}}e^y_{\omega\beta}(t)$$

$$=\sum_{\omega\beta}\frac{e^{i\omega t+i\beta x}}{\sqrt{ST}}F_{\omega\beta}(z)\left[\mu_o\varepsilon(z)\left(2i\omega\dot{e}^y_{\omega\beta}\right)+\mu_o\sigma\left(\dot{e}^y_{\omega\beta}+i\omega e^y_{\omega\beta}\right)-\mu_o\omega^2p^y_{\omega\beta}\right] \tag{3.26}$$

For functions in z, the over-dot signifies a derivative wrt z. In time, an over-dot signifies a derivative wrt time. Two over-dots signify the second derivative.

The LHS of equation (3.26) is just the source-free homogeneous equation and hence is zero. Multiplying the RHS by

$$\int_{t-T/2}^{t+T/2}\int_0^L\int_S dtd^3\mathbf{r}F^*(z)_{\omega\beta}\frac{e^{-i\beta x-i\omega t}}{\sqrt{ST}} \tag{3.27}$$

reduces this to

$$\dot{e}^y_{\omega\beta}\left(\bar{\varepsilon}2i\omega+\sigma\right)+i\sigma\omega e-\omega^2p^y_{\omega\beta}=0 \tag{3.28}$$

where $\bar{\varepsilon}=\int dz|F_{\omega\beta}(z)|^2\varepsilon(z)$ It is assumed $\sigma^2<<\omega^2\bar{\varepsilon}^2$ (low losses) so that equation (3.28) can be rearranged to

$$\dot{e}^y_{\omega\beta}\approx-\left(\frac{\sigma}{2\bar{\varepsilon}}-i\frac{\sigma}{4\bar{\varepsilon}^2\omega}\right)e^y_{\omega\beta}-\left(\frac{i\omega}{2\bar{\varepsilon}}-\frac{\sigma}{4\bar{\varepsilon}^2}\right)p^y_{\omega\beta} \tag{3.29}$$

If the last term of equation (3.29) is written as $g^{TE}_{\omega\beta}e^y_{\omega\beta}/2$ then the solution to equation (3.29) would be

$$e^y_{\omega\beta}(t)=e^y_{\omega\beta}(0)e^{(-\alpha+g^{TE}_{\omega\beta})t/2}\ ,\ \alpha=2\left(\frac{\sigma}{2\bar{\varepsilon}}-i\frac{\sigma}{4\bar{\varepsilon}^2\omega}\right) \tag{3.30}$$

Expanding E^y and H^z into the slowly-varying and passive mode basis, it can be shown from equation (3.21) that the components are related by

$$h^z_{\omega\beta}(t)=\frac{\beta}{\omega\mu}e^y_{\omega\beta}(t)$$

If this is substituted into equation (3.19), the power is

$$\begin{aligned} < S > (T) \quad &= \sum_{\omega\beta} \frac{\beta}{\mu\omega} (e^y_{\omega\beta}(T))^2 \\ &= \sum_{\omega\beta} \frac{\beta}{\mu\omega} (e^y_{\omega\beta}(0))^2 e^{(-\alpha + g^{TE}_{\omega\beta})T} \end{aligned} \tag{3.31}$$

which is of the form of equation (3.1) so that the term $g^{TE}_{\omega\beta}$ is the power gain of this mode. The term α represents the losses.

The purpose of this section is to find the relation between $e^y_{\omega\beta}(t)$ and $p^y_{\omega\beta}(t)$ so that the above definition of $g^{TE}_{\omega\beta}$ can then be made. Again, only the amplitude component of the gain will be considered and thus only the real part of $g^{TE}_{\omega\beta}$ is used.

To find the relation between $e^y_{\omega\beta}(t)$ and $p^y_{\omega\beta}(t)$, equation (3.17) is analyzed. This is multiplied by $\int d^3\mathbf{r} F^*_{\omega\beta}(z) \frac{e^{-i\beta x}}{\sqrt{S}}$ to give the y component of the polarization mode as

$$\begin{aligned} p^y_{\omega,\beta}(t) \quad &= \quad -\frac{\hbar q^2}{\omega m_o^2 \tau} \sum_{c,v} \frac{(f_c - f_v)}{(E_c - E_v - \hbar\omega)^2 + \hbar^2/\tau^2} \int_0^L \int_S d^3\mathbf{r} F^*_{\omega\beta}(z) \frac{e^{-i\beta x}}{\sqrt{S}} \\ &\times \quad \int d^3\mathbf{r}' a^y_\omega(\mathbf{r}', t) \left\{ \begin{array}{l} < c|\mathbf{r}' >< \mathbf{r}'|p^y|v >< v|p^y|\mathbf{r} >< \mathbf{r}|c > \\ + < v|p^y|\mathbf{r}' >< \mathbf{r}'|c >< c|\mathbf{r} >< \mathbf{r}|p^y|v > \end{array} \right\} \end{aligned} \tag{3.32}$$

The only non-zero component of the vector potential is a^y_ω because $\mathbf{E} = -\frac{\partial}{\partial t}\mathbf{A}$ in the Coulomb gauge.

The vector potential is also expanded into the previously discussed passive mode basis

$$a^y_\omega(\mathbf{r}, t) = \sum_\beta F_{\omega,\beta}(z) \frac{e^{i\beta x}}{\sqrt{S}} a^y_{\omega,\beta}(t) \tag{3.33}$$

so that equation (3.32) becomes

$$\begin{aligned} p^y_{\omega,\beta}(t) \quad &= \quad -\frac{\hbar q^2}{\omega m_o^2 \tau S} \sum_{c,v} \frac{(f_c - f_v)}{(E_c - E_v - \hbar\omega)^2 + \hbar^2/\tau^2} \int d^3\mathbf{r} d^3\mathbf{r}' \sum_{\beta'} F_{\omega,\beta'}(z') F^*_{\omega\beta}(z) \\ &\times e^{-i\beta x + i\beta' x'} a^y_{\omega,\beta'}(t) \left\{ \begin{array}{l} < c|\mathbf{r}' >< \mathbf{r}'|p^y|v >< v|p^y|\mathbf{r} >< \mathbf{r}|c > \\ + < v|p^y|\mathbf{r}' >< \mathbf{r}'|c >< c|\mathbf{r} >< \mathbf{r}|p^y|v > \end{array} \right\} \end{aligned} \tag{3.34}$$

The states $c,\ v$ are now written more explicitly as $\{n_c, \mathbf{k}_{c_\perp}, s_c\}$ and $\{n_v, \mathbf{k}_{v_\perp}, \alpha\}$. where s_c are the two S-spin states of the conduction band and α are the LK subbands. Using the expansions for these states from equations (2.12) and (2.23) so that equation (3.34) can be written as

$$
\begin{aligned}
p^y_{\omega,\beta}(t) &= -\frac{\hbar q^2}{\omega m_o^2 \tau S^3 L} \sum_{n_c,n_v,\mathbf{k}_c,\mathbf{k}_v} \frac{(f_{n_c}(\mathbf{k}_c) - f_{n_v}(\mathbf{k}_v))}{(E_{n_c}(\mathbf{k}_c) - E_{n_v}(\mathbf{k}_v) - \hbar\omega)^2 + \hbar^2/\tau^2} \qquad (3.35)\\
&\times \int d^3\mathbf{r} d^3\mathbf{r}' \sum_{\beta'} F_{\omega,\beta'}(z') F^*_{\omega\beta}(z) e^{i(\beta' x' - \beta x)} a^y_{\omega,\beta'}(t)\\
&\times \sum_{m,m',\alpha,\alpha',s_c,s'_c} p^y_{s_c,\alpha} p^{y*}_{s'_c,\alpha'} \left\{ \begin{array}{l} F^{c*}_{n_c}(z') e^{i(\mathbf{k}_v - \mathbf{k}_c)\cdot\mathbf{x}'} e^{iK_m z'} f_{m,\alpha,(n_v)} \\ \times F^c_{n_c}(z) e^{-i(\mathbf{k}_v - \mathbf{k}_c)\cdot\mathbf{x}} e^{-iK_{m'} z} f^*_{m',\alpha',(n_v)} \\ + F^{c*}_{n_c}(z) e^{i(\mathbf{k}_v - \mathbf{k}_c)\cdot\mathbf{x}} e^{iK_{m'} z} f_{m',\alpha',(n'_v)} \\ \times F^c_{n_c}(z') e^{-i(\mathbf{k}_v - \mathbf{k}_c)\cdot\mathbf{x}'} e^{-iK_m z'} f^*_{m,\alpha,(n_v)} \end{array} \right\}\\
&= -\frac{\hbar q^2}{\omega m_o^2 \tau L} \sum_{n_c,n_v,\mathbf{k}_c,\mathbf{k}_v} \frac{(f_{n_c}(\mathbf{k}_c) - f_{n_v}(\mathbf{k}_v))}{(E_{n_c}(\mathbf{k}_c) - E_{n_v}(\mathbf{k}_v) - \hbar\omega)^2 + \hbar^2/\tau^2}\\
&\int dz dz' \sum_{\beta'} F_{\omega,\beta'}(z') F^*_{\omega\beta}(z) a^y_{\omega,\beta'}(t)\\
&\times \sum_{m,m',\alpha,\alpha',s_c,s'_c} p^y_{s_c,\alpha} p^{y*}_{s'_c,\alpha'} \left\{ \begin{array}{l} F^{c*}_{n_c}(z') e^{iK_m z'} f_{m,\alpha n_v} F^c_{n_c}(z) e^{-iK_{m'} z} f^*_{m',\alpha' n_v} \delta_{\beta,\beta'} \delta_{\mathbf{k}_v,\mathbf{k}_c-\beta} \\ F^{c*}_{n_c}(z) e^{iK_{m'} z} f_{m',\alpha' n'_v} F^c_{n_c}(z') e^{-iK_m z'} f^*_{m,\alpha n_v} \delta_{\beta,\beta'} \delta_{\mathbf{k}_v,\mathbf{k}_c+\beta'} \end{array} \right\}
\end{aligned}
$$

where $p^y_{s_c,\alpha'} = \int\limits_{cell} d^3\mathbf{r} u^*_{s_c}(\mathbf{r}) \hat{p}^y u^v_\alpha(\mathbf{r})$ are the momentum matrix elements shown in Appendix A.

The photon momentum (β) is negligible compared to the carrier momentum so that the common approximation $\mathbf{k}_c \approx \mathbf{k}_v \equiv \mathbf{k}$ (known as k conservation) is used. This simplifies equation (3.35) to

$$
p^y_{\omega,\beta}(t) = -\frac{\hbar q^2}{\omega m_o^2 \tau} \sum_{n_c,n_v,\mathbf{k}} \frac{(f_{n_c}(\mathbf{k}) - f_{n_v}(\mathbf{k}))|\sum\limits_{m,\alpha,s_c} p^y_{s_c,\alpha} I^{n_c m}_{\omega\beta} f_{m\alpha,(n_v)}(\mathbf{k})|^2}{(E_{n_c}(\mathbf{k}) - E_{n_v}(\mathbf{k}) - \hbar\omega)^2 + \hbar^2/\tau^2} \mathbf{a}_{\omega,\beta}(t) \qquad (3.36)
$$

where

$$
I^{n_c m}_{\omega\beta} = \int dz F_{\omega,\beta}(z) F^{c*}_{n_c}(z) \frac{e^{iK_m z}}{\sqrt{L}}
$$

Substituting the momentum matrix elements of Appendix A into the absolute value term of equation (3.36) and averaging over the azimuthal angle (ϕ) in the plane of the QW's[12] reduces this term to

$$\sum_{\alpha} {M^y_{c\alpha}}^2 \left| \sum_m I^{n_c m}_{\omega\beta} f_{m,\alpha,(n_c)}(\mathbf{k}) \right|$$

where, near the band-edge ${M^y_{c\pm 3/2}}^2 \approx \frac{P_X^2}{2}$, ${M^y_{c\pm 1/2}}^2 \approx \frac{P_X^2}{6}$ these are described in Appendix A.

3.4.1 TE Power Gain

In the Coulomb gauge, the relation between electric field and vector potential is $\mathbf{E}(\mathbf{r},t) = -\frac{\partial \mathbf{A}(\mathbf{r},t)}{\partial t}$ which gives a relation between the slowly varying components in this basis

$$e^y_{\omega\beta}(t) = -i\omega a^y_{\omega\beta}(t) \tag{3.37}$$

$$a^y_{\omega}(\mathbf{r},t) = \sum_{\beta} F_{\omega,\beta}(z) \frac{e^{i\beta x}}{\sqrt{S}} a^y_{\omega,\beta}(t) = -\frac{i}{\omega} F_{\omega,\beta}(z) \frac{e^{i\beta x}}{\sqrt{S}} e^y_{\omega,\beta}(t) \tag{3.38}$$

so that equation (3.35) can be written as

$$p^y_{\omega,\beta}(t) = -iC_o \sum_{n_c,n_v,\mathbf{k}} \frac{(f_{n_c}(\mathbf{k}) - f_{n_v}(\mathbf{k})) \sum_{\alpha} {M^y_{c\alpha}}^2 |\sum_m I^{n_c m}_{\omega\beta} f_{m\alpha,(n_v)}(\mathbf{k})|^2}{(E_{n_c}(\mathbf{k}) - E_{n_v}(\mathbf{k}) - \hbar\omega)^2 + \hbar^2/\tau^2} e^y_{\omega,\beta}(t) \tag{3.39}$$

where $C_o = \frac{\hbar q^2}{\omega^2 m_o^2 \tau}$. This is the desired relation between $e^y_{\omega\beta}(t)$ and $p^y_{\omega\beta}(t)$.

Substituting this into equation (3.26) then gives the gain

$$g^{TE}_{\omega,\beta} = \frac{C_o}{\bar{\varepsilon}} \sum_{n_c,n_v,\mathbf{k}} \frac{(f_{n_c}(\mathbf{k}) - f_{n_v}(\mathbf{k})) \sum_{\alpha} {M^y_{c\alpha}}^2 |\sum_m I^{n_c m}_{\omega\beta} f_{m\alpha,(n_v)}(\mathbf{k})|^2}{(E_{n_c}(\mathbf{k}) - E_{n_v}(\mathbf{k}) - \hbar\omega)^2 + \hbar^2/\tau^2} \tag{3.40}$$

3.5 TM Modes

The derivation of the TM gain follows similar arguments to the TE gain except for some technical differences. The relation that will be important for this mode is the y component of equation (3.3). The field is expanded in this orthonormal passive mode basis

$$H^y = \sum_{\omega\beta} h^y_{\omega\beta}(t) G_{\omega\beta}(z) \frac{e^{i\beta x + i\omega t}}{\sqrt{ST}} \tag{3.41}$$

Similar to the TE method, $h^y_{\omega\beta}(t)$ is the slowly varying magnetic field component in the basis of equation (2.27) In this case, both the x and z components of the polarization are needed which are in this basis

$$P^\alpha = \sum_{\omega\beta} p^\alpha_{\omega\beta}(t) G_{\omega\beta}(z) \frac{e^{i\beta x + i\omega t}}{\sqrt{ST}} \tag{3.42}$$

where $\alpha = x, z$. These are substituted into equation (3.3) to get terms up to first derivative and then multiplied by

$$\int_{t-T/2}^{t+T/2} \int d^3\mathbf{r} \frac{e^{-i\omega t - i\beta x}}{\sqrt{ST}} \frac{G^*_{\omega\beta}(z)}{\varepsilon(z)} \tag{3.43}$$

to get

$$\dot{h}^y_{\omega\beta}(t) = -\frac{\sigma}{2 < \varepsilon G_{\omega\beta} >} h^y_{\omega\beta}(t) - \frac{i\beta}{2\mu_o < \varepsilon G_{\omega\beta} >} p^z_{\omega\beta}(t) + \frac{< \dot{G}_{\omega\beta} >}{2\omega\mu_o < \varepsilon G_{\omega\beta} >} p^x_{\omega\beta}(t) \tag{3.44}$$

where $< f >= \int \frac{G^*_{\omega\beta}(z)}{\varepsilon(z)} f(z) dz$. The factor $G^*_{\omega\beta}/\varepsilon$ is used instead of $G^*_{\omega\beta}$ due to the orthogonality relations of magnetic fields (Appendix B). Using a similar argument to the TE modes, the last two terms or equation (3.44) will be written as $g^{TM}_{\omega\beta} h^y_{\omega\beta}/2$. The relation of equation(3.23) and the Poynting vector shows that the TM power gain is $g^{TM}_{\omega\beta}$.

From equation (3.17), the components of the polarization in this basis are

$$\begin{aligned}
\mathbf{p}_{\omega,\beta}(t) &= -\frac{\hbar q^2}{\omega m_o^2 \tau} \sum_{c,v} \frac{(f_c - f_v)}{(E_c - E_v - \hbar\omega)^2 + \hbar^2/\tau^2} \int_0^L \int_S d^3\mathbf{r} \frac{G^*_{\omega\beta}(z)}{\varepsilon(z)} \frac{e^{-i\beta x}}{\sqrt{S}} \\
&\times \int d^3\mathbf{r}' \mathbf{a}_\omega(\mathbf{r}', t) \cdot \left\{ \begin{array}{l} < c|\mathbf{r}' >< \mathbf{r}'|\mathbf{p}|v >< v|\mathbf{p}|\mathbf{r} >< \mathbf{r}|c > \\ + < v|\mathbf{p}|\mathbf{r}' >< \mathbf{r}'|c >< c|\mathbf{r} >< \mathbf{r}|\mathbf{p}|v > \end{array} \right\} \\
&= -\frac{\hbar q^2}{\omega m_o^2 \tau S} \sum_{c,v} \frac{(f_c - f_v)}{(E_c - E_v - \hbar\omega)^2 + \hbar^2/\tau^2} \int_0^L \int_S d^3\mathbf{r} \sum_\beta G_{\omega,\beta'}(z') e^{i(\beta' x' - \beta x)} \frac{G^*_{\omega\beta}(z)}{\varepsilon(z)} \\
&\times \int d^3\mathbf{r}' \mathbf{a}_{\omega\beta'}(\mathbf{r}', t) \cdot \left\{ \begin{array}{l} < c|\mathbf{r}' >< \mathbf{r}'|\mathbf{p}|v >< v|\mathbf{p}|\mathbf{r} >< \mathbf{r}|c > \\ + < v|\mathbf{p}|\mathbf{r}' >< \mathbf{r}'|c >< c|\mathbf{r} >< \mathbf{r}|\mathbf{p}|v > \end{array} \right\} \qquad (3.45)
\end{aligned}$$

where the vector potential in this basis is

$$\mathbf{a}_\omega(\mathbf{r}, t) = \sum_\beta G_{\omega,\beta}(z) \frac{e^{i\beta x}}{\sqrt{S}} \mathbf{a}_{\omega,\beta}(t) \qquad (3.46)$$

The electron and hole basis are once again written explicitly and are expanded as equations (2.12) and (2.23)

$$\begin{aligned}
p^\gamma_{\omega,\beta}(t) &= -\frac{\hbar q^2}{\omega m_o^2 \tau S} \sum_{n_c, n_v, \mathbf{k}} \frac{(f_{n_c}(\mathbf{k}) - f_{n_v}(\mathbf{k}))}{(E_{n_c}(\mathbf{k}) - E_{n_v}(\mathbf{k}) - \hbar\omega)^2 + \hbar^2/\tau^2} \\
&\times a^{\gamma'}_{\omega\beta}(t) \sum_{\alpha,m,m'} {M^\gamma_{c\alpha}}^2 Re\left[J^{\omega\beta}_{m' n_v n_c} K^{\omega\beta}_{m n_v n_c} \right] f^*_{m'\alpha n_v} f_{m\alpha n_v} \qquad (3.47)
\end{aligned}$$

where

$$J^{\omega\beta}_{m' n_v n_c} = \int dz \frac{G^*_{\omega\beta}(z)}{\varepsilon(z)} \frac{e^{-iK_{m'} z}}{\sqrt{L}} F^c_{n_c}(z) \ , \ K^{\omega\beta}_{m' n_v n_c} = \int dz' G_{\omega\beta}(z') \frac{e^{iK_m z'}}{\sqrt{L}} F^{c*}_{n_c}(z')$$

The azimuthal angle (ϕ) has again been integrated over and $\gamma = (x, z)$ denotes the polarization directions. The only non-zero matrix elements near the band-edge are[12] ${M^z_{c\pm 1/2}}^2 = \frac{2}{3} P_X^2$ ${M^x_{c\pm 1/2}}^2 = \frac{1}{6} P_X^2$ ${M^x_{c\pm 3/2}}^2 = \frac{1}{2} P_X^2$

3.5.1 TM Power Gain

Similar to the TE method, the vector potential is written in terms of the TM fields. This is a bit more subtle than the relations for the TE field. Start with the Maxwell relation[54] $\mu\mathbf{H} = \nabla \times \mathbf{A}$. In vector notation, the TM mode reduces to

$$\mu_o \begin{bmatrix} 0 \\ H^y \\ 0 \end{bmatrix} = \begin{bmatrix} \partial_y A^z - \partial_z A^y \\ \partial_z A^x - \partial_x A^z \\ \partial_x A^y - \partial_y A^x \end{bmatrix} = \begin{bmatrix} -\partial_z A^y \\ \partial_z A^x - \partial_x A^z \\ \partial_x A^y \end{bmatrix} \tag{3.48}$$

The last equality in (3.48) is from the assumption that there is no variation in the field in the y direction. This equation implies $A^y = f(t)$ (some function with time dependence only) since all the partial derivatives of this component vanish. By gauge freedom, the function $\mathbf{A}' = \mathbf{A} + \nabla(-\gamma f(t))$ also satisfies Maxwell's equations so that $A^y = 0$ in this gauge.

Next, from the relation $\nabla \times \mathbf{H} = \mathbf{J} + \partial_t(\varepsilon\mathbf{E}) = \mathbf{J} - \varepsilon(\partial_t^2\mathbf{A} + \partial_t\nabla\phi)$, the approximations are then made

$$-\partial_z H^y(t) \approx -\varepsilon(z)\partial_t^2 A^x(t)\ ,\ \partial_x H^y(t) \approx -\varepsilon(z)\partial_t^2 A^z(t) \tag{3.49}$$

In terms of the TM passive mode basis being used, these relations can be written as

$$a^x_{\omega\beta}(t) = -\frac{<\dot{G}>}{\omega^2 < \varepsilon G >} h^y_{\omega\beta}(t)\ ,\ a^z_{\omega\beta}(t) = \frac{i\beta}{\omega^2 < \varepsilon G >} h^y_{\omega\beta}(t) \tag{3.50}$$

Substituting these into (3.47) gives the required relation between $p^x_{\omega\beta}(t)$, $p^z_{\omega\beta}(t)$ and $h^y_{\omega\beta}(t)$ and therefore using this in equation (3.44) leads to the TM power gain

$$\begin{aligned} g^{TM}_{\omega\beta} &= \frac{C_o P_X^2}{\mu_o < \varepsilon G >^2 \omega^2 S} \sum_{n_c, n_v, \mathbf{k}} \frac{(f_{n_c}(\mathbf{k}) - f_{n_v}(\mathbf{k})) \sum_{mm'} Re\left[J^{\omega\beta}_{m' n_v n_c} K^{\omega\beta}_{m n_v n_c}\right]}{(E_{n_c}(\mathbf{k}) - E_{n_v}(\mathbf{k}) - \hbar\omega)^2 + \hbar^2/\tau^2} \\ &\times \left(\sum_{\alpha=\pm 1/2} f^*_{m',\alpha n_v} f_{m,\alpha n_v} \left[\frac{2\beta^2}{3} - \frac{<\dot{G}>^2}{6}\right] - \sum_{\alpha=\pm 3/2} f^*_{m',\alpha n_v} f_{m,\alpha n_v} \frac{<\dot{G}>^2}{2} \right) \end{aligned} \tag{3.51}$$

3.6 Ab-initio approximations

There are various other effects that must be taken into account for an accurate simulation. Unfortunately, they cannot be incorporated consistently into this simplified model and require a more detailed derivation. The results from a more detailed model are therefore added into this model in an approximate ab-initio manner. This section will discuss some of these effects.

3.6.1 Electrostatic Interactions

The method presented to find the electron and hole wave-functions does not take into account what can be a significant effect, especially for InGaAsP based structures. The potential wells in the structure will cause charge carriers to be concentrated around them. This concentration of charged carriers will modify the potential due to their electrostatic interactions. To account for this Schrödinger's equation needs to be solved simultaneously with Poisson's equation[21, 56, 57]. There are various techniques to do this, the method used here will be referred to as the self-consistency method.

To start with, Poisson's equation is

$$\frac{\partial}{\partial z}\left[\varepsilon(z)\frac{\partial}{\partial z}\phi(z)\right] = -\rho(z) \tag{3.52}$$

where $\rho(z)$ is the total charge density which is a sum of the conduction band electrons, valence band holes and the total doping (the dopants will contribute a magnitude of one charge only)

$$\rho(z) = q(n(z) - p(z) + N_D(z)) \tag{3.53}$$

The term $\varepsilon(z)$ is the dielectric permitivity and $\phi(z)$ is the electrostatic potential generated by the charge distribution and it is assumed to vanish at the ends of the heterostructure. It has been found numerically that it is sufficient to use only the parabolic approximation for both electrons and holes when considering electrostatic effects. This is because the density is most dependent on carriers very near the band-edge. In the parabolic model, it can be shown that the carrier densities can be written as[21, 58]

$$\rho_\alpha(z) = \frac{k_B T}{\pi\hbar^2}\left(\sum_n \bar{m}^*_\alpha |F^\alpha_n(z)|^2 \ln\left[1 + \exp\left(\frac{E^f_\alpha - E^\alpha_n}{k_B T}\right)\right]\right) \tag{3.54}$$

The symbol α represents the conduction, HH (LK 3/2,$\pm$3/2) and LH (LK 3/2,$\pm$1/2) bands. E_c^f is the conduction band Fermi-level and $E_{HH}^f = E_{LH}^f$ is the hole Fermi-level. These are determined by standard methods[58] and $\bar{m}_\alpha^*$ is the average effective mass for the particular band, which will be taken as approximately the effective mass in the wells since most of the carriers are confined there. The term $F_n^\alpha(z)$ is the band's envelope function determined by the parabolic method of equation (2.13).

The self-consistency method is as follows. Let $V_\gamma^{(o)}(z) = V_\gamma(z)$, $\gamma = c, v$, the original heterostructure potential found using band-offset and effective mass theory. One uses these potentials in equation (2.13) to find the envelope functions. These are substituted into equation (3.54) to solve for the carrier densities. Substitute these into equation (3.53) and then (3.52) and update the potential

$$V_\gamma^{(1)}(z) = V_\gamma^{(o)}(z) + \eta q \phi(z)$$

Use these new values of the potential to recalculate the envelope functions, density and updated potential. Repeat this process until

$$\int \frac{V_\gamma^{(n+1)}(z) - V_\gamma^{(n)}(z)}{V_\gamma^{(n)}(z)} dz < \delta$$

where δ is some convergence criteria and $\eta < 1$ is a factor to assist numerically in the convergence.

3.6.2 Non-Markovian distribution

The model used so far describes a non-Markovian system. That is, a system which at time t is not affected by the system at time $t - \delta t$. In reality interactions such as scattering interactions are slightly time-retarded and will therefore have time-delayed effects. The simplest accounting of these time-delayed effects will be examined.

First, note that a system with no scattering interactions can be incorporated into the model by taking the limit of $\tau \to \infty$ in equations (3.40) and (3.51). A definition of the Dirac-delta function of use here is[59]

$$\delta(u) = \frac{1}{\pi} \frac{c}{c^2 + u^2} \ , \ c \to 0 \tag{3.55}$$

Using this relation, these two gain formula's can be shown to give the same results as a derivation of gain from Fermi's golden rule[12]. This is essentially the gain formulas used here but with the term $\frac{\hbar/\tau}{\Delta^2+\hbar^2/\tau^2}$ replaced by $\delta(\Delta_k)$ where $\Delta_k = E_{n_c}(\mathbf{k}) - E_{n_v}(\mathbf{k}) - \hbar\omega$. Thus, the incorporation of the Markovian scattering used can be viewed as convolving the no-scattering gain results with a Lorentzian

$$L = \frac{\hbar/\tau}{\Delta^2 + \hbar^2/\tau^2}$$

The incorporation of non-Markovian scattering is approached analogously by using a non-Markovian scattering function in place of the Markovian scattering Lorentzian L. It can be shown[18, 19] that the simplest non-Markovian function that can be used is the Maxwellian function

$$\Theta(\Delta_k) = \sqrt{\frac{\tau^2\pi}{2}} e^{-\tau^2\Delta_k^2/2} \tag{3.56}$$

This is a simplified from [19] by assuming the scattering time for the electrons and holes are the same and $\mathbf{k}$ independent.

3.6.3 Many-Body Effects

There are additional effects due to the coulombic interactions between the electrons and the holes. The general method to calculate these is by including the interactions into the Hamiltonian of equation (3.9) to determine the effects on the density matrix which will therefore lead to changes in the polarization and the gain. The Coulombic effects are examined in detail in the Greens function calculation in Appendix E although this is only for parabolic bands. These calculations will be referenced to show how the density matrix of equation (3.10) is affected by these interactions. These will be extended to the multi-band model used in this section by simply replacing the terms used in Appendix E with the multi-band equivalent[18]. As this is a more phenomenological model, it will just be pointed out here what each effect corresponds to and the common approximations that are used to incorporate it.

Band-gap renormalization (BGR)

Equation (6.89) shows how the transition energy is renormalized by the so-called *screened exchange*. Another energy renormalization term called the *coulomb-hole* renormalization is not readily apparent from this equation. It is due to the fact that screening processes affect the hole effective mass but the data for the hole effective mass is usually given for the low-density limit. This effect must therefore be added in. Equations (4.48) and (4.49) of [44] are formulas that can be used for this. A phenomenological approximation to this model is to use the relation [60, 44] $\delta\varepsilon \approx \beta N^{1/3}$ where β is known as the BGR factor and N is the average carrier density in the well. The BGR factor is often taken from tabulated values or as a fitting parameter. Alternatively, (4.48) and (4.49) can be used to calculate β at a known value of N and this is assumed to remain constant.

In the gain calculations done here, the independent variable is N so BGR is approximated by adding the calculated $\delta\varepsilon$ to E_g in the well. It is assumed the LH and HH bands have the same parameter.

Coulombic Enhancement

Coulombic enhancement is due to the renormalization of the Rabi frequency (for example the last term in equation (6.88)). This is approximated by convolving the gain equation with an extra broadening function[18, 19, 20, 60]

$$\frac{1}{1 - q_{n_c,n_v}(\mathbf{k}_{\|})} \tag{3.57}$$

where

$$q_{n_c,n_v}(\mathbf{k}_{\|}) = \frac{1}{V}\sum_{\mathbf{q}_{\|}} V^{eh}_{n_c,n_v,n_v,n_c}(|\mathbf{k}_{\|} - \mathbf{q}_{\|}|)(f_{n_c}(\mathbf{q}_{\|}) - f_{n_v}(\mathbf{q}_{\|}))\Theta(\Delta_k) \tag{3.58}$$

The term

$$V^{eh}_{n_c,n_v,n_v,n_c}(\mathbf{q}_{\|}) = \sum_{m,m',\alpha,\alpha'} \int dz'dz \frac{e^2}{2\varepsilon_s \mathbf{q}_{\|} A} F^{c*}_{n_c}(z') e^{i(K_m z' - K_{m'})z} f_{m,\alpha,(n_v)} F^{c}_{n_c}(z) f^{*}_{m',\alpha',(n_v)} \tag{3.59}$$

is the overlap of the carrier wave-functions and the coulombic interaction. This term must be used because the calculations here are for LK bands and not the parabolic bands of the Appendix. Evaluation of this factor is shown in [18].

An example of the qualitative dependence of gain on photon energy is shown in figure 3.1. For the no-scattering curve, there is no gain below $\hbar\omega = E_{min} = E_{c1}(0) - E_{v1}(0)$ and this is the energy of maximum gain. This is because the gain is proportional to

$$\delta(E_{nc}(\mathbf{k}) - E_{nv}(\mathbf{k}) - \hbar\omega)(f_{nc}(\mathbf{k}) - f_{nv}(\mathbf{k})) \tag{3.60}$$

and E_{min} of figure 3.1 is the lowest energy that will satisfy this. It will also give the greatest difference for $f_{nc}(\mathbf{k}) - f_{nv}(\mathbf{k})$. Physically this means that below this energy separation there are no electrons and holes to recombine and it is also the energy of greatest occupation number. The energy $\hbar\omega = E_{max} = E_{nc}(\mathbf{k}_{max}) - E_{nv}(\mathbf{k}_{max})$ is the largest energy where the gain will be be positive. Beyond this the gain will be negative (absorption) because $f_{nc}(\mathbf{k}) - f_{nv}(\mathbf{k})$ is negative (there are more valence electrons than conduction electrons).

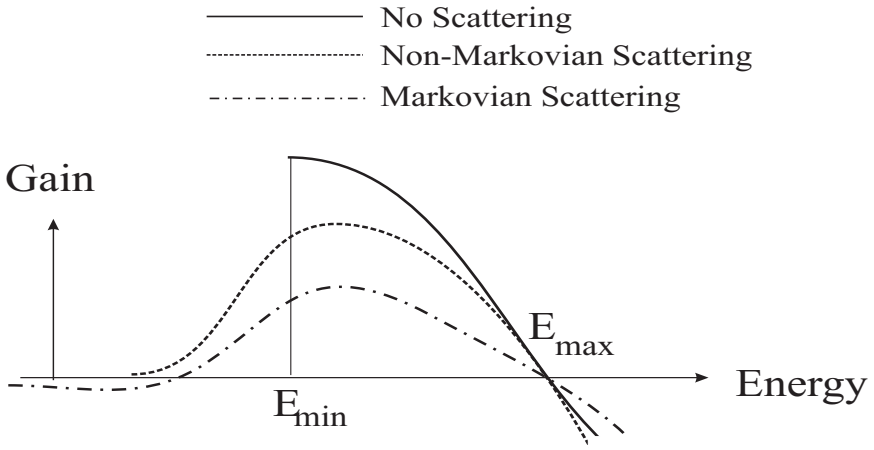

Figure 3.1: A Representation of Gain Versus Photon Energy for a QW Laser for the Cases of No Scattering, Markovian Scattering and Non-Markovian Scattering

Recall that the Fermi functions are also dependent on the carrier density so that the higher the carrier density, the more states will be involved in the stimulated emission. Thus

the next interband transition $n_{ci} - n_{vj}$ will become involved in the gain when $f_{n_{ci}}(0) - f_{nvj}(0) > 0$ barring omission due to symmetry considerations of the momentum overlap integral of Appendix A.

Figure 3.1 also shows how scattering broadens the gain curves. For Markovian scattering, the gain can actually drop below zero at energies less than E_{min}. This is an unphysical effect that is corrected by using the non-Markovian scattering function. The Coulombic interactions affect the curves in two ways. The band-gap renormalization will shift these curves horizontally and the scattering will contribute to further broadening.

3.7 Summary

This chapter describes calculation of the spectral property of amplitude gain in the conventional model. There are many similar formulas that are used for this quantity [18, 19, 25]. The author has generalized a method used by Aversa [17] by extending this to non-parabolic bands. The TE and TM modal gain equations derived use the plane-wave expansion of the Luttinger-Kohn approximation for the valence bands as described in Chapter 2. The purpose of the modified version of gain is for a description that does not depend on the definition of an "active region" in the laser structure, a benefit when examining the coupled quantum wells of Chapter 5. Included ab-initio are terms for Coulombic scattering and energy renormalizations deduced by other authors.

Chapter 4

Dynamics

In this chapter the kinetic and transport properties of the laser will be examined. The problem to be solved is determining the photon power output given an input, in this case, an injection current. What will be discussed here are the simplest models used. These are highly phenomenological and are deduced from more complex models.

4.1 Rate-Equations

A very common model used is the rate equation model[12, 22, 23, 24]. The main advantage of this model is it's simplicity and the speed of the numerical calculations arising from it. The disadvantage is the large number of fitting parameters involved (which necessitates some experimental input or approximations) as well as the simplifications of the physical processes involved. For predicting the properties of a known laser at different input parameters or of a laser of very similar construction it can be quite useful.

A schematic of a MQW using this model is shown in figure 4.1. The electrons and holes are described in an approximate way by lumping them into various groups localized over certain regions. These groupings are not accurately enough modeled to be considered density distributions but average carrier densities within these regions. N_S are the electrons localized around the separate confinement heterostructure (SCH) region (a certain region of layers used for confining the EM field around the heterostructure), this is where electrons injected by the injection current density (J) will enter the system. $N_i^{(3)}$ are electrons that

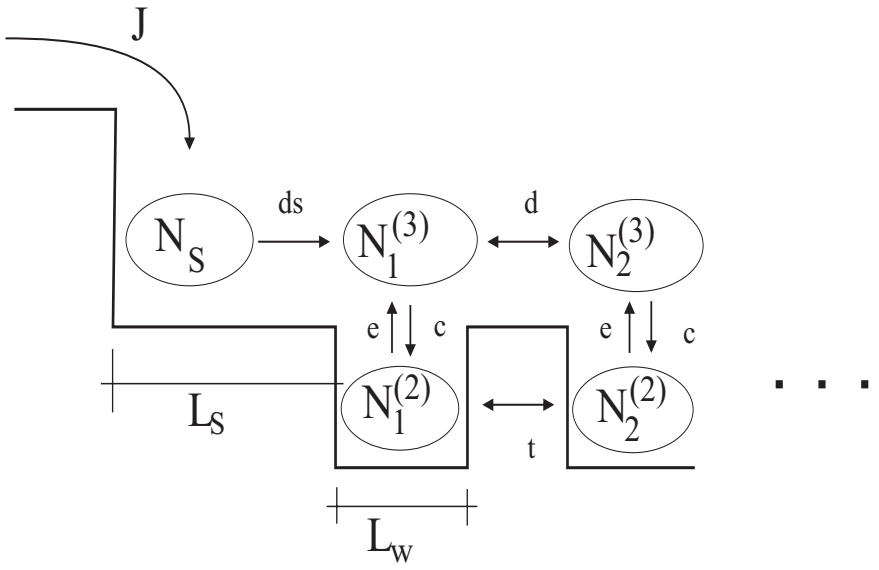

Figure 4.1: A Schematic Representation of the Carriers and Parameters Involved in the Rate Equation Model

are localized around the active region but have energy above the potential well. The superscript (3) is used to imply that they are free to move in all 3 dimensions. $N_i^{(2)}$ represents carriers that are localized around the active region but, due to various processes, have lost energy and have "fallen" into the well. The superscript (2) implies that they are no longer free to move in all 3 directions but only in the 2 in the plane of the well. The subscript i for both of these carrier types refers to the well they are localized around. The holes can be described similarly however, they generally have faster overall transport times which means the electron densities are the limiting factors. Often, as done here, only electron transport is explicitly modeled with the assumption that enough holes will localize around the wells to satisfy local charge neutrality. The electrons are then simply referred to as carriers.

The various physical processes that describe how the carriers move from one region to another are modeled by time constants shown schematically in figure 4.1 and mathemati-

cally in the rate equations of equations (4.1) to (4.8)[22, 23, 24, 61].

$$\frac{dN_S}{dt} = \frac{J}{qL_S} - N_S\left(\frac{1}{\tau_{ds}} + \frac{1}{\tau_n(N_S)}\right) \tag{4.1}$$

$$\frac{dN_1^{(3)}}{dt} = \frac{N_S L_S}{\tau_{ds} L_w} - N_1^{(3)}\left(\frac{1}{\tau_d} + \frac{1}{\tau_c} + \frac{1}{\tau_n(N_1^{(3)})}\right) + \frac{N_2^{(3)}}{\tau_d} + \frac{N_1^{(2)}}{\tau_e} \tag{4.2}$$

$$\frac{dN_1^{(2)}}{dt} = -N_1^{(2)}\left(\frac{1}{\tau_t} + \frac{1}{\tau_e} + \frac{1}{\tau_n(N_1^{(2)})}\right) + \frac{N_2^{(2)}}{\tau_t} + \frac{N_1^{(3)}}{\tau_c} - \sum_\omega \frac{v_g g(N_1^{(2)},\omega) S_\omega}{1+\epsilon S_\omega} \tag{4.3}$$

for i=2,nwells-1

$$\frac{dN_i^{(3)}}{dt} = -N_i^{(3)}\left(\frac{2}{\tau_d} + \frac{1}{\tau_c} + \frac{1}{\tau_n(N_i^{(3)})}\right) + \frac{N_{i-1}^{(3)}}{\tau_d} + \frac{N_{i+1}^{(3)}}{\tau_d} + \frac{N_i^{(2)}}{\tau_e} \tag{4.4}$$

$$\frac{dN_i^{(2)}}{dt} = -N_i^{(2)}\left(\frac{2}{\tau_t} + \frac{1}{\tau_e} + \frac{1}{\tau_n(N_i^{(2)})}\right) + \frac{N_{i-1}^{(2)}}{\tau_t} + \frac{N_{i+1}^{(2)}}{\tau_t} + \frac{N_i^{(3)}}{\tau_c} - \sum_\omega \frac{v_g g(N_i^{(2)},\omega) S_\omega}{1+\epsilon S_\omega} \tag{4.5}$$

$$\frac{dN_{nw}^{(3)}}{dt} = -N_{nw}^{(3)}\left(\frac{1}{\tau_d} + \frac{1}{\tau_c} + \frac{1}{\tau_n(N_{nw}^{(3)})}\right) + \frac{N_{nw-1}^{(3)}}{\tau_d} + \frac{N_{nw}^{(2)}}{\tau_e} \tag{4.6}$$

$$\frac{dN_{nw}^{(2)}}{dt} = -N_{nw}^{(2)}\left(\frac{1}{\tau_t} + \frac{1}{\tau_e} + \frac{1}{\tau_n(N_{nw}^{(2)})}\right) + \frac{N_{nw-1}^{(2)}}{\tau_t} + \frac{N_{nw}^{(3)}}{\tau_c} - \sum_\omega \frac{v_g g(N_{nw}^{(2)},\omega) S_\omega}{1+\epsilon S_\omega} \tag{4.7}$$

and

$$\frac{dS_\omega}{dt} = \frac{S_\omega}{1+\epsilon S_\omega}\sum_{i=1}^{nw} \Gamma_i v_g g(N_i^{(2)},\omega) - \frac{S_\omega}{\tau_p} + \beta R_{sp,\omega} \tag{4.8}$$

Transport between N_S and the various $N_i^{(3)}$ is by diffusion and are characterized by the diffusion times τ_{ds} and τ_d. Transport between $N_i^{(3)}$ and $N_i^{(2)}$ happens by various energy loss and gain processes such as phonon and carrier-carrier interactions, these are modeled

by the capture time τ_c and escape time τ_e. Transport between the various $N_i^{(2)}$ occur by quantum tunneling and are described by the tunneling time τ_t.

The lasing process occurs when electrons and holes recombine via EM interactions in the active regions. This interaction is modeled by the term $v_g g_\omega(N_i^{(2)})$, the group velocity times the *material gain*. The material gain can be related to the previous chapter which actually calculated the *modal gain* by the relation $g_{\omega,material}(N_i^{(2)}) = g_{\omega,modal}(N_i^{(2)})/\Gamma_{i,\omega}$ where

$$\Gamma_{i\omega} = \frac{\int\limits_{L_i} |E_\omega(z)|^2 \, dz}{\int\limits_{L_z} |E_\omega(z)|^2 \, dz} \tag{4.9}$$

is the optical confinement factor (essentially the fraction of the electric field around the active region that will interact with the carriers). $E_\omega(z)$ represents the transverse passive envelope function $F_{\omega,\beta}(z)$ or $G_{\omega,\beta}(z)$ of equations (2.26) and (2.27). The symbol L_z is the total length of the structure and L_i is the length of each well. It is assumed there is only a single longitudinal mode.

Spontaneous emission is incorporated explicitly into the equation for photon density by the term $\beta R_{sp,\omega}$ which is the spontaneous emission factor (amount of spontaneous emission entering the lasing mode [12]) multiplied by the spontaneous emission rate for each mode. The spontaneous emission rate is actually carrier dependent and can be related to the gain coefficient by [12] $R_{sp} = v_g n_{sp}$ where

$$n_{sp} = \frac{1}{1 + e^{(\hbar\omega - \Delta F)/k_B T}} \tag{4.10}$$

where ΔF is the separation of the quasi-Fermi levels between the electron and hole (which can be estimated using their average densities in the well).

The material gain does not represent the true power gain, but the gain of a QW (in an MQW or SQW structure) which is independent of the optical confinement factor[12] and coupling effects between other wells . The well's modal gain is then the material gain of the well times it's confinement factor (calculated for the various wells using equation (4.9)). This saves time in the calculations as it is now not required to calculated the gain of the entire structure, which is very time consuming, but just a single well and it's local surroundings. This approximation is only valid if the wells don't interact appreciably with each other (as examined in chapter 5).

Since the gain calculations implicitly assume the carriers to be in an equilibrium distribution, a temperature will have to be assumed. Often the material gain is calculated from a simple phenomenological approximation such as

$$g(N) = g_o \ln(N/N^{th}) \tag{4.11}$$

where g_o is a gain factor and N^{th} is the threshold carrier density (the carrier density where the gain balances the losses to give zero photon output). The gain is multiplied by group velocity to convert from gain/distance to gain/time. There are various losses in the system which are incorporated by the τ_n time constants, determined by the formula[20]

$$\tau_n = \frac{1}{A + BN + CN^2 + D_{leak}N^{4.5}} \tag{4.12}$$

These are the linear and bimolecular radiative and non-radiative terms A and B which includes spontaneous emission, the Auger recombination coefficient C and the carrier leakage coefficient D_{leak}. There are commonly tabulated values that are used[20].

L_S is the SCH length, ϵ is the gain saturation coefficient which accounts for *spectral hole burning*, the fact that it is mainly carriers around a certain energy that will recombine for lasing and thus will become depleted faster than the average number of carriers. τ_p is the photon lifetime which is related to mirror losses and intrinsic absorption by the equation

$$\frac{1}{\tau_p} = v_g \left(\alpha_i + \frac{1}{L} \ln \frac{1}{R^2} \right) \tag{4.13}$$

R is the refractive index of the facets (assumed to be the same on each side).

The rate equations above are often referred to as being multi-modal as they are the sum over different photon frequency modes. For a Fabry-Perot laser these are [61]

$$\omega = \frac{mc}{2Ln_{eff}};\ m = 0, 1, 2... \tag{4.14}$$

where n_{eff} is the effective refractive index of the cavity. Often the rate equation model will only use a single mode because the laser is designed such that only one mode has positive gain. Notice that the first and last wells equations have been separated from the wells in between. This is because the edge wells only interact with one adjacent well and the first well is the only one that interacts with the SCH region.

4.1.1 Analysis

Some of the methods of analysis of the rate equations will be presented.

Steady-State

Assume the system starts in equilibrium (no current applied, no photon output). If a constant current density is applied, there will be an initial transient spike of photon output. In time the system will settle (all transient oscillations die out) to constant photon output (and constant densities for the various carriers). This final state is known as the steady-state. The steady-state can be solved quite easily as all time derivatives in the rate equations vanish. A (non-linear) matrix method can then be used to solve equations (4.1) to (4.8). From now on, the steady-state solutions of these equations will have an extra subscript of "o" appended to them.

An important term to extract is the steady state photon density. This is when

$$0 = \frac{S_{\omega o}}{1 + \epsilon S_{\omega o}} \sum_{i=1}^{nw} \Gamma_i v_g g(N_i^{(2)}, \omega) - \frac{S_{\omega o}}{\tau_p} + \beta R_{sp,\omega} \tag{4.15}$$

By rearranging this equation, assuming ϵ is small, and taking the appropriate root from the quadratic equation gives the photon density as

$$S_{\omega o} = \frac{\beta R_{sp\omega}}{\frac{1}{\tau_p} - \sum_i g(N_{io}^{(2)}, \omega) - \epsilon \beta R_{sp\omega)}} \tag{4.16}$$

This is a very important result as it shows that without spontaneous emission, there is no photon density. Spontaneous emission is required for lasing to commence. This will come up again in later chapters.

The rate equations find the carrier and photon densities given an input current density. The important results to extract from this are the threshold current, gain-current and and power-current relations. The threshold current is the current at which the light output is zero and anything above this current will give positive light output. It is desirable to have the threshold current as low as possible.

The calculations of the previous chapter show the relation between gain and average carrier density (equations (3.40) and (3.51)) where the Fermi levels can be written in terms

of carrier density. However, in experiments, what is actually measured is the gain-input current relationship. The steady-state rate equations can convert between these two relationships because they relate the current input to carrier density. Comparing experimental and theoretical gain-current relations, it is possible to fit the various parameters in the rate equations. An example of this is presented in chapter 5.

Small-signal

Of interest is the response of the system to an oscillating input. This can be used in a qualitative way to determine the best frequency or time response of the system. Starting from the steady-state, a small, periodic modulation j to the steady-state input current density is applied[12, 22, 23, 24]

$$J = J_o + je^{i\Omega t} \tag{4.17}$$

this will result in small deviations to the carrier and photon densities of the form

$$X \approx X_o + xe^{i\Omega t} \tag{4.18}$$

where X_o represents the steady-state solutions to the respective densities in equations (4.1) - (4.8) and x are the resulting small-signal amplitudes of these densities. It is assumed that all the densities will have the same periodic form.

The rate equations to first order will be

$$i\Omega n_S = \frac{j}{qL_S} - n_S\left(\frac{1}{\tau_{ds}} + \frac{1}{\tau_n(N_{So}}\right) \tag{4.19}$$

$$i\Omega n_1^{(3)} = \frac{n_S L_S}{\tau_{ds} L_w} - n_1^{(3)}\left(\frac{1}{\tau_d} + \frac{1}{\tau_c} + \frac{1}{\tau_n(N_{1o}^{(3)})}\right) + \frac{n_2^{(3)}}{\tau_d} + \frac{n_1^{(2)}}{\tau_e} \tag{4.20}$$

$$\begin{aligned} i\Omega n_1^{(2)} &= -n_1^{(2)}\left(\frac{1}{\tau_t} + \frac{1}{\tau_e} + \frac{1}{\tau_n(N_{1o}^{(2)})}\right) + \frac{n_2^{(2)}}{\tau_t} + \frac{n_1^{(3)}}{\tau_c} \\ &- \sum_\omega \frac{v_g g'(N_{1o}^{(2)}, \omega) S_{\omega o}}{1 + \epsilon S_{\omega o}} + \sum_\omega \frac{v_g g(N_{1o}^{(2)}, \omega) s_\omega}{(1 + \epsilon S_{\omega o})^2} \end{aligned} \tag{4.21}$$

for i=2,nwells-1

$$i\Omega n_i^{(3)} = -n_i^{(3)}\left(\frac{2}{\tau_d}+\frac{1}{\tau_c}+\frac{1}{\tau_n(N_{io}^{(3)})}\right)+\frac{n_{i-1}^{(3)}}{\tau_d}+\frac{n_{i+1}^{(3)}}{\tau_d}+\frac{n_i^{(2)}}{\tau_e} \tag{4.22}$$

$$\begin{aligned} i\Omega n_i^{(2)} &= -n_i^{(2)}\left(\frac{2}{\tau_t}+\frac{1}{\tau_e}+\frac{1}{\tau_n(N_{io}^{(2)})}\right)+\frac{n_{i-1}^{(2)}}{\tau_t}+\frac{n_{i+1}^{(2)}}{\tau_t}+\frac{n_i^{(3)}}{\tau_c} \\ &- \sum_\omega \frac{v_g g'(N_{io}^{(2)},\omega)S_{\omega o}}{1+\epsilon S_{\omega o}}+\sum_\omega \frac{v_g g(N_{io}^{(2)},\omega)s_\omega}{(1+\epsilon S_{\omega o})^2} \end{aligned} \tag{4.23}$$

$$i\Omega n_{nw}^{(3)} = -n_{nw}^{(3)}\left(\frac{1}{\tau_d}+\frac{1}{\tau_c}+\frac{1}{\tau_n(N_{nwo}^{(3)})}\right)+\frac{n_{nw-1}^{(3)}}{\tau_d}+\frac{n_{nw}^{(2)}}{\tau_e} \tag{4.24}$$

$$\begin{aligned} i\Omega n_{nw}^{(2)} &= -n_{nw}^{(2)}\left(\frac{1}{\tau_t}+\frac{1}{\tau_e}+\frac{1}{\tau_n(N_{nwo}^{(2)})}\right)+\frac{n_{nw-1}^{(2)}}{\tau_t}+\frac{n_{nw}^{(3)}}{\tau_c} \\ &- \sum_\omega \frac{v_g g'(N_{nwo}^{(2)},\omega)S_{\omega o}}{1+\epsilon S_{\omega o}}+\sum_\omega \frac{v_g g(N_{nwo}^{(2)},\omega)s_\omega}{(1+\epsilon S_{\omega o})^2} \end{aligned} \tag{4.25}$$

and

$$i\Omega s_\omega = \frac{S_{\omega o}}{1+\epsilon S_{\omega o}}\sum_{i=1}^{nw}\Gamma_i v_g g'(N_{io}^{(2)})+\frac{s_\omega}{(1+\epsilon S_{\omega o})^2}\sum_{i=1}^{nw}\Gamma_i v_g g(N_{io}^{(2)})-\frac{s_\omega}{\tau_p} \tag{4.26}$$

The information obtained from this is primarily *quality factors*, an engineering term for making qualitative comparisons between two systems. Some of these parameters are the *modulation response*, *3dB bandwidth*, *resonant frequency* and *damping factor*. The idea is to design a system that has the highest of the first three parameters and lowest damping factor possible. The modulation response is defined as

$$response = \left|\frac{s(\Omega)}{j(\Omega)}\right| \tag{4.27}$$

An example of a modulation response is shown in figure 4.2. It shows the 3dB and resonant frequencies.

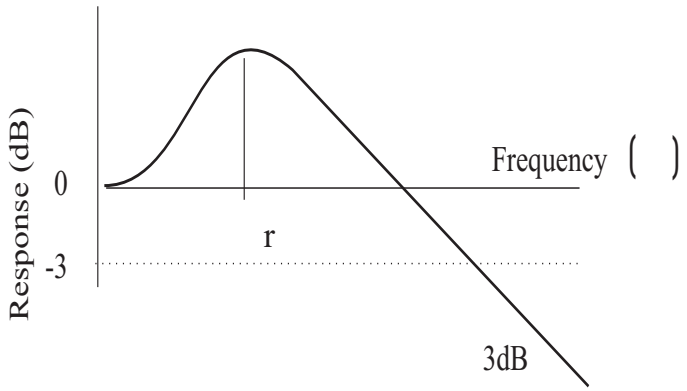

Figure 4.2: A Representation of the Modulation Response for a QW Laser Found from Small-signal Analysis of the Rate Equation Model

It is helpful to examine a simplified model of the laser. Assume there is only one well and there is now only one carrier type that the current injects into and also recombines for the lasing process. This would form a simple set of rate equations[12]

$$\frac{dN}{dt} = \frac{J}{qd} - \frac{N}{\tau} - \frac{vg(N)S}{1+\epsilon S} \tag{4.28}$$

$$\frac{dS}{dt} = \frac{\Gamma v_g g(N)S}{1+\epsilon S} - \frac{S}{\tau_p} + \beta R_{sp} \tag{4.29}$$

Here there are no time-constants but a loss term described by τ. In this case the steady-state solution for photon density is

$$S_o = \frac{\beta R_{sp}}{\frac{1}{\tau_p} - g(N) - \epsilon \beta R_{sp}} \tag{4.30}$$

proceeding with a small-signal analysis, the modulation response can be shown to be approximately

$$\left|\frac{s(\Omega)}{j(\Omega)}\right|^2 \approx \left(\frac{\Gamma \tau_p}{qd}\right)^2 \frac{\Omega_r^4}{(\Omega^2 - \Omega_r^2)^2 + \Omega^2 \gamma^2} \tag{4.31}$$

where

$$\Omega_r^2 \approx v_g g'(N) \frac{S_o}{\tau_p} \tag{4.32}$$

$$\gamma \approx 8\pi^3 \left(\tau_p + \frac{\epsilon}{v_g g'} \right) \Omega_r^2 + \frac{1}{\tau} \tag{4.33}$$

So this simple model has a damped harmonic oscillator form. Numerically, it is noted that the modulation response of the more complicated model is also very similar in form to that of a damped harmonic oscillator. This gives very important information as the more complicated system will qualitatively have similar parameter dependencies on differential gain and loss terms. It is because of this similarity that the damping coefficient (γ) and resonant frequency have been defined for the modulation response. They are determined by fitting equation (4.31) as close as possible to the modulation response of figure 4.2 by varying Ω_r and γ. Note that the resonant frequency is proportional to the square root of the differential gain. This is a very important relation as it is one of the major design parameters for modulation response. Also, the 3dB cutoff occurs at

$$(\Omega_{3dB}^2 - \Omega_r^2)^2 + \Omega_{3dB}^2 \gamma^2 = 2\Omega_r^4 \tag{4.34}$$

and the maximum bandwidth is when

$$2\Omega_r^2 = \gamma^2 \tag{4.35}$$

Therefore there is a major emphasis to increase differential gain and reduce losses. In fact, it is one of the main benefits of quantum well lasers that they have a much higher differential gain than bulk or simple heterojunction lasers.

4.1.2 Numerical Method

The methods for solving the steady-state and small-signal equations are quite simple. These are a set of coupled non-linear equations. A multi-dimension Newton's iteration method is used to solve for the steady-state. Sometimes a convergence factor is introduced for stability because it is non-linear due to the gain and τ_n. The small-signal case is even simpler as it is linearized and can therefore be solved by normal matrix methods once the inputs from the steady-state are obtained.

4.2 Carrier heating model

A deficiency of the rate equation model is the absence of any consideration of the carrier energies other than very generally by dividing the carriers into the classes of 2-D and 3-D. This is inaccurate because the gain is actually dependent on the carrier energy. The carrier heating model[26] adds extra rate equations to describe the energies of the carriers. This is based on the idea that the carrier transport processes will also involve an exchange of energies. For example, if a 3-D carrier is captured by a 2-D well, some of the energy difference between these two levels will be added to the 2-D carriers to increase it's average energy density. Another part of this energy will be radiated away (extra phenomenological parameters are used to determine these). To simplify matters more, it will be assumed that the carriers are all in local "quasi-equilibrium" so that instead of energies, temperatures can be used. From the gain calculations of the previous chapter it is assumed that the carriers are in equilibrium at a certain temperature. The general procedure will then be to include temperature rate equations into the model. This will be done by first writing the more intuitive energy rate equations and then converting these to temperature rate equations.

In this model, the rate equations of equations (4.1) to (4.8) will be the same except each of the carrier densities will now be dependent on temperature T_i were the index i indicates the well or SCH region. It is assumed that the temperatures for the carriers above the well and in the SCH region remain constant so the only varying temperatures are for the carriers in the well. The rate equations for the energy density of the carriers in the wells ($U_i(T_i)$) are[26]

$$\begin{aligned}\frac{dU_1}{dt} &= -N_1^{(2)}\left[\frac{<E_1^{(2)}>}{\tau_t} - \frac{<E_1^{(e)}>}{\tau_e} - \frac{E_1^{(n2)}}{\tau_{n2}}\right] + \frac{N_2^{(2)}}{\tau_t} < E_2^{(2)} > - \frac{N_1^{(3)}}{\tau_c} < E_1^{(c)} > \\ &- \sum_{\omega} \frac{v_g g(N_1^{(2)}), T_1, \omega)}{1+\epsilon S_\omega} S_\omega < E_1^{(st)} > + \hbar\omega v_g \alpha_f S_\omega + \frac{U_1(T_1) - U_1(T_L)}{\tau_L} \qquad (4.36)\end{aligned}$$

for i=2,nw-1

$$\begin{aligned}\frac{dU_i}{dt} &= -N_i^{(2)}\left[2\frac{<E_i^{(2)}>}{\tau_t} - \frac{<E_i^{(e)}>}{\tau_e} - \frac{E_i^{(n2)}}{\tau_{n2}}\right] + \frac{N_{i-1}^{(2)}}{\tau_t} < E_{i-1}^{(2)} > + \frac{N_{i+1}^{(2)}}{\tau_t} < E_{i+1}^{(2)} > \\ &+ \frac{N_i^{(3)}}{\tau_c} < E_i^{(c)} > - \sum_\omega \frac{v_g g(N_i^{(2)}), T_i, \omega)}{1+\epsilon S_\omega} S_\omega < E_i^{(st)} > + \hbar\omega v_g \alpha_f S_\omega \\ &+ \frac{U_i(T_i) - U_i(T_L)}{\tau_L} \qquad (4.37)\end{aligned}$$

for i=nw

$$\begin{aligned}\frac{dU_{nw}}{dt} &= -N_{nw}^{(2)}\left[\frac{<E_{nw}^{(2)}>}{\tau_t} - \frac{<E_{nw}^{(e)}>}{\tau_e} - \frac{E_{nw}^{(n2)}}{\tau_{n2}}\right] + \frac{N_{nw-1}^{(2)}}{\tau_t} < E_{nw-1}^{(2)} > + \frac{N_{nw}^{(3)}}{\tau_c} < E_{nw}^{(c)} > \\ &- \sum_\omega \frac{v_g g(N_{nw}^{(2)}), T_{nw}, \omega)}{1+\epsilon S_\omega} S_\omega < E_{nw}^{(st)} > + \hbar\omega v_g \alpha_f S_\omega + \frac{U_{nw}(T_{nw}) - U_{nw}(T_L)}{\tau_L} \qquad (4.38)\end{aligned}$$

where many new parameters have been used. These are the average energy of the carriers in the well $< E_i^{(2)} >$, the average energy loss due to escape from the well $< E_i^{(e)} >$, the average energy loss due to recombination in the well $< E_i^{(n2)} >$, the average energy gain due to capture in the well $< E_i^{(c)} >$, the average energy loss due to stimulated emission in the well $< E_i^{(st)} >$ and the coefficient of facet heating α_f which is due to photons being re-absorbed into the media to cause carrier heating. The energy wishes to equilibrate itself with its surroundings (the lattice temperature) thus the loss term $\frac{U_i(T_i)-U_i(T_L)}{\tau_L}$, τ_L is the time constant that governs this which is mainly due to phonon interactions.

Since the carriers in the well are in equilibrium, the average energy density in the well can be shown to be

$$U_i(T_I) = N_I^{(2)} k_B T_i \frac{F_1(\eta_i)}{F_0(\eta_i) + N_i^{(2)} E_{i,c}} \qquad (4.39)$$

where

$$F_n(x) = \frac{1}{\Gamma(n+1)} \int_0^\infty \frac{y^n}{1 + /exp(y-x)} dy$$

is the Fermi-Dirac integral[12], $E_{i,c}$ is the conduction band energy, and $\eta_i = (E_{n,i}^f - E_{i,c})/k_B T$, $E_{n,i}^f$ is the Fermi-level of electrons in the ith well. So that

$$\frac{\partial U_i}{\partial T} = N_i^{(2)} k_B \left[\frac{F_1(\eta_i)}{F_0(\eta_i)} + \eta_i \left(\frac{F_1(\eta_i) F_{-1}(\eta_i)}{F_0^2(\eta_i)} - 1\right)\right] \qquad (4.40)$$

and

$$\frac{\partial U_i}{\partial N_i^{(2)}} = k_B T_i \frac{F_0(\eta_i)}{F_{-1}(\eta_i)} + E_{i,c} \tag{4.41}$$

From the definition of a total differential,

$$\frac{dU_i}{dt} = \frac{\partial U_i}{\partial N_i^{(2)}} \frac{dN_i^{(2)}}{dt} + \frac{\partial U_i}{\partial T_i} \frac{dT_i}{dt}$$

the relation between the energy rate equations and temperature rate equations is

$$\frac{dT_i}{dt} = \left(\frac{\partial U_i}{\partial T_i} \right)^{-1} \left(\frac{dU_i}{dt} - \frac{\partial U_i}{\partial N_i^{(2)}} \frac{dN_i^{(2)}}{dt} \right) \tag{4.42}$$

The well carrier rate equations in (4.1) to (4.7), equations (4.36) to (4.38), (4.40), and (4.41) can then be substituted into equation (4.42) to get rate equations for the temperatures and therefore a complete set of equations for the carrier heating model.

The analysis for this model is similar to the rate equation model. The steady-state and small-signal analysis can be performed on this set of equations to again extract terms like the modulation response and bandwidth. This set of equations describes the system more accurately, but has introduced more phenomenological parameters in the different energy exchange terms. These are actually quite difficult to determine, which limits the usefulness of this model. An example of this model is shown in chapter 5. It has estimated parameters that are varied to examine their effects and is basically used just to demonstrate the importance of these effects.

4.3 Summary

This chapter describes calculations of the dynamic properties for the conventional model of the laser. The equations shown are a summary of others' work [12, 22, 26] for the rate equation and carrier heating models. The dynamical calculations require a formula for gain which can be the relations of Chapter 3 or a simple approximation. The next chapter will show numerical results for the spectral and dynamical calculations.

Chapter 5

Examples

In this chapter some research will be presented that uses the theory of the conventional model.

5.1 Effect of well coupling on the TE modal gain

A double QW system is analyzed for the effect of well-coupling on the TE gain with electrostatic effects included[21]. The structure simulated consists of two 5 nm QW's with a separation barrier of varying length (ΔL) between them and 500 nm fixed barriers on either side for the SCH. All barriers are InGaAsP with a band-gap of 1.1μm. The cladding and substrate surrounding the structure are InP. The wells are also InGaAsP. The wells and barriers are lattice matched to InP so there is no strain in the system. The composition of the wells is chosen so that the maximum gain occurs around 1.55μm (this is an approximate relation because the energy at maximum gain will change depending on carrier density and separation barrier width, see figure 5.3).

The description above is a common way to define the semiconductor layers. Instead of giving the x and y composition of each InGaAsP layer, it is more intuitive for readers to see them in terms of the parameters of band-gap and strain. Equation (2.11) and (2.18) with a_o being the lattice size of InP and a given by the interpolation formula (2.10) define two equations with the two unknowns x and y that can be solved. The structure given this description is represented in the table below

Layer	*Material*	*Thickness(nm)*
1	InP	"∞"
2	$In_{0.74}Ga_{0.26}As_{0.56}P_{0.44}$	500
3	$In_{0.53}Ga_{0.47}As$	5
4	$In_{0.74}Ga_{0.26}As_{0.56}P_{0.44}$	ΔL
5	$In_{0.53}Ga_{0.47}As$	5
6	$In_{0.74}Ga_{0.26}As_{0.56}P_{0.44}$	500
7	InP	"∞"

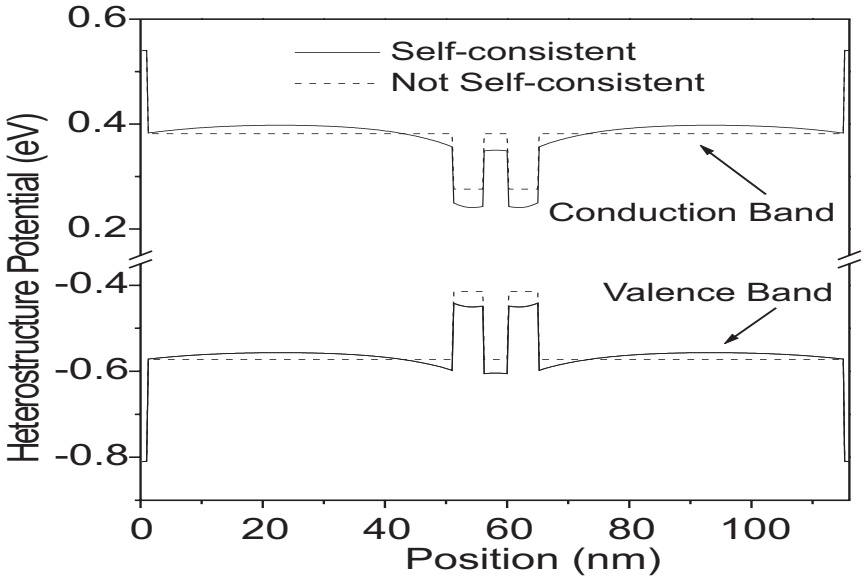

Figure 5.1: The Potential Profile of a DQW Laser Structure with and without Electrostatic Effects Using the Parameters of the Above Table. This is at Average Well Carrier Density $4.5\times10^{18}/\mathrm{cm}^3$.

Figure 5.1 shows how the self-consistent electrostatic effects modify the original heterostructure potential, it modifies the system so as to move it closer to local charge neutrality[56]. This modification causes more conduction electrons and fewer holes to be confined within the wells (figure 5.2). Since conduction electrons are normally the limiting factor to gain, the higher confinement of electrons in the wells results in larger gain amplitude (figures 5.3, 5.4).

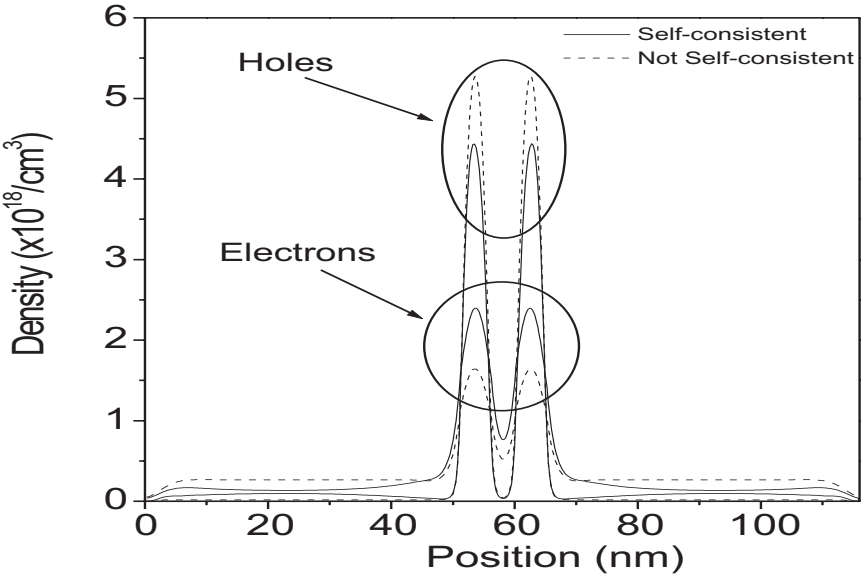

Figure 5.2: Density of Electrons and Holes in the DQW Laser Structure of Fig 5.1 with and without Electrostatic Effects. This is at Average Well Carrier Density $4.5\times10^{18}/\mathrm{cm}^3$.

Electrostatic effects also cause the photon energy dependence of gain to change. As noted by others[62], varying separation barrier widths will change the relative strength of each subband transition. Evidence of different subband transitions is apparent when there is a large change in the energy of the peak gain or local peaks. Electrostatics modifies the potential profile and consequently the relative transition strengths. Therefore, the gain versus photon energy will depend on the well separation and electrostatics as shown in figure 5.3. In figure 5.4 the maximum gain is significantly larger for the electrostatic case for most barrier widths. As well, the barrier separation for minimum gain is smaller when electrostatics is included. This can be explained by figure 5.3, where it is apparent that the dominant transition has changed between the 1.0 and 2.0 nm barriers when electrostatics is included, but not when there are no electrostatics included.

The effects discussed have a large practical importance. The coupling and electrostatics modify the maximum gain in both amplitude and position of the maximum. These are important considerations on the design of an efficient laser. Also, it can be determined the minimum separation barrier width above which the gain will remain relatively uniform,

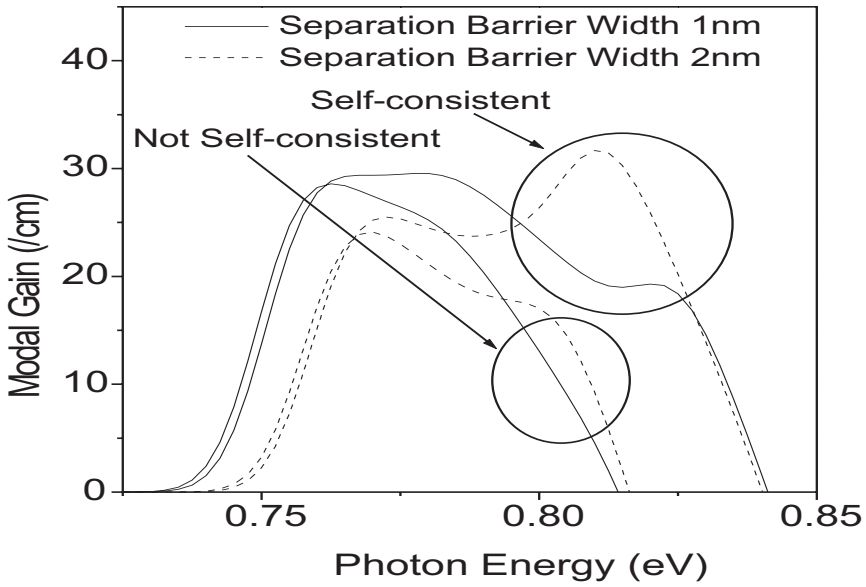

Figure 5.3: TE Modal Gain versus Photon Energy for two Barrier Widths (ΔL) for the DQW Laser in Fig. 5.1 with and without Electrostatic Effects. This is at Average Well Carrier Density $4.5\times10^{18}/\mathrm{cm}^3$.

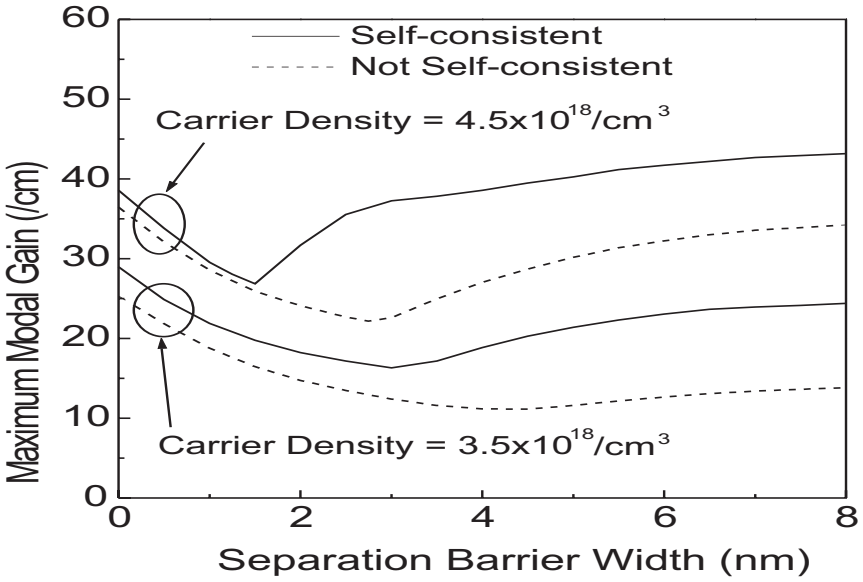

Figure 5.4: Maximum Modal Gain Versus Barrier Width for the DQW Laser of Fig 5.1 with and without Electrostatic Effects.

which can be used to estimate how large barriers must be for the coupling effects to be negligible. An accurate model of the DQW will therefore have to take into account coupling and electrostatic effects.

5.2 Polarization dependence of delta-strained SOA's

SOA's are a key element for optical switching and signal processing[13, 14, 15, 16, 63]. They have the advantages of a wide gain bandwidth and ease of integrability into photonic integrated circuits. The major disadvantage is the polarization sensitivity. That is, the TE and TM gain of the SOA can differ significantly. This can be a serious problem if the input polarization cannot be tightly controlled.

There is ongoing research to design a SOA structure that has less polarization sensitivity. This subject has been analyzed by several groups using combinations of tensile and/or compressive strain in wells and/or barriers[13, 14]. By adjusting the ratio of the number of tensile and compressively strained wells, the TE and TM gains can be matched. Recently

a new method of achieving insensitivity in MQW structures has been proposed[15, 16] by adding a thin layer of GaAs (known as a delta-strain layer) to an otherwise unstrained system.

The structure to be simulated has the layers shown in the table

Layer	*Material*	*Thickness(nm)*
1	InP	50
2	$In_{0.72}Ga_{0.28}As_{0.61}P_{0.39}$	10
3	$In_{0.47}Ga_{0.53}P$	ΔL
4	GaAs	0.9
5	$In_{0.47}Ga_{0.53}P$	13.2-ΔL
6	$In_{0.72}Ga_{0.28}As_{0.61}P_{0.39}$	10
7	InP	50

A delta layer (the GaAs layer which has significantly different lattice size than the other layers) is placed in one large well to effectively make two wells. The positioning of the delta layer is variable (ΔL). The purpose of varying this position is to determine where the best position for polarization independence is. The heterostructure for the delta layer positioned in the center is shown in figure 5.5.

Figure 5.6 shows the valence band dispersion for two positions of the delta layer. The energy is measured with respect to the well band-edge. The band dispersion plays a significant role because changes in the positions of the HH and LH subbands will change which mode is the dominant transition. This can be seen in the momentum matrix elements of Appendix A. For the TE mode, the HH transition is dominant and for the TM transition the LH transitions is dominant (although the HH is still quite significant). The TE and TM modal gain for these two positions are shown in figs 5.7 and 5.8.

In this case, electrostatic effects do not play a significant role as can be seen in figure 5.9. This is because the GaAs barrier potential is so much higher than the electrostatic modification to the heterostructure shown in fig 5.5.

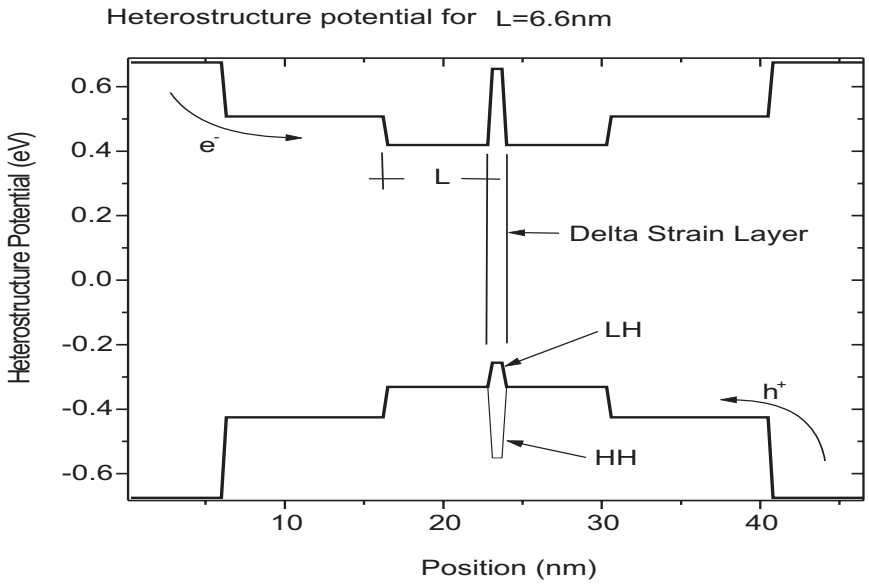

Figure 5.5: Potential Profile of Delta-Strained SOA with the Delta Layer at the Center of the Well.

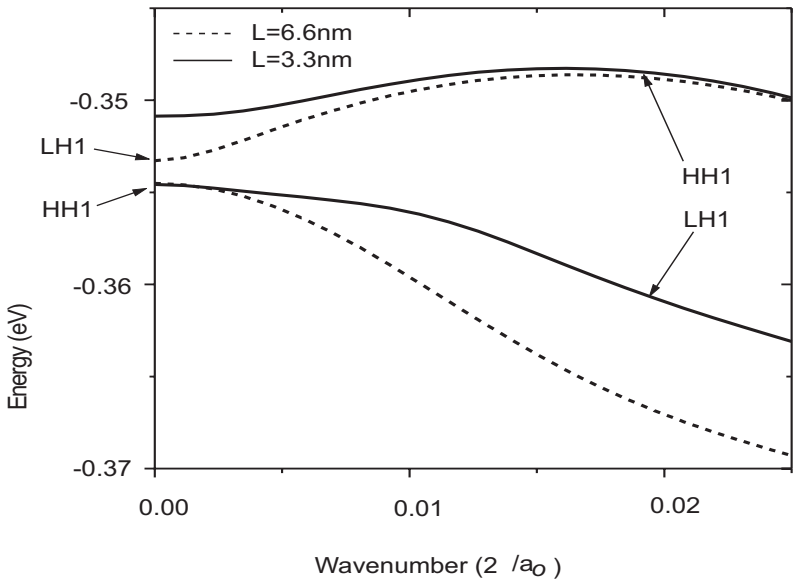

Figure 5.6: Valence Band Dispersion for the first HH and LH Subbands of the SOA for two Different Delta Layer Positions.

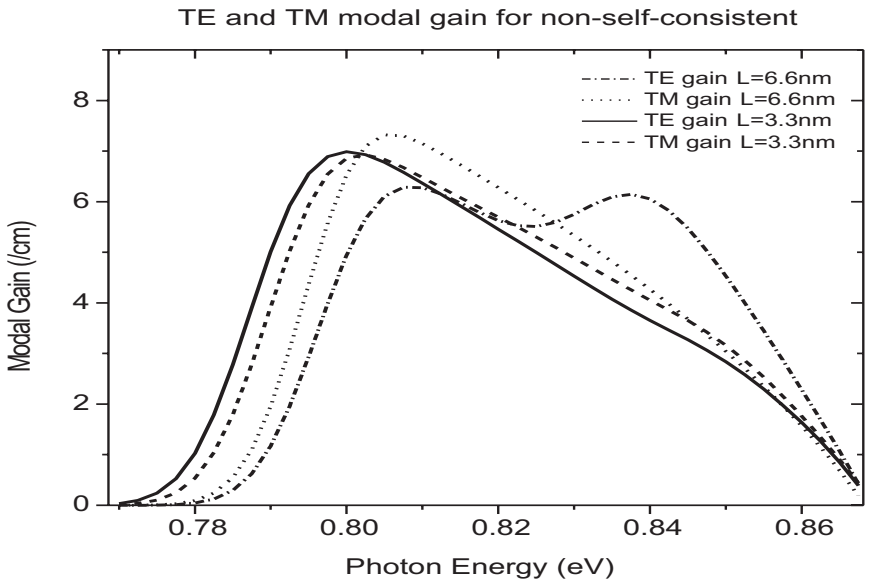

Figure 5.7: TE Modal Gain Versus Photon Energy for the SOA at Delta Layer Position ΔL = 3.3nm from the Left of the Well (no Electrostatic Effects).

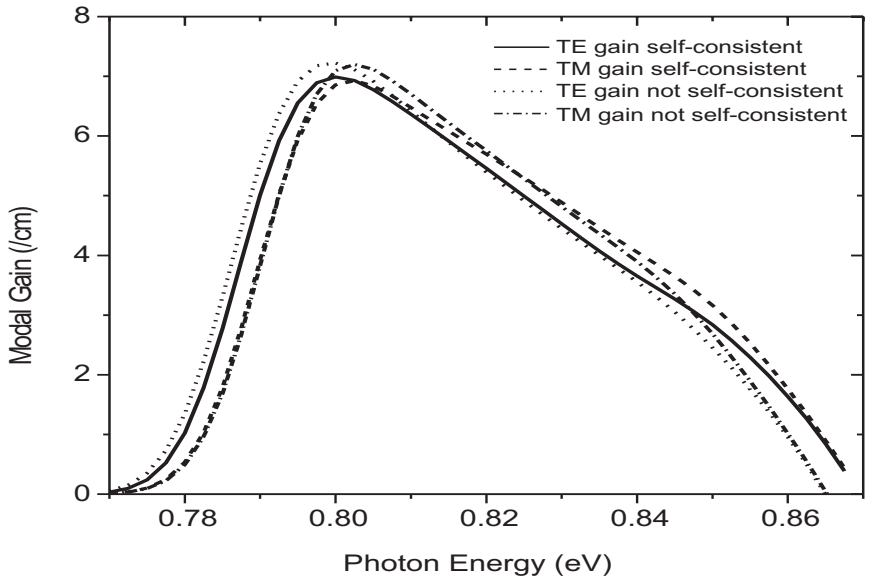

Figure 5.8: TE and TM Modal Gain Versus Photon Energy of the SOA for Delta Layer Position ΔL = 3.3nm from the Left of the Well with and without Electrostatic Effects.

5.3 Comparison of Classical and Tunneling Injection Schemes in QW Lasers

One of the problems that exists in the present generation of MQW lasers is related to the current injection scheme and is generally termed as carrier transport effects[22, 23, 24]. These transport effects are the diffusion in the SCH and the capture-escape in the well regions. It is believed that carrier transport can severely reduce the modulation bandwidth[4, 64, 65].

One possible solution to the carrier transport problem is to consider a different mechanism of carrier injection into the wells based on resonant and non-resonant tunneling instead of carrier capture by energy loss interactions. This mechanism is currently applied to other semiconductor devices such as the resonant tunneling diode. In this case carriers will thermalize in the SCH region and then tunnel into the first QW. This has benefits because thermalization in the SCH region is faster than in the well region because it is larger and therefore there are more energy states available which means a higher probability of scattering. Also, the quantum tunneling time τ_{ts} through the tunneling barrier is of the order of 10 times faster than the traditional capture time τ_c. Since the carriers are more likely thermalizing in the SCH region, the temperature within the well region is lower which will mean lower losses and a higher probability of carriers being around the lasing energy (lower spectral hole burning ε).

The tunneling mechanism of injection in a SQW laser was recently proposed[4, 64, 65]. Those devices have been successfully fabricated. Some of the improvements observed with these devices are a significant reduction of the Auger coefficient (which implies longer τ_n in the rate equations) due to the lower temperature of carriers within the wells. Also, there will be an increase in the modulation bandwidth due to the shorter injection times into the wells.

Comparisons will be made between two MQW designs called here classical injection (CI) and tunneling injection (TI). The CI laser has been shown already in figure 4.1, the TI laser is similar but an extra tunneling barrier is added as shown in figure 5.9.

The analysis will be done with the rate equation model and the characteristic that will be examined is the modulation response. The modulation response of a MQW TI laser

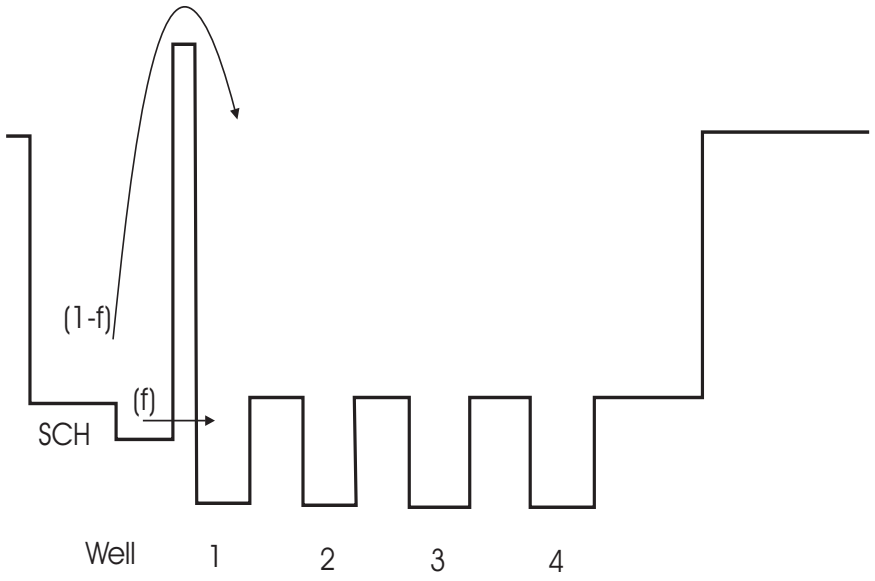

Figure 5.9: Schematic of the Tunneling Injection Laser Heterostructure

will be simulated using the small signal rate equations. These will be compared with the modulation response of a comparable CI laser (the same structure as figure 5.10 but with the tunneling barrier removed). A fraction parameter (f) has been introduced to model the fraction of carriers injected by tunneling into the first confined region of the first well and by tunneling and diffusion into the first unconfined region of the first well. Pure TI(CI) injection is when $f = 1(0)$ and injection schemes "in between" when $0 < f < 1$. The $f = 0$ case gives the same equations from chapter 4. To incorporate this fraction parameter, the rate equations (4.1) to (4.3) must be slightly modified to account for this extra injection mechanism.

$$\frac{dN_S}{dt} = \frac{J}{qL_S} - N_S\left((1-f)\frac{1}{\tau_{ds}} + f\frac{1}{\tau_{ts}} + \frac{1}{\tau_n(N_S)}\right) \tag{5.1}$$

$$\frac{dN_1^{(3)}}{dt} = (1-f)\frac{N_S L_S}{\tau_{ds} L_w} - N_1^{(3)}\left(\frac{1}{\tau_d} + \frac{1}{\tau_c} + \frac{1}{\tau_n(N_1^{(3)})}\right) + \frac{N_2^{(3)}}{\tau_d} + \frac{N_1^{(2)}}{\tau_e} \tag{5.2}$$

$$\frac{dN_1^{(2)}}{dt} = f\frac{N_S L_S}{\tau_{ts} L_w} - N_1^{(2)}\left(\frac{1}{\tau_t} + \frac{1}{\tau_e} + \frac{1}{\tau_n(N_1^{(2)})}\right) + \frac{N_2^{(2)}}{\tau_t} + \frac{N_1^{(3)}}{\tau_c} - \frac{v_g g(N_1^{(2)})S}{1+\epsilon S} \tag{5.3}$$

In this case it is assumed that there is only one frequency mode for the laser and the gain is given by the simplified model of equation (4.11). A steady-state and small signal analysis can then be performed on the rate equations.

It may be asked why complicate matters by adding in one more term? Due to the large number of fitting parameters already present, it would be possible to change the existing parameters of the classical model (namely by reducing τ_c) to model any response desired. The purpose of the extra parameter is that tunneling time is considered to be significantly different from the capture time. As such, any modifications to the parameters of the classical model to obtain the tunneling results is deemed too unphysical. This new parameter is expected to model the system more accurately.

The number of wells was chosen to be four. The cavity length and stripe width were 200 and 3 μm. It is assumed that the electrodes as shown in fig 1.1 have the same cross-sectional area so that these dimensions give the area of the laser perpendicular to the injection direction. The injection current I can then be found from the injection current density by $I = (200\mu m)(3\mu m)J$. The tunneling time through the tunneling barrier was taken as 2ps, the capture times were 20ps, the SCH length 100mm and gain suppression coefficient $\varepsilon = 1.7 \times 10^{-17}$. These parameters are taken directly from [4] as it is these experimental results that the model is being compared to. The average length in each well was 5.4nm and instead of calculation the optical confinement factors it was approximated as 0.01875 for each well. The photon lifetime was inferred from their results to be 2ps and standard values for the group velocity and the threshold carrier density of $8.5 \times 10^9\ cm/s$ and $1.5x10^{18}/cm^3$ were chosen.

Normally the tunneling time τ_{ds} is $<<$ 1ps however, this parameter is meant to approximate the time of traversal over *and* through the tunneling barrier into the first unconfined state hence it will be $\leq$ 2ps so it was chosen as 1ps (actually this time had little effect on the results due to the large capture time). The escape time is in the ns range so for simplicity was chosen as 1ns, this also had little effect on the results. The diffusion and tunneling time between the wells had little effect on the results so they were taken to be the same as those used for the tunneling barrier. The results were highly dependent on the final two parameters of gain coefficient and carrier loss time in the wells, g_o and τ_n these were chosen to fit the threshold current (the current when S_o from the steady-state

solution is zero) and maximum modulation response of the experimental values. The best match to experimental results was when $\tau_n = 1.3ns$ (taken the same for all well densities) and $g_o = 3800/cm$.

The 3dB bandwidth versus current injection for a range of tunneling injection fractions (f) is shown in figure 5.11 for a SQW laser and in figure 5.12 for a 4QW laser. Comparing these two figures shows that the 3dB bandwidth increases as the number of wells increase. It is also seen that the greater the fraction of tunneling injection, the greater the bandwidth. The discrepancy between the fractions increases as the current increases.

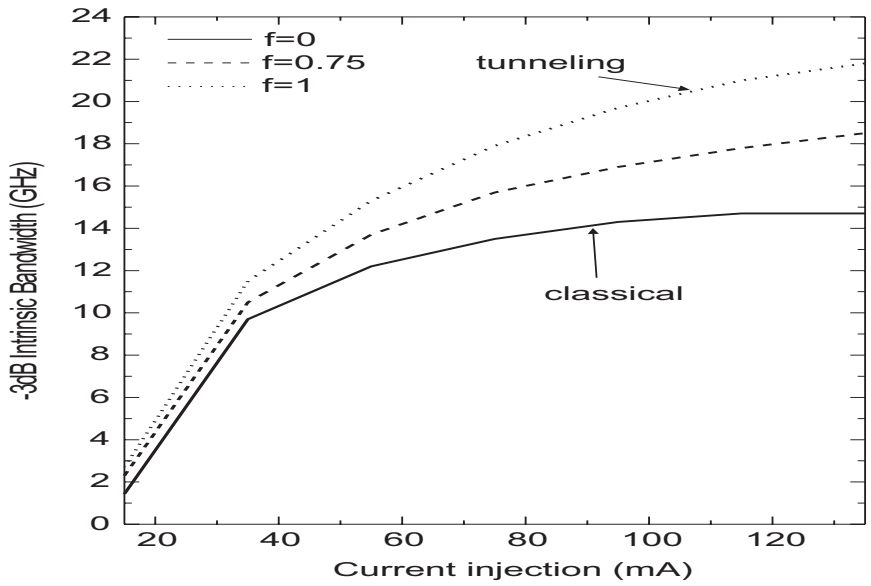

Figure 5.10: 3dB Bandwidth Versus Injection Current for an SQW Laser with and without Tunneling Effects. This is Found Using Small-signal Analysis of the Rate Equations.

Zhang et al[4] found that for a 4 QW TI laser, the 3dB frequency was 76GHz. In these simulations for f=1, the 3dB bandwidth was found to be 70GHz. The threshold current for all values of f was relatively constant as 3.0mA which is the same as the experimental result. The average differential gain in the wells was $2.0 \times 10^{-15} cm^2$ and the experimental result was $1.86 \times 10^{-15} cm^2$. In figure 5.12 it is clearly demonstrated that the modulation response increases as f increases. Figure 5.13 shows that the modulation response also increases as injected current increases.

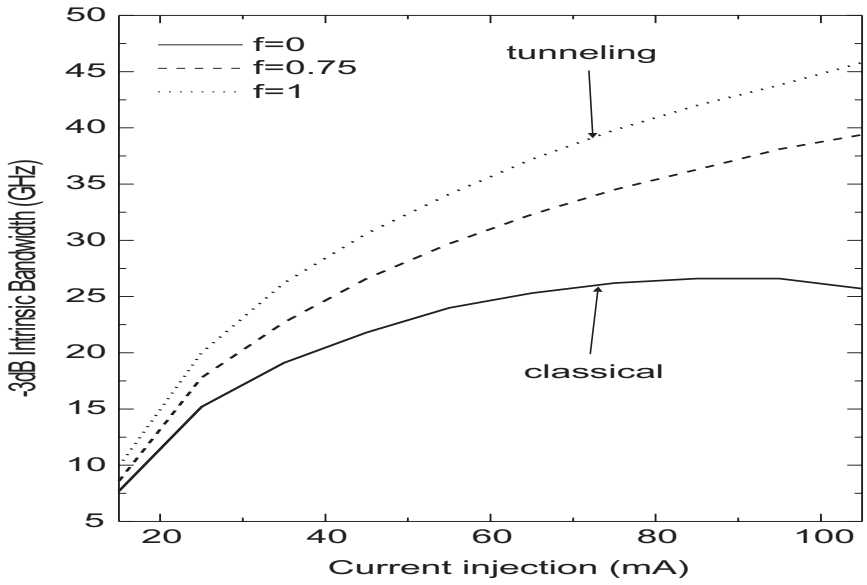

Figure 5.11: 3dB Bandwidth Versus Injection Current for a 4QW Laser with and without Tunneling Effects. This is Found Using Small-signal Analysis of the Rate Equations.

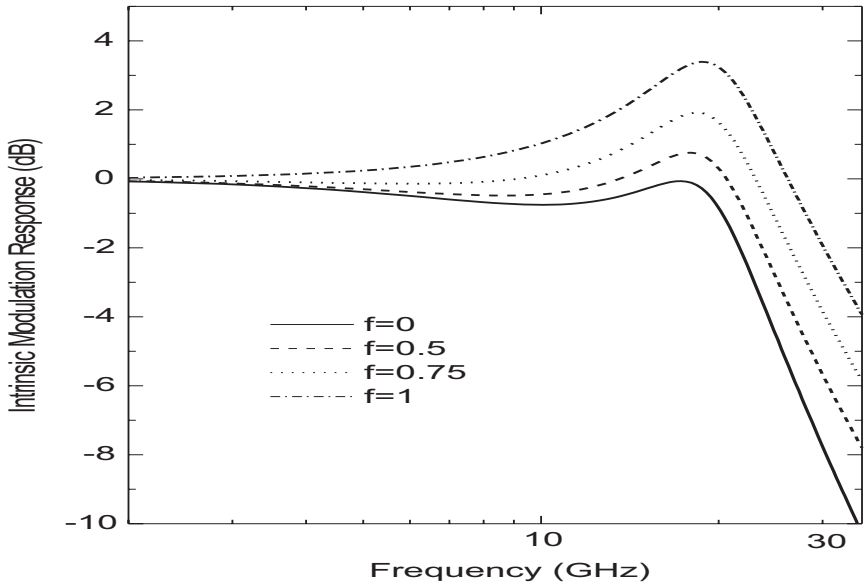

Figure 5.12: Modulation Response Versus Frequency for Various Fractions of Tunneling Injection at 50mA Injection Current

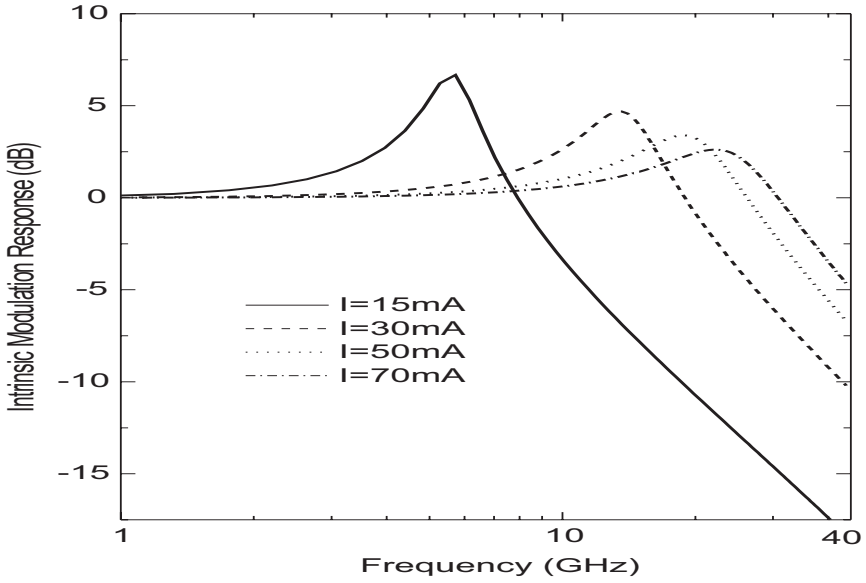

Figure 5.13: Modulation Response Versus Frequency for Various Injection Currents for Complete Tunneling Injection

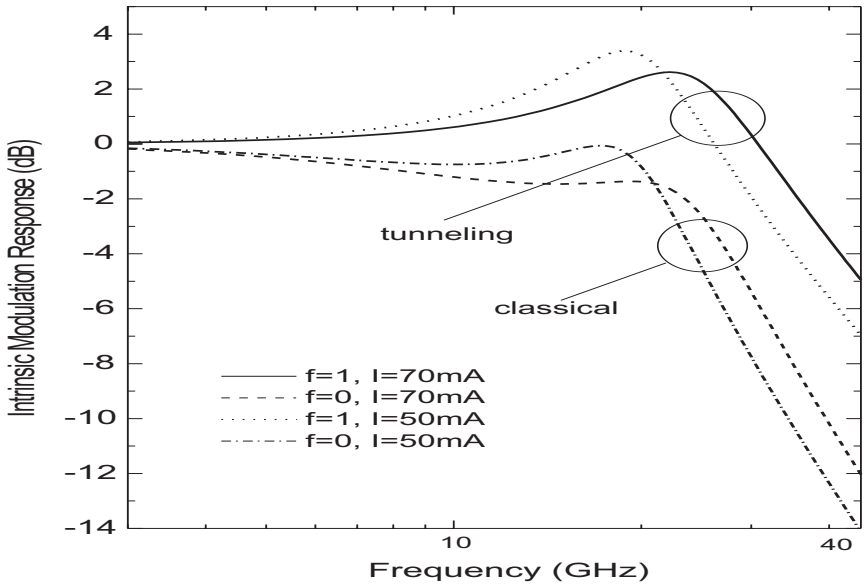

Figure 5.14: Modulation Response Versus Frequency at Various Injection Currents and Fractions of Tunneling Injection

5.4 TE Modal Gain: Theory and Experiment

The purpose of this model is to estimate the parameters used in the conventional method by fitting the results obtained by the theory to some experimental data[66]. Of particular interest is the carrier leakage coefficient (D_{leak}) of equation (4.12). Calculations for the TE modal gain in a 4-well QW laser were performed and compared to experiment. In this case the gain calculations of chapter 3 and the rate equation calculations of chapter 4 were used together for a self-consistent solution.

In the rate equations, the input is the injection current and the output are the various carrier and photon densities. The steady-state rate equations are solved by a Newton's iterative method. It is impractical to recalculate the gain at each iteration using the updated guesses for the carrier and photon densities. Instead, gain is calculated at a number of carrier densities that will cover the range of densities the Newton's iteration will use. This range was determined by trial and error. The gain at these various points will then be used as a basis for interpolation to find gain for any density within the appropriate range. For increased generality, the gain is also on calculated at a range of photon energies and then interpolated for arbitrary energy within this range. Therefore the input of gain into the rate equations is a surface map versus density and energy. From equation (4.9) it can be seen that the confinement factor depends on ω therefore it is interpolated also, which happens to be be almost linear.

For a 4-well system, it is computationally impractical to calculate the gain for a fully coupled system. Fortunately the wells are separated by large enough barriers that the coupling effects are small (see figure 5.4) and so the calculations can be simplified by calculating the material gain for a SQW laser and assuming the material gain is the same for each in the 4-well laser. As discussed in 4.1, the modal gain for each well will be different since the confinement factor will change for the wells. Therefore, the total modal gain as a function of injection current will be a sum of the modal gains for each well

$$G_{total}(I,\omega) = \sum_i \Gamma_i(\omega) g_{net}(N_{if}^{(2)},\omega) \tag{5.4}$$

where $N_{if}^{(2)}$ symbolizes the value of the densities found in the rate equations for this injection current.

The structure is shown in the table below

Layer	*Type*	*Material*	*Thickness(nm)*
1	Cladding	InP	∞
2	Barrier	$In_{0.8}Ga_{0.2}As_{0.75}P_{0.25}$	10
3	Well	$In_{0.8}Ga_{0.2}As_{0.43}P_{0.57}$	5
4	Barrier	$In_{0.8}Ga_{0.2}As_{0.75}P_{0.25}$	10
5	Well	$In_{0.8}Ga_{0.2}As_{0.43}P_{0.57}$	5
6	Barrier	$In_{0.8}Ga_{0.2}As_{0.75}P_{0.25}$	10
7	Well	$In_{0.8}Ga_{0.2}As_{0.43}P_{0.57}$	5
8	Barrier	$In_{0.8}Ga_{0.2}As_{0.75}P_{0.25}$	10
9	Well	$In_{0.8}Ga_{0.2}As_{0.43}P_{0.57}$	5
10	Barrier	$In_{0.8}Ga_{0.2}As_{0.75}P_{0.25}$	10
11	Substrate	InP	∞

This model has many phenomenological parameters that must be fitted. These parameters are from both the gain calculations and rate equations. The parameters needed to fit various aspects of the gain curves are β (band renormalization coefficient) for position of gain maximum, the time constants $\tau_c = 4ps$, $\tau_e = 3ns$, $\tau_t = 8ps$, $\tau_d = \tau_{sd} = 7ps$ of the well equations as well as A(SCH:$3\times10^7/s$, Well:$1\times10^6/s$), C(SCH:0, Well:$1.25\times10^{-41}m^6/s$) and D_{leak} to fit the amplitude. In order to calculate the gain correctly for different currents it is especially important to find appropriate Auger and leakage coefficients. The values chosen for the leakage coefficient correspond to leakage currents of approximately 2.5mA in the SCH region and 0.7mA in the wells. The intrinsic loss term ($\approx 30.0/cmd - 750.0I/(mAcm)$) where I is the injection current is used to get the appropriate offset for the net gain[25]. The B coefficient can be determined by the relationships between the gain, spontaneous emission rate and this coefficient (equations (30) and (33) of [25]).

Figure 5.16 shows the experimental and theoretical total modal gain for this laser. Figures 5.17 and 5.18 show how important the leakage term is to the gain, in figure 5.17 all parameters are kept the same as those used in figure 5.16 except the leakage terms are set to zero. In figure 5.18 the best fit is attempted without using leakage effects.

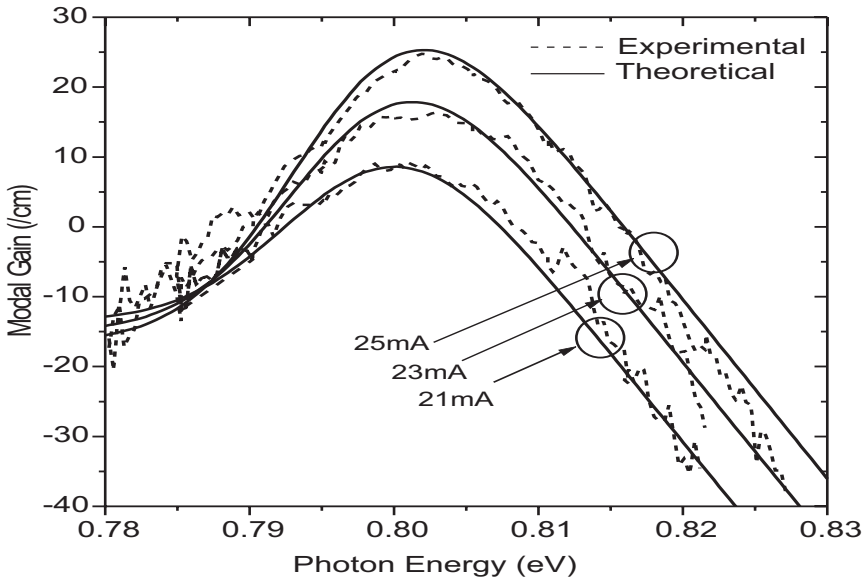

Figure 5.15: Experimental and Theoretically Fitted Modal Gain Versus Photon Energy for Three Injection Currents. All Parameters are Varied (Within Physical Reason) for Best Fit.

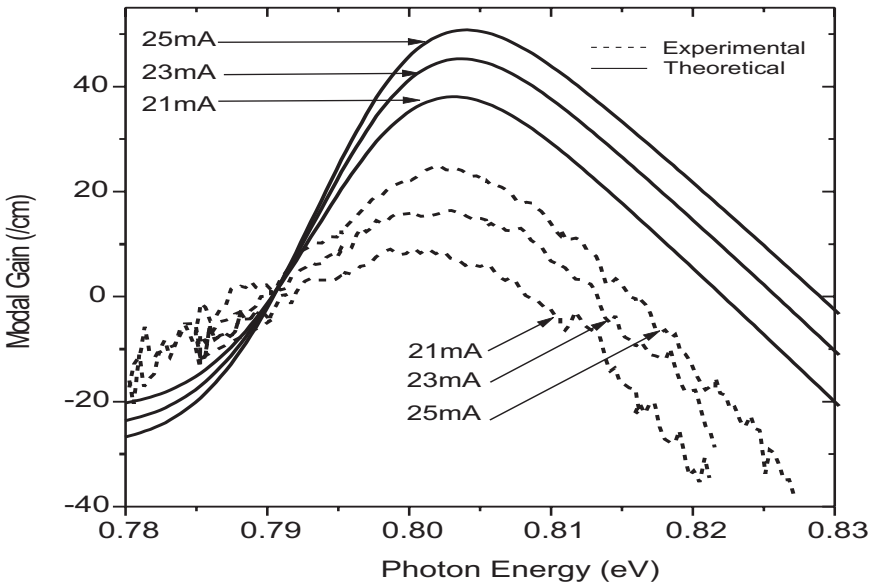

Figure 5.16: Experimental and Theoretically Modal Gain Versus Photon Energy for Three Injection Currents. All Parameters are the Same as Fig 5.15 Except the Leakage has been Ignored.

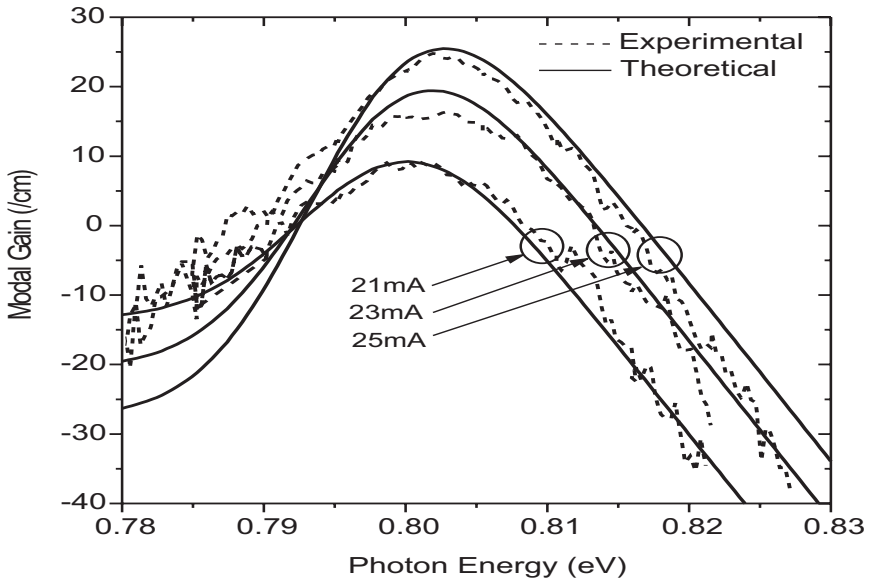

Figure 5.17: Experimental and Theoretical Modal Gain Versus Photon Energy for Three Injection Currents. All Parameters are Varied, Carrier Leakage has been Ignored.

5.5 Modulation Response in the Carrier Heating Model

This model demonstrates how increasing the carrier capture energy ($< E_i^{(c)} >$ in section 4.2) leads to an increase in the temperature of the carriers in the well[67]. If the energy loss time of the carriers (τ_L) is decreased, this will lead to a reduction of the carrier temperatures. Actual values of this are shown in the table below for an injection current of 20mA.

$< E^{(c)} > (eV)$	$\tau_L(ps)$	$AverageTemperature(K)$	$ThresholdCurrent(mA)$
0.13	1	308	2.64
	3	320	2.66
	5	335	2.68
	10	365	2.72
	15	391	2.75
0.026	3	301	2.62
	10	305	2.63

For the higher $< E^{(c)} >$ there is a significant change in the temperature and threshold current dependence of τ_L. For the lower $< E^{(c)} >$ this is not so critical.

The modulation responses for the $< E^{(c)} >$ and τ_L at 20mA are show in figures 5.19 and 5.20 and shows a decreasing modulation response to the increasing temperatures.

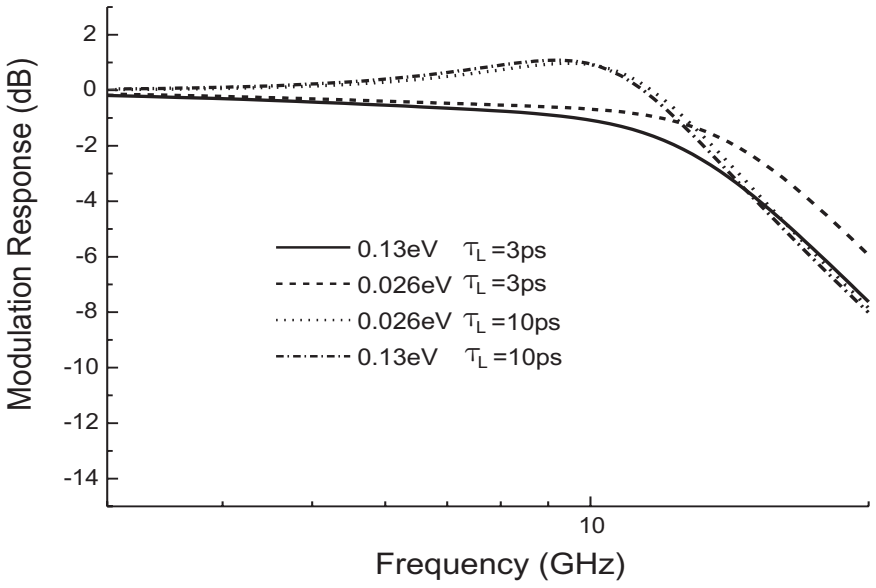

Figure 5.18: Modulation Response Versus Frequency at 20mA Injection Current and Various $< E^{(c)} >$, τ_L. This is found from Small-signal Analysis of the Carrier Heating Model

5.6 Summary

This chapter presents the author's original numerical calculations for spectral and dynamical properties of various lasers and semiconductor optical amplifiers. The rate-equation model of the tunneling injection laser in section 5.2 has a new parameter introduced by the author to describe the fraction of carriers injected into the well by tunneling injection.

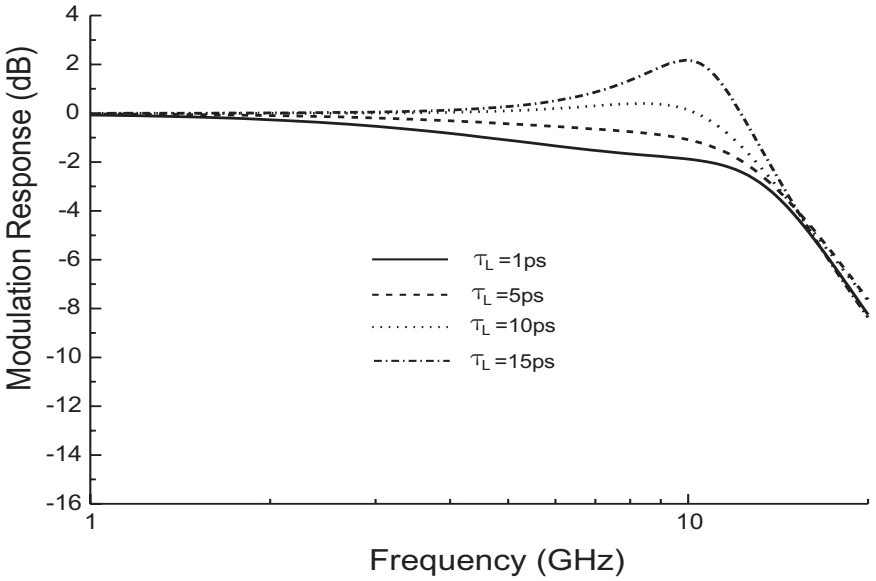

Figure 5.19: Modulation Response Versus Frequency at 20mA Injection Current with $< E^{(c)} >$=0.13eV and various τ_L. This is found from Small-signal Analysis of the Carrier Heating Model.

Part II

Wigner Function Theory

This part will describe the derivation and use of the Wigner functions and quantum Boltzmann equation (QBE) that describe their evolution. Chapter 6 will derive the Wigner functions and the QBE starting from two-particle non-equilibrium Greens functions and Dyson's equations. Chapter 7 discuss the implementation of these equations and a sample calculation using this model.

Chapter 6

Deriving the Quantum Boltzmann Equation

The goal of this chapter is to derive the quantum Boltzmann equations. There are various approaches that can be used to derive them. A common starting point (which is actually simpler than the method to be presented) is density matrix theory and Heisenberg's equation of motion (becomes the Loiuville-von Neuman equation) [29, 43] which can be transformed to the QBEs. This is a convenient method to use if all interactions in the system are "simple" (classical interactions or scattering modeled by Fermi's golden rule). When the interactions become more complicated such as more detailed phonon or Coulombic interactions, the density matrix method is unsatisfying because the new interactions can be difficult to define. In Greens function theory, it is always possible to add in new interactions in a straightforward manner by adding more self-energy terms. The model used in this work is intended to be a general method to derive the QBEs for all types of interactions and we therefore start with the Greens function theory.

6.1 Greens Functions

6.1.1 Real-Time Greens Functions

Physically, the systems being analyzed are clearly not in equilibrium (even if they are in steady-state). A potential is applied across the electrodes which causes carriers to move and recombine. The standard zero-temperature Greens functions are therefore not sufficient for this system. To model a system not in equilibrium, the real-time Greens functions on a Schwinger-Keldysh contour (figure 6.1) are used[27, 68]. The purpose of using this time contour is because in non-equilibrium, it is not possible to define a final state of the system beforehand.

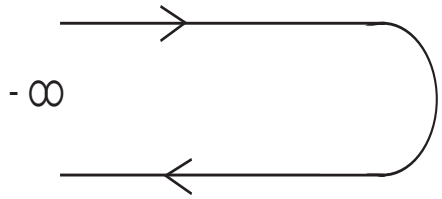

Figure 6.1: A Representation of the Keldysh Time Contour used for Real-Time Greens Functions

The time τ can be set to go to infinity. The cost of using this time contour is the necessity to use more than one Greens function. There are various ways of doing this[27, 30, 32] which are essentially equivalent. The method used here will be to use six Greens functions which are the advanced G^a, retarded G^r, time-ordered G^t, anti time-ordered $G^{\bar{t}}$

and $G^<$ and $G^>$ which have no name. These are defined as

$$\begin{aligned}
G^>(x_1,x_2) &= -\frac{i}{\hbar}\left\langle \hat{\psi}(x_1)\hat{\psi}^+(x_2)\right\rangle \\
G^<(x_1,x_2) &= \frac{i}{\hbar}\left\langle \hat{\psi}^+(x_2)\hat{\psi}(x_1)\right\rangle \\
G^r(x_1,x_2) &= -\frac{i}{\hbar}\Theta(t_1-t_2)\left\langle \hat{\psi}(x_1)\hat{\psi}^+(x_2)\right\rangle \\
G^a(x_1,x_2) &= -\frac{i}{\hbar}\Theta(t_2-t_1)\left\langle \hat{\psi}(x_1)\hat{\psi}^+(x_2)\right\rangle \\
G^t(x_1,x_2) &= \Theta(t_1-t_2)G^>(x_1,x_2)+\Theta(t_2-t_1)G^<(x_1,x_2) \\
G^{\bar{t}}(x_1,x_2) &= \Theta(t_2-t_1)G^>(x_1,x_2)+\Theta(t_1-t_2)G^<(x_1,x_2)
\end{aligned} \tag{6.1}$$

where $x=(\mathbf{r},t)$ and $\hat{\psi}^+(x)$ and $\hat{\psi}(x)$ are the particle creation and annihilation operators.

These Greens functions are defined on different sections of the time contour, four of these are represented in figure 6.2. The other two Greens functions are related by

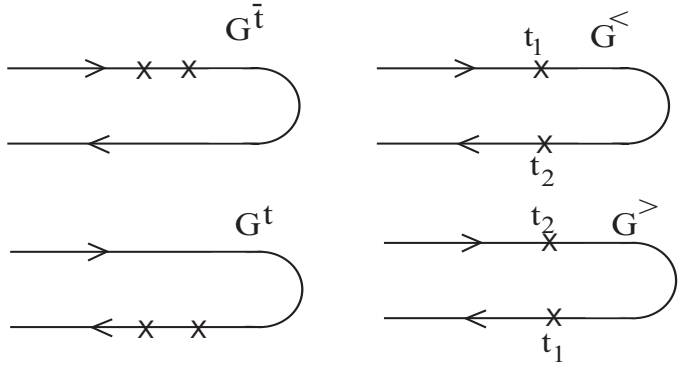

Figure 6.2: The Representation of the Various Real-Time Greens Functions on the Keldysh Time Contour

$$G^r = G^t - G^< = G^> - G^{\bar{t}}\ ,\ G^a = G^t - G^> = G^< - G^{\bar{t}} \tag{6.2}$$

so that the six Greens functions are not mutually independent. It is possible to use less Greens functions, but this set is convenient because the matrix representation of Craig[27, 69]

$$\tilde{G}(x_1,x_2) = \begin{bmatrix} G^t(x_1,x_2) & -G^<(x_1,x_2) \\ G^>(x_1,x_2) & -G^{\bar{t}}(x_1,x_2) \end{bmatrix} \tag{6.3}$$

is formally similar to the zero temperature Dyson's equations and also has a Wick's decomposition (the standard decomposition method to reduce the many-particle Greens functions that arise in the perturbation expansion to a combination of single-particle Greens functions). Once the Dyson equations have been sufficiently defined and simplified for this matrix, G^t and $G^{\bar{t}}$ will be written in terms of $G^<$, $G^>$ and G^r by equation (6.2) because of further simplifications that can be applied in this form.

The Greens function $G^<$ has a special importance as it is the one used to calculate the expectation values of a one-particle operator $(O(x)\hat{\psi}^+(x)\hat{\psi}(x))$ is given by[27, 28]

$$i\int d^3\mathbf{r}_1 \lim_{x_2\to x_1} O(x_1)G^<(x_1,x_2) \tag{6.4}$$

The limit is used in case the operator is not continuous.

6.1.2 Dyson's Equations

In the Greens function method, all interactions can be incorporated by the *self-energies*. They can be used as a basis of a perturbative expansion by choosing the order of self-energies which are included (eg, only keeping the single phonon interaction). For a self-consistent solution, it is actually the *minimum irreducible* self-energies that are used[28] (and only a subset of these are chosen in the Hartree-Fock approximation) but they will just be referred to as the self-energies. The total self-energy is the sum over the self-energies for each type of interaction so that they can be examined separately. It can be shown that the self-energies also have relations like equation (6.2)[27].

These can also be written in Craig's matrix form[27, 69]

$$\tilde{\Sigma}(x_1,x_2) = \begin{bmatrix} \Sigma^t(x_1,x_2) & -\Sigma^<(x_1,x_2) \\ \Sigma^>(x_1,x_2) & -\Sigma^{\bar{t}}(x_1,x_2) \end{bmatrix} \tag{6.5}$$

The perturbation expansion for the real-time Greens functions matrix using these self-energies are Dyson's equations[27, 34]

$$\tilde{G}(x_1,x_2) = \tilde{G}_o(x_1,x_2) + \int dx_3 \int dx_4 \tilde{G}_o(x_1,x_3)\tilde{\Sigma}(x_3,x_4)\tilde{G}(x_4,x_2) \tag{6.6}$$

and

$$\tilde{G}(x_1,x_2) = \tilde{G}_o(x_1,x_2) + \int dx_3 \int dx_4 \tilde{G}(x_1,x_3)\tilde{\Sigma}(x_3,x_4)\tilde{G}_o(x_4,x_2) \tag{6.7}$$

where $\tilde{G}_o$ is the Greens function solution for an unperturbed system. Equations (6.6) and (6.7) could be solved by a massive self-consistency operation. This is not practical. Instead, perform the following steps:

i) Operate on equation (6.6) by $i\hbar\frac{\partial}{\partial t_1} - H_o(\mathbf{r}_1)$ to get

$$\left[i\hbar\frac{\partial}{\partial t_1} - H_o(\mathbf{r}_1)\right]\tilde{G}(x_1,x_2) = \hbar\delta^4(x_1-x_2)\tilde{I} + \hbar\int dx_3\tilde{\Sigma}(x_1,x_3)\tilde{G}(x_3,x_2) \tag{6.8}$$

ii) Operate on equation (6.7) by $-i\hbar\frac{\partial}{\partial t_2} - H_o(\mathbf{r}_2)$ to get

$$\left[-i\hbar\frac{\partial}{\partial t_2} - H_o(\mathbf{r}_2)\right]\tilde{G}(x_1,x_2) = \hbar\delta^4(x_1-x_2)\tilde{I} + \hbar\int dx_3\tilde{G}(x_1,x_3)\tilde{\Sigma}(x_3,x_2) \tag{6.9}$$

iii) Subtract equation (6.9) from (6.8)

$$\left[i\hbar\left(\frac{\partial}{\partial t_1}+\frac{\partial}{\partial t_2}\right) - (H_o(\mathbf{r}_1)-H_o(\mathbf{r}_2))\right]\tilde{G}(x_1,x_2) = \hbar\int dx_3\begin{bmatrix}\tilde{\Sigma}(x_1,x_2)\tilde{G}(x_3,x_2)\\ -\tilde{G}(x_1,x_3)\tilde{\Sigma}(x_3,x_2)\end{bmatrix} \tag{6.10}$$

where $H_o(\mathbf{r})$ is the unperturbed Hamiltonian (which has only $\mathbf{r}$ dependence) and the relation

$$\left[i\hbar\frac{\partial}{\partial t_1} - H_o(x_1)\right]\tilde{G}_o(x_1,x_2) = \left[-i\hbar\frac{\partial}{\partial t_2} - H_o(x_2)\right]\tilde{G}_o(x_1,x_2) = \hbar\delta^4(x_1-x_2)\tilde{I} \tag{6.11}$$

$\tilde{I}$ is the identity matrix in this space. Equation (6.10) is the Dyson equation that is required to solve.

6.1.3 Expansions into the Band Basis

The equations in the previous section will be expanded in terms of the periodic functions in the Bloch basis. The creation and annihilation operators in terms of that for each band are

$$\hat{\psi}^+(x) = \sum_i u_i^*(\mathbf{r})\hat{\psi}_i^+(x)\ ,\ \hat{\psi}(x) = \sum_i u_i(\mathbf{r})\hat{\psi}_i(x) \tag{6.12}$$

where $u_i(\mathbf{r})$ is a normalized function periodic in the unit cell and $\hat{\psi}^+/\hat{\psi}$ is the creation/annihilation operator for an electron in this band. Because of this, the Greens functions can also be

expanded into this basis as

$$\tilde{G}(x_1, x_2) = \sum_{i,j} u_i(\mathbf{r}_1) u_j^*(\mathbf{r}_2) \tilde{G}_{i,j}(x_1, x_2) \tag{6.13}$$

where $\tilde{G}_{i,j}$ can be written with elements similar to equation (6.1) such as

$$G^{>}_{i,j}(x_1, x_2) = -\frac{i}{\hbar} \left\langle \hat{\psi}_i(x_1) \hat{\psi}_j^{+}(x_2) \right\rangle \tag{6.14}$$

The self-energies will also be expanded into this basis as.

$$\hat{\Sigma}(x_1, x_2) = \sum_{i,j} u_i(\mathbf{r}_1) u_j^*(\mathbf{r}_2) \tilde{\Sigma}_{i,j}(x_1, x_2) \tag{6.15}$$

Substituting equations (6.13) and (6.15) into (6.10),

$$\begin{aligned} &\left[i\hbar \left(\frac{\partial}{\partial t_1} + \frac{\partial}{\partial t_2} \right) - (H_o(\mathbf{r}_1) - H_o(\mathbf{r}_2)) \right] \sum_{i',j'} u_{i'}(\mathbf{r}_1) u_{j'}^*(\mathbf{r}_2) \tilde{G}_{i',j'}(x_1, x_2) \\ &= \hbar \int dx_3 \sum_{i',j',i'',j''} \begin{bmatrix} \tilde{\Sigma}_{i',j'}(x_1, x_3) u_{i'}(\mathbf{r}_1) u_{j'}^*(\mathbf{r}_3) \tilde{G}_{i'',j''}(x_3, x_2) u_{i''}(\mathbf{r}_3) u_{j''}^*(\mathbf{r}) \\ -\tilde{G}_{i',j'}(x_1, x_3) u_{i'}(\mathbf{r}_1) u_{j'}^*(\mathbf{r}_3) \tilde{\Sigma}_{i'',j''}(x_3, x_2) u_{i''}(\mathbf{r}_3) u_{j''}^*(\mathbf{r}) \end{bmatrix} \end{aligned} \tag{6.16}$$

It is important to recognize that the Greens functions and self-energies are slowly varying over the distance of the unit cells because of the definitions of the expansions. Therefore multiplying equation (6.16) by $\int_{\Omega} u_i^*(\mathbf{r}_1) u_j(\mathbf{r}_2) d^3\mathbf{r}_1 d^3\mathbf{r}_2 d^3\mathbf{r}_3$ reduces this to

$$\begin{aligned} &\left[i\hbar \left(\frac{\partial}{\partial t_1} + \frac{\partial}{\partial t_2} \right) - (H_i(\mathbf{r}_1) - H_j(\mathbf{r}_2)) \right] \sum_{i',j'} \tilde{G}_{i',j'}(x_1, x_2) \\ &= \hbar \int dx_3 \sum_{j'} \begin{bmatrix} \tilde{\Sigma}_{i,j'}(x_1, x_3) \tilde{G}_{j',j}(x_3, x_2) \\ -\tilde{G}_{i,j'}(x_1, x_3) \tilde{\Sigma}_{j',j}(x_3, x_2) \end{bmatrix} \end{aligned} \tag{6.17}$$

where $H_i(\mathbf{r})$ is the unperturbed energy for the i^{th} band. The effective mass theory implies the relation

$$H_i(\mathbf{r}) = \frac{\hbar^2}{2m_i^*} \nabla_{\mathbf{r}}^2 + V_i(\mathbf{r}) \tag{6.18}$$

where $V_i(\mathbf{r})$ again is the potential profile constructed from the band-gaps and band-offsets of each layer of the structure.

Equation (6.17) is an important form because it allows definitions of Greens functions for different bands. The diagonal ($i = j$) Greens functions can be used to determine the properties of the carriers for the various bands such as the conduction ($i = c$) or valence ($i = v$) band densities. The off-diagonal ($i \neq j$) Greens functions will be shown to be used to determine the polarization functions. Therefore, with equation (6.17) a model of the coupling between carriers and the polarizations can be obtained which will form a basis for modelling the system. These relations will be shown in later sections after the transition to the Wigner function model.

6.1.4 Self-Energies

Dyson's equation in the format used requires the interactions to be expressed in terms of the self-energies. The self-energies used in this thesis are listed here with more detail in the Appendices.

Classical Single Particle Interactions

The classical interaction written in second-quantization form is

$$\hat{V}(x_1, x_2) = V(x_1)\delta^4(x_1 - x_2)\hat{\psi}(x_1)\hat{\psi}^+(x_2) \tag{6.19}$$

where $V(x_1)$ is a general classical interaction potential. The delta function in time is because classical interactions like this are assumed to act instantaneously in time (no retardation effects). In this work, the classical interaction is used to describe both an applied potential bias as well as the electromagnetic interactions. It is also often used to for the heterostructure potential as well[32] instead of incorporating it into H_i as done here.

The general self-energy for any classical single particle interaction is[32]

$$\tilde{\Sigma}(x_1, x_2) = \frac{1}{\hbar}\tilde{I}\delta^4(x_1 - x_2)V(x_1) \tag{6.20}$$

Substituting this into (6.15) results in the classical self-energy

$$\tilde{\Sigma}_{i,j}(x_1, x_2) = \frac{1}{\hbar}\tilde{I}\delta^4(x_1 - x_2)\int_{\Omega} d^3\mathbf{r}_1 u_i^*(\mathbf{r})u_j(\mathbf{r})V(\mathbf{r}_1, t_1) \tag{6.21}$$

Slowly Varying Applied Potential

For a slowly varying applied bias potential $V(x) = V^{app}(x)$, the potential can be moved out of the integral over the unit cell in equation (6.21) to simplify this self-energy to

$$\tilde{\Sigma}^{app}_{i,j}(x_1, x_2) = \frac{1}{\hbar}\tilde{I}\delta(x_1 - x_2)\delta^4_{i,j}V^{app}(\mathbf{r}_1, t_1) \tag{6.22}$$

This slowly varying applied potential includes the applied bias and the modifications of the heterostructure due to electrostatic effects.

Classical Electromagnetic Interaction

The classical electromagnetic interaction is written as $V(x) = -e\mathbf{E}(\mathbf{r}, t)\cdot\mathbf{r}$ where the electric field $\mathbf{E}$ is assumed to be slowly varying. This is a different form than the electromagnetic interaction used in Chapter 3 ($e\mathbf{p}\cdot\mathbf{A}$). In this part it is more convenient to have expressions for $\mathbf{E}$ because of the well-known Greens function expansions of the electric field discussed in section 6.3. Substituting this into equation (6.21) gives

$$\tilde{\Sigma}^{EM}_{i,j} = -\frac{1}{\hbar}\tilde{I}\delta^4(x_1 - x_2)\mathbf{d}_{ij}\cdot\mathbf{E}(\mathbf{r}_1, t_1) \tag{6.23}$$

where $\mathbf{d}_{ij} = e\int d^3\mathbf{r}u^*_i(\mathbf{r})u_j(\mathbf{r})\mathbf{r}$ is the interband polarization. This is the basis of the lasing action and since the system is designed to be operating around the band-gap, it is assumed this is negligible when $i = j$.

Note that since a classical interaction is being used for the electromagnetic field, there will be consequences because the important effect of spontaneous emission cannot be modeled by this. Recall from equation (4.16) the photon output is directly proportional to spontaneous emission. Without it, the lasing action cannot start. It will have to be added *ab initio* in an accurate manner. This is done with the Quantum Langevin equations in a later section.

Phonon Interactions

In this case it is assumed that the phonons are unconfined and are therefore described by plane-waves. The electron phonon interaction in second quantization form is[27, 28]

$$H^{phon}(x_1, x_2) = \delta(x_1 - x_2)\hat{\phi}(x_1)\hat{\psi}^+(x_1)\hat{\psi}(x_2) \tag{6.24}$$

where $\hat{\phi}(x_1)$ is the quantization of the potential that arises from the oscillation in the crystal. This is defined in Appendix D in the Frölich coupling model. The interaction is assumed to be instantaneous (no *phonon drag*). The self-energies in the matrix representation and in the band basis resulting from this interaction are (Appendix D, [27, 34])

$$\tilde{\Sigma}^{phon}_{i,j}(x_1,x_2) = i \begin{bmatrix} G^{t}_{i,j}(x_1,x_2)D^{t}(x_1,x_2) & -G^{<}_{i,j}(x_1,x_2)D^{<}(x_1,x_2) \\ G^{>}_{i,j}(x_1,x_2)D^{>}(x_1,x_2) & -G^{\bar{t}}_{i,j}(x_1,x_2)D^{\bar{t}}(x_1,x_2) \end{bmatrix} \tag{6.25}$$

D^{α} are the phonon Greens functions which, in this notation contain the Frölich coupling coefficients. These phonon Greens functions are for the longitudinal optical type (LO) as all others have weaker interactions with carriers[70]. They are assumed to be in equilibrium because LO phonons quickly equilibrate by decaying into acoustic phonons and propagating away from the active regions. The expressions for D^{α} of use here are shown in the Appendix D.

Coulomb Interaction

The Coulombic interaction is a two-particle interaction expressed in second-quantization form as

$$H^{coul}(x_1,x_2) = \frac{\delta(t_1-t_2)}{2}\int d^3\mathbf{r}_1 d^3\mathbf{r}_2 \hat{\psi}^{+}(x_1)\hat{\psi}^{+}(x_2)V_s(|\mathbf{r}_1-\mathbf{r}_2|)\hat{\psi}(x_2)\hat{\psi}(x_1) \tag{6.26}$$

where $V_s(|\mathbf{r}_1-\mathbf{r}_2|)$ is the scattering-renormalized Coulomb interaction potential $\frac{e^2}{|\mathbf{r}_1-\mathbf{r}_2|\varepsilon_s}$ in the quasi-static Hartree-Fock approximation (also referred to as the random phase approximation). The symbol ε_s is the dielectric constant incorporating scattering effects using the plasmon-pole approximation.

This gives the self energy (Appendix E)

$$\tilde{\Sigma}^{coul}_{i,j}(x_1,x_2) = \begin{bmatrix} C^{t}_{i,j}(x_1,x_2) & 0 \\ 0 & C^{\bar{t}}_{i,j}(x_1,x_2) \end{bmatrix} \tag{6.27}$$

The terms $C^{\alpha}_{i,j}(x_1,x_2)$ are shown in Appendix E.

Dyson's equation

Substituting the self-energy terms of section 6.1.4 into equation (6.17) gives the Dyson equation

$$\begin{aligned}
&\left[i\hbar\left(\frac{\partial}{\partial t_1}+\frac{\partial}{\partial t_2}\right)-(H_i(\mathbf{r}_1)-H_j(\mathbf{r}_2))\right]\tilde{G}_{i,j}(x_1,x_2)\\
&=\sum_{j'}\left[V^{app}_{i,j'}(x_1)\tilde{G}_{j',j}(x_1,x_2)-\tilde{G}_{i,j'}(x_1,x_2)V^{app}_{j',j}(x_2)\right]\\
&-\sum_{j'}\left[\mathbf{d}_{ij'}\cdot\mathbf{E}(x_1)\tilde{G}_{j',j}(x_1,x_2)-\tilde{G}_{i,j'}(x_1,x_2)\mathbf{d}_{j',j}\cdot\mathbf{E}(x_2)\right]\\
&+\hbar\int dx_3\sum\left[\tilde{\Sigma}^{phon}_{i,j'}(x_1,x_3)\tilde{G}_{j',j}(x_3,x_2)-\tilde{G}_{i,j'}(x_1,x_3)\tilde{\Sigma}^{phon}_{j',j}(x_3,x_2)\right]\\
&+\hbar\int dx_3\sum\left[\tilde{\Sigma}^{coul}_{i,j'}(x_1,x_3)\tilde{G}_{j',j}(x_3,x_2)-\tilde{G}_{i,j'}(x_1,x_3)\tilde{\Sigma}^{coul}_{j',j}(x_3,x_2)\right] \qquad (6.28)
\end{aligned}$$

The terms for the phonon and coulomb interactions are not expanded yet here due to their length, they will be shown in greater detail after some approximations and reductions.

6.2 Wigner Functions

In this section the Wigner functions and their corresponding evolution equations will be derived. This is essentially just a change of the independent variables used in the Greens functions, self-energies and Dyson equations and then the application of the Markovian approximation. The Wigner functions are then related to the $^<$ and $^>$ Greens functions by the Kadanoff-Baym Ansatz[30, 35]. The QBE describes the evolution of the Wigner functions and it is derived from the Dyson equations by applying the various variable transformations and approximations.

6.2.1 Change of Variables

The Greens functions and self-energies used so far are of the form $\tilde{H}_{i,j}(x_1,x_2)$ where $\tilde{H}$ represents either $\tilde{G}$ or $\tilde{\Sigma}$. A new set of variables is defined called the *center of mass (CM)*

variables,

$$T = \frac{t_1 + t_2}{2} \ , \ t = t_1 - t_2 \ \Rightarrow t_1 = T + \frac{t}{2} \ , \ t_2 = T - \frac{t}{2} \tag{6.29}$$

$$\mathbf{R} = \frac{\mathbf{r}_1 + \mathbf{r}_2}{2} \ , \ \mathbf{r} = \mathbf{r}_1 - \mathbf{r}_2 \ \Rightarrow \mathbf{r}_1 = \mathbf{R} + \frac{\mathbf{r}}{2} \ , \ \mathbf{r}_2 = \mathbf{R} - \frac{\mathbf{r}}{2} \tag{6.30}$$

The rationale for this is that for a spatially homogeneous system in equilibrium, the time and position dependence is only on t and $\mathbf{r}$. It is therefore a convenient form for the boundary conditions which are approximated being in equilibrium. The Greens functions and self-energies are thus rewritten with this variable dependence as $\tilde{H}_{i,j}(\mathbf{r}, \mathbf{R}, t, T)$. Next, $\tilde{H}$ is Fourier transformed to a function that has independent variables which correspond to phase space in the classical limit. This transformation is known as the Wigner-Weyl transformation and is given by

$$\tilde{H}_{i,j}(\mathbf{k}, \mathbf{R}, T, \omega) = \int \int dt d^3\mathbf{r} \frac{e^{-i(\mathbf{k}\cdot\mathbf{r} - \omega t)}}{(2\pi)^2} \tilde{H}_{i,j}(\mathbf{r}, \mathbf{R}, t, T) \tag{6.31}$$

6.2.2 Kadanoff-Baym Ansatz (KBA)

The set of four coupled Greens functions in the real time model is prohibitive to solve. It is very desirable to reduce the number of Greens functions that are required[35]. To reduce this, recall that the $G^<$ Greens function is the Greens function of most interest here[27, 32]. Thus it will be attempted to find the minimal amount of equations required to determine it. When examining this Greens function it is apparent that the functions of $G^>$, G^t and $G^{\bar{t}}$ are also required. However, equation (6.2) shows that both G^t and $G^{\bar{t}}$ can be written in terms of $G^<$, $G^>$ and G^r. Therefore to solve for $G^<$ it is also necessary to solve for $G^>$ and G^r. The purpose of the KBA is to uncouple this dependence.

For a homogeneous system in equilibrium, the following relations are exact[27],

$$G^<(\mathbf{k}, \omega) = iA(\mathbf{k}, \omega) n_F(\mathbf{k}) \tag{6.32}$$

$$G^>(\mathbf{k}, \omega) = -iA(\mathbf{k}, \omega)[1 - n_F(\mathbf{k})] \tag{6.33}$$

where $n_F(\mathbf{k})$ is the Fermi-Dirac function and $A(\mathbf{k}, \omega) = -2\mathrm{Im}G^r(\mathbf{k}, \omega)$, which is known as the spectral density function.

The KBA is based on the assumption that as interactions and structure are added, the functions become T and $\mathbf{R}$ dependent, but in a way that they are slow as compared to t and $\mathbf{r}$. In general, the relation like equation (6.32) for arbitrary systems would have to be written in the position-time coordinates as

$$G^<(x_1, x_2) = iA(x_1, x_3)f(x_3, x_2) \tag{6.34}$$

Just looking at the time coordinates now for simplicity, equation (6.60) shows that the Wigner-Weyl transformation can be written in the form

$$\int dtdt_3 \frac{e^{i\omega(t+t_3)}}{(2\pi)^{1/2}} A(T + \frac{t_3}{2}, t)B(T - \frac{t}{2}, t_3) \tag{6.35}$$

It is also assumed that the functions will decay in their time-difference coordinates due to equilibrating scatterings in the system. Because they are quickly varying and decaying, this can approximately be written as

$$\int dtdt_3 \frac{e^{i\omega(t+t_3)}}{(2\pi)^{1/2}} A(T, t)B(T, t_3) = (2\pi)^{1/2} A(T, \omega)B(T, \omega) \tag{6.36}$$

This is essentially the Markovian approximation (and the zeroth order gradient expansion to be discussed). A similar relation holds for the position variables. Thus equation (6.34) is approximated in the transformed coordinates as

$$G^<(\mathbf{k}, \mathbf{R}, \omega, T) \approx iA(\mathbf{k}, \mathbf{R}, \omega, T)f(\mathbf{k}, \mathbf{R}, T) \tag{6.37}$$

$$G^>(\mathbf{k}, \mathbf{R}, \omega, T) = -iA(\mathbf{k}, \mathbf{R}, \omega, T)[1 - f(\mathbf{k}, \mathbf{R}, T)] \tag{6.38}$$

The function $f(\mathbf{k}, \mathbf{R}, T)$ is the *Wigner function* which is assumed to have no ω dependence because n_F doesn't. This is the famous KBA[30] and reduces the coupling in the set of equations from $G^<$, $G^>$ and G^r to just f and G^r.

To simplify this even more, it is assumed the retarded Greens function remain relatively unchanged from a homogeneous system in equilibrium and are therefore approximated by their equilibrium values[27, 30]. This assumption changes the spectral broadening slightly which can be compensated for by the inclusion of a scattering time to be discussed.

$$G^{ro}_{i,j}(\mathbf{k}, \omega) = \frac{\delta_{i,j}}{\omega - \frac{\varepsilon_{i,\mathbf{k}}}{\hbar} + i\eta} \tag{6.39}$$

where η is a vanishingly small number to assist in convergence. When this is placed in an integral, complex analysis states that this can be replaced by

$$G^{ro}_{i,j}(\mathbf{k},\omega) = \Pr \frac{\delta_{i,j}}{\omega - \frac{\varepsilon_{i,\mathbf{k}}}{\hbar}} - i\pi\delta(\omega - \frac{\varepsilon_{i,\mathbf{k}}}{\hbar}) \tag{6.40}$$

where Pr denotes the principal value and $\varepsilon_{i,\mathbf{k}}$ is the band's energy (including band-edge).

The KBA ansatz consists of the following approximations when expanded in the band basis[30]

$$G^{<}_{i,j}(\mathbf{k},\mathbf{R},\omega,T) = i\left[G^{ro}_{i,i}(\mathbf{k},\omega)G^{<}_{i,j}(\mathbf{k},\mathbf{R},T) - G^{<}_{i,j}(\mathbf{k},\mathbf{r},T)G^{ro*}_{j,j}(\mathbf{k},\omega)\right] \tag{6.41}$$

$$G^{>}_{i,j}(\mathbf{k},\mathbf{R},\omega,T) = i\left[G^{ro}_{i,i}(\mathbf{k},\omega)G^{>}_{i,j}(\mathbf{k},\mathbf{R},T) - G^{>}_{i,j}(\mathbf{k},\mathbf{R},T)G^{ro*}_{j,j}(\mathbf{k},\omega)\right] \tag{6.42}$$

where

$$G^{>,<}_{i,j}(\mathbf{k},\mathbf{R},T) = \int \frac{d\omega}{2\pi} G^{>,<}_{i,j}(\mathbf{k},\mathbf{R},\omega,T) \tag{6.43}$$

In this case the spectral function is

$$A_{i,j}(\mathbf{k},\omega) = i\left(G^{ro}_{i,i}(\mathbf{k},\omega) - G^{ro*}_{j,j}(\mathbf{k},\omega)\right) \tag{6.44}$$

Note that when i=j, the spectral density becomes $-2\mathrm{Im}(G^{ro}_{i,i}(\mathbf{k},\omega))$ as used previously. From equation (6.2),

$$G^{>}_{i,j}(\mathbf{k},\mathbf{R},\omega,T) = G^{<}_{i,j}(\mathbf{k},\mathbf{R},\omega,T) - iA_{i,j}(\mathbf{k}) \tag{6.45}$$

Multiplying equation (6.45) by $\int \frac{d\omega}{(2\pi)}$ gives

$$G^{>}_{i,j}(\mathbf{k},\mathbf{R},T) = G^{<}_{i,j}(\mathbf{k},\mathbf{R},T) - i \tag{6.46}$$

which is because of the relationship $\int \frac{d\omega}{(2\pi)} A_{i,j}(\mathbf{k},\omega) = 1$ (substitute equation (6.40) into (6.44) and multiply by $\int \frac{d\omega}{(2\pi)}$). The KBA can therefore be written as

$$G^{<}_{i,j}(\mathbf{k},\mathbf{R},\omega,T) \approx iA_{i,j}(\mathbf{k},\omega) f_{i,j}(\mathbf{k},\mathbf{R},T) \tag{6.47}$$

and

$$G^{>}_{i,j}(\mathbf{k},\mathbf{R},\omega,T) \approx iA_{i,j}(\mathbf{k},\omega)\left(f_{i,j}(\mathbf{k},\mathbf{R},T) - 1\right) \tag{6.48}$$

where $f_{i,j}(\mathbf{k},\mathbf{R},T) = -iG^{<}_{i,j}(\mathbf{k},\mathbf{R},T)$ are the Wigner functions in the band basis.

6.2.3 QBE

The QBE is the evolution of the Wigner function as derived from Dyson's equation (6.28) for $G^<$. The following steps are performed to obtain the Wigner functions and the QBE from $G^<$ and Dyson's equations:

1. Isolate the Dyson equation for the $<$ component, write G^t and $G^{\bar{t}}$ in terms of $G^<$, $G^>$ and G^r using equation (6.2).
2. Change to the CM variables of (6.29) and then write the functions in terms of the Wigner-Weyl transformed functions by applying the inverse transformation of equation (6.31).
3. Multiply the Dyson equation by $\int \frac{dtd^3\mathbf{r}}{(2\pi)^2} e^{-i(\mathbf{k}\cdot\mathbf{r}-\omega t)}$ to express this equation completely in the Wigner coordinates.
4. Apply the KBA to write $G^<$ and $G^>$ in terms of f and G^r
5. Assume G^r takes the form of equation (6.39).
6. Multiply the equation by $-\frac{1}{\hbar}\int \frac{d\omega}{2\pi}$. The $-\frac{1}{\hbar}$ is for convenience, $\int \frac{d\omega}{2\pi}$ is the Markovian approximation which will remove the $A_{i,j}(\mathbf{K},\omega)$ terms when there is a linear dependence on this.

Each term in equation (6.28) will be examined to see the effects of the above steps.

LHS

The LHS of equation (6.28) for the $G^<$ term in the CM coordinates is

$$\left[i\hbar\frac{\partial}{\partial T} - \left\{ \begin{array}{c} \left(V_i(\mathbf{R}+\frac{\mathbf{r}}{2}) - \frac{\hbar^2}{2m_i^*}\nabla^2_{\mathbf{R}+\mathbf{r}/2}\right) \\ -\left(V_j(\mathbf{R}-\frac{\mathbf{r}}{2}) - \frac{\hbar^2}{2m_j^*}\nabla^2_{\mathbf{R}-\mathbf{r}/2}\right) \end{array} \right\}\right] G^<_{i,j}(\mathbf{r},\mathbf{R},t,T) \tag{6.49}$$

Which can be written as, after applying steps 2 to 6 and some algebra

$$\left[\frac{\partial}{\partial T} + \frac{i\hbar}{2}\left(\frac{1}{m_i^*}-\frac{1}{m_j^*}\right)\left(\mathbf{k}^2 - \frac{\nabla^2_{\mathbf{R}}}{4}\right) + \frac{\hbar}{2}\left(\frac{1}{m_i^*}+\frac{1}{m_j^*}\right)\mathbf{k}\cdot\nabla_{\mathbf{R}}\right] f_{i,j}(\mathbf{k},\mathbf{R},T)$$
$$+\frac{i}{\hbar(2\pi)^3}\int d^3\mathbf{k}'\left[V_i(\mathbf{k}-\mathbf{k}',\mathbf{R}) - V_j(\mathbf{k}'-\mathbf{k},\mathbf{R})\right] f_{i,j}(\mathbf{k}',\mathbf{R},T) \tag{6.50}$$

where

$$V_i(\mathbf{k},\mathbf{R}) = 2\int d^3\mathbf{R}' e^{-\mathbf{k}\cdot(\mathbf{R}'-\mathbf{R})} V_i(\mathbf{R}') \tag{6.51}$$

For simplicity, this derivation assumes the effective mass is constant. For a spatially varying effective mass, more technical detail is required[71]. The derivation involves some straightforward Fourier transforms and is shown in Appendix F. These terms can be replaced by the varying ones if so desired.

Applied potential

This looks very similar to the heterostructure potential part of the LHS above except the potential now has a time dependence. Applying steps 1 to 5 gives

$$\int d\Omega \frac{e^{i\Omega T}}{(2\pi)^{7/2}} \int d^3\mathbf{k}' \begin{bmatrix} V_i^{app}(\mathbf{k}-\mathbf{k}',\mathbf{R},\Omega) G_{i,j}^{<}(\mathbf{k}',\mathbf{R},\omega-\frac{\Omega}{2},T) \\ -G_{i,j}^{<}(\mathbf{k}',\mathbf{R},\omega+\frac{\Omega}{2},T) V_j^{app}(\mathbf{k}'-\mathbf{k},\mathbf{R},\Omega) \end{bmatrix} \tag{6.52}$$

where

$$V_i^{app}(\mathbf{k},\mathbf{R},\Omega) = \int dT \frac{e^{-i\Omega T}}{(2\pi)^{1/2}} 2\int d^3\mathbf{R}' e^{-\mathbf{k}\cdot(\mathbf{R}'-\mathbf{R})} V_i(\mathbf{R}',T) \tag{6.53}$$

Applying step 6 to this will reduce it to

$$\begin{array}{l} -\int d\Omega e^{i\Omega T} \frac{i}{\hbar(2\pi)^{7/2}} \int d^3\mathbf{k}' \left[V_i^{app}(\mathbf{k}-\mathbf{k}',\mathbf{R},\Omega) - V_j^{app}(\mathbf{k}'-\mathbf{k},\mathbf{R},\Omega)\right] f_{i,j}(\mathbf{k}',\mathbf{R},T) \\ = -\frac{i}{\hbar(2\pi)^3} \int d^3\mathbf{k}' \left[V_i^{app}(\mathbf{k}-\mathbf{k}',\mathbf{R},T) - V_j^{app}(\mathbf{k}'-\mathbf{k},\mathbf{R},T)\right] f_{i,j}(\mathbf{k}',\mathbf{R},T) \end{array} \tag{6.54}$$

Electromagnetic term

Expand the electric field as

$$\mathbf{E}(\mathbf{R},T) = \int d\Omega d^3\mathbf{k} \frac{e^{-i(\Omega T - \mathbf{k}\cdot\mathbf{R})}}{(2\pi)^2} \mathbf{E}(\mathbf{k},\Omega) \tag{6.55}$$

so that steps 1 to 6 will reduce this term to

$$\int d\Omega e^{-i\Omega T} \frac{i}{\hbar(2\pi)^2} \int d^3\mathbf{k}' e^{i\mathbf{k}'\cdot\mathbf{R}} \sum_{j'} \begin{bmatrix} \mathbf{d}_{ij'} \cdot \mathbf{E}(\mathbf{k}',\Omega) f_{j',j}(\mathbf{R},\mathbf{k}-\mathbf{k}'/2,T) \\ -f_{i,j'}(\mathbf{k}+\mathbf{k}'/2,\mathbf{R},T) \mathbf{d}_{j'j} \cdot \mathbf{E}(\mathbf{k}',\Omega) \end{bmatrix} \tag{6.56}$$

It has a similar time dependence to the applied potential term. The $\mathbf{k}'$ variable corresponds to the photon wavenumber. Since photon momentum ($\hbar\mathbf{k}'$) is assumed to be negligible compared to the electron momentum (k conservation again), this can be approximated as

$$\frac{i}{\hbar}\sum_{j'}\left[\mathbf{d}_{ij'}\cdot\mathbf{E}(\mathbf{R},T)f_{j',j}(\mathbf{k},\mathbf{R},T)-f_{i,j'}(\mathbf{k},\mathbf{R},T)\mathbf{d}_{j'j}\cdot\mathbf{E}(\mathbf{R},T)\right] \tag{6.57}$$

Gradient Expansion

The transformation for the phonon and Coulombic terms in Dyson's equations into the QBE is more difficult due to the complicated forms of these self-energies. This means integrals arising from terms like

$$\int\frac{dx}{(2\pi)^2}e^{-i(\mathbf{k}\cdot\mathbf{R}-\omega t)}\int dx_3\tilde{G}(x_1,x_3)\tilde{\Sigma}(x_3,x_2) \tag{6.58}$$

cannot be reduced and so would have to be evaluated numerically. This is very undesirable because of the large amount of time involved. To simplify this, a perturbative method for these terms is used called the *gradient expansion*[27, 32].

Consider first a simpler expression just for the time variables $\int\frac{dt}{(2\pi)^{1/2}}e^{i\omega t}dt_3A(t_1,t_3)B(t_3,t_2)$. In the CM coordinates this is

$$\int dtdt_3\frac{e^{-i\omega t}}{(2\pi)^{1/2}}A(\frac{T+t/2+t_3}{2},T+t/2-t_3)B(\frac{T-t/2+t_3}{2},-T+t/2+t_3) \tag{6.59}$$

Make the replacements $t_3\to t_3-T+t/2$ and then $t\to t+t_3$ to simplify this to

$$\int dtdt_3\frac{e^{i\omega(t+t_3)}}{(2\pi)^{1/2}}A(T+\frac{t_3}{2},t)B(T-\frac{t}{2},t_3) \tag{6.60}$$

Expand this into a Taylor series

$$\int dtdt_3\frac{e^{i\omega(t+t_3)}}{(2\pi)^{1/2}}\sum_{n,m}\frac{1}{2^{n+m}n!m!}\left(t_3\frac{\partial}{\partial T}\right)^n A(T,t)\left(-t\frac{\partial}{\partial T}\right)^m B(T,t) \tag{6.61}$$

and use the Fourier relation

$$\int dtt^ne^{i\omega t}C(t)=\left(-i\frac{\partial}{\partial\omega}\right)^n\int dte^{-i\omega t}C(t) \tag{6.62}$$

to get

$$\sum_{n,m} \frac{1}{2^{n+m} n! m!} \left[\left(\frac{\partial}{\partial \omega} \right)^m \left(\frac{\partial}{\partial T} \right)^n A(T,\omega) \right] \left[\left(-\frac{\partial}{\partial \omega} \right)^n \left(\frac{\partial}{\partial T} \right)^m B(T,\omega) \right] \tag{6.63}$$

There exists a similar method for the position variables except for the sign change in equation (6.62) so that the term

$$\int dx \frac{e^{-i(\mathbf{k}\cdot\mathbf{R}-\omega t)}}{(2\pi)^2} \int dx_3 \sum_{j'} \begin{bmatrix} \tilde{\Sigma}_{i,j'}(x_1,x_3)\tilde{G}_{j',j}(x_3,x_2) \\ -\tilde{G}_{i,j'}(x_1,x_3)\tilde{\Sigma}_{j',j}(x_3,x_2) \end{bmatrix} \tag{6.64}$$

can be written as

$$\sum_{j'} \left[L(\tilde{\Sigma}_{i,j'}(\mathbf{k},\mathbf{R},\omega,T)\tilde{G}_{j',j}(\mathbf{K},\mathbf{R},\omega,T)) - L(\tilde{G}_{i,j'}(\mathbf{k},\mathbf{R},\omega,T)\tilde{\Sigma}_{j',j}(\mathbf{k},\mathbf{R},\omega,T)) \right] \tag{6.65}$$

where

$$L(A(\mathbf{k},\mathbf{R},\omega,T)B(\mathbf{k},\mathbf{R},\omega,T)) = \prod_{\alpha} \sum_{n_\alpha, m_\alpha} \frac{1}{2^{n_\alpha+m_\alpha} n_\alpha! m_\alpha!} \times \tag{6.66}$$

$$\left[\left(a(\alpha) \frac{\partial}{\partial \bar{x}_\alpha} \right)^{m_\alpha} \left(\frac{\partial}{\partial x_\alpha} \right)^{n_\alpha} A(\mathbf{K},\mathbf{R},\omega,T) \right] \left[\left(-a(\alpha) \frac{\partial}{\partial \bar{x}_\alpha} \right)^{n_\alpha} \left(\frac{\partial}{\partial x_\alpha} \right)^{m_\alpha} B(\mathbf{K},\mathbf{R},\omega,T) \right]$$

and $\alpha = 1$ to 4 is an index for the sets of variables $x = \{X, Y, Z, T\}$, $\bar{x} = \{k_x, k_y, k_z, \omega\}$, n_α, m_α are integers from zero to the order of approximation and $a(\alpha) = -1$ for $\alpha = 1, 2, 3$ and 1 for $\alpha = 4$ (to account for the sign difference between the position and time expansions). The function L is a linear function. It is apparent that the zeroth order approximation is simply

$$\sum_{j'} \left[\tilde{\Sigma}_{i,j'}(\mathbf{K},\mathbf{R},\omega,T)\tilde{G}_{j',j}(\mathbf{K},\mathbf{R},\omega,T) - \tilde{G}_{i,j'}(\mathbf{K},\mathbf{R},\omega,T)\tilde{\Sigma}_{j',j}(\mathbf{K},\mathbf{R},\omega,T) \right] \tag{6.67}$$

The zeroth order approximation is equivalent to the Markovian approximation in position and time. This accounts for step 1 to 3 of 6.2.3.

Since it is only required that $G^<$ be solved for in the Dyson equation, only the $<$ component of equation (6.65) is needed. By matrix multiplication, this is

$$\sum_{j'} L \left[\Sigma^t_{i,j'} G^<_{j',j} - \Sigma^<_{i,j'} G^{\bar{t}}_{j',j} - G^t_{i,j'} \Sigma^<_{j',j} + G^<_{i,j'} \Sigma^{\bar{t}}_{j',j} \right] \tag{6.68}$$

This expansion can now be applied to find the phonon and Coulombic terms in the QBE derivation. In all the work following, only the 0th order contributions will be kept (a Markovian approximation).

Phonons

Using the relations of equation (6.25), the phonon terms and applying steps 1 to 3 of the procedure to convert to the QBE, these terms can be written as

$$\hbar(2\pi)^2 \sum_{j'} \left[\begin{array}{c} \Sigma^{phon,<}_{i,j'}(G^{<}_{j',j'} - G^{>}_{j',j'}) - G^{<}_{i,j'}(\Sigma^{phon,<}_{j',j} - \Sigma^{phon,>}_{j',j}) \\ +\Sigma^{phon,r}_{i,j'} G^{<}_{j',j} - G^{<}_{i,j'}\Sigma^{phon,r}_{j',j} + \Sigma^{phon,<}_{i,j'} G^{r}_{j',j} - G^{r}_{i,j'}\Sigma^{phon,<}_{j',j} \end{array} \right] \tag{6.69}$$

where each Greens function and self-energy is in the Wigner coordinates $(\mathbf{k}, \mathbf{R}, \omega, T)$. The self-energies for phonons in the Wigner coordinates are shown in Appendix D. Applying steps 4 to 6 on equation (6.69) results in the phonon contribution to the QBE as

$$-\int d^3_{\mathbf{q}} \left\{ \sum_{j'} \left(\begin{array}{c} \left[Z^{i,j'}_{j',j}(\mathbf{k},\mathbf{q},\omega_L) f_{i,j'}(\mathbf{k},\mathbf{R},T) - f_{i,j'}(\mathbf{q},\mathbf{R},T) Z^{i,j'}_{j',j}(\mathbf{q},\mathbf{k},\omega_L) \right] \\ +i \sum_{\nu=\pm 1} \left[\begin{array}{c} \nu B(j,\mathbf{k},i,\mathbf{q},\nu\omega_L) f_{i,j'}(\mathbf{q},\mathbf{R},T) f_{j',j}(\mathbf{k},\mathbf{R},T) \\ -\nu B(j,\mathbf{q},i,\mathbf{k},\nu\omega_L) f_{i,j'}(\mathbf{k},\mathbf{R},T) f_{j',j}(\mathbf{q},\mathbf{R},T) \end{array} \right] \end{array} \right) \right\} \tag{6.70}$$

Coulombic Interactions

Using equation (6.68) and the Coulombic self-energy of (E.7), the $<$ component of the Dyson equation can be written as

$$\sum_{j'} \left[C^{t}_{i,j'} G^{<}_{j',j} + G^{<}_{i,j'} C^{\bar{t}}_{j',j} \right] \tag{6.71}$$

Where $C^{\alpha}_{i,j}$ is defined in Appendix E. Applying steps 1 to 6 gives the QBE contribution of this term as

$$\frac{i}{\hbar} \sum_{j'} \int d^3\mathbf{k}' V_{s,\mathbf{k}-\mathbf{k}'} \left\{ \begin{array}{c} f_{i,j'}(\mathbf{k},\mathbf{R},T) f_{j',j}(\mathbf{k}',\mathbf{R},T) - f_{i,j'}(\mathbf{k}',\mathbf{R},T) f_{j',j}(\mathbf{k},\mathbf{R},T) \\ -f_{i,j\neq i}(\mathbf{k},\mathbf{R},T) \end{array} \right\} \tag{6.72}$$

where $V_{s,\mathbf{k}-\mathbf{k}'}$ is defined in Appendix E.

QBE

Putting all these components together gives the QBE

$$\begin{aligned}
&\left[\frac{\partial}{\partial T}+\frac{i\hbar}{2}\left[\frac{1}{m^{*-}_{i,j}}\left(k^2-\frac{\nabla^2_{\mathbf{R}}}{4}\right)-\frac{i}{m^{*+}_{i,j}}\mathbf{k}\cdot\nabla_{\mathbf{R}}\right]\right]f_{i,j}(\mathbf{k},\mathbf{R},T)\\
&=\int\frac{d^3\mathbf{k}'}{i\hbar(2\pi)^3}\left(V_i(\mathbf{k}-\mathbf{k}',\mathbf{R})-V_i(\mathbf{k}'-\mathbf{k},\mathbf{R})\right)f_{i,j}(\mathbf{k}',\mathbf{R},T)\\
&+\int\frac{d^3\mathbf{k}'}{i\hbar(2\pi)^3}\left[V^{app}_i(\mathbf{k}-\mathbf{k}',\mathbf{R},T)-V^{app}_i(\mathbf{k}'-\mathbf{k},\mathbf{R},T)\right]f_{i,j}(\mathbf{k}',\mathbf{R},T)\\
&+\frac{i}{\hbar}\sum_{j'}\left[\mathbf{d}_{ij'}\cdot\mathbf{E}(\mathbf{R},T)f_{j',j}(\mathbf{k},\mathbf{R},T)-f_{i,j'}(\mathbf{k},\mathbf{R},T)\mathbf{d}_{j'j}\cdot\mathbf{E}(\mathbf{R},T)\right]\\
&-\int d^3_{\mathbf{q}}\left\{\sum_{j'}\left(\begin{array}{c}\left[Z^{i,j'}_{j',j}(\mathbf{k},\mathbf{q},\omega_L)f_{i,j'}(\mathbf{k},\mathbf{R},T)-f_{i,j'}(\mathbf{q},\mathbf{R},T)Z^{i,j'}_{j',j}(\mathbf{q},\mathbf{k},\omega_L)\right]\\+i\sum\limits_{\nu=\pm1}\left[\begin{array}{c}\nu B(j,\mathbf{k},i,\mathbf{q},\nu\omega_L)f_{i,j'}(\mathbf{q},\mathbf{R},T)f_{j',j}(\mathbf{k},\mathbf{R},T)\\-\nu B(j,\mathbf{k},i,\mathbf{q},\nu\omega_L)f_{i,j'}(\mathbf{k},\mathbf{R},T)f_{j',j}(\mathbf{q},\mathbf{R},T)\end{array}\right]\end{array}\right)\right\}\\
&+\frac{i}{\hbar}\sum_{j'}\int d^3\mathbf{k}'V_{s,\mathbf{k}-\mathbf{k}'}\left\{\begin{array}{c}f_{i,j'}(\mathbf{k},\mathbf{R},T)f_{j',j}(\mathbf{k}',\mathbf{R},T)-f_{i,j'}(\mathbf{k}',\mathbf{R},T)f_{j',j}(\mathbf{k},\mathbf{R},T)\\-f_{i,j\neq i}(\mathbf{k},\mathbf{R},T)\end{array}\right\}
\end{aligned}\tag{6.73}$$

where $\frac{1}{m^{*\pm}}{}_{i,j}=\left(\frac{1}{m^*_i}\pm\frac{1}{m^*_j}\right)$

From now on, the applied potential and heterostructure potential terms will be combined into a single classical potential term $V^t_i(\mathbf{k},\mathbf{R},T)=V_i(\mathbf{k},\mathbf{R})+V^{app}_i(\mathbf{k},\mathbf{R},T)$

6.2.4 Rotating Wave Approximation

The rotating wave approximation is a common technique used to separate the quickly and slowly varying functions in time T[72]. This idea has been seen already in chapter 3 when the slowly varying quantities were used. Examining equation (6.73), it is apparent that if there are no external interactions except for a constant band-gap from the heterostructure term, the equation for $f_{i,j}$ can be written as

$$\left[i\hbar\frac{\partial}{\partial T}-(\epsilon_{i,\mathbf{k}}-\epsilon_{j,\mathbf{k}})-\varepsilon_{ij}\right]f_{i,j}(\mathbf{k},T)=0\tag{6.74}$$

where kinetic energy is represented by $\epsilon_{i,\mathbf{k}}$ and the constant band-gap by ε_{ij}. Equation (6.74) has the solution

$$f_{i,j}(\mathbf{k},T) = f_{i,j}(\mathbf{k},0)e^{-\frac{i}{\hbar}(\epsilon_{i,\mathbf{k}}-\epsilon_{j,\mathbf{k}}+\varepsilon_{ij})T} \tag{6.75}$$

Note that, although the oscillating part of equation (6.75) is dependent on momentum, the most significant factor comes from the band-gap component because $\epsilon_{i,\mathbf{k}} - \epsilon_{j,\mathbf{k}} << \varepsilon_{ij}$. Therefore the off-diagonal components will be considered quickly varying and the diagonal components will be relatively slowly varying.

When interactions are incorporated into the system, the Wigner functions will change, but they will still oscillate close to the resonance frequency $\Omega_{i,j}^{res} = \frac{\varepsilon_{ij}}{\hbar} + \delta\Omega$. where $\delta\Omega$ is a small additional term added for reasons discussed below. Therefore the general solution of (6.73) can be approximated as

$$f_{i,j}(\mathbf{k},\mathbf{R},T) \approx \tilde{f}_{i,j}(\mathbf{k},\mathbf{R},T)e^{-i\Omega_{i,j}^{res}T} \tag{6.76}$$

where $\tilde{f}_{i,j}$ is the slow moving component. The diagonal components have $f_{ii} \approx \tilde{f}_{ii}$ because they are already slowly varying.

Assume that the device to be simulated will be operating around a single optical frequency Ω_{op}. In practice, the laser will be designed so that it's operating frequency will be at maximum gain. This means it will be very close to (but not exactly at) the band-gap frequency as was seen in Chapter 3. The exact frequency of the oscillation is the aforementioned resonance frequency between the conduction and valence band ($\Omega_{op} = \Omega_{c,v}^{res}$). The electric field can then be separated into slow and fast varying components

$$\mathbf{E}(\mathbf{R},T) \approx \mathbf{E}^{+}(\mathbf{R},T)e^{-i\Omega_{op}T} + \mathbf{E}^{-}(\mathbf{R},T)e^{i\Omega_{op}T} \tag{6.77}$$

Therefore, the Wigner functions will be of the form

$$f_{c,v}(\mathbf{k},\mathbf{R},T) \approx \tilde{f}_{c,v}(\mathbf{k},\mathbf{R},T)e^{-i\Omega_{op}T} \ , \ f_{v,c}(\mathbf{k},\mathbf{R},T) \approx \tilde{f}_{v,c}(\mathbf{k},\mathbf{R},T)e^{i\Omega_{op}T} \ , \ f_{i,i} \approx \tilde{f}_{i,i} \tag{6.78}$$

The approximations of equations (6.77) and (6.78) are substituted into equation (6.73) and analyzed for each combination of i,j.

For the i=j=c term this is

$$
\begin{aligned}
&\left[\frac{\partial}{\partial T}+\frac{\hbar}{m_c^*}\mathbf{K}\cdot\nabla_{\mathbf{R}}\right]f_{c,c}(\mathbf{k},\mathbf{R},T)\\
&=\int\frac{d^3\mathbf{k}'}{i\hbar(2\pi)^3}\left(V_c^t(\mathbf{k}-\mathbf{k}',\mathbf{R})-V_c^t(\mathbf{k}'-\mathbf{k},\mathbf{R})\right)f_{c,c}(\mathbf{k}',\mathbf{R},T) \qquad (6.79)\\
&+\frac{i}{\hbar}\left[\begin{array}{c} f_{v,c}(\mathbf{k},\mathbf{R},T)e^{i\Omega_{op}T}\mathbf{d}_{cv}\cdot\left(\mathbf{E}^+(\mathbf{R},T)e^{-i\Omega_{op}T}+\mathbf{E}^-(\mathbf{R},T)e^{i\Omega_{op}T}\right)\\ -f_{c,v}(\mathbf{k},\mathbf{R},T)e^{-i\Omega_{op}T}\mathbf{d}_{vc}\cdot\left(\mathbf{E}^+(\mathbf{R},T)e^{-i\Omega_{op}T}+\mathbf{E}^-(\mathbf{R},T)e^{i\Omega_{op}T}\right)\end{array}\right]\\
&-\int d^3\mathbf{q}\left\{\begin{array}{c}\left[\begin{array}{l} Z_{c,c}^{c,c}(\mathbf{k},\mathbf{q},\omega_L)f_{c,c}(\mathbf{k},\mathbf{R},T)-f_{c,c}(\mathbf{q},\mathbf{R},T)Z_{c,c}^{c,c}(\mathbf{q},\mathbf{k},\omega_L)\\ +Z_{v,c}^{c,v}(\mathbf{k},\mathbf{q},\omega_L)f_{c,v}(\mathbf{k},\mathbf{R},T)e^{-i\Omega_{op}T}\\ -f_{c,v}(\mathbf{q},\mathbf{R},T)e^{-i\Omega_{op}T}Z_{v,c}^{c,v}(\mathbf{q},\mathbf{k},\omega_L)\end{array}\right]\\ +i\sum\limits_{\nu=\pm1}\left[\begin{array}{c}\nu\left(B(c,\mathbf{k},c,\mathbf{q},\nu\omega_L)-B^*(c,\mathbf{k},c,\mathbf{q},\nu\omega_L)\right)\\ \times f_{c,c}(\mathbf{q},\mathbf{R},T)f_{c,c}(\mathbf{k},\mathbf{R},T)\\ +\nu B(c,\mathbf{k},c,\mathbf{q},\nu\omega_L)f_{c,v}(\mathbf{q},\mathbf{R},T)f_{v,c}(\mathbf{k},\mathbf{R},T)\\ -\nu B^*(c,\mathbf{k},c,\mathbf{q},\nu\omega_L)f_{c,v}(\mathbf{k},\mathbf{R},T)f_{v,c}(\mathbf{q},\mathbf{R},T)\end{array}\right]\end{array}\right\}\\
&+\frac{i}{\hbar}\int d^3\mathbf{k}'V_{s,\mathbf{k}-\mathbf{k}'}\left\{\begin{array}{c} f_{c,v}(\mathbf{k},\mathbf{R},T)f_{v,c}(\mathbf{k}',\mathbf{R},T)-f_{c,v}(\mathbf{k}',\mathbf{R},T)f_{v,c}(\mathbf{k},\mathbf{R},T)\\ -f_{c,v}(\mathbf{k},\mathbf{R},T)\end{array}\right\}
\end{aligned}
$$

Equation (6.79) is multiplied by $\int\limits_{T-\tau}^{T+\tau}dT'$ where $\tau=\frac{2\pi}{\Omega_{op}}$. The slowly varying components have negligible change over this time, while any components with terms of $e^{n\Omega_{op}T}$, $n=\pm1\ ,\ \pm2...$ will average to zero. This is the rotating wave approximation and gives the simplification

$$
\begin{aligned}
&\left[\frac{\partial}{\partial T}+\frac{\hbar}{m_c^*}\mathbf{k}\cdot\nabla_{\mathbf{R}}\right]f_{c,c}(\mathbf{k},\mathbf{R},T)\\
&=\int\frac{d^3\mathbf{k}'}{i\hbar(2\pi)^3}\left(V_c^t(\mathbf{k}-\mathbf{k}',\mathbf{R})-V_c^t(\mathbf{k}'-\mathbf{k},\mathbf{R})\right)f_{c,c}(\mathbf{k}',\mathbf{R},T)\\
&+\frac{i}{\hbar}\left[f_{v,c}(\mathbf{k},\mathbf{R},T)\mathbf{d}_{cv}\cdot\mathbf{E}^+(\mathbf{R},T)-f_{c,v}(\mathbf{k},\mathbf{R},T)\mathbf{d}_{vc}\cdot\mathbf{E}^-(\mathbf{R},T)\right]\\
&-\int d^3\mathbf{q}\left\{\begin{array}{c}\left[Z_{c,c}^{c,c}(\mathbf{k},\mathbf{q},\omega_L)f_{c,c}(\mathbf{k},\mathbf{R},T)-f_{c,c}(\mathbf{q},\mathbf{R},T)Z_{c,c}^{c,c}(\mathbf{q},\mathbf{k},\omega_L)\right]\\ +i\sum\limits_{\nu=\pm1}\left[\begin{array}{c}\nu\left(B(c,\mathbf{k},c,\mathbf{q},\nu\omega_L)-B^*(c,\mathbf{k},c,\mathbf{q},\nu\omega_L)\right)\\ \times f_{c,c}(\mathbf{q},\mathbf{R},T)f_{c,c}(\mathbf{k},\mathbf{R},T)\\ +\nu B(c,\mathbf{k},c,\mathbf{q},\nu\omega_L)f_{c,v}(\mathbf{q},\mathbf{R},T)f_{v,c}(\mathbf{k},\mathbf{R},T)\\ -\nu B^*(c,\mathbf{k},c,\mathbf{q},\nu\omega_L)f_{c,v}(\mathbf{k},\mathbf{R},T)f_{v,c}(\mathbf{q},\mathbf{R},T)\end{array}\right]\end{array}\right\}\\
&+\frac{i}{\hbar}\int d^3\mathbf{k}'V_{s,\mathbf{k}-\mathbf{k}'}\left\{f_{c,v}(\mathbf{k},\mathbf{R},T)f_{v,c}(\mathbf{k}',\mathbf{R},T)-f_{c,v}(\mathbf{k}',\mathbf{R},T)f_{v,c}(\mathbf{k},\mathbf{R},T)\right\}
\end{aligned}
\tag{6.80}
$$

It has been assumed that the time dependence of the applied potential is slow compared τ. The term $\frac{1}{\hbar}\mathbf{d}_{cv}\cdot\mathbf{E}^+(\mathbf{R},T)$ is commonly referred to as the Rabi frequency.

Similarly, i=j=v is

$$
\begin{aligned}
&\left[\frac{\partial}{\partial T}+\frac{\hbar}{m_v^*}\mathbf{k}\cdot\nabla_{\mathbf{R}}\right]f_{v,v}(\mathbf{k},\mathbf{R},T)\\
&=\int\frac{d^3\mathbf{k}'}{i\hbar(2\pi)^3}\left(V_v^t(\mathbf{k}-\mathbf{k}',\mathbf{R})-V_v^t(\mathbf{k}'-\mathbf{k},\mathbf{R})\right)f_{v,v}(\mathbf{k}',\mathbf{R},T)\\
&+\frac{i}{\hbar}\left[f_{c,v}(\mathbf{k},\mathbf{R},T)\mathbf{d}_{vc}\cdot\mathbf{E}^-(\mathbf{R},T)-f_{v,c}(\mathbf{k},\mathbf{R},T)\mathbf{d}_{cv}\cdot\mathbf{E}^+(\mathbf{R},T)\right]\\
&-\int d^3\mathbf{q}\left\{\begin{array}{c}\left[Z_{v,v}^{v,v}(\mathbf{k},\mathbf{q},\omega_L)f_{v,v}(\mathbf{k},\mathbf{R},T)-f_{v,v}(\mathbf{q},\mathbf{R},T)Z_{v,v}^{v,v}(\mathbf{q},\mathbf{k},\omega_L)\right]\\ +i\sum\limits_{\nu=\pm1}\left[\begin{array}{c}\nu\left(B(v,\mathbf{k},v,\mathbf{q},\nu\omega_L)-B^*(v,\mathbf{k},v,\mathbf{q},\nu\omega_L)\right)\\ \times f_{v,v}(\mathbf{q},\mathbf{R},T)f_{v,v}(\mathbf{k},\mathbf{R},T)\\ +\nu B(v,\mathbf{k},v,\mathbf{q},\nu\omega_L)f_{v,c}(\mathbf{q},\mathbf{R},T)f_{c,v}(\mathbf{k},\mathbf{R},T)\\ -\nu B^*(v,\mathbf{k},v,\mathbf{q},\nu\omega_L)f_{v,c}(\mathbf{k},\mathbf{R},T)f_{c,v}(\mathbf{q},\mathbf{R},T)\end{array}\right]\end{array}\right\}\\
&+\frac{i}{\hbar}\int d^3\mathbf{k}'V_{s,\mathbf{k}-\mathbf{k}'}\left\{f_{v,c}(\mathbf{k},\mathbf{R},T)f_{c,v}(\mathbf{k}',\mathbf{R},T)-f_{v,c}(\mathbf{k}',\mathbf{R},T)f_{c,v}(\mathbf{k},\mathbf{R},T)\right\}
\end{aligned}
\tag{6.81}
$$

For the i=c, j=v term, substitute the expansions of (6.78) into (6.73) again, cancel out a factor of $e^{-i\Omega_{op}T}$ and then make the rotating wave approximation,

$$
\begin{aligned}
&\left[\frac{\partial}{\partial T} - i\Omega_{op} + \frac{\hbar}{2}\left[\frac{i}{m^{*-}_{c,v}}\left(k^2 - \frac{\nabla^2_{\mathbf{R}}}{4}\right) + \frac{1}{m^{*+}_{c,v}}\mathbf{k}\cdot\nabla_{\mathbf{R}}\right]\right] f_{c,v}(\mathbf{k},\mathbf{R},T) \\
&= \int \frac{d^3\mathbf{k}'}{i\hbar(2\pi)^3}\left(V^t_c(\mathbf{k}-\mathbf{k}',\mathbf{R}) - V^t_v(\mathbf{k}'-\mathbf{k},\mathbf{R})\right) f_{c,v}(\mathbf{k}',\mathbf{R},T) \qquad (6.82)\\
&+\frac{i}{\hbar}\mathbf{d}_{cv}\cdot\mathbf{E}^+(\mathbf{R},T)\left(f_{v,v}(\mathbf{k},\mathbf{R},T) - f_{c,c}(\mathbf{k},\mathbf{R},T)\right) \\
&-\int d^3\mathbf{q}\left\{\begin{array}{l}\left[\ Z^{c,v}_{v,v}(\mathbf{k},\mathbf{q},\omega_L)f_{c,v}(\mathbf{k},\mathbf{R},T) - f_{c,v}(\mathbf{q},\mathbf{R},T)Z^{c,v}_{v,v}(\mathbf{q},\mathbf{k},\omega_L)\ \right] \\ +i\sum\limits_{\nu=\pm1}\left[\begin{array}{c}\nu B(v,\mathbf{k},c,\mathbf{q},\nu\omega_L)\begin{pmatrix} f_{c,c}(\mathbf{q},\mathbf{R},T)f_{c,v}(\mathbf{k},\mathbf{R},T) \\ -f_{c,v}(\mathbf{q},\mathbf{R},T)f_{v,v}(\mathbf{k},\mathbf{R},T)\end{pmatrix} \\ -\nu B(v,\mathbf{q},c,\mathbf{k},\nu\omega_L)\begin{pmatrix} f_{c,c}(\mathbf{k},\mathbf{R},T)f_{c,v}(\mathbf{q},\mathbf{R},T) \\ -f_{c,v}(\mathbf{k},\mathbf{R},T)f_{v,v}(\mathbf{q},\mathbf{R},T)\end{pmatrix}\end{array}\right]\end{array}\right\} \\
&+\frac{i}{\hbar}\int d^3\mathbf{k}' V_{s,\mathbf{k}-\mathbf{k}'}\left\{\begin{array}{l} f_{c,v}(\mathbf{k},\mathbf{R},T)\left(f_{v,v}(\mathbf{k}',\mathbf{R},T) - f_{c,c}(\mathbf{k}',\mathbf{R},T) - 1\right) \\ +f_{c,v}(\mathbf{k}',\mathbf{R},T)\left(f_{c,c}(\mathbf{k},\mathbf{R},T) - f_{v,v}(\mathbf{k},\mathbf{R},T)\right)\end{array}\right\}
\end{aligned}
$$

Similarly i=v, j=c is

$$
\begin{aligned}
&\left[\frac{\partial}{\partial T} + i\Omega_{op} + \frac{i\hbar}{2}\left[\frac{1}{m^{*-}_{v,c}}\left(k^2 - \frac{\nabla^2_{\mathbf{R}}}{4}\right) - \frac{i}{m^{*+}_{v,c}}\mathbf{k}\cdot\nabla_{\mathbf{R}}\right]\right] f_{v,c}(\mathbf{k},\mathbf{R},T) \\
&= \int \frac{d^3\mathbf{k}'}{i\hbar(2\pi)^3}\left(V^t_v(\mathbf{k}-\mathbf{k}',\mathbf{R}) - V^t_c(\mathbf{k}'-\mathbf{k},\mathbf{R})\right) f_{v,c}(\mathbf{k}',\mathbf{R},T) \qquad (6.83)\\
&+\frac{i}{\hbar}\mathbf{d}_{vc}\cdot\mathbf{E}^-(\mathbf{R},T)\left(f_{c,c}(\mathbf{K},\mathbf{R},T) - f_{v,v}(\mathbf{k},\mathbf{R},T)\right) \\
&-\int d^3\mathbf{q}\left\{\begin{array}{l}\left[\ Z^{v,c}_{c,c}(\mathbf{k},\mathbf{q},\omega_L)f_{v,c}(\mathbf{k},\mathbf{R},T) - f_{v,c}(\mathbf{q},\mathbf{R},T)Z^{v,c}_{c,c}(\mathbf{q},\mathbf{k},\omega_L)\ \right] \\ +i\sum\limits_{\nu=\pm1}\left[\begin{array}{c}\nu B(c,\mathbf{k},v,\mathbf{q},\nu\omega_L)\begin{pmatrix} f_{v,v}(\mathbf{q},\mathbf{R},T)f_{v,c}(\mathbf{k},\mathbf{R},T) \\ -f_{v,c}(\mathbf{q},\mathbf{R},T)f_{c,c}(\mathbf{k},\mathbf{R},T)\end{pmatrix} \\ -\nu B(c,\mathbf{q},v,\mathbf{k},\nu\omega_L)\begin{pmatrix} f_{v,v}(\mathbf{k},\mathbf{R},T)f_{v,c}(\mathbf{q},\mathbf{R},T) \\ -f_{v,c}(\mathbf{k},\mathbf{R},T)f_{c,c}(\mathbf{q},\mathbf{R},T)\end{pmatrix}\end{array}\right]\end{array}\right\} \\
&+\frac{i}{\hbar}\int d^3\mathbf{k}' V_{s,\mathbf{k}-\mathbf{k}'}\left\{\begin{array}{l} f_{v,c}(\mathbf{k},\mathbf{R},T)\left(f_{c,c}(\mathbf{k}',\mathbf{R},T) - f_{v,v}(\mathbf{k}',\mathbf{R},T) + 1\right) \\ +f_{v,c}(\mathbf{k}',\mathbf{R},T)\left(f_{v,v}(\mathbf{k},\mathbf{R},T) - f_{c,c}(\mathbf{k},\mathbf{R},T)\right)\end{array}\right\}
\end{aligned}
$$

An extra manipulation had to be made to arrive at the +1 term on the second last line of equation (6.83). This follows the argument of Schäfer and Truesch, and Binder and

Koch[30, 73] where any zero-excitation effects due to the coulomb interaction (non-zero terms for the coulombic contribution when $f_{cc} = 0$ and $f_{vv} = 1$) have to be subtracted because they are already included in the effective mass of the Hamiltonian.

Additional Comments

All remaining phonon terms in the off-diagonal equations are of the form

$$B(c,\mathbf{k},v,\mathbf{k}',\nu\omega_L) \propto \frac{1}{\nu\omega_L + \frac{\varepsilon_{cv}}{\hbar} + \frac{\hbar}{2}\left(\frac{k^2}{m_c} - \frac{k'^2}{m_v}\right) + i\xi} \tag{6.84}$$

or the conjugate. Since $\varepsilon_{cv} >> \hbar\omega_L$, these terms will be small and hence they will from now on be neglected.

Since the electric field being considered is classical, the relation $E^{(+)} = E^{(-)*}$ is true. It can then be shown that $f_{vc} = f^*_{cv}$ by applying the complex conjugate to equation (6.82) to show that f^*_{cv} satisfies equation (6.83) as well. Therefore, from now on f_{vc} will be replaced by f^*_{cv} and equation (6.83) will be neglected.

The coulombic terms are often incorporated into the evolution equations as renormalization terms. That is, the QBE's are rewritten as

$$\begin{aligned}
&\left[\frac{\partial}{\partial T} + \frac{\hbar}{m^*_c}\mathbf{k}\cdot\nabla_{\mathbf{R}}\right] f_{c,c}(\mathbf{k},\mathbf{R},T) \\
&= \int \frac{d^3\mathbf{k}'}{i\hbar(2\pi)^3}\left(V^t_c(\mathbf{k}-\mathbf{k}',\mathbf{R}) - V^t_c(\mathbf{k}'-\mathbf{k},\mathbf{R})\right) f_{c,c}(\mathbf{k}',\mathbf{R},T) \\
&+i\left[f^*_{c,v}(\mathbf{k},\mathbf{R},T)\Omega^+_R(\mathbf{k},\mathbf{R},T) - f_{c,v}(\mathbf{k},\mathbf{R},T)\Omega^{+*}_R(\mathbf{k},\mathbf{R},T)\right] \\
&- \int d^3\mathbf{q}\left\{\begin{array}{l}
\left[Z^{c,c}_{c,c}(\mathbf{k},\mathbf{q},\omega_L)f_{c,c}(\mathbf{k},\mathbf{R},T) - f_{c,c}(\mathbf{q},\mathbf{R},T)Z^{c,c}_{c,c}(\mathbf{q},\mathbf{k},\omega_L)\right] \\
+i\sum\limits_{\nu=\pm 1}\left[\begin{array}{c}
\nu\left(B(c,\mathbf{k},c,\mathbf{q},\nu\omega_L) - B^*(c,\mathbf{k},c,\mathbf{q},\nu\omega_L)\right) \\
\times f_{c,c}(\mathbf{q},\mathbf{R},T)f_{c,c}(\mathbf{k},\mathbf{R},T) \\
+\nu B(c,\mathbf{k},c,\mathbf{q},\nu\omega_L)f_{c,v}(\mathbf{q},\mathbf{R},T)f^*_{c,v}(\mathbf{k},\mathbf{R},T) \\
-\nu B^*(c,\mathbf{k},c,\mathbf{q},\nu\omega_L)f_{c,v}(\mathbf{k},\mathbf{R},T)f^*_{c,v}(\mathbf{q},\mathbf{R},T)
\end{array}\right]
\end{array}\right\}
\end{aligned} \tag{6.85}$$

and

$$\begin{aligned}
&\left[\frac{\partial}{\partial T}+\frac{\hbar}{m_v^*}\mathbf{k}\cdot\nabla_{\mathbf{R}}\right]f_{v,v}(\mathbf{k},\mathbf{R},T)\\
&=\int\frac{d^3\mathbf{k}'}{i\hbar(2\pi)^3}\left(V_v^t(\mathbf{k}-\mathbf{k}',\mathbf{R})-V_v^t(\mathbf{k}'-\mathbf{k},\mathbf{R})\right)f_{v,v}(\mathbf{k}',\mathbf{R},T)\\
&+i\left[f_{c,v}(\mathbf{k},\mathbf{R},T)\Omega_R^{+*}(\mathbf{k},\mathbf{R},T)-f_{c,v}^*(\mathbf{k},\mathbf{R},T)\Omega_R^+(\mathbf{k},\mathbf{R},T)\right]\\
&-\int d^3\mathbf{q}\left\{\begin{array}{l}\left[Z_{v,v}^{v,v}(\mathbf{k},\mathbf{q},\omega_L)f_{v,v}(\mathbf{k},\mathbf{R},T)-f_{v,v}(\mathbf{q},\mathbf{R},T)Z_{v,v}^{v,v}(\mathbf{q},\mathbf{k},\omega_L)\right]\\ +i\sum\limits_{\nu=\pm1}\left[\begin{array}{c}\nu\left(B(v,\mathbf{k},v,\mathbf{q},\nu\omega_L)-B^*(v,\mathbf{k},v,\mathbf{q},\nu\omega_L)\right)\\ \times f_{v,v}(\mathbf{q},\mathbf{R},T)f_{v,v}(\mathbf{k},\mathbf{R},T)\\ +\nu B(v,\mathbf{k},v,\mathbf{q},\nu\omega_L)f_{c,v}^*(\mathbf{q},\mathbf{R},T)f_{c,v}(\mathbf{k},\mathbf{R},T)\\ -\nu B^*(v,\mathbf{k},v,\mathbf{q},\nu\omega_L)f_{c,v}^*(\mathbf{k},\mathbf{R},T)f_{c,v}(\mathbf{q},\mathbf{R},T)\end{array}\right]\end{array}\right\}
\end{aligned}\tag{6.86}$$

and

$$\begin{aligned}
&\left[\frac{\partial}{\partial T}-i\Omega_{op}+i\omega_R(\mathbf{k},\mathbf{R},T)+\frac{\hbar}{2}\left[\frac{i}{m_{c,v}^{*-}}\left(k^2-\frac{\nabla_{\mathbf{R}}^2}{4}\right)+\frac{1}{m_{c,v}^{*+}}\mathbf{k}\cdot\nabla_{\mathbf{R}}\right]\right]f_{c,v}(\mathbf{k},\mathbf{R},T)\\
&=\int\frac{d^3\mathbf{k}'}{i\hbar(2\pi)^3}\left(V_c^t(\mathbf{k}-\mathbf{k}',\mathbf{R})-V_v^t(\mathbf{k}'-\mathbf{k},\mathbf{R})\right)f_{c,v}(\mathbf{k}',\mathbf{R},T)\\
&+i\Omega_R^+(\mathbf{k},\mathbf{R},T)\left(f_{v,v}(\mathbf{k},\mathbf{R},T)-f_{c,c}(\mathbf{k},\mathbf{R},T)\right)
\end{aligned}\tag{6.87}$$

Where

$$\Omega_R^+(\mathbf{k},\mathbf{R},T)=\frac{1}{\hbar}\mathbf{d}_{cv}\cdot\mathbf{E}^+(\mathbf{R},T)+\int d^3\mathbf{k}'V_{s\mathbf{k}-\mathbf{k}'}f_{cv}(\mathbf{k}',\mathbf{R},T)\tag{6.88}$$

is known as the renormalized Rabi frequency and

$$\hbar\omega_R(\mathbf{k},\mathbf{R},T)=\int d^3\mathbf{k}'V_{s,\mathbf{k}-\mathbf{k}'}\left(f_{v,v}(\mathbf{k}',\mathbf{R},T)-f_{c,c}(\mathbf{k}',\mathbf{R},T)-1\right)\tag{6.89}$$

is the renormalization to the transition energy.

In section 3.6.3 the renormalization factors included the coulomb-hole energy. This has not been incorporated here yet because the effective masses are taken as their screened values. During a practical calculation, this will have to be added in if the masses used are the unscreened values.

6.3 Electric Field

The Quantum Boltzmann equation as derived so far is incomplete because there are not yet expressions for the electric field. In this section, it will be shown how the electric field and Wigner functions are related. This will give a fully self-consistent model.

6.3.1 Macroscopic Polarization

The energy density of a system is described by[54]

$$W(T) = \int d^3\mathbf{R}\mathbf{E}(\mathbf{R},T)\cdot\mathbf{D}(\mathbf{R},T) \tag{6.90}$$

where the displacement is

$$\mathbf{D}(\mathbf{R},T) = \mathbf{E}(\mathbf{R},T) + \mathbf{P}_{nr}(\mathbf{R},T) - \mathbf{P}_r(\mathbf{R},T) \tag{6.91}$$

The polarization has been separated into two components, the resonant and non-resonant. The non-resonant polarization ($\mathbf{P}_{nr}$) is the background polarization that generally exists in the material. It is known as non-resonant because it is not at the frequency of the laser light. It is assumed to have a linear relationship to the electric field ($\mathbf{P}_{nr}(\mathbf{R},T) = \chi(\mathbf{R})\mathbf{E}(\mathbf{R},T)$) The resonant polarization ($\mathbf{P}_r$) is the polarization resonant with the laser light. This is negative because the polarization is induced. This is what controls the gain and is related to the Wigner functions. To see this, from (6.90) the energy density due to the resonant polarization is

$$\delta W(T) = -\int d^3\mathbf{R}\mathbf{E}(\mathbf{r},T)\cdot\mathbf{P}_r(\mathbf{R},T) \tag{6.92}$$

The electromagnetic interaction has a perturbation energy $\mathbf{R}\cdot\mathbf{E}$ so that the energy density can also be written as, using the relation between $G^<$ and the expectation value in equation (6.4),

$$\begin{aligned}
\delta W(T) &= -i\int d^3\mathbf{R}e\mathbf{R}\cdot\mathbf{E}(\mathbf{R},T)G^<(X,X) \\
&= -i\int d^3\mathbf{R}e\mathbf{R}\cdot\mathbf{E}(\mathbf{R},T)\sum_{i,j}u_i(\mathbf{R})u_j^*(\mathbf{R})G^<_{i,j}(X,X) \\
&\approx \frac{1}{2\pi}\sum_{i,j}\mathbf{d}_{ji}\cdot\int d^3\mathbf{R}d^3\mathbf{k}\mathbf{E}(\mathbf{R},T)f_{i,j}(\mathbf{k},\mathbf{R},T)
\end{aligned} \tag{6.93}$$

Note the Wigner function used here is **before** the rotating wave approximation has been made, which will be applied shortly.

From the equality of equations (6.92) and (6.93) the identification

$$\mathbf{P}_r(\mathbf{R},T) = -\frac{1}{2\pi}\sum_{i,j}\mathbf{d}_{ji}\cdot\int d^3\mathbf{k} f_{i,j}(\mathbf{k},\mathbf{R},T) \tag{6.94}$$

can then be made. This is a very important result as it relates the off-diagonal Wigner functions to the macroscopic Polarization and therefore the electric field can be related to the Wigner functions through Maxwell's equations.

6.3.2 Maxwell's equations

The evolution of a TE field, assuming no current flows in the transverse direction is

$$\left[\mu_o\varepsilon(\mathbf{R})\frac{\partial^2}{\partial T^2} - \nabla^2\right]\mathbf{E}(\mathbf{R},T) = -\mu_o\frac{\partial^2}{\partial T^2}\mathbf{P}_r(\mathbf{R},T) \tag{6.95}$$

where the polarization is separated into the resonant and non-resonant parts. The non-resonant part is included in the dielectric constant by $\varepsilon(\mathbf{R}) = 1 + \chi(\mathbf{R})$. It is simpler to solve this in frequency space so make the transformation

$$\mathbf{E}(\mathbf{R},T) = \int d\Omega\frac{e^{i\Omega T}}{(2\pi)^{1/2}}\mathbf{E}(\mathbf{R},\Omega)\ ,\ \mathbf{P}_r(\mathbf{R},T) = \int d\Omega\frac{e^{i\Omega T}}{(2\pi)^{1/2}}\mathbf{P}_r(\mathbf{R},\Omega) \tag{6.96}$$

Equation (6.95) in this space is

$$\left[\nabla^2 + \Omega^2\mu_o\varepsilon(\mathbf{R})\right]\mathbf{E}(\mathbf{R},\Omega) = -\mu_o\Omega^2\mathbf{P}_r(\mathbf{R},\Omega) \tag{6.97}$$

The difficulty with solving this equation is that the resonant polarization can be quite complicated, as evident in equation (6.94). To solve when the polarization is arbitrary, another Greens function method will be used. This is the *electromagnetic Greens function*, which is the solution of

$$\left[\nabla^2 + \Omega^2\mu_o\varepsilon(\mathbf{R})\right]G^{EM}(\mathbf{R},\mathbf{R}',\Omega) = \delta^3(\mathbf{R}-\mathbf{R}') \tag{6.98}$$

so that the electric field is then

$$\mathbf{E}(\mathbf{R},\Omega) = \int d^3\mathbf{R}' G^{EM}(\mathbf{R},\mathbf{R}',\Omega)\left[-\mu_o\Omega^2\mathbf{P}(\mathbf{R}',\Omega)\right] \quad (6.99)$$

$$= \frac{\mu_o}{2\pi}\sum_{i,j}\mathbf{d}_{ij}\int d^3\mathbf{R}' G^{EM}(\mathbf{R},\mathbf{R}',\Omega)\Omega^2\int d^3\mathbf{k} f_{i,j}(\mathbf{k},\mathbf{R},\Omega) \quad (6.100)$$

where equation (6.94) has been used in the last line and the Wigner function is Fourier transformed as in equation (6.96). This is the general relation between the electric field and the Wigner functions. The electromagnetic Greens functions in frequency space were chosen as there are already known solutions for this for the structures under consideration.

Fabry-Perot (FP) Cavity

The FP cavity is a standard structure, it consists of two partially reflecting mirrors placed perpendicular to the direction of optical propagation. The dielectric is constant along this direction and therefore a simple resonant cavity is formed. This cavity has been implicitly used in chapter 3 and is shown in figure (6.3).

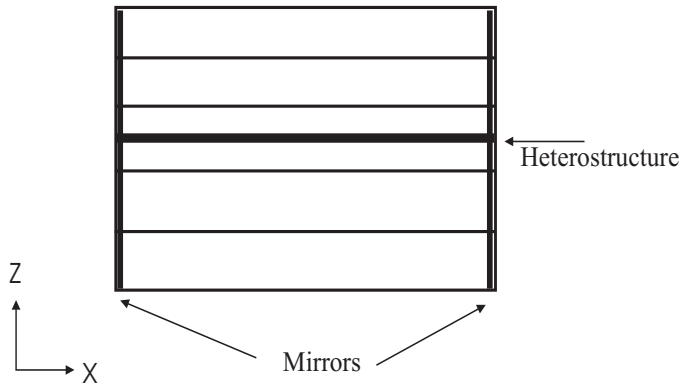

Figure 6.3: A Schematic Representation of a Fabry-Perot Laser Cavity

The electromagnetic Greens function for the FP cavity has standard solutions[74, 75, 76]

$$G^{EM}(\mathbf{R},\mathbf{R}',\Omega) = \sum_n g_n(X,X',\Omega)\frac{\phi_{n,\Omega}(Z)\phi_{n,\Omega}(Z')}{<\phi_{n,\Omega}\phi_{n,\Omega}>} = \sum_n g_n(X,X',\Omega)g_n(Z,Z',\Omega) \quad (6.101)$$

The variation in the Y direction has been neglected as it is assumed in this direction it is an infinite waveguide. The subscript n denotes the transverse mode solution which is determined by annotating the solutions of the one-dimensional waveguide problem

$$\left[\frac{d^2}{dZ^2} + \Omega^2 \mu_o \varepsilon(Z)\right] \phi_{n,\Omega}(Z) = k_{n,\Omega}^2 \phi_{n,\Omega}(Z) \tag{6.102}$$

Which has been solved in Chapter 2. The denominator in (6.101) is for normalization. Since the transverse modes are orthogonal, this gives an equation for the one-dimensional Greens function[74, 75]

$$\left[\frac{d^2}{dX^2} + k_{n,\Omega}^2\right] g_n(X, X', \Omega) = \delta(X - X') \tag{6.103}$$

which has solutions

$$g_n(X, X', \Omega) = \frac{Z_{R,n,\Omega}(X) Z_{L,n,\Omega}(X') \Theta(X - X') + Z_{R,n,\Omega}(X') Z_{L,n,\Omega}(X) \Theta(X' - X)}{W_{n,\Omega}} \tag{6.104}$$

where $Z_{L,n\Omega}$ is the solution of the homogeneous equation which satisfies the boundary condition at the left laser facet and $Z_{R,n\Omega}$ is the solution that satisfies the boundary condition at the right laser facet. The denominator is the Wronskian which is defined by

$$W_{n,\Omega} = Z_{L,n,\Omega}(X) \frac{d}{dX} Z_{R,n\Omega}(X) - Z_{R,n,\Omega}(X) \frac{d}{dX} Z_{L,n,\Omega}(X) \tag{6.105}$$

For the first mode of the Fabry-Perot cavity extending from X=0 to X=L with reflectivities r_1 and r_2, these have the solutions

$$Z_{L,o,\Omega}(X) = r_1 e^{ik_{o,\Omega}X} + e^{-ik_{o,\Omega}X} \ , \ Z_{R,o,\Omega}(X) = r_1 \left[e^{ik_{o,\Omega}X} + r_2 e^{ik_{o,\Omega}(2L-X)}\right] \tag{6.106}$$

$$W_{o,\Omega} = 2ik_{o,\Omega} \left[1 - r_1 r_2 e^{2ik_{o,\Omega}L}\right] \tag{6.107}$$

Distributed Feedback (DFB) Cavity

Another common cavity design is a DFB cavity. It gives a sharper spectral resolution than the FP cavity. Instead of the dielectric being constant in the field propagation direction,

a periodic grating structure is formed in one or more of the layers. A schematic of this is shown in figure 6.4 by the solid lines. An exact solution of this problem is quite complicated so that usually perturbation method in $\delta\varepsilon(X,Z)$ (the difference between dielectric over the grating structure and the "average" as shown in figure 6.4 by the dashed line) is used such as the coupled wave solutions[77]. Instead of this method, a Greens function solution will be used. Note that the average structure of figure 6.4 is just a FP cavity, therefore, the DFB Greens function can be considered a perturbation on the Greens function solution of the FP structure.

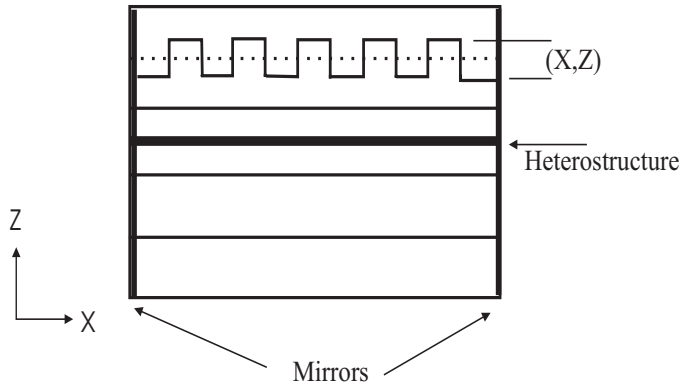

Figure 6.4: A Schematic Representation of a DFB Laser Cavity

Let $\varepsilon(X,Z) = \varepsilon_o(Z) + \delta\varepsilon(X,Z)$ where ε_o is the dielectric profile of a FP type cavity as shown in figure 6.3 and figure 6.4 by the dashed lines and $\delta\varepsilon$ is the perturbation to this to modify this structure to a DFB as shown in figure 6.4 by the solid lines. The unperturbed Greens function G_o^{EM} is thus the solution to

$$\left[\nabla^2 + \Omega^2\mu_o\varepsilon_o(\mathbf{R})\right] G_o^{EM}(\mathbf{R},\mathbf{R}',\Omega) = \delta^3(\mathbf{R}-\mathbf{R}') \tag{6.108}$$

and is determined in the above section. The first order perturbation to this is then[76]

$$G^{EM}(\mathbf{R},\mathbf{R}',\Omega) = G_o^{EM}(\mathbf{R},\mathbf{R}',\Omega) + G_1^{EM}(\mathbf{R},\mathbf{R}',\Omega) \tag{6.109}$$

where

$$G_1^{EM}(\mathbf{R},\mathbf{R}',\Omega) = -\int d^3\mathbf{R}'' G_o^{EM}(\mathbf{R},\mathbf{R}'',\Omega)\delta\varepsilon(\mathbf{R}'')G_o^{EM}(\mathbf{R}'',\mathbf{R}',\Omega) \tag{6.110}$$

6.3.3 Rotating Wave Components

The above section shows how to determine the electric field $\mathbf{E}$ from the Wigner functions. Now, it is required to show the relation between the slowly vary components $\mathbf{E}^+$, $\mathbf{E}^-$ and $\tilde{f}_{c,v}$ and $\tilde{f}_{v,c}$. The relation is a bit subtle because these are not straight Fourier transforms.

A time dependent function $A(T)$ is expanded into Fourier components $A(\Omega)$ as well as the slowly rotating components $\tilde{A}(T)$

$$A(T) = \int d\Omega \frac{e^{-i\Omega T}}{(2\pi)^{1/2}} A(\Omega) \approx \tilde{A}(T) e^{-i\Omega_r T} \tag{6.111}$$

Ω_r is the frequency about which the function is peaked. Multiply equation (6.111) by $\int_{T-\tau}^{T+\tau} dT' \frac{1}{2\tau} e^{i\Omega_r T'}$ where $\tau = \frac{n2\pi}{\Omega_r}$ and n>>1 but small enough such that $\tilde{A}(T+\tau) \approx \tilde{A}(T)$ to get the approximate relation

$$\tilde{A}(T) \approx \int d\Omega \left[\frac{1}{2(2\pi)^{1/2}\tau} \int_{T-\tau}^{T+\tau} dT' e^{-i(\Omega-\Omega_r)T'} \right] A(\Omega) = \int d\Omega g(\Omega, \Omega_r, T) A(\Omega) \tag{6.112}$$

It is not necessary to explicitly evaluate the term in the square brackets, simply call it $g(\Omega, \Omega_r, T)$ and note that it is a function that is sharply peaked around Ω_r.

All of the slowly varying electric field and Wigner functions used have this form and can therefore be expanded as

$$\begin{aligned}
\mathbf{E}^+(\mathbf{R}, T) &\approx \int d\Omega g(\Omega, \Omega_{op}, T) \mathbf{E}(\mathbf{R}, \Omega) \\
\mathbf{E}^-(\mathbf{R}, T) &\approx \int d\Omega g(\Omega, -\Omega_{op}, T) \mathbf{E}(\mathbf{R}, \Omega) \\
\tilde{f}_{c,v}(\mathbf{k}, \mathbf{R}, T) &\approx \int d\Omega g(\Omega, \Omega_{op}, T) f_{c,v}(\mathbf{k}, \mathbf{R}, \Omega) \\
\tilde{f}_{v,c}(\mathbf{k}, \mathbf{R}, T) &\approx \int d\Omega g(\Omega, -\Omega_{op}, T) f_{v,c}(\mathbf{k}, \mathbf{R}, \Omega)
\end{aligned} \tag{6.113}$$

The terms $\mathbf{E}^-$ and $f_{v,c}$ are being kept instead of simply using the complex conjugates of $\mathbf{E}^+$ and $f_{c,v}$ because of a key piece of information about the electromagnetic Greens function to be explained at the end of this section.

Substituting the relations in equation (6.99) into the above expansions of the fields gives

$$\begin{aligned}\mathbf{E}^{+}(\mathbf{R},T) &= \frac{\mu_o}{2\pi}\int d\Omega\Omega^2 g(\Omega,\Omega_{op},T)\int d^3\mathbf{R}' G^{EM}(\mathbf{R},\mathbf{R}',\Omega) \\ &\times \int d^3\mathbf{k}\left(\mathbf{d}_{vc}f_{c,v}(\mathbf{k},\mathbf{R}',\Omega)+\mathbf{d}_{cv}f_{v,c}(\mathbf{k},\mathbf{R}',\Omega)\right) \qquad (6.114)\end{aligned}$$

but Ω^2 and $G^{EM}(\mathbf{R},\mathbf{R}',\Omega)$ are much slower varying functions in Ω than $g(\Omega,\Omega_{op},T)$ and $f_{i,j}(\mathbf{k},\mathbf{R},T)$ so that this can be approximately written as

$$\begin{aligned}\mathbf{E}^{+}(\mathbf{R},T) &\approx \frac{\mu_o\Omega_{op}^2}{2\pi}\int d^3\mathbf{R}' G^{EM}(\mathbf{R},\mathbf{R}',\Omega_{op})\int d\Omega g(\Omega,\Omega_{op},T) \\ &\times \int d^3\mathbf{k}\left(\mathbf{d}_{vc}f_{c,v}(\mathbf{k},\mathbf{R}',\Omega)+\mathbf{d}_{cv}f_{v,c}(\mathbf{k},\mathbf{R}',\Omega)\right) \qquad (6.115)\end{aligned}$$

Since $f_{c,v}$ is peaked around Ω_{op}, whereas $f_{v,c}$ is peaked around $-\Omega_{op}$, this can be approximated as

$$\mathbf{E}^{+}(\mathbf{R},T)=\frac{\mu_o\Omega_{op}^2}{2\pi}\int d^3\mathbf{R}' G^{EM}(\mathbf{R},\mathbf{R}',\Omega_{op})\int d^3\mathbf{k}\mathbf{d}_{vc}\tilde{f}_{c,v}(\mathbf{k},\mathbf{R}',T) \qquad (6.116)$$

similarly,

$$\mathbf{E}^{-}(\mathbf{R},T)=\frac{\mu_o\Omega_{op}^2}{2\pi}\int d^3\mathbf{R}' G^{EM}(\mathbf{R},\mathbf{R}',\Omega_{op})\int d^3\mathbf{k}\mathbf{d}_{cv}\tilde{f}_{v,c}(\mathbf{k},\mathbf{R}',T) \qquad (6.117)$$

where the relation $G^{EM}(\mathbf{R},\mathbf{R}',\Omega_{op})=G^{EM}(\mathbf{R},\mathbf{R}',-\Omega_{op})$ has been used (which comes out of section 6.3.2). Equations (6.116) and (6.117) can then be substituted into equations (6.80) to (6.83) to couple the electric field with the QBE.

Equation (6.117) might be cause for concern because the relation $\mathbf{E}^{+}=\mathbf{E}^{-*}$ implies from equation (6.116) that

$$\mathbf{E}^{-}(\mathbf{R},T)=\frac{\mu_o\Omega_{op}^2}{2\pi}\int d^3\mathbf{R}' G^{EM*}(\mathbf{R},\mathbf{R}',\Omega_{op})\int d^3\mathbf{k}\mathbf{d}_{cv}\tilde{f}^{*}_{c,v}(\mathbf{k},\mathbf{R}',T) \qquad (6.118)$$

Since $G^{EM}\neq G^{EM*}$, when comparing equations (6.117) and (6.118) it would seem $f_{v,c}\neq f^{*}_{c,v}$ which was asserted previously. However, it can be shown that the complex conjugate of the electromagnetic Greens functions also satisfies the equations and boundary conditions of the FP and DFB structures. This means it is acceptable to replace G^{EM*} by G^{EM} because they'll both yield the same expectation values. Thus the relation $f_{c,v}=f^{*}_{v,c}$ still holds.

6.4 The Electron-Hole Representation

The conduction-valence band representation has been convenient to use to derive the QBE. However in practice, the conduction-hole band representation is preferable because doping is given in terms of donors and acceptors which are free conduction electrons and holes. Thus the boundary conditions, which will be related to the doping are more convenient to formulate in terms of holes. This is accomplished by replacing the valence band Wigner function with a hole band Wigner function.

These are related by[44]

$$f_{v,v}(\mathbf{k},\mathbf{R},T) = 1 - f_{h,h}(-\mathbf{k},\mathbf{R},T) \tag{6.119}$$

Where $f_{h,h}(-\mathbf{k},\mathbf{R},T)$ is the hole band Wigner function. Note that the momentum indice is the opposite sign because the valence and hole creation and annihilation operators in the momentum representation are related by[43, 44, 28]

$$\hat{a}_v(\mathbf{k},t) = \hat{a}_h^+(-\mathbf{k},t)\ ,\ \hat{a}_v^+(\mathbf{k},t) = \hat{a}_h(-\mathbf{k},t) \tag{6.120}$$

It can be shown that the hole creation and annihilation operators also obey the commutation relations[28] and hence are an equivalent method of describing the system. Therefore the Greens functions and Wigner functions can be defined in this representation.

Substituting the relations of (6.119) into equations (6.80) to (6.82) as well as using the relations between the electric field and Wigner functions gives the equations in the hole representation

$$
\begin{aligned}
&\left[\frac{\partial}{\partial T}+\frac{\hbar}{m_c^*}\mathbf{k}\cdot\nabla_{\mathbf{R}}\right] f_{c,c}(\mathbf{k},\mathbf{R},T)\\
&=\int\frac{d^3\mathbf{k}'}{i\hbar(2\pi)^3}\left(V_c^t(\mathbf{k}-\mathbf{k}',\mathbf{R})-V_c^t(\mathbf{k}'-\mathbf{k},\mathbf{R})\right)f_{c,c}(\mathbf{k}',\mathbf{R},T)\\
&+\frac{i}{\hbar}\left[f_{c,h}(\mathbf{k},\mathbf{R},T)\mathbf{d}_{ch}^*\cdot\mathbf{E}^-(\mathbf{R},T)-f_{c,h}^*(\mathbf{k},\mathbf{R},T)\mathbf{d}_{ch}\cdot\mathbf{E}^+(\mathbf{R},T)\right]\\
&-\int d^3\mathbf{q}\left\{\begin{array}{l}\left[Z_{c,c}^{c,c}(\mathbf{k},\mathbf{q},\omega_L)f_{c,c}(\mathbf{k},\mathbf{R},T)-f_{c,c}(\mathbf{q},\mathbf{R},T)Z_{c,c}^{c,c}(\mathbf{q},\mathbf{k},\omega_L)\right]\\ +i\sum\limits_{\nu=\pm1}\left[\begin{array}{c}\nu\left(B(c,\mathbf{k},c,\mathbf{q},\nu\omega_L)-B^*(c,\mathbf{k},c,\mathbf{q},\nu\omega_L)\right)\\ \times f_{c,c}(\mathbf{q},\mathbf{R},T)f_{c,c}(\mathbf{k},\mathbf{R},T)\\ +\nu B(c,\mathbf{k},c,\mathbf{q},\nu\omega_L)f_{c,h}(\mathbf{q},\mathbf{R},T)f_{c,h}^*(\mathbf{k},\mathbf{R},T)\\ -\nu B^*(c,\mathbf{k},c,\mathbf{q},\nu\omega_L)f_{c,h}(\mathbf{k},\mathbf{R},T)f_{c,h}^*(\mathbf{q},\mathbf{R},T)\end{array}\right]\end{array}\right\}\\
&+\frac{i}{\hbar}\int d^3\mathbf{k}'V_{s,\mathbf{k}-\mathbf{k}'}\left\{f_{c,h}(\mathbf{k},\mathbf{R},T)f_{c,h}^*(\mathbf{k}',\mathbf{R},T)-f_{c,h}(\mathbf{k}',\mathbf{R},T)f_{c,h}^*(\mathbf{k},\mathbf{R},T)\right\}
\end{aligned}
\tag{6.121}
$$

$$
\begin{aligned}
&\left[-\frac{\partial}{\partial T}+\frac{\hbar}{m_h^*}\mathbf{k}\cdot\nabla_{\mathbf{R}}\right] f_{h,h}(\mathbf{k},\mathbf{R},T)\\
&=\int\frac{d^3\mathbf{k}'}{i\hbar(2\pi)^3}\left(V_h^t(\mathbf{k}-\mathbf{k}',\mathbf{R})-V_h^t(\mathbf{k}'-\mathbf{k},\mathbf{R})\right)f_{h,h}(\mathbf{k}',\mathbf{R},T)\\
&+\frac{i}{\hbar}\left[f_{c,h}^*(\mathbf{k},\mathbf{R},T)\mathbf{d}_{ch}\cdot\mathbf{E}^+(\mathbf{R},T)-f_{c,h}(\mathbf{k},\mathbf{R},T)\mathbf{d}_{ch}^*\cdot\mathbf{E}^-(\mathbf{R},T)\right]\\
&-\int d^3\mathbf{q}\left\{\begin{array}{l}\left[-Z_{h,h}^{h,h}(\mathbf{k},\mathbf{q},\omega_L)f_{h,h}(\mathbf{k},\mathbf{R},T)+f_{h,h}(\mathbf{q},\mathbf{R},T)Z_{h,h}^{h,h}(\mathbf{q},\mathbf{k},\omega_L)\right]\\ +i\sum\limits_{\nu=\pm1}\left[\begin{array}{c}\nu\left(B(h,\mathbf{k},h,\mathbf{q},\nu\omega_L)-B^*(h,\mathbf{k},h,\mathbf{q},\nu\omega_L)\right)\\ \times f_{h,h}(\mathbf{q},\mathbf{R},T)f_{h,h}(\mathbf{k},\mathbf{R},T)\\ +\nu B(h,\mathbf{k},h,\mathbf{q},\nu\omega_L)f_{c,h}^*(\mathbf{q},\mathbf{R},T)f_{c,h}(\mathbf{k},\mathbf{R},T)\\ -\nu B^*(h,\mathbf{k},h,\mathbf{q},\nu\omega_L)f_{c,h}^*(\mathbf{k},\mathbf{R},T)f_{c,h}(\mathbf{q},\mathbf{R},T)\end{array}\right]\end{array}\right\}\\
&+\frac{i}{\hbar}\int d^3\mathbf{k}'V_{s,\mathbf{k}-\mathbf{k}'}\left\{f_{c,h}^*(\mathbf{k},\mathbf{R},T)f_{c,h}(\mathbf{k}',\mathbf{R},T)-f_{c,h}^*(\mathbf{k}',\mathbf{R},T)f_{c,h}(\mathbf{k},\mathbf{R},T)\right\}
\end{aligned}
\tag{6.122}
$$

$$\left[\frac{\partial}{\partial T} - i\Omega_{op} + \frac{\hbar}{2}\left[\frac{i}{m^{*+}_{c,h}}\left(k^2 - \frac{\nabla^2_{\mathbf{R}}}{4}\right) + \frac{1}{m^{*-}_{c,h}}\mathbf{k}\cdot\nabla_{\mathbf{R}}\right]\right] f_{c,h}(\mathbf{k},\mathbf{R},T)$$
$$= \int \frac{d^3\mathbf{k}'}{i\hbar(2\pi)^3}\left(V^t_c(\mathbf{k}-\mathbf{k}',\mathbf{R}) + V^t_h(\mathbf{k}'-\mathbf{k},\mathbf{R})\right) f_{c,h}(\mathbf{k}',\mathbf{R},T) \tag{6.123}$$
$$+\frac{i}{\hbar}\mathbf{d}_{ch}\cdot\mathbf{E}^+(\mathbf{R},T)\left(1 - f_{h,h}(\mathbf{k},\mathbf{R},T) - f_{c,c}(\mathbf{k},\mathbf{R},T)\right)$$
$$+\frac{i}{\hbar}\int d^3\mathbf{k}' V_{s,\mathbf{k}-\mathbf{k}'}\left\{\begin{array}{l} f_{c,h}(\mathbf{k},\mathbf{R},T)\left(-f_{h,h}(\mathbf{k}',\mathbf{R},T) - f_{c,c}(\mathbf{k}',\mathbf{R},T)\right) \\ +f_{c,h}(\mathbf{k}',\mathbf{R},T)\left(f_{c,c}(\mathbf{k},\mathbf{R},T) + f_{h,h}(\mathbf{k},\mathbf{R},T) - 1\right)\end{array}\right\}$$

where $f_{c,v} = f_{c,h}$, $V^t_v = -V^t_h$, $m_h = -m_v$ and $|d|^2 = \mathbf{d}_{cv}\cdot\mathbf{d}^*_{cv}$. The $f_{h,h}$ functions have also simply been redefined so that they are $f_{h,h}(\mathbf{k},\mathbf{R},T)$ instead of $f_{h,h}(-\mathbf{k},\mathbf{R},T)$. The phonon terms have indices v replaced by h which signifies that any components within these terms that depend on m_v will be replaced by $-m_h$. It can be shown that all terms of the form $\sum_{\nu=\pm1}\int d^3\mathbf{q} Im(B(i,\mathbf{q},i,\mathbf{k},\nu\omega_L))$ will cancel by virtue of some relations of the Dirac-delta functions. This reduces the number of phonon terms when the hole replacement is made.

6.5 Higher Order Scattering

The Hartree-Fock approximation to the Phonon and Coulombic scattering ignores the higher order processes. These are usually incorporated by assuming they generally contribute in a form that can be modeled by the relaxation time approximation in classical Boltzmann scattering[30, 31, 44].

$$\left.\frac{\partial f_{i,i}}{\partial T}\right|_{coll} = \frac{1}{\tau_i}\left[\frac{f^{eq}_{i,i}}{\int d^3\mathbf{k} f^{eq}_{i,i}}\int d^3\mathbf{k} f_{i,i} - f_{i,i}\right] \tag{6.124}$$

for the diagonal components where f^{eq} is the equilibrium Wigner function, which is normally found by calculating the Wigner functions (excluding scattering) at zero-bias potential. For the off-diagonal components, the term used is

$$\left.\frac{\partial f_{c,h}}{\partial T}\right|_{coll} = -\frac{f_{c,h}}{\tau_{ch}} \tag{6.125}$$

This is because in equilibrium the off-diagonal components don't exist. The symbol τ_i is the relaxation time for the diagonal Wigner function components, τ_{ch} is the relaxation time of the off-diagonal component given by $\tau_{ch} = \frac{\tau_c + \tau_h}{2}$. These times can also be used to include the other phenomenological effects used in the conventional model.

The time constants describe a further factor of irreversibility in the system (recall the system is already irreversible by virtue of the boundary conditions). The scattering processes cause a decay in the non-equilibrium Wigner functions and a drive to the equilibrium state ($f^{eq}_{i,i}$ for diagonal, 0 for off-diagonal). The shorter the scattering time, the closer to equilibrium the system will be. In the numerical example that follows, the scattering times are such that there is some broadening because of it, but the system is still in a highly non-equilibrium state.

6.6 Spontaneous Emission

If equations (6.121) to (6.123) are solved simultaneously, it is quickly realized that $f_{c,h} = 0$ for vanishing boundary conditions. Thus there is no polarization and no electric field. The reason for this is because spontaneous emission, which is critical to start the lasing process, is not yet accounted for since the electric field was treated classically. It must therefore be added to complete the model.

Equation (6.123) can be represented schematically as

$$\frac{\partial}{\partial T} f_{c,h} = -\frac{f_{c,h}}{\tau_{ch}} + L f_{c,h} \tag{6.126}$$

where L represents all other terms that operate on $f_{c,h}$. A semi-classical method to add spontaneous emission is to consider it a random force originating from the vacuum fluctuations. A random force of this type can be accounted for in this case using Langevin theory by adding a random fluctuating force $F_{c,h}$ to equation (6.126) to get[44, 78]

$$\frac{\partial}{\partial T} f_{c,h} = -\frac{f_{c,h}}{\tau_{ch}} + L f_{c,h} + F_{c,h} \tag{6.127}$$

This force has zero mean when averaged over the vacuum fluctuations. The diffusion coefficient ($D_{c,h}$) is related to the correlation of the random fluctuations by

$$< F^*_{c,h}(\mathbf{k}, \mathbf{R}, t) F_{c,h}(\mathbf{k}, \mathbf{R}', t' >= \delta(t - t')\delta^3(\mathbf{R} - \mathbf{R}') 2 D_{c,h}(\mathbf{k}, \mathbf{R}, t) \tag{6.128}$$

It is estimated by making the identification of equation (6.127) with semi-classical laser theories. This will give an approximate diffusion coefficient relation[44]

$$D_{c,h} \approx \frac{f_{c,c} f_{h,h}}{\tau_{c,h}} \tag{6.129}$$

To solve equation (6.126) simultaneously with equations (6.121) and (6.122) it is required to solve these equations a large number of times using $F_{c,h}$ as Gaussian random variable and then taking a statistical average of the solutions. This is a very time consuming method, in the next section a method will be shown to avoid this.

6.7 Summary

This chapter describes the general quantum Boltzmann equations for the QW laser derived from non-equilibrium Greens function theory. Various manipulations have been performed which are schematically represented in the flow chart below.

The concepts and components used in this chapter are not original. However, to the author's knowledge the QBE combined with the electromagnetic Greens functions and spontaneous emission have not been performed before. Wigner function modelling is more commonly used for resonant tunneling diodes than active laser devices. Including the electromagnetic coupling to the model introduces off-diagonal Wigner functions that we have not seen modeled in this way before. The phonon terms in equation (6.73) also have new components due to the off-diagonal Wigner functions. In addition, we have not seen an electromagnetic Greens function of the DFB cavity described as a perturbation of the Fabry-Perot cavity as shown in section 6.3, but it is a quite straightforward extension of the FP Greens function and therefore likely to not be original.

Although this chapter ends with a complete model of the QW laser in the QBE formulation, it is still not practical to numerically solve on a computer. The next chapter will apply some simplifying approximations to the QBE for practical calculations.

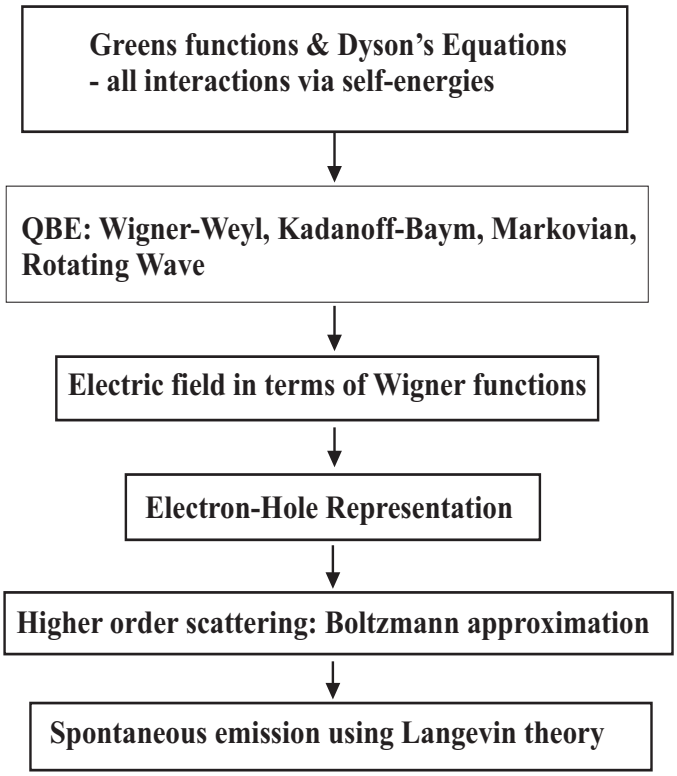
Greens functions & Dyson's Equations
- all interactions via self-energies
QBE: Wigner-Weyl, Kadanoff-Baym, Markovian, Rotating Wave
Electric field in terms of Wigner functions
Electron-Hole Representation
Higher order scattering: Boltzmann approximation
Spontaneous emission using Langevin theory

Chapter 7

Solving the QBE and a Sample Solution

In this chapter, an example will be given of how to solve the Wigner functions for a certain structure. In this case, the system will be solved for steady-state (all T dependence vanishes) and phonon, coulombic interactions will only be accounted for in the decay constants.

7.1 Linear and Non-Linear Polarization

It is convenient to separate the off-diagonal Wigner function into "linear" and "non-linear" components[43]. Essentially, this is an approximation where the off-diagonal Wigner function can be split into terms weakly varying in $\mathbf{k}$-space and those quickly varying.

$$\begin{aligned}
&\left[-i\Omega_{op} + \frac{\hbar}{2}\left[\frac{i}{m^{*+}_{c,h}}\left(k^2 - \frac{\nabla^2_{\mathbf{R}}}{4}\right) + \frac{1}{m^{*-}_{c,h}}\mathbf{k}\cdot\nabla_{\mathbf{R}}\right]\right] f_{c,h:l}(\mathbf{k},\mathbf{R}) \\
&= \int \frac{d^3\mathbf{k}'}{i\hbar(2\pi)^3}\left(V^t_c(\mathbf{k}-\mathbf{k}',\mathbf{R}) + V^t_h(\mathbf{k}'-\mathbf{k},\mathbf{R})\right) f_{c,h:l}(\mathbf{k}',\mathbf{R}) \\
&+ \frac{i}{\hbar}\mathbf{d}_{ch}\cdot\mathbf{E}^+(\mathbf{R}) - \frac{f_{c,h:l}(\mathbf{k},\mathbf{R})}{\tau_{ch}}
\end{aligned} \tag{7.1}$$

and

$$\left[-i\Omega_{op}+\frac{\hbar}{2}\left[\frac{i}{m_{c,h}^{*+}}\left(k^2-\frac{\nabla_{\mathbf{R}}^2}{4}\right)+\frac{1}{m_{c,h}^{*-}}\mathbf{k}\cdot\nabla_{\mathbf{R}}\right]\right]f_{c,h:nl}(\mathbf{k},\mathbf{R})$$
$$=\int\frac{d^3\mathbf{k}'}{i\hbar(2\pi)^3}\left(V_c^t(\mathbf{k}-\mathbf{k}',\mathbf{R})+V_h^t(\mathbf{k}'-\mathbf{k},\mathbf{R})\right)f_{c,h:nl}(\mathbf{k}',\mathbf{R}) \tag{7.2}$$
$$+\frac{i}{\hbar}\mathbf{d}_{ch}\cdot\mathbf{E}^+(\mathbf{R})\left(-f_{h,h}(\mathbf{k},\mathbf{R})-f_{c,c}(\mathbf{k},\mathbf{R})\right)$$
$$-\frac{f_{c,h:nl}(\mathbf{k},\mathbf{R})}{\tau_{ch}}+F_{c,h}(\mathbf{k},\mathbf{R})$$

It is assumed the linear Wigner function $f_{c,h:l}$ changes slowly with position so that these derivatives can be removed and the random $F_{c,h}$ will only apply to the non-linear part. It may seem contradictory to have a random force in the steady-state solutions but as Chow, Koch and Sargent argue[44] this term results in an operator that decays exponentially in time ($\tau_{c,h}$) which gives a noise spectrum, but slowly varying quantities such as $f_{c,h:nl}$ are not sensitive to this.

The most significant contributions to the linear term will be within the well region. Equation (7.1) can then be approximately written as

$$f_{c,h:l}(\mathbf{k},\mathbf{R})\approx\frac{\mathbf{d}_{ch}\cdot\mathbf{E}^+(\mathbf{R})\Theta(Z)}{\frac{\hbar^2k^2}{2m_{c,h}^{*+}}+\varepsilon_{ch}-\hbar\Omega_{op}-\frac{i\hbar}{\tau_{ch}}} \tag{7.3}$$

where ε_{ch} is the band-gap in the well and $\Theta(Z)$ is just a function that is 1 within the well region and 0 elsewhere.

From equation (6.94), the macroscopic resonant polarization is

$$\mathbf{P}_r^+(\mathbf{R})=-\frac{1}{2\pi}\mathbf{d}_{ch}^*\int d^3\mathbf{k}'\left[f_{c,h:l}(\mathbf{k}',\mathbf{R})+f_{c,h:nl}(\mathbf{k}',\mathbf{R})\right]=\mathbf{P}_{r:l}^+(\mathbf{R})+\mathbf{P}_{r:nl}^+(\mathbf{R}) \tag{7.4}$$

Thus using equation (7.3), the linear part of the resonant polarization is

$$\mathbf{P}_{r:l}^+(\mathbf{R})=-\frac{|d|^2\Theta(Z)}{2\pi}\mathbf{E}^+(\mathbf{R})\int d^3\mathbf{k}\frac{1}{\frac{\hbar^2k^2}{2m_{c,h}^{*+}}+\varepsilon_{ch}-\hbar\Omega_{op}-\frac{i}{\tau_{ch}}} \tag{7.5}$$

The linear susceptibility is defined as

$$\chi_l(Z)=\int d^3\mathbf{k}\chi_l(\mathbf{k},Z)=|d|^2\int d^3\mathbf{k}\frac{\Theta(Z)}{\frac{\hbar^2k^2}{2m_{c,h}^{*+}}+\varepsilon_{ch}-\hbar\Omega_{op}-\frac{i}{\tau_{ch}}} \tag{7.6}$$

$\chi_l(Z)$ can then be added to the system's dielectric $\tilde{\epsilon} = \epsilon - \chi_l/2\pi$ which is incorporated into the electromagnetic analysis of section 6.3. So that the electric field can be expressed as

$$\mathbf{E}^+(\mathbf{R}) = \frac{\mu_o \Omega_{op}^2 \mathbf{d}_{ch}^*}{2\pi} \int d^3\mathbf{R}' d^3\mathbf{k}' \tilde{G}^{EM}(\mathbf{R}, \mathbf{R}', \Omega_{op}) f_{c,h:nl}(\mathbf{k}', \mathbf{R}') \tag{7.7}$$

where $\tilde{G}^{EM}(\ \mathbf{R}, \mathbf{R}', \Omega_{op})$ is a new electromagnetic Greens function found using $\tilde{\epsilon}$ in place of ϵ in equation (6.98). The terms for the components of this electromagnetic Greens function $\tilde{G}^{EM}(\mathbf{R}, \mathbf{R}') = \tilde{g}(X, X', \Omega_{op})\tilde{g}(Z, Z', \Omega_{op})$ are found similarly to the components of the FP cavity of section 6.3.2 but with $\tilde{\epsilon}$ in place of ϵ.

Substituting equation (7.7) back into (7.3) gives

$$f_{c,h:l}(\mathbf{k}, \mathbf{R}) = \frac{\mu_o \Omega_{op}^2}{2\pi} \chi_l(\mathbf{k}, Z) \int d^3\mathbf{R}' d^3\mathbf{k}' \tilde{G}^{EM}(\mathbf{R}, \mathbf{R}', \Omega_{op}) f_{c,h:nl}(\mathbf{k}', \mathbf{R}') \tag{7.8}$$

Substituting equation (7.8) into equations (6.121), (6.122) and (7.2) gives

$$\left[+ \frac{\hbar}{m_c^*} \mathbf{k} \cdot \nabla_{\mathbf{R}} \right] f_{c,c}(\mathbf{k}, \mathbf{R})$$

$$= \int \frac{d^3\mathbf{k}'}{i\hbar(2\pi)^3} \left(V_c^t(\mathbf{k} - \mathbf{k}', \mathbf{R}) - V_c^t(\mathbf{k}' - \mathbf{k}, \mathbf{R}) \right) f_{c,c}(\mathbf{k}', \mathbf{R}) \tag{7.9}$$

$$+ \frac{i\mu_o \Omega_{op}^2 |d|^2}{2\pi\hbar} \times \tag{7.10}$$

$$\left[\begin{array}{c} \left[f_{c,h:nl}(\mathbf{k}, \mathbf{R}) + \chi_l(\mathbf{k}, Z) \int d^3\mathbf{R}' d^3\mathbf{k}' \tilde{G}^{EM}(\mathbf{R}, \mathbf{R}', \Omega_{op}) f_{c,h:nl}(\mathbf{k}', \mathbf{R}') \right] \\ \left[\int d^3\mathbf{R}' d^3\mathbf{k}' \tilde{G}^{EM}(\mathbf{R}, \mathbf{R}', \Omega_{op}) f_{c,h:nl}(\mathbf{k}', \mathbf{R}') \right]^* \\ - \left[f_{c,h:nl}(\mathbf{k}, \mathbf{R}) + \chi_l(\mathbf{k}, Z) \int d^3\mathbf{R}' d^3\mathbf{k}' \tilde{G}^{EM}(\mathbf{R}, \mathbf{R}', \Omega_{op}) f_{c,h:nl}(\mathbf{k}', \mathbf{R}',) \right]^* \\ \left[\int d^3\mathbf{R}' d^3\mathbf{k}' \tilde{G}^{EM}(\mathbf{R}, \mathbf{R}', \Omega_{op}) f_{c,h:nl}(\mathbf{k}', \mathbf{R}') \right] \end{array} \right]$$

$$+ \frac{1}{\tau_c} \left[\frac{f_{c,c}^{eq}(\mathbf{k}, \mathbf{R})}{\int d^3\mathbf{k}' f_{c,c}^{eq}(\mathbf{k}', \mathbf{R})} \int d^3\mathbf{k}'' f_{c,c}(\mathbf{k}'', \mathbf{R}) - f_{c,c}(\mathbf{k}, \mathbf{R}) \right]$$

$$
\begin{aligned}
&\left[\frac{\hbar}{m_h^*}\mathbf{k}\cdot\nabla_{\mathbf{R}}\right] f_{h,h}(\mathbf{k},\mathbf{R}) \\
&= \int \frac{d^3\mathbf{k}'}{i\hbar(2\pi)^3}\left(V_h^t(\mathbf{k}-\mathbf{k}',\mathbf{R}) - V_h^t(\mathbf{k}'-\mathbf{k},\mathbf{R})\right) f_{h,h}(\mathbf{k}',\mathbf{R}) \\
&+\frac{i\mu_o\Omega_{op}^2|d|^2}{2\pi\hbar}\times \\
&\left[\begin{array}{c}
\left[f_{c,h:nl}(\mathbf{k},\mathbf{R}) + \chi_l(\mathbf{k},Z)\int d^3\mathbf{R}'d^3\mathbf{k}'\tilde{G}^{EM}(\mathbf{R},\mathbf{R}',\Omega_{op})f_{c,h:nl}(\mathbf{k}',\mathbf{R}')\right]^* \\
\left[\int d^3\mathbf{R}'d^3\mathbf{k}'\tilde{G}^{EM}(\mathbf{R},\mathbf{R}',\Omega_{op})f_{c,h:nl}(\mathbf{k}',\mathbf{R}')\right] \\
-\left[f_{c,h:nl}(\mathbf{k},\mathbf{R}) + \chi_l(\mathbf{k},Z)\int d^3\mathbf{R}'d^3\mathbf{k}'\tilde{G}^{EM}(\mathbf{R},\mathbf{R}',\Omega_{op})f_{c,h:nl}(\mathbf{k}',\mathbf{R}')\right] \\
\left[\int d^3\mathbf{R}'d^3\mathbf{k}'\tilde{G}^{EM}(\mathbf{R},\mathbf{R}',\Omega_{op})f_{c,h:nl}(\mathbf{k}',\mathbf{R}')\right]^*
\end{array}\right] \\
&+\frac{1}{\tau_h}\left[\frac{f_{h,h}^{eq}(\mathbf{k},\mathbf{R})}{\int d^3\mathbf{k}' f_{h,h}^{eq}(\mathbf{k}',\mathbf{R})}\int d^3\mathbf{k}'' f_{h,h}(\mathbf{k}'',\mathbf{R}) - f_{h,h}(\mathbf{k},\mathbf{R})\right]
\end{aligned}
\tag{7.11}
$$

and

$$
\begin{aligned}
&\left[-i\Omega_{op} + \frac{\hbar}{2}\left[\frac{i}{m_{c,h}^{*+}}\left(k^2 - \frac{\nabla_{\mathbf{R}}^2}{4}\right) + \frac{1}{m_{c,h}^{*-}}\mathbf{k}\cdot\nabla_{\mathbf{R}}\right]\right] f_{c,h:nl}(\mathbf{k},\mathbf{R}) \\
&= \int \frac{d^3\mathbf{k}'}{i\hbar(2\pi)^3}\left(V_c^t(\mathbf{k}-\mathbf{k}',\mathbf{R}) + V_h^t(\mathbf{k}'-\mathbf{k},\mathbf{R})\right) f_{c,h:nl}(\mathbf{k}',\mathbf{R}) \\
&-\frac{i\mu_o\Omega_{op}^2|d|^2}{2\pi\hbar}\int d^3\mathbf{R}'d^3\mathbf{k}'\tilde{G}^{EM}(\mathbf{R},\mathbf{R}',\Omega_{op})f_{c,h:nl}(\mathbf{k}',\mathbf{R}')\left[\begin{array}{c} f_{h,h}(\mathbf{k},\mathbf{R}) \\ +f_{c,c}(\mathbf{k},\mathbf{R})\end{array}\right] \\
&-\frac{f_{c,h:nl}(\mathbf{k},\mathbf{R})}{\tau_{ch}} + F_{c,h}(\mathbf{k},\mathbf{R})
\end{aligned}
\tag{7.12}
$$

7.2 Reducing Dimensionality

To reduce computation time of the Wigner functions of equations (6.121) to (6.123) approximations will be made so that there are no transverse directions in the independent variables. That is, it is desirable to remove the (X,Y) and (k_x, k_y) dependence. The subsections below will use various approximations to accomplish this.

7.2.1 Position

In the Y-direction, there is very little variation as the semiconductor layers are homogeneous and no cavity modes are formed in this direction. Therefore all Y-dependence will be removed. The X-direction is a bit more complicated because this is the direction of propagation of the electric field and, as has been shown there is therefore an X dependence on the polarization P and by equation (6.94) there is then an X dependence for f_{ch}.

From here on, only the fundamental mode (n=0) will be considered. When the cavity is near an oscillating mode the one-dimensional Greens function of equation (6.103) can be approximated as[74, 75]

$$\tilde{g}^{EM}(X, X', \Omega) \approx \frac{Z_{L,\Omega}(X) Z_{R,\Omega}(X')}{W_\Omega} \tag{7.13}$$

Substituting this into equation (6.99),

$$E(\mathbf{R}, \Omega) = \int dX' dZ' \frac{Z_{L,\Omega}(X) Z_{R\Omega}(X')}{W_\Omega} \tilde{g}^{EM}(Z, Z', \Omega)[-\mu_o \Omega^2 P(\mathbf{R}', \Omega)] = Z_{L,\Omega}(X) E(Z, \Omega) \tag{7.14}$$

where

$$E(Z, \Omega) = \int dX' dZ' \frac{Z_{R\Omega}(X')}{W_\Omega} \tilde{g}^{EM}(Z, Z', \Omega)[-\mu_o \Omega^2 P(\mathbf{R}', \Omega)] \tag{7.15}$$

Recall that the functions are peaked around Ω_{op} so that the approximate relation $E(\mathbf{R}, T) \propto Z_{L,\Omega_{op}}(X)$ can be used. Equations (6.95) and (6.94) then also imply $f_{c,h}(\mathbf{k}, \mathbf{R}, T) \approx Z_{L,\Omega_{op}}(X) f_{c,h}(\mathbf{k}, Z, T)$. From here on, the Ω_{op} term will be dropped.

At resonance, $k_o L \approx n\pi$ so that $W \approx 2ik_o(1 - r^2)$ and

$$\int_0^L dX Z_R(X) Z_L(X) \approx [r^2 + 1]L \ , \quad \int_0^L dX Z_L(X) Z_L(X) \approx 2rL \tag{7.16}$$

Equation (7.9) is multiplied by $\int_0^L \frac{dX}{L}$ to remove the X-dependence

$$\begin{aligned}
&\left[\frac{\hbar}{m_c^*}k_z\frac{\partial}{\partial Z}\right] f_{c,c}(\mathbf{k},Z) \\
&= \int \frac{dk_z'}{i\hbar(2\pi)}\left(V_c^t(k_z-k_z',Z)-V_c^t(k_z'-k_z,Z)\right) f_{c,c}(\mathbf{k}',Z) \qquad (7.17)\\
&+\frac{\mu_o\Omega_{op}^2|d|^2 rL(1+r^2)}{2\pi\hbar k_o(1-r^2)}\times \\
&\left[\begin{array}{c}
\left[f_{c,h:nl}(\mathbf{k},Z)+\frac{2rL}{k_o}\chi_l(\mathbf{k},Z)\int dZ'd^3\mathbf{k}'\tilde{g}^{EM}(Z,Z',\Omega_{op})f_{c,h:nl}(\mathbf{k}',Z')\right] \\
\left[\int dZ'd^3\mathbf{k}'\tilde{g}^{EM}(Z,Z',\Omega_{op})f_{c,h:nl}(\mathbf{k}',Z')\right]^* \\
-\left[f_{c,h:nl}(\mathbf{k},Z)+\frac{2rL}{k_o}\chi_l(\mathbf{k},Z)\int d^3Z'd^3\mathbf{k}'\tilde{g}^{EM}(Z,Z',\Omega_{op})f_{c,h:nl}(\mathbf{k}',Z',)\right]^* \\
\left[\int dZ'd^3\mathbf{k}'\tilde{g}^{EM}(Z,Z',\Omega_{op})f_{c,h:nl}(\mathbf{k}',Z')\right]
\end{array}\right] \\
&+\frac{1}{\tau_c}\left[\frac{f_{c,c}^{eq}(\mathbf{k},Z)}{\int d^3\mathbf{k}' f_{c,c}^{eq}(\mathbf{k}',Z)}\int d^3\mathbf{k}'' f_{c,c}(\mathbf{k}'',Z)-f_{c,c}(\mathbf{k},Z)\right]
\end{aligned}$$

where

$$\frac{V_i(\mathbf{k},\mathbf{R})}{(2\pi)^3}=\frac{2}{(2\pi)^3}\int d^3\mathbf{R}' e^{-2i\mathbf{k}\cdot(\mathbf{R}'-\mathbf{R})}V_i(\mathbf{R}')=\frac{2}{(2\pi)}\int dZ' e^{-2ik_z(Z'-Z)}V_i(Z')=\frac{V_i(k_z,Z)}{2\pi} \qquad (7.18)$$

This is because the applied and heterostructure potentials only vary in the Z direction. The term $|d|^2$ is the magnitude of the interband polarization ($\mathbf{d}_{c,h}\mathbf{d}_{c,h}^*$). It is assumed that the X component of the $\nabla_{\mathbf{R}}$ is small compared to the other terms as the variation over the cavity length is much slower than variation in the Z direction.

Similarly, equation (7.11) is averaged to

$$
\begin{aligned}
&\left[\frac{\hbar}{m_h^*}k_z\frac{\partial}{\partial Z}\right] f_{h,h}(\mathbf{k},Z) \\
&= \int \frac{dk_z'}{i\hbar(2\pi)}\left(V_h^t(k_z-k_z',Z)-V_h^t(k_z'-k_z,Z)\right) f_{h,h}(\mathbf{k}',Z) \qquad (7.19)\\
&+\frac{\mu_o\Omega_{op}^2|d|^2 rL(1+r^2)}{2\pi\hbar k_o(1-r^2)}\times \\
&\left[\begin{array}{c}
\left[f_{c,h:nl}(\mathbf{k},Z)+\frac{2rL}{k_o}\chi_l(\mathbf{k},Z)\int dZ'd^3\mathbf{k}'\tilde{g}^{EM}(Z,Z',\Omega_{op})f_{c,h:nl}(\mathbf{k}',Z')\right]^* \\
\left[\int dZ'd^3\mathbf{k}'\tilde{g}^{EM}(Z,Z',\Omega_{op})f_{c,h:nl}(\mathbf{k}',Z')\right] \\
-\left[f_{c,h:nl}(\mathbf{k},Z)+\frac{2rL}{k_o}\chi_l(\mathbf{k},Z)\int dZ'd^3\mathbf{k}'\tilde{g}^{EM}(Z,Z',\Omega_{op})f_{c,h:nl}(\mathbf{k}',Z',)\right] \\
\left[\int dZ'd^3\mathbf{k}'\tilde{g}^{EM}(Z,Z',\Omega_{op})f_{c,h:nl}(\mathbf{k}',Z')\right]^*
\end{array}\right] \\
&+\frac{1}{\tau_h}\left[\frac{f_{h,h}^{eq}(\mathbf{k},Z)}{\int d^3\mathbf{k}' f_{h,h}^{eq}(\mathbf{k}',Z)}\int d^3\mathbf{k}'' f_{h,h}(\mathbf{k}'',Z)-f_{h,h}(\mathbf{k},Z)\right]
\end{aligned}
$$

The terms $f_{c,c}(\mathbf{k},Z)$ and $f_{v,v}(\mathbf{k},Z)$ denote the averages of these Wigner functions over the X direction.

Equation (6.123) is multiplied by $\int_0^L \frac{dX}{2r_1L}Z_L(X)$ to remove the X dependence

$$
\begin{aligned}
&\left[-i\Omega_{op}+\frac{i\hbar}{2}\left[\frac{1}{m_{c,h}^{*+}}\left(k^2-\frac{1}{4}\frac{\partial^2}{\partial Z^2}\right)-\frac{i}{m_{c,h}^{*-}}k_z\frac{\partial}{\partial Z}\right]\right] f_{c,h:nl}(\mathbf{k},Z) \\
&= \int \frac{dk_z'}{i\hbar(2\pi)}\left(V_c^t(k_z-k_z',Z)+V_h^t(k_z'-k_z,Z)\right) f_{c,h:nl}(\mathbf{k}',Z) \qquad (7.20)\\
&-\frac{\mu_o\Omega_{op}^2|d|^2 rL}{2\pi\hbar k_o(1-r^2)}\int dZ'd^3\mathbf{k}'\tilde{g}^{EM}(Z,Z',\Omega_{op})f_{c,h:nl}(\mathbf{k}',Z')\left[f_{c,c}(\mathbf{k},Z)+f_{h,h}(\mathbf{k},Z)\right] \\
&+\frac{i}{\hbar}\int d^3\mathbf{k}' V_{s,\mathbf{k}-\mathbf{k}'}\left\{\begin{array}{l} f_{c,h:nl}(\mathbf{k},Z)\left(-f_{h,h}(\mathbf{k}',Z)-f_{c,c}(\mathbf{k}',Z)\right) \\ +f_{c,h:nl}(\mathbf{k}',Z)\left(f_{c,c}(\mathbf{k},Z)+f_{h,h}(\mathbf{k},Z)-1\right)\end{array}\right\} \\
&-\frac{f_{c,h:nl}(\mathbf{k},Z)}{\tau_{ch}}+F_{c,h}(\mathbf{k},Z)
\end{aligned}
$$

In this equation, the diagonal elements $f_{i,i}(\mathbf{k},\mathbf{R})$ have been replaced by their X-averages. The force $F_{c,h}$ is assumed to have the same position dependence as $f_{c,h:nl}$.

7.2.2 Momentum

Since there is little structure in the X-Y directions, it is assumed that the Wigner functions in momentum space in these directions will be similar to an equilibrium distribution[29]. Therefore the approximation for the Wigner functions is made[29]

$$f_{i,i}(\mathbf{k}, Z) \approx f_{i,i}(k_z, Z) 2\pi\lambda_{ij} e^{-\lambda_{ij}\frac{\mathbf{k}_\perp^2}{2}} \ , \ \lambda_{ij} = \begin{cases} \frac{\hbar^2\beta}{m_i^*} & i = j \\ \frac{\hbar^2\beta}{m_{ch}^{*+}} & i \neq j \end{cases} \tag{7.21}$$

This is a normalized Maxwellian distribution that is peaked around $\mathbf{k}_\perp^2 = 0$

Substituting these relations into equations (7.17) to (7.20), multiplying them by $\int d^2\mathbf{k}_\perp$ and performing any integrals of the form $\int d^2\mathbf{k}'_\perp$ and $\int d^2\mathbf{q}_\perp$ reduces them to

$$\begin{aligned}
&\left[\frac{\hbar}{m_c^*} k_z \frac{\partial}{\partial Z}\right] f_{c,c}(k_z, Z) \\
&= \int \frac{dk'_z}{i\hbar(2\pi)} \left(V_c^t(k_z - k'_z, Z) - V_c^t(k'_z - k_z, Z)\right) f_{c,c}(k'_z, Z) \\
&+ \frac{\mu_o \Omega_{op}^2 |d|^2 r L (1 + r^2)}{2\pi\hbar k_o (1 - r^2)} \times \\
&\left[\begin{array}{c} \left[f_{c,h:nl}(\mathbf{k}, Z) + \frac{2rL}{k_o}\chi_l(k_z, Z) \int dZ' dk'_z \tilde{g}^{EM}(Z, Z', \Omega_{op}) f_{c,h:nl}(k'_z, Z')\right] \\ \left[\int dZ' dk'_z \tilde{g}^{EM}(Z, Z', \Omega_{op}) f_{c,h:nl}(k'_z, Z')\right]^* \\ - \left[f_{c,h:nl}(k_z, Z) + \frac{2rL}{k_o}\chi_l(k_Z, Z) \int d^3Z' dk'_z \tilde{g}^{EM}(Z, Z', \Omega_{op}) f_{c,h:nl}(k'_z, Z',)\right]^* \\ \left[\int dZ' dk'_z \tilde{g}^{EM}(Z, Z', \Omega_{op}) f_{c,h:nl}(k'_z, Z')\right] \end{array} \right] \\
&+ \frac{1}{\tau_c} \left[\frac{f_{c,c}^{eq}(k_z, Z)}{\int dk'_z f_{c,c}^{eq}(k'_z, Z)} \int dk''_z f_{c,c}(k''_z, Z) - f_{c,c}(k_z, Z) \right]
\end{aligned} \tag{7.22}$$

$$
\begin{aligned}
&\left[\frac{\hbar}{m_h^*}k_z\frac{\partial}{\partial Z}\right] f_{h,h}(k_z,Z) \\
&= \int \frac{dk_z'}{i\hbar(2\pi)}\left(V_h^t(k_z-k_z',Z)-V_h^t(k_z'-k_z,Z)\right) f_{h,h}(k_z',Z) \\
&+\frac{\mu_o\Omega_{op}^2|d|^2 rL(1+r^2)}{2\pi\hbar k_o(1-r^2)}\times \\
&\left[\begin{array}{c}
\left[f_{c,h:nl}(k_z,Z)+\frac{2rL}{k_o}\chi_l(k_z,Z)\int dZ'dk_z'\tilde{g}^{EM}(Z,Z',\Omega_{op})f_{c,h:nl}(k_z',Z')\right]^* \\
\left[\int dZ'dk_z'\tilde{g}^{EM}(Z,Z',\Omega_{op})f_{c,h:nl}(k_z',Z')\right] \\
-\left[f_{c,h:nl}(k_z,Z)+\frac{2rL}{k_o}\chi_l(k_z,Z)\int dZ'dk_z'\tilde{g}^{EM}(Z,Z',\Omega_{op})f_{c,h:nl}(k_z',Z',)\right] \\
\left[\int dZ'dk_z'\tilde{g}^{EM}(Z,Z',\Omega_{op})f_{c,h:nl}(k_z',Z')\right]^*
\end{array}\right] \\
&+\frac{1}{\tau_h}\left[\frac{f_{h,h}^{eq}(k_z,Z)}{\int dk_z' f_{h,h}^{eq}(k_z',Z)}\int dk_z'' f_{h,h}(k_z'',Z)-f_{h,h}(k_z,Z)\right]
\end{aligned}
\tag{7.23}
$$

and

$$
\begin{aligned}
&\left[-i\Omega_{op}+\frac{i\hbar}{2}\left[\frac{1}{m_{c,h}^{*+}}\left(k_z^2+\Gamma-\frac{1}{4}\frac{\partial^2}{\partial Z^2}\right)-\frac{i}{m_{c,h}^{*-}}k_z\frac{\partial}{\partial Z}\right]\right] f_{c,h:nl}(k_z,Z) \\
&= \int \frac{dk_z'}{i\hbar(2\pi)}\left(V_c^t(k_z-k_z',Z)+V_h^t(k_z'-k_z,Z)\right) f_{c,h}(k_z',Z) \\
&-\frac{\mu_o\Omega_{op}^2|d|^2 rL}{2\pi\hbar k_o(1-r^2)}\int dZ'dk_z'\tilde{g}(Z,Z',\Omega_{op})f_{c,h}(k_z',Z')\left[f_{c,c}(k_z,Z)+f_{h,h}(k_z,Z)\right] \\
&+\frac{i}{\hbar}\int dk_z' V_{s,\mathbf{k}-\mathbf{k}'}\left\{\begin{array}{l}
f_{c,h:nl}(k_z,Z)\left(-f_{h,h}(k_z',Z)-f_{c,c}(k_z',Z)\right) \\
+f_{c,h:nl}(k_z',Z)\left(f_{c,c}(k_z,Z)+f_{h,h}(k_z,Z)-1\right)
\end{array}\right\} \\
&-\frac{f_{c,h:nl}(k_z,Z)}{\tau_{ch}}+F_{c,h}(k_z,Z)
\end{aligned}
\tag{7.24}
$$

where $\chi_l(k_z,Z)=\int d^2\mathbf{k}_\perp\chi_l(\mathbf{k},Z)$

The term

$$
\Gamma = 2\pi\lambda_{cv}\int d^2\mathbf{k}_\perp\mathbf{k}_\perp^2 e^{-\lambda_{ch}\frac{\mathbf{k}_\perp^2}{2}} = \frac{(\pi)^{5/2}}{\lambda_{ch}^{1/2}}
$$

is negligible. It is assumed that the random force will also have a similar momentum dependence.

7.3 Spontaneous Emission

Instead of solving equation (7.24) many times for the random force and then taking the statistical average, it is desirable to solve this only once incorporating this force in an average way. Unfortunately, this force has zero mean. However, notice that what is important in equations (7.22) and (7.23) is not actually $f_{c,h}(k_z, Z)$ but $f^*_{c,h}(k'_z, Z')f_{c,h}(k_z, Z)$. It can be also be shown that[44, 70]

$$\begin{aligned} &< f^*_{c,h:nl}(k'_z, Z')F_{c,h}(k_z, Z) >= \delta(k_z - k'_z)\delta(Z - Z')D_{c,h}(k_z, Z) \\ &\approx \delta(k_z - k'_z)\delta(Z - Z')\frac{f_{c,c}(k_z, Z)f_{h,h}(k_z, Z)}{\tau_{ch}} \end{aligned} \tag{7.25}$$

Therefore define a new function $p(k_z, Z) = \int dk'_z dZ' f^*_{c,h:nl}(k'_z, Z')f_{c,h:nl}(k_z, Z)$ which can be substituted into equations (7.22) and (7.23) to get

$$\begin{aligned} &\left[\frac{\hbar}{m^*_c}k_z\frac{\partial}{\partial Z}\right] f_{c,c}(\mathbf{k}, Z) \\ &= \int \frac{dk'_z}{i\hbar(2\pi)}\left(V^t_c(k_z - k'_z, Z) - V^t_c(k'_z - k_z, Z)\right) f_{c,c}(k'_z, Z) \\ &+ \frac{\mu_o\Omega^2_{op}|d|^2 rL(1+r^2)\tilde{g}}{2\pi\hbar k_o(1-r^2)}\left[\begin{array}{c}\left[p(k_z, Z) + \frac{2rL\tilde{g}}{k_o}\chi_l(k_z, Z)\int dZ'dk'_z p(k'_z, Z')\right] \\ -\left[p^*(k_z, Z) + \frac{2rL\tilde{g}}{k_o}\chi_l(k_Z, Z)\int d^3Z'dk'_z p^*(k'_z, Z',)\right]\end{array}\right] \\ &+ \frac{1}{\tau_c}\left[\frac{f^{eq}_{c,c}(k_z, Z)}{\int dk'_z f^{eq}_{c,c}(k'_z, Z)}\int dk''_z f_{c,c}(k''_z, Z) - f_{c,c}(k_z, Z)\right] \end{aligned} \tag{7.26}$$

and

$$\begin{aligned}
&\left[\frac{\hbar}{m_h^*}k_z\frac{\partial}{\partial Z}\right]f_{h,h}(k_z,Z)\\
&=\int\frac{dk_z'}{i\hbar(2\pi)}\left(V_h^t(k_z-k_z',Z)-V_h^t(k_z'-k_z,Z)\right)f_{h,h}(k_z',Z) \qquad (7.27)\\
&+\frac{\mu_o\Omega_{op}^2|d|^2rL(1+r^2)\tilde{g}}{2\pi\hbar k_o(1-r^2)}\left[\begin{array}{l}\left[p^*(k_z,Z)+\frac{2rL\tilde{g}}{k_o}\chi_l(k_z,Z)\int dZ'dk_z'p^*(k_z',Z')\right]\\ -\left[p(k_z,Z)+\frac{2rL\tilde{g}}{k_o}\chi_l(k_Z,Z)\int d^3Z'dk_z'p(k_z',Z',)\right]\end{array}\right]\\
&+\frac{1}{\tau_h}\left[\frac{f_{h,h}^{eq}(k_z,Z)}{\int dk_z'f_{h,h}^{eq}(k_z',Z)}\int dk_z''f_{h,h}(k_z'',Z)-f_{h,h}(k_z,Z)\right]
\end{aligned}$$

It was verified numerically that to a very high degree of accuracy, the Z component of the electromagnetic Greens function ($\tilde{g}(Z,Z',\Omega_{op})$) is approximately constant over the heterostructure being used. It is thus replaced by an average term labelled $\tilde{g}$

Equation (7.24) is then multiplied by $\int dk_z'dZ'f_{c,h}^*(k_z',Z')$ to give the equation

$$\begin{aligned}
&\left[-i\Omega_{op}+\frac{i\hbar}{2}\left[\frac{1}{m_{c,h}^{*+}}\left(k_z^2-\frac{1}{4}\frac{\partial^2}{\partial Z^2}\right)-\frac{i}{m_{c,h}^{*-}}k_z\frac{\partial}{\partial Z}\right]\right]p(k_z,Z)\\
&=\int\frac{dk_z'}{i\hbar(2\pi)}\left(V_c^t(k_z-k_z',Z)+V_h^t(k_z'-k_z,Z)\right)p(k_z',Z) \qquad (7.28)\\
&-\frac{\mu_o\Omega_{op}^2|d|^2rL\tilde{g}}{2\pi\hbar k_o(1-r^2)}\int dZ'dk_z'p(k_z',Z')\left[f_{c,c}(k_z,Z)+f_{h,h}(k_z,Z)\right]\\
&+\frac{i}{\hbar}\int dk_z'V_{s,\mathbf{k}-\mathbf{k}'}\left\{\begin{array}{l}p(k_z,Z)\left(-f_{h,h}(k_z',Z)-f_{c,c}(k_z',Z)\right)\\ +p(k_z',Z)\left(f_{c,c}(k_z,Z)+f_{h,h}(k_z,Z)-1\right)\end{array}\right\}\\
&-\frac{p(k_z,Z)}{\tau_{ch}}+\frac{f_{c,c}(k_z,Z)f_{h,h}(k_z,Z)}{\tau_{ch}}
\end{aligned}$$

The random fluctuation has been replaced by the average over the vacuum. Also, use has been made of the following fact: for a general function in two variables $f(x,y)$ that satisfies the relation

$$f^*(x',y')L_{x,y}f(x,y)=\delta(x-x')\delta(y-y')D(x,y)$$

the function $P(x,y)=\int dx'dy'f^*(x',y')f(x,y)$ will satisfy the relation

$$L_{x,y}P(x,y)=D(x,y)$$

Equations (7.26), (7.27) and (7.28) are the final results for this model. With these, the operating characteristics of interest can be determined simply from the input applied potential, heterostructure, cavity structure and the time constants τ_c, τ_h and τ_{ch}.

To summarize, equation (7.26) describes the conduction band Wigner functions under various effects. The second row of this equation describes the total potential, which is the combined heterostructure, applied bias and electrostatic (to be discussed in more detail shortly) effects. The third row describes the interaction with a classical electric field using the approximation of separating the polarization into linear and non-linear components.. The fourth row is a phenomenological approximation for the phonon and Coulombic effects. These can be expanded in more detail as shown in equation (6.121) if desired. Equation (7.27) is similar except that it describes the holes.

Equation (7.28) describes the evolution of a function that is related to the non-linear off-diagonal components. The first row describes kinetic effects. As with the previous equation second and third lines describe the total potential and classical electric field interactions. The fourth row has a phenomenological term for the phonon and Coulombic scattering as well as a term for spontaneous emission.

These equations will be solved in the next section for a sample case to demonstrate some of the numerical techniques involved as well as some of the information that can be extracted.

7.4 Numerical Method

This section discusses the numerical implementation of equations (7.26) to (7.28). This is solved in a manner similar to those used to solve the Wigner functions of resonant tunneling diodes[29, 31].

7.4.1 Grid

The simulated region is discreetized according to the grid shown in figure 7.1 [29]. It is discreetized this way to take advantage of the equilibrium incoming and outgoing boundary conditions that can be assumed if the boundaries are far enough away from any structure.

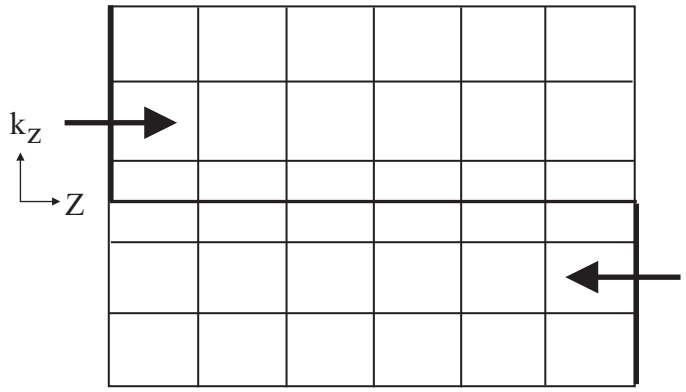

Figure 7.1: A Representation of the Grid Wigner Functions are Discreetized upon for Numerical Solutions

On this grid, the Wigner functions are discreetized as [29, 31]

$$f(k_z, Z) \rightarrow f(k_n, Z_m) = f(n, m) \tag{7.29}$$

where f is any one of the Wigner functions. The grid position variable is

$$Z_m = m\Delta_z,\ m = 0...N_z,\ N_z = L/\Delta_z \tag{7.30}$$

the momentum are discreetized as

$$k_n = \Delta_k \left[n - \left(\frac{N_k + 1}{2} \right) \right],\ n = 1...N_k,\ \Delta_k = \frac{\pi}{N_k \Delta_z} \tag{7.31}$$

The choice of Δ_k is motivated by the desire to avoid $k_z = 0$ and to satisfy the Fourier completeness relation which implies that this discreet model exactly satisfies the continuity equation for the diagonal Wigner functions[29].

7.4.2 Center Upwind Finite Difference

From figure 7.1 there are the two types of carriers, outgoing ($k_z > 0$) and incoming ($k_z < 0$). The discreetization will be different for each type of carrier in order to incorporate boundary conditions correctly. Outgoing carriers will depend on the left boundary condition and

incoming carriers will depend on the right boundary condition. For the first derivative discreetize as [31]

$$\frac{\partial}{\partial z}f(z,K_z)=\begin{cases}\frac{-f(m+2,n)+4f(m+1,n)-3f(m,n)}{2\Delta_z} & n\leq\frac{N_k}{2}\\ \frac{f(m-2,n)-4f(m-1,n)+3f(m,n)}{2\Delta_z} & n>\frac{N_k}{2}\end{cases} \tag{7.32}$$

and second derivatives

$$\frac{\partial^2}{\partial z^2}f(z,K_z)=\begin{cases}\frac{f(m+4,n)-8f(m+3,n)+22f(m+2,n)-24f(m+1,n)+9f(m,n)}{4\Delta_z^2} & n\leq\frac{N_k}{2}\\ \frac{f(m-4,n)-8f(m-3,n)+22f(m-2,n)-24f(m-1,n)+9f(m,n)}{4\Delta_z^2} & n>\frac{N_k}{2}\end{cases} \tag{7.33}$$

The integrals over momentum are converted to sums as $\sum_{n=-N_k/2+1}^{N_k/2}$ the integral in position for the EM contribution will be $\sum_{m=0}^{N_z}$ because the functions vanish outside this region.

Integrals are replaced by sums in the usual way. For the integral of the potential terms like

$$V^a(k_z,Z)=2\int dZ' e^{-ik_z(Z'-Z)}V^a(Z')$$

this must be replaced by the discreetized version

$$V^a(n,m)=2\sum_{m'=-N_k/2+1}^{N_k/2} e^{-i\Delta_k\Delta_Z(m'-m)}V^a(m')$$

because it is a finite Fourier transform.

There will be cases when $m'-m$ is outside the region of calculation. It is found to be sufficient to just use the value of the potential at the boundary [29].

7.4.3 Boundary Conditions

A benefit of the Wigner functions that has been mentioned is the simplicity of the boundary conditions. The diagonal components at the Boundaries are Fermi functions averaged over $k_\perp$ [29, 31, 33, 58]

$$f_{cc}(k_z\begin{matrix}>\\<\end{matrix}0,Z=\begin{matrix}0\\L_z\end{matrix})=\frac{m_e k_B T}{\pi\hbar^2}\ln\left[1+\exp\left(\frac{-1}{k_BT}\left(\frac{\hbar^2k_z^2}{2m_e}+\varepsilon_e-E_e^f(\begin{matrix}0\\L_z\end{matrix})\right)\right)\right] \tag{7.34}$$

and

$$f_{hh}(k_z \begin{matrix} > \\ < \end{matrix} 0, \begin{matrix} 0 \\ L_z \end{matrix}) = \frac{m_h k_B T}{\pi \hbar^2} \ln \left[1 + \exp \left(\frac{+1}{k_B T} \left(\frac{\hbar^2 k_z^2}{2m_h} + \varepsilon_h - E_h^f(\begin{matrix} 0 \\ L_z \end{matrix}) \right) \right) \right] \tag{7.35}$$

where ε_α is the band-edge potential and $E_\alpha^f(\begin{matrix} 0 \\ L_z \end{matrix})$ are the Fermi energies at $Z = 0$ and L_z. L_z is the length of the structure. Since the boundaries are assumed to be in equilibrium, there really is only one Fermi level for each side [12] but E_e^f and E_h^f will be with respect to different energies. The Fermi levels are found by knowledge of the doping in the system, equation (3.54) and the knowledge that the total density in (3.53) is zero in equilibrium. As discussed in the next section, the carrier densities will change at each iteration thus the Fermi levels must be recalculated for each iteration.

The off-diagonal component $p(k_z, Z)$ can cause problems due to reflections at the boundaries. One solution to overcome this is to use absorbing boundary conditions [79]. This was done by setting periodic boundary conditions and adding an imaginary component to the heterostructure for the off-diagonal components for positions at and past the boundaries.

7.4.4 Self-Consistency

As with the conventional model, electrostatics has the effect of modifying the potential profile. A method similar to 3.6.1 must be used where the heterostructure potential is recalculated after each iteration. However, in this case the carrier density is not determined from equation (3.54) but by using the Wigner functions with

$$\rho_\alpha(z) = \int \frac{dk}{2\pi} f_{\alpha,\alpha}(k, z) \ \rightarrow n(i) = \sum_{n=1}^{N_k} f_{\alpha,\alpha}(n, m) \tag{7.36}$$

The boundary conditions for the potential $\phi(Z)$ in Poisson's equation are the band offset plus the Fermi-level at each end [12]. The first guess at the total potential term ($V^t = V + V^{app}$) is the flat-band heterostructure offsets (V) added to a linear-varying applied potential V^{app}. That is, for V^{app}, the applied bias is added to the Fermi-level difference. This is taken as the potential difference between the left and right side of the structure. A straight-line is then drawn between these two points and this line gives the initial guess

at the applied potential of each point along the structure. Each iteration will then update V^t.

7.5 Example

A structure that is similar to that by Tsuchiya and Miyoshi [33] (which was for electron and hole transport with no field coupling) is used for sample calculations to demonstrate the computational utility and as for comparisons to some of their calculations. This is more of a test system than a realistic situation. This is a system that consists of 5 layers, two barrier layers of 15 nm length and $In_{0.72}Ga_{0.28}As_{0.61}P_{0.39}$ composition and a 7 nm well with composition $In_{0.72}Ga_{0.47}As$. The outer cladding and substrate were taken to be 20μm InP layers. These are required in order to get confined electric field modes. The grid-size is chosen to be $\Delta_z = 0.5nm$ and then the appropriate momentum grid is found from equation (7.31). This will be referred to later as the *normal grid-size*. The effective mass was constant across the system and were $m_e = 0.05m_o$, $m_h = 0.48m_o$ where m_o is the bare electron mass. The band offset was estimated using the relation $\Delta_c/E_g = 0.4$. Dielectric constants for each layer were found by the interpolation formula and data in Appendix A. The structure is n-doped (introduction of impurity donor atoms) in the left barrier and p-doped (introduction of impurity acceptor atoms) in the right barrier both at magnitude $5{\times}10^{18}/\text{cm}^3$. The doping will affect the Fermi levels of these layers in such a way to prevent current flow until a potential bias counteracting this is applied. For example, figure 7.2 shows how the doping affects the potential profile when no bias is applied and figure 7.3 shows the effect on the structure when a bias is applied.

7.5.1 Power Out

One of the expectation values that can be found using the Wigner function has been shown already. That being the carrier density. Another that can be found is the power output. Here, it will be solved for the TE mode. Once again, the power is given using the Poynting Vector $\mathbf{S} = \mathbf{E} \times \mathbf{H}^*$. Maxwell's equation

$$\nabla \times \mathbf{E} = -\partial_T \mathbf{H}^* \tag{7.37}$$

implies $\mathbf{H}^{\pm}$ will be proportional to $\mathbf{E}^{\pm}$. In the rotating wave approximation, the Poynting vector can then be written as $\mathbf{S} = \mathbf{E}^{+} \times \mathbf{H}^{+*} + \mathbf{E}^{-} \times \mathbf{H}^{-*}$. The positive and negative frequency components will give the same power output so that this can be rewritten as $\mathbf{S} = 2\mathbf{E}^{+} \times \mathbf{H}^{+*}$ therefore it is only required to work with $\mathbf{E}^{+}$.

From (7.37)

$$\mathbf{H}^{+} = -\frac{i}{\mu\Omega} \begin{pmatrix} -\partial_Z E_Y^{+} \\ 0 \\ \partial_X E_Y^{+} \end{pmatrix} \tag{7.38}$$

The Poynting vector then propagating in the X-direction is

$$S^X = \frac{i}{\mu\omega} E_Y^{+} \partial_X E_Y^{+} \tag{7.39}$$

Recall $E_Y^{+}(\mathbf{R} = Z_L(X) E_Y^{+}(Z)$ so that

$$Z_L(X) \left[\partial_X Z_L(X)\right]^* = i k_o^* [(1 - r^2) - i2r \sin(2k_o X)] \tag{7.40}$$

thus

$$S^X = \frac{k_o^*}{\mu\Omega} \left[i2r \sin(k_o x) 0 (1 - r^2)\right] |E_Y^{+}(Z)|^2 \tag{7.41}$$

At the boundaries X=0,L so that this gives the power out as

$$S_{out}^X = \frac{2k_o^*}{\mu\Omega} (1 - r^2) |E_Y^{+}|^2 \tag{7.42}$$

The factor of 2 is introduced for the $^-$ components. Using equation (6.116) there is the relation

$$E_Y^{+}(Z) = \frac{\mu\Omega_{op}^2 d_{c,h,Y}^*}{2\pi} \frac{[1 + r^2] L_{cav} \tilde{g}}{i k_o [1 - r^2]} \int dk_z' dZ' f_{ch:nl}(k_z', Z') \tag{7.43}$$

Which gives the Poynting vector

$$\begin{aligned} S^X &= \frac{2k_o^* [1 - r^2]}{\mu\Omega_{op}} \left| \frac{\mu\Omega_{op}^2 d_{c,h,Y}^* [1 + r^2] L_{cav} \tilde{g}}{2\pi i k_o [1 - r^2]} \right|^2 \int dk_z' dZ' f_{c,h:nl}^*(k', z') \int dk_z dZ f_{c,h:nl}(k_z, Z) \\ &= \frac{2\mu\Omega_{op}^3 d_y^2 [1 + r^2] L_{cav}^2 \tilde{g}^2}{(2\pi)^2 k_o [1 - r^2]} \int dk_z dZ p(k_z, Z) \end{aligned} \tag{7.44}$$

where the real part of k_o is taken. This will give the power density. To get the total power, multiply this by the cross-sectional area perpendicular to X ($L_Y L_Z$). The field is assumed

constant in the Y direction so L_y is just the stripe width. L_Z must be found with a bit more care. This is the direction of the electric field envelope. To approximate the length to use in the direction, the FWHM of this function will be taken.

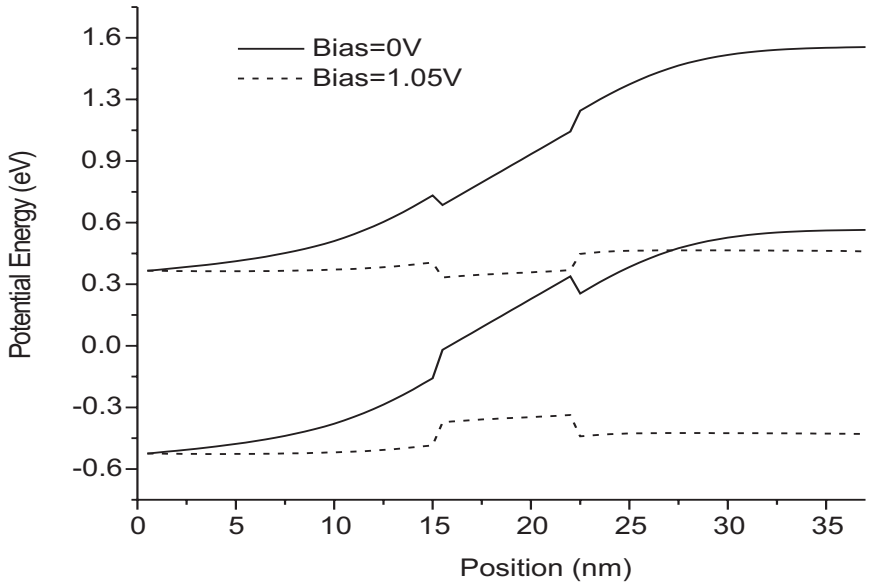

Figure 7.2: The Total Potential (Heterostructure Plus Applied Bias Plus Electrostatic Effects) of the Laser of Applied Biases 0 and 1.05V. No Electromagnetic Coupling.

Figures 7.2 and 7.3 show the total potential (V^t) that the carriers experience (heterostructure, Fermi potentials due to doping, applied potential bias and electrostatic effects) when uncoupled from the electric field. This is found by summing all these potentials after the system has reached self-consistency. At zero bias, the potential is such that no carriers can localize around the well as seen in figure 7.4. The application of the bias will tend to flatten the band. The flatter the potential the more carriers there are localized around the well as shown in figures 7.5 and 7.6 which give the densities for the corresponding potentials in 7.2 and 7.3. This is how the concentration of carriers is controlled in this system. The hole concentrations shown in figure 7.6 are not smooth in the well region because there is more than one confined mode energy in the well[33]. From here, it can be seen why the flat-band approximation used in the conventional model is not completely accurate. Note that the results presented are not identical to the ones in [33] because this

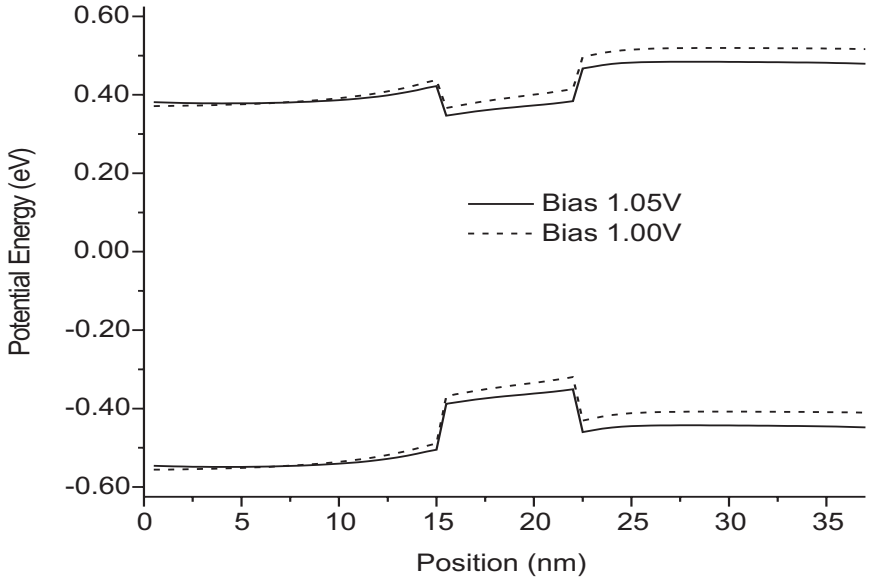

Figure 7.3: The Total Potential (Heterostructure Plus Applied Bias Plus Electrostatic Effects) of the Laser of Applied Biases 1.00 and 1.05V. No Electromagnetic Coupling.

solution does not have varying effective masses or the light-hole band.

Figures 7.7 and 7.8 show the Wigner functions for the case of 1.00 V bias applied across the structure. Once again, these look very much like phase-space distributions but they are not exactly due to Heisenberg uncertainty [29].

When the electric field is coupled to the system, some of the carriers will recombine and emit light. This can be seen in figures 7.9 and 7.10 where the concentration in the well is lower when electric field coupling is included. This causes the power output of figure 7.11. It can be seen that the power increases with increasing bias and has a resonant frequency near the band-gap energy. In this case, there is an energy shift between the two biases (compare this to figure 5.15) this is because coulombic renormalizations have not been included in this example which shift the energy. This is not exactly the gain found in the conventional model(indeed, gain is just an approximation that the power will be of a simple exponential form), but there is a close relationship between steady-state power and gain as can be seen by equation(4.16). This approximation could be used if one is interested in estimating a gain of the system.

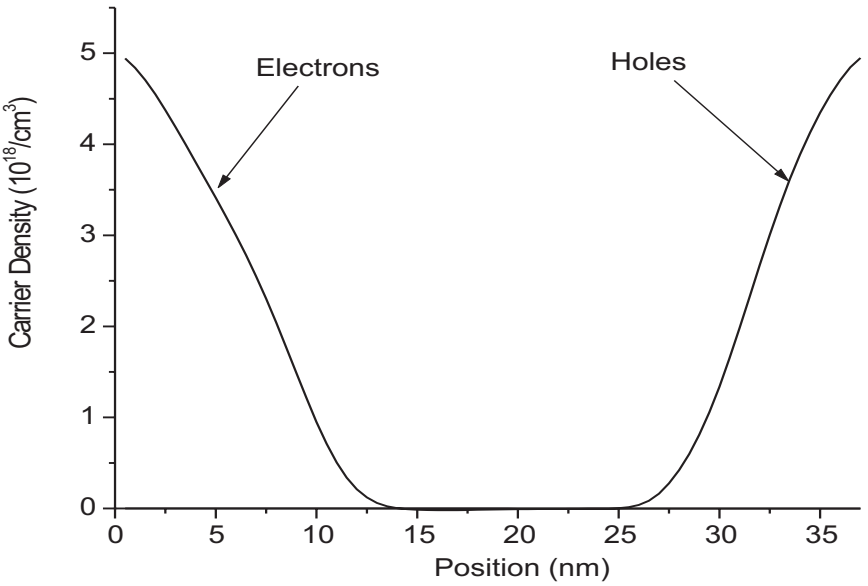

Figure 7.4: Concentration of the Electrons and Holes at Zero Applied Bias

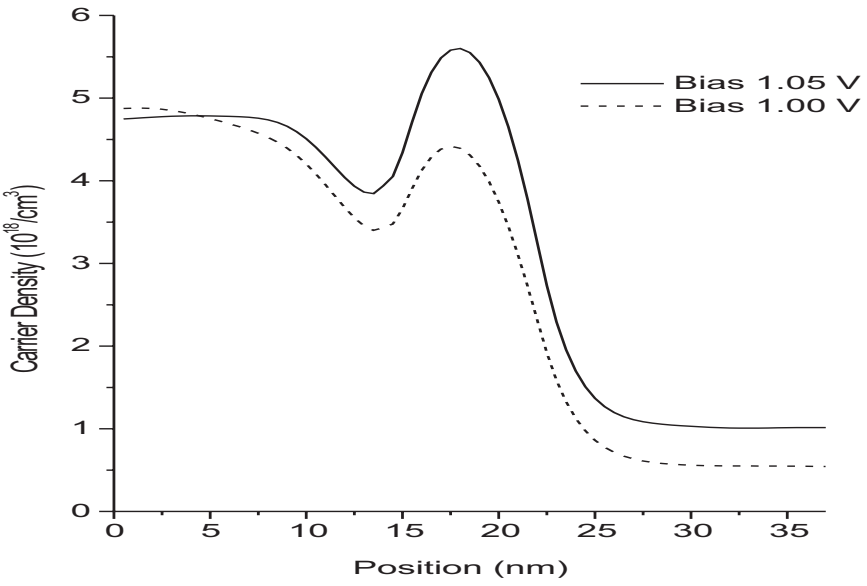

Figure 7.5: Electron Concentrations in the Laser Structure for Applied Potential Bias 1.00 and 1.05V. No Electromagnetic Coupling.

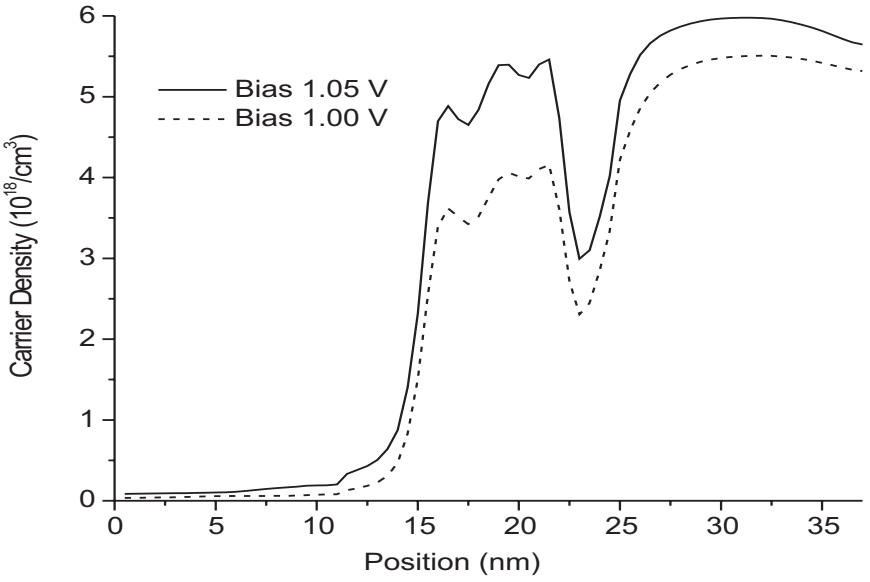

Figure 7.6: Hole Concentrations in the Laser Structure for Applied Potential Bias 1.00 and 1.05V. No Electromagnetic Coupling.

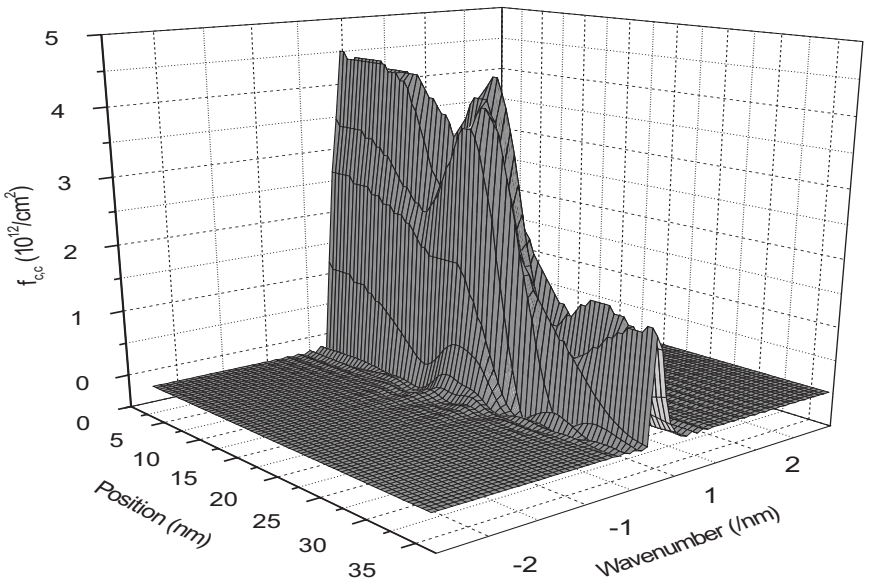

Figure 7.7: Electron Wigner Function for Bias 1.00V. No Electromagnetic Coupling.

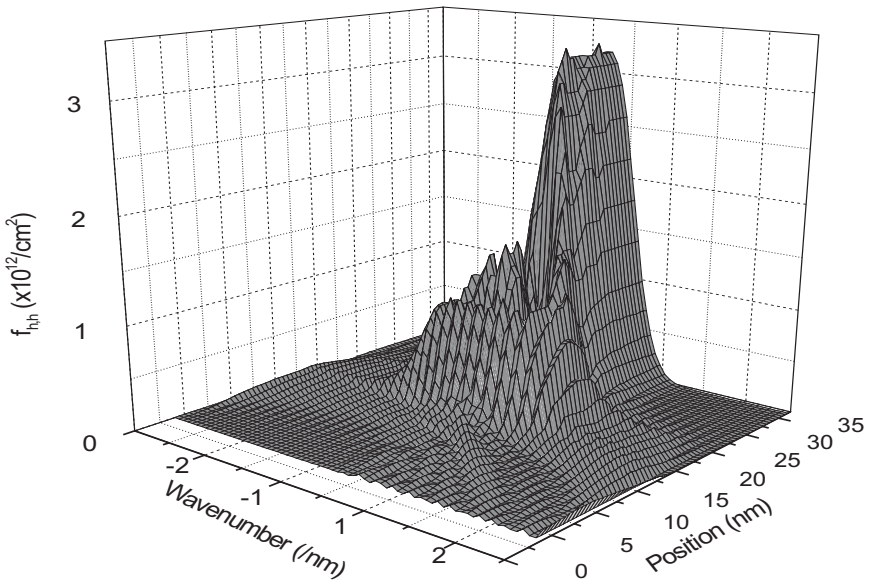

Figure 7.8: Hole Wigner Function for Bias 1.00V. No Electromagnetic Coupling.

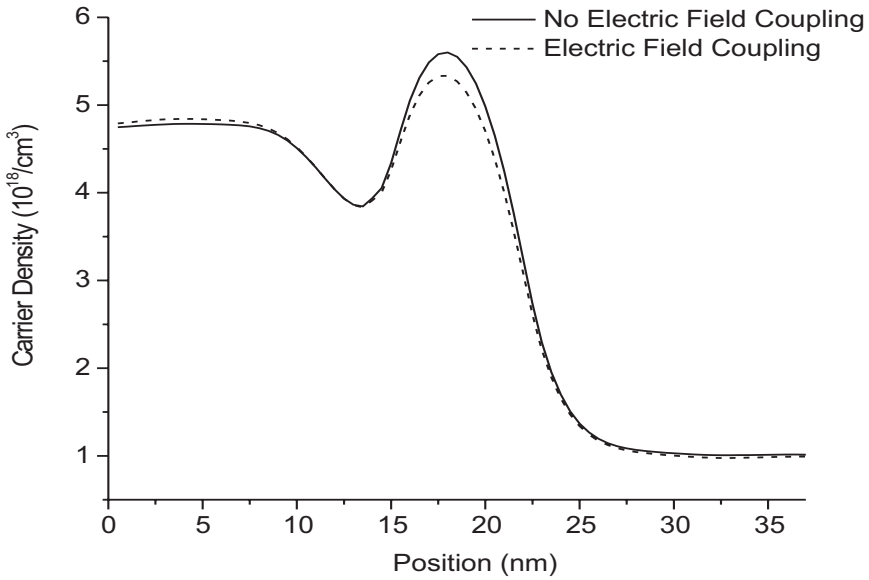

Figure 7.9: Electron Concentrations for Applied Bias 1.05V with and without Electromagnetic Coupling at Photon Energy 0.775 eV

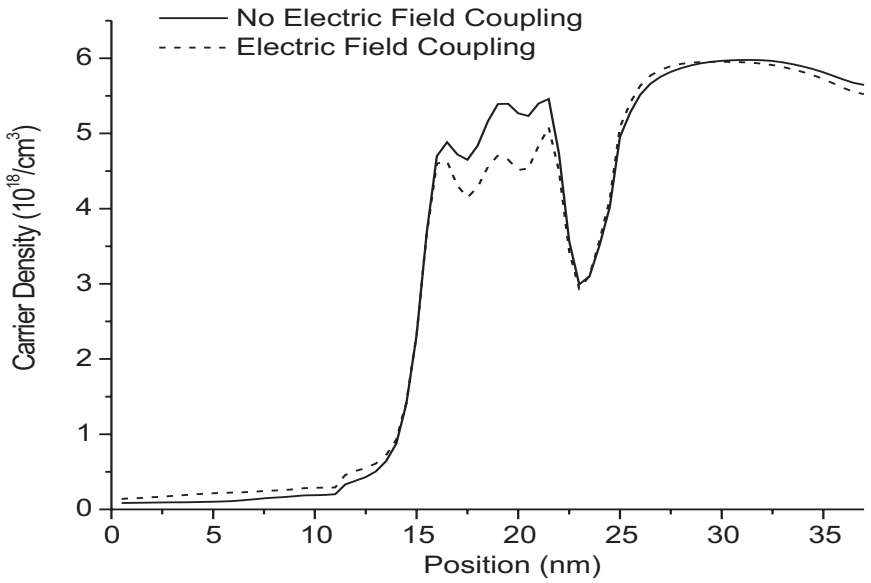

Figure 7.10: Hole Concentrations for Applied Bias 1.05V with and without Electromagnetic Coupling at Photon Energy 0.775 eV

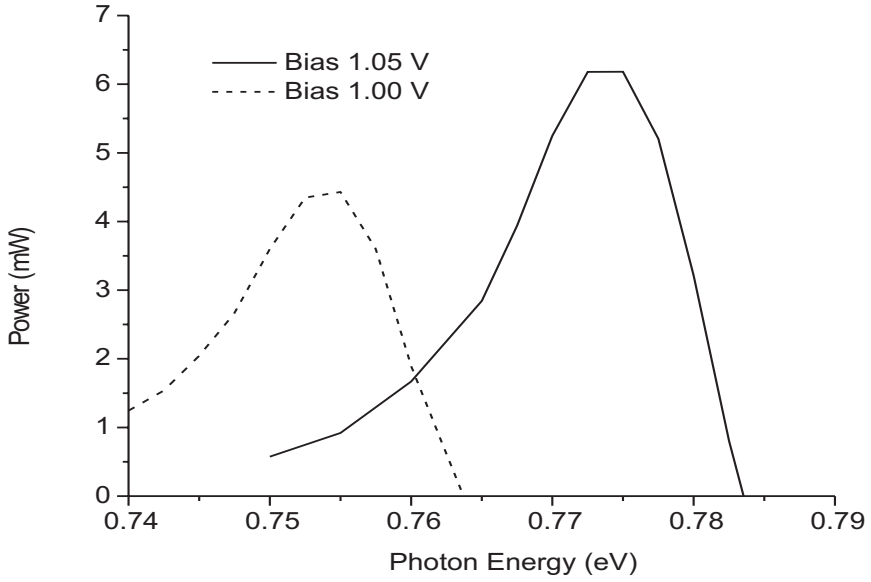

Figure 7.11: Photon Power Output Versus Photon Energy for Applied Bias Potential 1.00 and 1.05V

One can get a power-current relationship from the method as well since the current can be found with the formula

$$j_\alpha(Z) = q_\alpha \int \frac{dk_z}{2\pi} \frac{\hbar k_z}{m_\alpha} f_{\alpha,\alpha}(k_z, Z) \tag{7.45}$$

where q_α is the charge of this carrier type. Since the system is not in equilibrium,, the current will not be constant across the structure. This is shown in figure 7.12. It can be seen from this graph that this structure is not very efficient and has high electron leakage current (the relatively straight part of the graphs) and requires high injection currents (the spikes near the well) for lasing. This is interesting because in order to increase efficiency by lowering leakage current, this model will be very useful in determining a structure to do this.

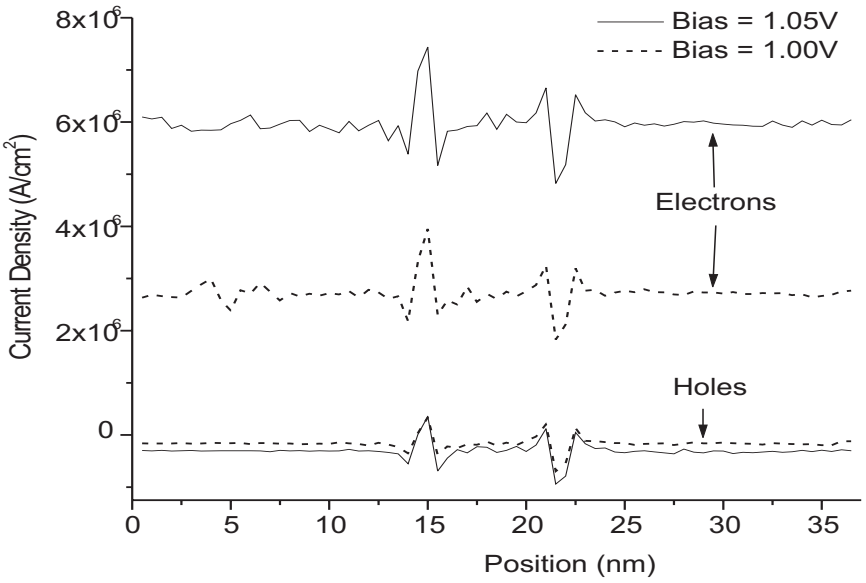

Figure 7.12: Electron and Hole Current in the Structure at Applied Potential Biases 1.00 and 1.05V. No Electromagnetic Coupling.

7.6 Errors

There are two major types of errors for these calculations. The first is due to the numerical methods and grid-size used. The errors due to the numerical differentiation will be of the order Δz^2 (that was the purpose of using center difference methods) and numerical integration of the order Δz. The system is too complicated to give an analytic estimate of the errors, but a numerical estimate is shown in figures 7.13 and 7.14 by calculating the concentrations of the electrons and holes in a system uncoupled with the EM field and a grid twice as fine as the normal grid-size. These calculations are compared to the calculations on the normal grid-size. As can be deduced from these figures, the error is small enough that the physical effects of EM coupling are not within this range of error.

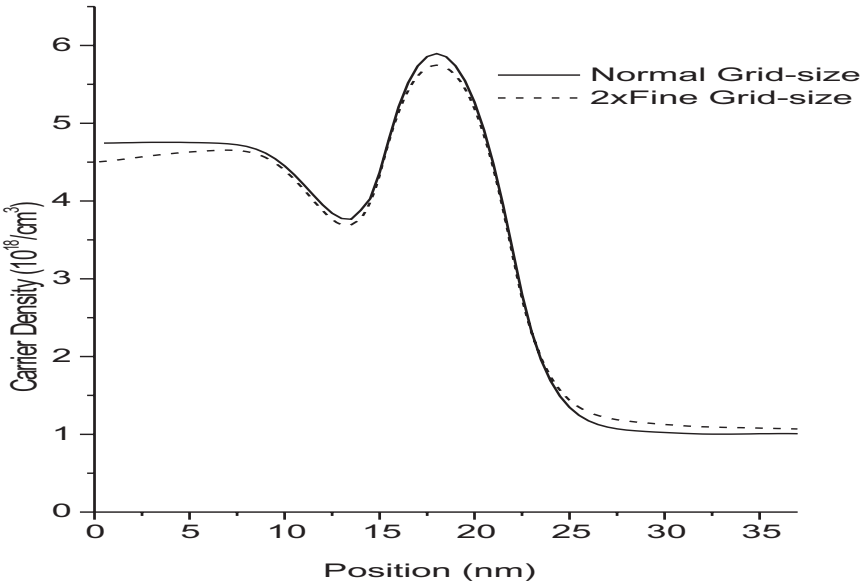

Figure 7.13: Electron Concentrations at Two Grid-sizes, the Normal Grid-size and one 2X as fine. The Applied Potential Bias is 1.05V and there is no Electromagnetic Coupling.

The second group of even more difficult to quantify errors are due to the physical approximations made to arrive at the QBE and the reduction for computational practicality. In particular the approximations of the phonon and Coulombic scattering will be the major sources of error. More intensive calculations with greater details of these interactions will

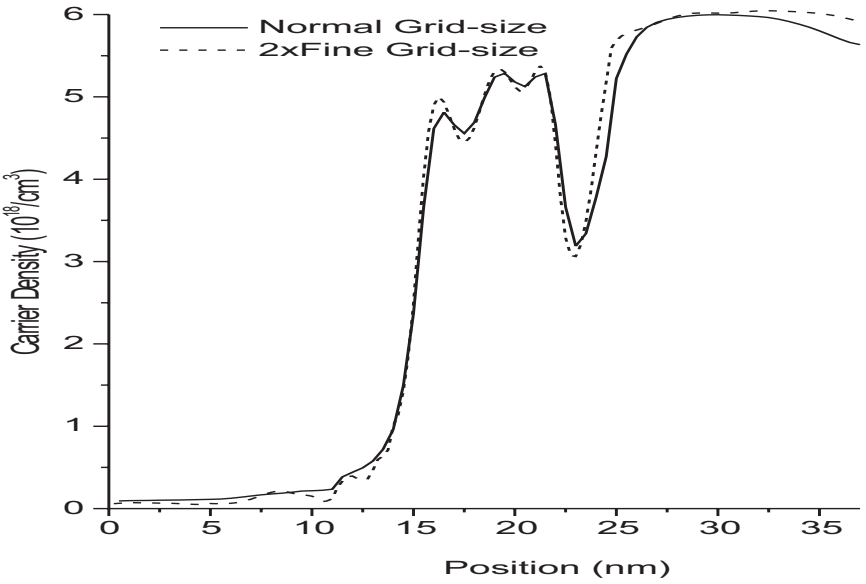

Figure 7.14: Hole Concentrations at Two Grid-sizes, the Normal Grid-size and one 2X as fine. The Applied Potential Bias is 1.05V and there is no Electromagnetic Coupling.

reduce these errors. To numerically determine the magnitudes of these errors, it will be necessary to compare the results obtained with this model to some experimental results. This will be done in the future when a more realistic heterostructure is modeled.

7.7 Summary

This chapter begins with specific simplifications to the general QBE of chapter 6 to arrive at a computationally practical set of equations. There are three major reductions made to the equations of chapter 6. The polarization is separated into linear and non-linear polarization. The purpose of this separation is so that the next approximation, the reduction in dimensionality can be performed. The final manipulation is to define a new function based on the off-diagonal Wigner functions that would allow spontaneous emission to be incorporated in an average way. The first manipulation has been used by others [43], the second manipulation contains approximations made before (diagonal Wigner function momentum [29]). The last manipulation has not been seen before by the author but builds on

some known relations of Langevin theory. The chapter concludes with some original sample calculations of this set of equations for a structure simplified from [33]. The numerical techniques for the diagonal Wigner functions are quite common.

Chapter 8

Conclusions

8.1 Conventional Model

A model of the quantum well laser has been derived using conventional methods. This model includes the spectral property of gain and dynamic properties of photon density and carrier densities. These can be used together for a complete model or can be calculated separately. Included in the gain calculations are the effects of electrostatic and Coulombic renormalization.

Results have been presented for the gain, steady-state power and modulation response of various lasers. Some of this data has been compared to experiment.

These models are very useful if what is required is to extract parameters or predict characteristics for a narrow class of lasers when there is some experimental or given data already available. It can also be used to estimate some *quality factors* when making slight modifications to known laser designs and input parameters. They are limited however by the large amount of phenomenological parameters required.

8.2 Wigner Model

The Wigner function model has been formulated (to the author's knowledge, for the first time) as a more rigorous description of the quantum well laser. This model includes in

a detailed manner phonon, electromagnetic, heterostructure and Coulombic interactions. Along the way, various simplifications and approximations have been made, these can be removed if certain aspects or increased details are required. As this model does not rely so heavily on phenomenological parameters, it can be used as a basis for a more advanced analysis of the QW laser than the conventional model with enhanced predictive power of quantum interference effects.

An example is given showing calculation techniques useful to extract data from this model. A single quantum well laser is modeled and the Wigner functions, carrier concentrations, current distribution and steady-state power output are presented. It is a great benefit that this method utilizes the combination of transport (current) and spectral (power - gain) properties. There are still practical challenges however, as it is quite numerically intensive. It is therefore necessary to simplify some of the calculations such as reducing the number of subbands considered. Methods to shorten the computation time must be researched.

8.3 Future Directions

The Wigner function model forms a solid basis for a more advanced analysis. Much work still needs to be done. It is desirable to extend this from two-bands to multi-bands by incorporating the spin coupling in the Luttinger-Kohn formalism. Other improvements of interest are more detailed phonon models with confined mode phonons, and varying effective mass through the structure. Also a significant development to enable this to be a practical complete model is to couple it with a semi-classical model such as drift-diffusion for regions far from the active region. When these more detailed effects are taken into account, the calculations can then be compared to experimental results to test the errors of various approximations and perform any parameter fitting depending on the simplifications utilized.

Part III

Appendices

Appendix A

Glossary of Terms and Data Tables

This section will list some of the variables and parameters used in this thesis. The variables listed chapter by chapter are those that may be confusing due to similar symbols used to represent other terms. In this thesis notation following the standard literature was used. Unfortunately, combining various theories together will sometimes result in an overlap of symbols.

A.1 Glossary

A.1.1 Chapter 2

V : Volume used in box-normalization.
S : A Term in the 4×4 LK Hamiltonian.
S : Area used in box-normalization. (In context not to be confused with above).
L : Length used in box-normalization.
T : Time used in box-normalization.
m_o : Bare electron mass.
γ_i : The various Luttinger coefficients.
E_g : Band-gap
β : Longitudinal EM field mode.

A.1.2 Chapter 3

g_α : Modal gain of the α (frequency and longitudinal) mode.
ε : Dielectric permitivity.
$\mathbf{J}$: Macroscopic current density.
$\mathbf{j}$: Microscopic current density.
$\mathbf{A}$: Electromagnetic vector potential.
τ : Scattering time.
$\mathbf{S}$, S^x Vector and x-component of Poynting vector.

A.1.3 Chapter 4

J : Injection current density.
L_S : SCH length.
ϵ : Spectral hole burning coefficient.
β : Spontaneous emission coefficient.
S_ω : Photon density for ω frequency mode.
S : Photon density for a single mode.
L : Cavity length.
T_i : Carrier temperature in carrier heating model.

A.1.4 Chapter 6

$x_i = (\mathbf{r}_i, t_i)$: General position and time coordinates.
G^α : Various real-time Greens functions
$\Theta(t)$: Step function.
Σ : Self-energies.
V^α : Various types of classical potentials.
$\mathbf{d}_{ij}$: Interband polarization.
$X = (\mathbf{R}, T)$: "Macroscopic" center of mass variables. (see section 6.2.1)
$x = (\mathbf{r}, t)$: "Microscopic" center of mass variables. (see section 6.2.1)
$(\mathbf{k}, \omega)$ Wigner coordinates.
$f_{i,j}$: Wigner function.

ϵ : Band-energies used for demonstration purposes in section 6.2.5.

ε_{ij} : Band-gap energy between i and j band.

ε : Dielectric permitivity.

Ω : Frequency mode.

$k_{n,\Omega}$: Propagation constant at nth Longitudinal and Ω frequency modes.

$r, r_1, r2$: Mirror reflectivities.

A.1.5 Chapter 7

p : Function defined from the off-diagonal Wigner functions in section 7.3.

A.2 Data Tables

$In_{1-x}Ga_xAs_yP_{1-y}$ interpolation:

(GaAs)xy+(InP)(1-x)(1-y)+(InAs)(1-x)y+(GaP)x(1-y)

Quantity	*GaAs*	*InAs*	*InP*	*GaP*
m_e/m_o	0.067	0.023	0.077	0.25
m_{hh}/m_o	0.5	0.40	0.60	0.67
γ_1	6.8	20.4	4.95	4.05
γ_2	1.9	8.3	1.65	0.49
γ_3	2.73	9.1	2.35	1.25
$a_o(x10^{-10}m)$	5.6533	6.0584	5.8688	5.4505
$E_p(eV)$	25.7	22.2	20.7	22.2
C_{11}dyne/cm^2	11.879	8.329	10.11	14.05
C_{12}dyne/cm^2	5.376	4.526	5.61	6.203

Band-gap[25] $E_g = 1.35+0.642x-1.101y+0.758x^2+0.101y^2-0.159xy-0.28x^2y+0.109xy^2$

Momentum Matrix Elements

heavy hole

$$\langle S\uparrow|\mathbf{p}|3/2,3/2\rangle = -\left[(\cos\phi - i\sin\phi\hat{x} + (\sin\phi + i\cos\phi)\hat{y}\right]\frac{P_x}{\sqrt{2}}$$

$$\langle S\downarrow|\mathbf{p}|3/2,3/2\rangle = 0$$

$$\langle S\uparrow|\mathbf{p}|3/2,-3/2\rangle = 0$$

$$\langle S\downarrow|\mathbf{p}|3/2,-3/2\rangle = -\left[(\cos\phi + i\sin\phi\hat{x} + (\sin\phi - i\cos\phi)\hat{y}\right]\frac{P_x}{\sqrt{2}}$$

light hole

$$\langle S\uparrow|\mathbf{p}|3/2,1/2\rangle = \sqrt{\frac{1}{6}}P_x\hat{z}$$

$$\langle S\downarrow|\mathbf{p}|3/2,1/2\rangle = \frac{-1}{\sqrt{6}}\left[(\cos\phi - i\sin\phi\hat{x} + (\sin\phi + i\cos\phi)\hat{y}\right]\frac{P_x}{\sqrt{2}}$$

$$\langle S\uparrow|\mathbf{p}|3/2,-1/2\rangle = \frac{1}{\sqrt{6}}\left[(\cos\phi + i\sin\phi\hat{x} + (\sin\phi - i\cos\phi)\hat{y}\right]\frac{P_x}{\sqrt{2}}$$

$$\langle S\downarrow|\mathbf{p}|3/2,-1/2\rangle = \sqrt{\frac{1}{6}}P_x\hat{z}$$

where $P_x^2 = m_o E_p/2$, $S\uparrow$ and $S\downarrow$ are the up and down spins for the conduction band Bloch functions.

Dipole matrix element: $|d|^2 = \frac{q^2 E_p}{3m_o\Omega_{op}^2}$

Appendix B

Orthogonality of Fields

The optical power density of the field is

$$\mathbf{S} = \frac{1}{2} Re[\mathbf{E} \times \mathbf{H}^*] \tag{B.1}$$

Thus for modes to be orthogonal, we define the orthogonality condition

$$\int d^3\mathbf{r}\mathbf{E}_{\omega\beta}(\mathbf{r},t) \times \mathbf{H}^*_{\omega\beta'}(\mathbf{r},t) \propto \delta_{\beta,\beta'} \tag{B.2}$$

This means that each component of the vector must be orthogonal.

Again, for the TE modes, only the x component of the electric field is non-zero then using equation (2.24) the orthogonality condition of equation (B.2) implies

$$\int d^3\mathbf{r} E^x_{\omega,\beta}(\mathbf{r}) \frac{\partial}{\partial x} E^{y*}_{\omega,\beta'}(\mathbf{r}) \propto \delta_{\beta,\beta'}$$

which implies

$$\int dz E^x_{\omega,\beta}(z) E^{y*}_{\omega,\beta'}(z) \propto \delta_{\beta,\beta'} \tag{B.3}$$

which then can be normalized to get

$$\int_0^L dz F_{\omega\beta}(z) F^*_{\omega\beta'}(z) \propto \delta_{\beta,\beta'} \tag{B.4}$$

For the TM modes, only the y component of the magnetic field is non-zero. Using equation (2.25) we can extract an orthogonality condition from equation (B.2) of

$$\int d^3\mathbf{r} \frac{1}{\varepsilon(z)} \frac{\partial}{\partial x} H^y_{\omega\beta'}(\mathbf{r}) \times H^{y*}_{\omega\beta'}(\mathbf{r}) \propto \delta_{\beta,\beta'}$$

which implies

$$\int dz \frac{H^y_{\omega\beta'}(z) H^{y*}_{\omega\beta'}(z)}{\varepsilon(z)} \propto \delta_{\beta,\beta'} \tag{B.5}$$

normalizing gives

$$\int_0^L dz \frac{G_{\omega\beta}(z) G^*_{\omega\beta'}(z)}{\varepsilon(z)} \propto \delta_{\beta,\beta'} \tag{B.6}$$

Appendix C

Relations for the Perturbation Hamiltonian

An argument is made for replacing $\mathbf{A} \cdot \mathbf{j}_{ab}$ by $\mathbf{A} \cdot \mathbf{p}_{ab}$ in the perturbation Hamiltonian.

The current operator is

$$\mathbf{j}_{ab} = \frac{q}{2m_o} \left[< a|\mathbf{p}|\mathbf{r} >< \mathbf{r}|b > + < a|\mathbf{r} >< \mathbf{r}|\mathbf{p}|b > \right] \tag{C.1}$$

The wave-functions will be written in the form

$$< \mathbf{r}|a >= \sum_i \phi_i^a(\mathbf{r}) u_i^a(\mathbf{r}) \tag{C.2}$$

where ϕ_i^a are slowly varying envelope functions and u_i^a are quickly varying spin functions. What is important in the analysis is the integral $\int d^3\mathbf{r}\mathbf{A}(\mathbf{r},t) \cdot \mathbf{j}_{ab}$, $\mathbf{A}(\mathbf{r},t)$ is a slowly varying function.

Substituting equation (C.2) into (C.1) gives

$$\begin{aligned}
&\int d^3\mathbf{r}\mathbf{A}(\mathbf{r},t) \cdot \mathbf{j}_{ab} \approx \frac{q}{2m_o} \sum_{i,i'} \left(\begin{array}{c} \left[d^3\mathbf{r}\phi_i^{a*}(\mathbf{r})\phi_{i'}^b(\mathbf{r})\mathbf{A}(\mathbf{r},t)\right] \cdot \\ \left[\int_\Omega \frac{d^3\mathbf{r}}{\Omega} \left(< u_i^a|\mathbf{p}| >< \mathbf{r}|u_{i'}^b > + < u_i^a|\mathbf{r} >< \mathbf{r}|\mathbf{p}|u_{i'}^b > \right) \right] \end{array} \right) \\
&\approx \frac{q}{2m_o} \sum_{i,i'} \left[d^3\mathbf{r}\phi_i^{a*}(\mathbf{r})\phi_{i'}^b(\mathbf{r})\mathbf{A}(\mathbf{r},t)\right] \cdot 2 < u_i^a|\mathbf{p}|u_{i'}^b > \\
&\approx \int d^3\mathbf{r}\mathbf{A}(\mathbf{r},t) \cdot \mathbf{p}_{ab}
\end{aligned} \tag{C.3}$$

A number of approximations have been made to get to the last line of equation (C.3). On the first line, the fast varying part and the slowly varying part have been separated. The gradient operator on ϕ_i^a has been neglected since this will lead to terms related to the intra-band electromagnetic transitions. The second term on the first line is reduce to the second term on the second line by using the completeness relation. Thus the last line shows that the replacement $\mathbf{j}_{ab} \rightarrow \mathbf{p}_{ab}$ is valid if it is used in an integral like this.

Appendix D

Phonon Relations

D.1 Self-Energies

The Hamiltonian density for the electron-phonon interaction is $H^{e-ph}(x) = e\phi(x)$ where $\phi(x)$ is the potential induced by the phonons. This is written, with electrons quantized as

$$\begin{aligned}\hat{H}^{e-ph}(x_1, x_2) &= \hat{\phi}(x_1)\delta^4(x_1 - x_2)\hat{\psi}^+(x_1)\hat{\psi}(x_2) \\ &= \hat{\phi}(x_1)\delta^4(x_1 - x_2)\sum_{i,j}\hat{\psi}_i^+(x_1)\hat{\psi}_j(x_2)u_i^*(\mathbf{r}_1)u_j(\mathbf{r}_2)\end{aligned} \tag{D.1}$$

The quantized potential due to lattice vibrations is written in terms of the phonon creation and annihilation operators as

$$\hat{\phi}(x) = \int d^3\mathbf{q}e^{i\mathbf{q}\cdot\mathbf{r}}M_{\mathbf{q}}(\hat{a}_{\mathbf{q}}(t) + \hat{a}^+_{-\mathbf{q}(t)}) \tag{D.2}$$

where

$$M_{\mathbf{q}} = \frac{e}{q}\left[\frac{\omega_{LO}\hbar}{(2\pi)^2}\left(\frac{1}{\varepsilon_o} - \frac{1}{\varepsilon_\infty}\right)\right]^{1/2}$$

This is in the Frölich coupling model and gives the Hamiltonian density

$$\hat{H}^{e-ph}(x) = \sum_{i,j}\int d^3\mathbf{q}e^{i\mathbf{q}\cdot\mathbf{r}}M_{\mathbf{q}}\hat{A}_{\mathbf{q}}(t)\hat{\psi}_i^+(x)\hat{\psi}_j(x)u_i^*(\mathbf{r})u_j(\mathbf{r}) \tag{D.3}$$

where $\hat{A}_{\mathbf{q}} = \hat{a}_{\mathbf{q}} + \hat{a}^+_{-\mathbf{q}}$ in this case, the delta function is removed and the variables are thus $x_1 = x_2 = x$.

The lowest order correction to the Greens function incorporating this perturbation will be the lowest order connected diagrams

$$\delta G_{i,j}(x_1,x_2) = -\sum_{connected}\int dx_1' dx_2' < |\hat{\psi}_i(x_1)\hat{H}^{e-p}(x_1')\hat{H}^{e-p}(x_2')\hat{\psi}_j^+(x_2)| >$$
$$= -\sum_{connected}\sum_{i_1,j_1,i_2,j_2}\int dx_1' dx_2' d^3\mathbf{q}_1 d^3\mathbf{q}_2 M_{\mathbf{q}_1} M_{\mathbf{q}_2} e^{i\mathbf{q}_1\cdot\mathbf{r}_1'} e^{i\mathbf{q}_2\cdot\mathbf{r}_2'} u_{i_1}^*(\mathbf{r}_1') u_{j_1}(\mathbf{r}_1') \tag{D.4}$$
$$\times u_{i_2'}^*(\mathbf{r}_2') u_{j_2}(\mathbf{r}_2) < |\hat{A}_{\mathbf{q}_1}(t_1')\hat{A}_{\mathbf{q}_2}(t_2')| >< |\hat{\psi}_i(x_1)\hat{\psi}_{i_1}^+(x_1')\hat{\psi}_{j_1}(x_1')\hat{\psi}_{i_2}^+(x_2')\hat{\psi}_{j_2}(x_2')\hat{\psi}_j^+(x_2)| >$$

Since the periodic u_i functions are the only quickly varying functions, they can be removed from the slowly-varying integral to get the approximate relations of δ_{i_1,j_1} and δ_{i_2,j_2}. To simplify calculations it is assumed that the phonons remain in equilibrium [29, 32]. The approximation is because the LO phonons being analyzed are quickly equilibrated by the decay into acoustic phonons [26].

If the phonons remain in equilibrium, then

$$M_{\mathbf{q}_1} M_{\mathbf{q}_2} < P|\hat{A}_{\mathbf{q}_1}(t_1')\hat{A}_{\mathbf{q}_2}(t_2') >= -iD^P(\mathbf{q}_1, t_1' - t_2')\delta(\mathbf{q}_1 + \mathbf{q}_2) \tag{D.5}$$

where $D^P(\mathbf{q}_1, t_1 - t_2)$ is the phonon Greens function in momentum space (in this case it includes the coupling coefficients for convenience). The superscript P denotes the various path ordering. Substituting this into (D.4) simplifies it to

$$\delta G_{i,j}(x_1,x_2) = i\sum_{connected}\sum_{i_1,i_2}\int dx_1' dx_2' D^P(x_1' - x_2')$$
$$\times < P|\hat{\psi}_i(x_1)\hat{\psi}_{i_1}^+(x_1')\hat{\psi}_{i_1}(x_1')\hat{\psi}_{i_2}^+(x_2')\hat{\psi}_{i_2}(x_2')\hat{\psi}_j^+(x_2)| >$$
$$= i\sum_{i_1,i_2}\int dx_1' dx_2' D^P(x_1' - x_2') G_{i,i_1}(x_1,x_1') G_{i_1,i_2}(x_1',x_2') G_{i_2,j}(x_2',x_2) \tag{D.6}$$

where $D^P(x_1', x_2') = \int d^3\mathbf{q}_1 e^{i\mathbf{q}_1\cdot(\mathbf{r}_1' - \mathbf{r}_2'} D^P(\mathbf{q}_1, t_1' - t_2')$ and in the last line, only the connected diagrams have been kept. For simplicity, the type of Greens function ($<,>$ etc) is not explicitly labeled, but can be inferred from the time indices. From the last line of equation (D.6) the path dependences are such that it can be shown

$$\Sigma_{i,j}^{phon,\alpha}(x_1,x_2) = iG_{i,j}^{\alpha}(x_1 - x_2)D^{\alpha}(x_1,x_2),\ \alpha =<,>,t,\bar{t} \tag{D.7}$$

This is the first order irreducible self-energy for the phonons.

D.2 Phonon Greens Functions

The phonons are assumed to be plane-wave and in equilibrium. These have known relations[27, 32, 34]

$$D^{<}(x) = -i \int d^3\mathbf{q} e^{i\mathbf{q}\cdot\mathbf{r}} M_{\mathbf{q}}^2 \left[(N_{\mathbf{q}}+1) e^{i\omega_{\mathbf{q}} t} + N_{\mathbf{q}} e^{-i\omega_{\mathbf{q}} t} \right] \tag{D.8}$$

and

$$D^{>}(x) = -i \int d^3\mathbf{q} e^{i\mathbf{q}\cdot\mathbf{r}} M_{\mathbf{q}}^2 \left[(N_{\mathbf{q}}+1) e^{-i\omega_{\mathbf{q}} t} + N_{\mathbf{q}} e^{i\omega_{\mathbf{q}} t} \right] \tag{D.9}$$

where $\omega_{\mathbf{q}}$ is the phonon frequency for this momentum. For this interaction it is only the longitudinal optical (LO) phonons that are significant. A common approximation for plane-wave LO phonons is that they all have the same frequency ($\omega_{\mathbf{q}} = \omega_{LO}$). To determine the advanced and retarded self-energies, the relations of equation (6.2) for D^r must be used which shows that

$$D^r(x) = -2 \int d^3\mathbf{q} e^{i\mathbf{q}\cdot\mathbf{r}} \Theta(t) \sin(\omega_{\mathbf{q}} t) \tag{D.10}$$

In Wigner space, these are

$$D^{<}(\mathbf{k},\omega) = -i(2\pi)^{1/2} \int d^3\mathbf{q} e^{i\mathbf{q}\cdot\mathbf{r}} M_{\mathbf{q}}^2 \left[(N_{\mathbf{q}}+1)\delta(\omega-\omega_L) + N_{\mathbf{q}}\delta(\omega+\omega_L) \right] \tag{D.11}$$

and

$$D^{>}(\mathbf{k},\omega) = -i(2\pi)^{1/2} \int d^3\mathbf{q} e^{i\mathbf{q}\cdot\mathbf{r}} M_{\mathbf{q}}^2 \left[(N_{\mathbf{q}}+1)\delta(\omega+\omega_L) + N_{\mathbf{q}}\delta(\omega-\omega_L) \right] \tag{D.12}$$

and

$$D^r(\mathbf{k},\omega) = -\frac{1}{(2\pi)^{1/2}} \int d^3\mathbf{q} M_{\mathbf{q}}^2 e^{i\mathbf{q}\cdot\mathbf{r}} \int \frac{d\Omega}{\Omega + i\xi} \left[\delta(\omega-\Omega+\omega_L) - \delta(\omega-\Omega-\omega_L) \right] \tag{D.13}$$

where use has been made of the relationship $\Theta(t) = \frac{i}{2\pi} \int \frac{d\Omega}{\Omega+i\xi} e^{-i\Omega t}$, ξ is a vanishingly small number.

D.3 QBE Terms

Equation (6.69) will require phonon self-energies $\Sigma^{<}$, $\Sigma^{>}$, and Σ^r. $\Sigma^{<}$ and $\Sigma^{>}$ are straightforward from equation (D.7) but the relations of (6.2) must be used to find Σ^r which

is

$$\begin{aligned}\Sigma^r_{i,j} &= \Sigma^t_{i,j} - \Sigma^<_{i,j} = i\left\{(D^r + D^<)(G^r_{i,j} + G^<_{i,j})\right\} - i\left\{D^< G^<_{i,j}\right\} \\ &= i\left[\left\{D^r G^r_{i,j}\right\} + \left\{D^< G^r_{i,j}\right\} + \left\{D^r G^<_{i,j}\right\}\right]\end{aligned}$$

In the Wigner coordinates, this requires functions of the form

$$\begin{aligned}\left\{D^\alpha G^\beta_{i,j}\right\}(\mathbf{k},\mathbf{R},\omega,T) &= \int \frac{dt d^3\mathbf{r}}{(2\pi)^2} e^{-i(\mathbf{k}\cdot\mathbf{r}-\omega t)} D^\alpha(\mathbf{r},t) G^\beta_{i,j}(\mathbf{r},\mathbf{R},t,T) \qquad \text{(D.14)} \\ &= \int \frac{d\omega' d\mathbf{q}}{(2\pi)^2} D^\alpha(\mathbf{k}-\mathbf{q},\omega-\omega') G^\beta_{i,j}(\mathbf{q},\mathbf{R},\omega',T)\end{aligned}$$

The terms required are shown below with the relevant Greens functions converted into Wigner functions using equations (D.10) to (D.13)

$$\begin{aligned}\left\{D^< G^<_{i,j}\right\} &= \frac{1}{(2\pi)^{3/2}} \int d^3\mathbf{q} M^2_{\mathbf{k}-\mathbf{q}} \left[(N_L+1)A_{i,j}(\mathbf{q},\omega+\omega_L) + N_L A_{i,j}(\mathbf{q},\omega-\omega_L)\right] \\ &\times \quad f_{i,j}(\mathbf{q},\mathbf{R},T) \qquad \text{(D.15)}\end{aligned}$$

$$\begin{aligned}\left\{D^> G^>_{i,j}\right\} &= \frac{1}{(2\pi)^{3/2}} \int d^3\mathbf{q} M^2_{\mathbf{k}-\mathbf{q}} \left[(N_L+1)A_{i,j}(\mathbf{q},\omega-\omega_L) + N_L A_{i,j}(\mathbf{q},\omega+\omega_L)\right] \\ &\times \quad \left[f_{i,j}(\mathbf{q},\mathbf{R},T) - 1\right] \qquad \text{(D.16)}\end{aligned}$$

$$\left\{D^r G^r_{i,j}\right\} = \frac{i\delta_{i,j}}{(2\pi)^{3/2}} \int d^3\mathbf{q} M^2_{\mathbf{k}-\mathbf{q}} \left[G^r_{i,i}(\mathbf{q},\omega+\omega_L) - G^r_{i,i}(\mathbf{q},\omega-\omega_L)\right] \qquad \text{(D.17)}$$

$$\left\{D^< G^r_{i,j}\right\} = \frac{-i\delta_{i,j}}{(2\pi)^{3/2}} \int d^3\mathbf{q} M^2_{\mathbf{k}-\mathbf{q}} \left[(N_L+1)G^r_{i,i}(\mathbf{q},\omega+\omega_L) + N_L G^r_{i,i}(\mathbf{q},\omega-\omega_L)\right] \qquad \text{(D.18)}$$

$$\left\{D^r G^<_{i,j}\right\} = \frac{-i}{(2\pi)^{3/2}} \int d^3\mathbf{q} M^2_{\mathbf{k}-\mathbf{q}} \left[G^r_{i,i}(\mathbf{q},\omega+\omega_L) - G^r_{i,i}(\mathbf{q},\omega-\omega_L)\right] f_{i,j}(\mathbf{q},\mathbf{R},T) \qquad \text{(D.19)}$$

Thus the retarded self energy is

$$\Sigma^r_{i,j} = \frac{1}{(2\pi)^{3/2}} \int d^3\mathbf{q} M^2_{\mathbf{k}-\mathbf{q}} \left[\begin{array}{l} \delta_{i,j}\left(N_L G^r_{i,i}(\mathbf{q},\omega+\omega_L) + (N_L+1)G^r_{i,i}(\mathbf{q},\omega-\omega_L)\right) \\ +\left(G^r_{i,i}(\mathbf{q},\omega+\omega_L) - G^r_{i,i}(\mathbf{q},\omega-\omega_L)\right) f_{i,j}(\mathbf{q},\mathbf{R},T) \end{array}\right]$$

Substituting these into equation (6.69) and performing the QBE steps of 6.2.3

$$-(2\pi)^{1/2}\int\frac{d\omega}{2\pi}d_{\mathbf{q}}^{3}M_{\mathbf{k}-\mathbf{q}}^{2}\sum_{\nu=\pm1}\times \tag{D.20}$$

$$\left\{\begin{array}{r}
\sum_{j'}\left[\begin{array}{c}A_{i,j'}(\mathbf{k},\omega)f_{i,j'}(\mathbf{k},\mathbf{R},T)\left\{(N_L+\frac{1}{2}-\frac{\nu}{2})A_{j',j}(\mathbf{q},\omega+\nu\omega_L)\right\}\\ -A_{i,j'}(\mathbf{q},\omega)f_{i,j'}(\mathbf{q},\mathbf{R},T)\left\{(N_L+\frac{1}{2}-\frac{\nu}{2})A_{j',j}(\mathbf{k},\omega+\nu\omega_L)\right\}\end{array}\right]\\
+\sum_{j'}\left[\begin{array}{c}i\left\{\nu G_{i,i}^{r}(\mathbf{q},\omega+\nu\omega_L)\right\}A_{j',j}(\mathbf{k},\omega)f_{i,j'}(\mathbf{q},\mathbf{R},T)f_{j',j}(\mathbf{k},\mathbf{R},T)\\ -iA_{i,j'}(\mathbf{k},\omega)\left\{\nu G_{j',j'}^{r}(\mathbf{q},\omega+\nu\omega_L)\right\}f_{i,j'}(\mathbf{k},\mathbf{R},T)f_{j',j}(\mathbf{q},\mathbf{R},T)\end{array}\right]\\
+iA_{i,j}(\mathbf{k},\omega)f_{i,j}(\mathbf{k},\mathbf{R},T)\left[\begin{array}{c}(N_L+\frac{1}{2}-\frac{\nu}{2})\left\{G_{i,i}^{r}(\mathbf{q},\omega+\nu\omega_L)-G_{j,j}^{r}(\mathbf{q},\omega+\nu\omega_L)\right\}\end{array}\right]\\
-iA_{i,j}(\mathbf{q},\omega)f_{i,j}(\mathbf{q},\mathbf{R},T)\left[\begin{array}{c}(N_L+\frac{1}{2}-\frac{\nu}{2})\left\{G_{i,i}^{r}(\mathbf{k},\omega+\nu\omega_L)-G_{j,j}^{r}(\mathbf{k},\omega+\omega_L)\right\}\end{array}\right]
\end{array}\right\}$$

Which can be simplified to

$$-\int d_{\mathbf{q}}^{3}\left\{\sum_{j'}\left(\begin{array}{c}\left[Z_{j',j}^{i,j'}(\mathbf{k},\mathbf{q},\omega_L)f_{i,j'}(\mathbf{k},\mathbf{R},T)-f_{i,j'}(\mathbf{q},\mathbf{R},T)z_{j',j}^{i,j'}(\mathbf{q},\mathbf{k},\omega_L)\right]\\ +i\sum_{\nu=\pm1}\left[\begin{array}{c}\nu B(j,\mathbf{k},i,\mathbf{q},\nu\omega_L)f_{i,j'}(\mathbf{q},\mathbf{R},T)f_{j',j}(\mathbf{k},\mathbf{R},T)\\ -\nu B(j,\mathbf{k},i,\mathbf{q},\nu\omega_L)f_{i,j'}(\mathbf{k},\mathbf{R},T)f_{j',j}(\mathbf{q},\mathbf{R},T)\end{array}\right]\end{array}\right)\right\} \tag{D.21}$$

where $Z_{j',j}^{i,j'}(\mathbf{k},\mathbf{q},\omega_L)=W_{j',j}^{i,j'}(\mathbf{k},\mathbf{q},\omega_L)+\delta_{j,j'}Y_{i,j}(\mathbf{k},\mathbf{q})$ with $W_{j',j}^{i,j'}$ a commonly used term[32]

$$\begin{aligned}W_{j',j}^{i,j'}(\mathbf{k},\mathbf{q},\omega_L)&=(2\pi)^{1/2}M_{\mathbf{k}-\mathbf{q}}^{2}\sum_{\nu=\pm1}\frac{d\omega}{2\pi}(N_L+\frac{1}{2}-\frac{\nu}{2})A_{i,j'}(\mathbf{k},\omega)A_{j',j}(\mathbf{q},\omega+\nu\omega_L)\\&=i\sum_{\nu=\pm1}(N_L+\frac{1}{2}-\frac{\nu}{2})\left(B(j',\mathbf{k},j',\mathbf{q},\nu\omega_L)+B(j,\mathbf{q},i,\mathbf{k},-\nu\omega_L)\right)\end{aligned} \tag{D.22}$$

and

$$Y_{i,j}(\mathbf{k},\mathbf{q})=i\sum_{\nu=\pm1}\left\{(N_L+\frac{1}{2}-\frac{\nu}{2})[B(j,\mathbf{k},i,\mathbf{q},\nu\omega_L)-B(j,\mathbf{k},j,\mathbf{q},\nu\omega_L)]\right\} \tag{D.23}$$

with

$$B(i,\mathbf{k},j,\mathbf{q},\omega)=\frac{(2\pi)^{1/2}M_{\mathbf{k}-\mathbf{q}}^{2}}{\omega+\omega_{i,\mathbf{k}}-\omega_{j,\mathbf{q}}+i\xi} \tag{D.24}$$

$\omega_{i,\mathbf{k}}=\varepsilon_{i,\mathbf{k}}/\hbar$.

Appendix E

Coulombic Interaction

E.1 Self-Energies

The two-body coulombic interaction Hamiltonian in second quantized form and in position space is

$$\hat{H}^{coul}(x_1,x_2) = \frac{\delta(t_1-t_2)}{2}\hat{\psi}^{+}(\mathbf{r}_1,t_1)\hat{\psi}^{+}(\mathbf{r}_2,t_2)V(|\mathbf{r}_1-\mathbf{r}_2|)\hat{\psi}(\mathbf{r}_2,t_2)\hat{\psi}(\mathbf{r}_1,t_1) \tag{E.1}$$

$$\begin{aligned}
\delta G_{i,j}(x_1,x_2) &= -\sum_{connected}\int dx_1' dx_2' < |\hat{\psi}_i(x_1)\hat{H}^{coul}(x_1',x_2')\hat{\psi}_j^{+}(x_2)| > \\
&\approx -\frac{1}{2}\sum_{conn}\sum_{i_1,j_1,i_2,j_2}\int dx_1' dx_2' \delta(t_1-t_2) < |\hat{\psi}_i(x_1)\hat{\psi}_{i_2}^{+}(\mathbf{r}_1',t_1')\hat{\psi}_{j_2}^{+}(\mathbf{r}_2',t_2') \\
&\times V_{i_1,j_1}^{i_2,j_2}(|\mathbf{r}_1'-\mathbf{r}_2'|)\hat{\psi}_{j_1}(\mathbf{r}_2',t_2')\hat{\psi}_{i_1}(\mathbf{r}_1',t_1')\hat{\psi}_j^{+}(x_2)| >
\end{aligned} \tag{E.2}$$

$$\begin{aligned}
V_{i,j}^{i',j'}(|\mathbf{r}_1-\mathbf{r}_2|) &= \int_{\Omega} d^3\mathbf{r}_1 d^3\mathbf{r}_2 u_{i'}^{*}(\mathbf{r}_1)u_{j'}^{*}(\mathbf{r}_2)V(|\mathbf{r}_1-\mathbf{r}_2|)u_i(\mathbf{r}_1)u_j(\mathbf{r}_2) \\
&\approx \delta_{i,i'}\delta_{j,j'}V(|\mathbf{r}_1-\mathbf{r}_2|)
\end{aligned} \tag{E.3}$$

This is a common approximation[30] so that equation (E.2) simplifies to

$$-\frac{1}{2}\sum_{conn}\sum_{i_1,j_1}\int dx_1' d^3\mathbf{r}_2' < |\hat{\psi}_i(x_1)\hat{\psi}_i^{+}(x_1')\hat{\psi}_j^{+}(\mathbf{r}_2',t_1')V(|\mathbf{r}_1'-\mathbf{r}_2'|)\hat{\psi}_j(\mathbf{r}_2',t_1')\hat{\psi}_i(x_1')\hat{\psi}_j^{+}(x_2)| > \tag{E.4}$$

There are four connected paths, but only two are unique so that this can be written as

$$\begin{aligned}
&\tfrac{i}{\hbar}\sum_{i_1,j_1}\int d^3\mathbf{r}_1' d^3\mathbf{r}_2' ds V(|\mathbf{r}_1-\mathbf{r}_2|)G^{Pt_1s}_{i,i_1}(\mathbf{r}_1,t_1,\mathbf{r}_1',s)G^{Pss}_{j_1,j_1}(\mathbf{r}_2',s,\mathbf{r}_2',s)G^{Pst_2}_{i_1,j}(\mathbf{r}_1',s,\mathbf{r}_2',t_2)\\
&-\tfrac{i}{\hbar}\sum_{i_1,j_1}\int d^3\mathbf{r}_1' d^3\mathbf{r}_2' ds V(|\mathbf{r}_1-\mathbf{r}_2|)G^{Pt_1s}_{i,i_1}(\mathbf{r}_1,t_1,\mathbf{r}_1',s)G^{Pss}_{i_1,j_1}(\mathbf{r}_1',s,\mathbf{r}_2',s)G^{Pst_2}_{j_1,j}(\mathbf{r}_2',s,\mathbf{r}_2,t_2)
\end{aligned} \tag{E.5}$$

where the superscripts on the Greens functions denote the various path orderings. The times t_1 and t_2 are fixed when looking at the various component of the perturbation and s will be on both paths. This is the method used by Mahan[27]. Using this method, it can be shown that the perturbation will be (shown in Craig's matrix form[27, 69])

$$\sum_{i_1,j_1}\int d^3\mathbf{r}_1' d^3\mathbf{r}_2' \tilde{G}_{i,i_1}(\mathbf{r}_1,t_1,\mathbf{r}_1',t)\tilde{\Sigma}_{i_1,j_1}(\mathbf{r}_1',t,\mathbf{r}_2',t)\tilde{G}_{j_1,j}(\mathbf{r}_2',t,\mathbf{r}_2,t_2) \tag{E.6}$$

where

$$\tilde{\Sigma}^{coul}_{i,j}(x_1,x_2)=\begin{bmatrix} C^t_{i,j}(x_1,x_2) & 0\\ 0 & C^{\bar{t}}_{i,j}(x_1,x_2)\end{bmatrix} \tag{E.7}$$

where

$$C^{\alpha}_{i,j}(x_1,x_2)=\frac{i}{\hbar}\delta(t_1-t_2)\begin{pmatrix}\sum_{j'}\int d^3\mathbf{r}'\delta_{i,j}\delta(\mathbf{r}_1-\mathbf{r}_2)V_s(|\mathbf{r}_1-\mathbf{r}'|)G^{\alpha}_{j',j'}(\mathbf{r}',t_1,\mathbf{r}',t_2)\\ -V_s(|\mathbf{r}_1-\mathbf{r}_2|)G^{\alpha}_{i,j}(x_1,x_2)\end{pmatrix} \tag{E.8}$$

where V has been replaced by V_s which is a renormalized potential for screening. In this case it is found using the quasi-static screening and Hartree-Fock approximations[30] (also known as the random-phase approximation) which gives this potential as $\frac{e^2}{|\mathbf{r}_1-\mathbf{r}_2|\varepsilon_s}$. In this approximation the only difference from the screened and unscreened potential is the dielectric, it will be modeled by the plasmon-pole approximation[44].

E.2 QBE Terms

In the center of mass coordinates, the term in the self-energy is

$$C^{\alpha}_{i_1,j_1}(\mathbf{r},\mathbf{R},t,T)=\frac{i}{\hbar}\delta(t=0)\left\{\begin{array}{l}\sum_{j''}\int d^3\mathbf{r}'\delta_{i_1,j_1}\delta(\mathbf{r}=0)V_s(|\mathbf{R}+\frac{\mathbf{r}}{2}-\mathbf{r}'|)G^{\alpha}_{j'',j''}(\mathbf{r}',0,T+t/2,0)\\ -V_s(|\mathbf{r}|)G^{\alpha}_{i_1,j_1}(\mathbf{R},\mathbf{r},T+t/2,0)\end{array}\right\} \tag{E.9}$$

In the Wigner coordinates this can be written as

$$\begin{aligned} C^{\alpha}_{i_1,j_1}(\mathbf{k},\mathbf{R},\omega,T) &= \left\{ \begin{array}{l} \sum\limits_{j''} \int \frac{d^3\mathbf{k}'d\omega'}{(2\pi)^4}\delta_{i_1,j_1}V_s(|\mathbf{R}-\mathbf{R}'|)G^{\alpha}_{j'',j''}(\mathbf{k}',\mathbf{R}',\omega',T) \\ -\int \frac{d^3\mathbf{r}}{(2\pi)^2}e^{-i\mathbf{k}\cdot\mathbf{r}}V_s(|\mathbf{r}|)\frac{d^3\mathbf{k}'d\omega'}{(2\pi)^2}e^{i\mathbf{k}'\cdot\mathbf{r}}G^{\alpha}_{i_1,j_1}(\mathbf{k}',\mathbf{R},\omega',T) \end{array} \right\} \\ &= \begin{array}{l} \sum\limits_{j''}\delta_{i_1,j_1}\int \frac{d(\mathbf{R}'\mathbf{q}\mathbf{k}'\omega')}{(2\pi)^{11/2}}e^{i\mathbf{q}\cdot(\mathbf{R}-\mathbf{R}')}V_{s,\mathbf{q}}G^{\alpha}_{j'',j''}(\mathbf{k}',\mathbf{r}',\omega',T) \\ -\int \frac{d(\mathbf{k}'\omega')}{(2\pi)^{5/2}}V_{s,\mathbf{k}-\mathbf{k}'}G^{\alpha}_{i_1,j_1}(\mathbf{k}',\mathbf{R},\omega',T) \end{array} \end{aligned} \tag{E.10}$$

where the shorthand $d(\mathbf{R}'\mathbf{q}\mathbf{k}'\omega')$ and $d(\mathbf{k}'\omega')$ are used to denote $d^3\mathbf{R}'d^3\mathbf{q}d^3\mathbf{k}'d\omega'$ and $d^3\mathbf{k}'d\omega'$. The potential $V_{\mathbf{q}} = \int \frac{d^3\mathbf{r}}{(2\pi)^{3/2}}e^{-i\mathbf{q}\cdot\mathbf{r}}V(|\mathbf{r}|)$ has been used. It is important to note that the component V_0, which diverges, is canceled by the $\mathbf{q}=0$ terms from the electron-ion and ion-ion Coulomb potentials and so will be ignored[44]. Using the random phase approximation, $V_{s\mathbf{q}} = \frac{V_{\mathbf{q}}}{\epsilon_{\mathbf{q}}(\omega)}$ where the renormalizing coefficient is given in the static plasmon-pole approximation

$$\frac{1}{\epsilon_{\mathbf{q}}(\omega)} = 1 - \frac{\omega_{pl}^2}{\omega_{\mathbf{q}}^2}\ ,\ \omega_{\mathbf{q}}^2 = \omega_{pl}^2\left(1+\frac{q^2}{\kappa^2}\right) + C\left(\frac{\hbar q^2}{4m_r}\right)^2 \tag{E.11}$$

where the square of the electron-hole frequency is $\omega_{pl}^2 = 16\pi N a_o^3(\varepsilon/\hbar)^2$ m_r is the reduced electron-hole mass, C is a numerical constant usually taken between 1 and 4 and κ is the inverse static screening length

$$\kappa\left[\frac{4\pi e^2}{\epsilon_b}\sum_{\alpha=e,h}\frac{\partial N}{\partial\mu}\right]^{1/2}$$

The values of N and $\partial N/\partial\mu$ will be approximated by averaging over these quantities in the well region in the case of no light coupling. The chemical potential μ is estimated by approximating the carriers as in equilibrium for this calculation.

The lowest order contribution to the gradient expansion on the $<$ term of equation

(6.68) is then

$$
\begin{aligned}
&(2\pi)^2\hbar\sum\left[\Sigma^t_{i,j'}(\mathbf{k},\mathbf{R},\omega,T)G^<_{j',j}(\mathbf{k},\mathbf{R},\omega,T)+G^<_{i,j'}(\mathbf{k},\mathbf{R},\omega,T)\Sigma^{\bar{t}}_{j',j}(\mathbf{k},\mathbf{R},\omega,T)\right]\\
&=\hbar\sum_{j'}\left[\begin{array}{l}
\left\{\begin{array}{l}\int\frac{d(\mathbf{R}'\mathbf{q}\mathbf{k}'\omega')}{(2\pi)^{7/2}}e^{i\mathbf{q}\cdot(\mathbf{R}-\mathbf{R}')}V_{s,\mathbf{q}}\sum\limits_{j''}G^t_{j'',j''}(\mathbf{k}',\mathbf{R}',\omega',T)\delta_{i,j'}\\ -\int\frac{d(\mathbf{k}'\omega')}{(2\pi)^{1/2}}V_{s,\mathbf{k}-\mathbf{k}'}G^t_{i,j'}(\mathbf{k}',\mathbf{R},\omega',T)\end{array}\right\}G^<_{j',j}(\mathbf{k},\mathbf{R},\omega,T)\\
-G^<_{i,j'}(\mathbf{k},\mathbf{R},\omega,T)\left\{\begin{array}{l}\int\frac{d(\mathbf{R}'\mathbf{q}\mathbf{k}'\omega')}{(2\pi)^{7/2}}e^{i\mathbf{q}\cdot(\mathbf{R}-\mathbf{R}')}V_{s,\mathbf{q}}\sum\limits_{j''}G^{\bar{t}}_{j'',j''}(\mathbf{k}',\mathbf{R}',\omega',T)\delta_{j',j}\\ -\int\frac{d(\mathbf{k}'\omega')}{(2\pi)^{1/2}}V_{s,\mathbf{k}-\mathbf{k}'}G^{\bar{t}}_{j',j}(\mathbf{k}',\mathbf{R},\omega',T)\end{array}\right\}
\end{array}\right]
\end{aligned}
\tag{E.12}
$$

Applying the steps 4-6 of the QBE method in section 6.2.3 gives

$$
\sum_{j'}\left[\begin{array}{l}
\frac{(2\pi)^{1/2}}{2}\int d^3\mathbf{k}'V_{\mathbf{k}-\mathbf{k}'}\delta_{i,j'}f_{j',j}(\mathbf{k},\mathbf{R},T)\\
+\left\{\begin{array}{l}\delta_{i,j'}\int\frac{d(\mathbf{R}'\mathbf{q}\mathbf{k}')}{(2\pi)^{5/2}}e^{i\mathbf{q}\cdot(\mathbf{R}-\mathbf{R}')}V_{\mathbf{q}}\sum\limits_{j''}f_{j'',j''}(\mathbf{k}',\mathbf{R}',T)\\ -(2\pi)^{1/2}\int d^3\mathbf{k}'V_{\mathbf{k}-\mathbf{k}'}f_{i,j'}(\mathbf{k}',\mathbf{R},T)\end{array}\right\}f_{j',j}(\mathbf{k},\mathbf{R},T)\\
-f_{i,j'}(\mathbf{k},\mathbf{R},T)\left\{\begin{array}{l}\delta_{j',j}\int\frac{d(\mathbf{R}'\mathbf{q}\mathbf{k}')}{(2\pi)^{5/2}}e^{i\mathbf{q}\cdot(\mathbf{R}-\mathbf{R}')}V_{\mathbf{q}}\sum\limits_{j''}\left[f_{j'',j''}(\mathbf{k}',\mathbf{R}',T)-1\right]\\ -(2\pi)^{1/2}\int d^3\mathbf{k}'V_{\mathbf{k}-\mathbf{k}'}\left[f_{j',j}(\mathbf{k}',\mathbf{R},T)-1\right]\end{array}\right\}\\
+\frac{(2\pi)^{1/2}}{2}\delta_{j',j}f_{i,j'}(\mathbf{k},\mathbf{R},T)\int d^3\mathbf{k}'V_{\mathbf{k}-\mathbf{k}'}
\end{array}\right]
\tag{E.13}
$$

Removing the $\mathbf{q}=0$ components and simplifying, this is

$$
\sum_{j'}(2\pi)^{1/2}\int d^3\mathbf{k}'V_{\mathbf{k}-\mathbf{k}'}\left\{\begin{array}{l}f_{i,j'}(\mathbf{k},\mathbf{R},T)f_{j',j}(\mathbf{k}',\mathbf{R},T)-f_{i,j'}(\mathbf{k}',\mathbf{R},T)f_{j',j}(\mathbf{k},\mathbf{R},T)\\ -f_{i,j'\neq i}(\mathbf{k},\mathbf{R},T)\end{array}\right\}
\tag{E.14}
$$

Appendix F

Spatially Varying Effective Mass

The effective masses in Dyson's equations can be taken as spatially varying. This is not too difficult, but leads to extra terms when the QBE steps are taken. The terms that would have to transformed are shown in equation (6.49)

$$\left[\frac{\hbar^2}{2m_i^*(\mathbf{R}+\mathbf{r}/2)}\nabla^2_{\mathbf{R}+\mathbf{r}/2} - \frac{\hbar^2}{2m_j^*(\mathbf{R}-\mathbf{r}/2)}\nabla^2_{\mathbf{R}-\mathbf{r}/2}\right] G^<_{i,j}(\mathbf{r},\mathbf{R},t,T) \tag{F.1}$$

where the spatial dependence has been added. The first step when including spatial dependence is to make the equation operators Hermitian, this accomplished by transforming these terms to

$$\frac{\hbar^2}{2}\left[\nabla_{\mathbf{R}+\mathbf{r}/2}m_i^*(\mathbf{R}+\mathbf{r}/2)\cdot\nabla_{\mathbf{R}+\mathbf{r}/2} - \nabla_{\mathbf{R}-\mathbf{r}/2}m_j^*(\mathbf{R}-\mathbf{r}/2)\cdot\nabla_{\mathbf{R}-\mathbf{r}/2}\right] G^<_{i,j}(\mathbf{r},\mathbf{R},t,T) \tag{F.2}$$

Some mathematical properties will be shown. From straightforward Fourier transformations, it can be shown that

$$\int d^3\mathbf{r}e^{-i\mathbf{k}\cdot\mathbf{r}}A(\mathbf{r}_1,\mathbf{r}_2)B(\mathbf{r}_1,\mathbf{r}_2) = \int d^3\mathbf{q}A(\mathbf{k}-\mathbf{q},\mathbf{R})B(\mathbf{R},\mathbf{q}) \tag{F.3}$$

where A and B are functions in the original position space on the LHS of this equation and functions in the Wigner coordinates on the RHS.

$$\int d^3\mathbf{r}e^{-i\mathbf{k}\cdot\mathbf{r}}\nabla_{\mathbf{r}_1}A(\mathbf{r}_1,\mathbf{r}_2) = \left(\frac{1}{2}\nabla_{\mathbf{R}}+i\mathbf{k}\right)A(\mathbf{k},\mathbf{R}) \tag{F.4}$$

$$\int d^3\mathbf{r} e^{-i\mathbf{k}\cdot\mathbf{r}} \nabla_{\mathbf{r}_2} A(\mathbf{r}_1, \mathbf{r}_2) = \left(\frac{1}{2}\nabla_{\mathbf{R}} - i\mathbf{k}\right) A(\mathbf{k}, \mathbf{R}) \tag{F.5}$$

$$\int d^3\mathbf{r} e^{-i\mathbf{k}\cdot\mathbf{r}} \nabla^2_{\mathbf{r}_1} A(\mathbf{r}_1, \mathbf{r}_2) = \int d^3\mathbf{r} e^{-i\mathbf{k}\cdot\mathbf{r}} \nabla^2_{\mathbf{r}_2} A(\mathbf{r}_1, \mathbf{r}_2) = \left(\frac{1}{4}\nabla^2_{\mathbf{R}} - k^2\right) A(\mathbf{k}, \mathbf{R}) \tag{F.6}$$

$$\int d^3\mathbf{r} e^{-i\mathbf{k}\cdot\mathbf{r}} A(\mathbf{r}_1) = 2\int d^3\mathbf{R}' e^{-i\mathbf{k}\cdot(\mathbf{R}'-\mathbf{R})} A(\mathbf{R}') \tag{F.7}$$

$$\int d^3\mathbf{r} e^{-i\mathbf{k}\cdot\mathbf{r}} A(\mathbf{r}_2) = 2\int d^3\mathbf{R}' e^{i\mathbf{k}\cdot(\mathbf{R}'-\mathbf{R})} A(\mathbf{R}') \tag{F.8}$$

Next define $M_i^*(\mathbf{r}_1) = \frac{1}{m_i^*(\mathbf{r}_1)}$. Using the relations of equations (F.3) to (F.8) it can then be shown with some manipulation that the terms of equation (F.2) can be written in the Wigner coordinates as

$$\frac{\hbar^2}{2(2\pi)^3}\int d^3\mathbf{q} \begin{bmatrix} \tilde{M}_i^*(\mathbf{R}, \mathbf{k}-\mathbf{q}) \begin{pmatrix} i(\mathbf{k}-\mathbf{q})\left[\frac{1}{2}\nabla_{\mathbf{R}} + i\mathbf{q}\right] \\ +\left[\frac{1}{4}\nabla^2_{\mathbf{R}} - q^2\right] \end{pmatrix} \\ -\tilde{M}_j^*(\mathbf{R}, \mathbf{k}-\mathbf{q}) \begin{pmatrix} -i(\mathbf{k}-\mathbf{q})\left[\frac{1}{2}\nabla_{\mathbf{R}} - i\mathbf{q}\right] \\ +\left[\frac{1}{4}\nabla^2_{\mathbf{R}} - q^2\right] \end{pmatrix} \end{bmatrix} G^<_{i,j}(\mathbf{q}, \mathbf{R}, \omega, T) \tag{F.9}$$

where

$$\tilde{M}_i^*(\mathbf{k}, \mathbf{R}) = 2\int d^3\mathbf{R}' e^{-\mathbf{k}\cdot(\mathbf{R}'-\mathbf{R})} M_i^*(\mathbf{R}') \tag{F.10}$$

Bibliography

[1] J.D. Ralston, S. Weisser, K. Eisele, R.E. Sha, E.C. Larkins, J. Rosenzweig, J. Fleissiner, and K. Bender. Low-bias-current direct modulation up to 33 GHz in InGaAs/AlGaAs psuedomorphic MQW ridge waveguide lasers. *IEEE Photonics Technol. Lett.*, 6:1076–1079, 1994.

[2] S. Weisser, E. C. Larkins, K. Cetscher, W. Benz, J. Daleiden, I. Esquivias, J. Fleissner nad J. D. Ralston, B. Romero, R.E. Sah, A. Schönfeld, and J. Rosenzweig. Damping-limited modulation bandwidths up to 40 GHz in undoped short-cavity $In_{0.35}Ga_{0.65}As$-GaAs multiple-quantum-well lasers. *IEEE Photonics Technol. Lett.*, 8:608–610, 1996.

[3] O. Kjebon, R. Schatz, S. Lourdudoss, S. Nisson, B. Stalnacke, and L. Backom. 30 GHz direct modulation bandwidth in detuned loaded InGaAsP DBR lasers at 1.55 μm wavelength. *Electron. Lett.*, 33:488–489, 1997.

[4] X. Zhang, A. Gutierrez-Aitken, D. Klotzkin, P Bhattacharya, C. Caneau, and R. Bhat. 0.98 μm multiple-quantum-well tunneling injection laser with 98-GHz intrinsic modulation bandwidth. *IEEE Journal of Selected Topics in Quantum Electronics*, 3:309–314, 1997.

[5] R. N. Hall, G. E. Fenner, J.D. Kingsley, T.J. Soltys, and R. O. Carlson. Coherent light emission from GaAs junctions. *Phys. Rev. Lett.*, 9:366–368, 1962.

[6] M. I. Nathan, W. P. Dumke, G. Burns amd F. H. Dill Jr., and G. Lascher. Stimulated emission of radiation from GaAs p-n junctions. *Appl. Phys. Lett.*, 1:62–64, 1962.

[7] N. Holonyak Jr. and S. F. Bevacques. Coherent (visible) light emission from $Ga(As_{1-x}P_x$ junctions. *Appl. Phys. Lett*, 1:82–83, 1962.

[8] H. Kroemer. A proposed class of heterojunction injection lasers. *Proc. IEEE*, 51:1782–1783, 1963.

[9] H. Kressel and H. Nelson. Close confinement gallium arsenide p-n junction lasers with reduced optical loss at room temperature. *RCA Rev.*, 30:106–113, 1969.

[10] E. Yablonovitch and E. O. Kane. Reduction of lasing threshold current density by the lowering of valence band effective mass. *Journal of Lightwave Technology*, LT-4:504–506, 1986.

[11] A. R. Adams. Band-Structure engineering for low-threshold high-efficiency. *Electron. Lett.*, 22:249–250, 1986.

[12] S. L. Chuang. *Physics of Optoelectronic Devices*. Wiley, New York, 1995.

[13] P. Doussier, P. Garabedian, C. Graven, D. Bonnevic, T. Filion, E. Derouin, M. Mannot, J. G. Provost, D. Leclerc, and M. Klonk. 1.55 μm Polarisation Independent Semiconductor Optical Amplifier with 25 dB Fiber to Fiber Gain. *IEEE Photonics Technol. Lett.*, 6:170–173, 1994.

[14] A. Godefroy, A. Le Corre, F. Clérot, S. Salaän, S. Loualiche, J. C. Simon, L. Henry, C. Vandry, J. C. Kèromnès, G. Jouliè, and P. Lamouler. 1.55 μm Polarization-Insensitive Optical Amplifier with Strain-Balanced Superlattice Active Layer. *IEEE Photonics Technol. Lett.*, 10:657–649, 1998.

[15] M. Hovinen, B. Gopalan, F. G. Johnson, and M. Dagenais. A novel structure of delta-strained quantum well for polarization insensitive semiconductor devices at 1.55 μm. *Proc. IEEE Lasers and Electro-Optical Soc. Annu. Meet.*, 1966.

[16] Y.S. Cho and W. Y. Choi. Polarization-Dependent Optical Gain Characteristics of Delta-Strained Quantum Wells for Semiconductor Optical Amplifiers. *Physics and Simulation of Optoelectronic Devices, Proc. of SPIE*, 3944, 2000.

[17] C. Aversa and K. Iizuka. Gain of TE-TM Modes in Quantum-Well Lasers. *IEEE Journal of Quantum Electronics*, 28:1864–1873, 1992.

[18] D. Ahn and S. L. Chuang. The Theory of Strained-Layer Quantum-Well Lasers with Bandgap Renormalization. *IEEE Journal of Quantum Electronics*, 30:350–365, 1994.

[19] D. Ahn. Optical Gain of a Quantum-Well Laser with Non-Markovian Relaxation and Many-Body Effects. *IEEE Journal of Quantum Electronics*, 1996:960–965, 1996.

[20] M. J. Connelly. Wideband Semiconductor Optical Amplifier Steady-State Numerical Model. *IEEE Journal of Quantum Electronics*, 37:439–447, 2001.

[21] P. Weetman, M. Kucharczyk, and M. S. Wartak. Effect of Well Coupling on the TE optical modal gain in quantum-well-based semiconductor lasers. *J. Phys. Condens. Matter*, 14:L83–L87, 2002.

[22] R. Nagarajan, M. Ishikawa, T. Fukushima, R. S. Geels, and J. E. Bowers. High Speed Quantum-Well Lasers and Carrier Transport Effects. *IEEE Journal of Quantum Electronics*, 28:1990–2008, 1992.

[23] M. Kucharczyk, M. S. Wartak, P. Weetman, and P.K. Lau. Theoretical modelling of multiple quantum well lasers with tunneling injection and tunneling transport between quantum wells. *J. App. Phys.*, 86:3218–3228, 1999.

[24] P. Weetman, M. S. Wartak, and P. Rusek. Comparison of Classical and Tunneling Injection Schemes in Quantum-Well Lasers. *IEEE Photonics Technol. Lett.*, 10:648–650, 1998.

[25] J. Minch, S. H. Park, T. Keating, and S. L. Chuang. Theory and Experiment of $In_{1-x}Ga_xAs_yP_{1-y}$ and $In_{1-x-y}Ga_xAl_yAs$ Long-Wavelength Strained Quantum-Well Lasers. *IEEE Journal of Quantum Electronics*, 35:771–782, 1999.

[26] C. Y. Tsai, F. P. Shih, T. L. Sung, T. Y. Wu, C. H. Chen, and C. Y. Tsai. A Small-Signal Analysis of the Modulation Response of High-Speed Quantum-Well Lasers: Effects of Spectral Hole Burning, Carrier Heating, and Carrier Diffusion-Capture-Escape. *IEEE Journal of Quantum Electronics*, 33:2084–2096, 1997.

[27] G. D. Mahan. *Many-Particle Physics*. Plenum Press, New York, second edition, 1990.

[28] A. L. Fetter amd J. D. Walecka. *Quantum Theory of Many-Particle Systems*. McGraw-Hill, New York, 1971.

[29] W. R. Frensley. Boundary Conditions for open quantum systems driven far from equilibrium. *Rev. Mod. Phys.*, 62:745–783, 1990.

[30] R. Binder and S. W. Koch. Nonequilibrium Semiconductor Dynamics. *Prog. Quant. Elec.*, 19:307–462, 1995.

[31] B. A. Biegel and J. D. Plummer. Comparison of Self-Consistency Iteration Options fot the Wigner Function Method of Quantum Devices Simulation. *Phys. Rev.B*, 54:8070–8082, 1996.

[32] H. Tsuchiya and T. Miyoshi. Nonequilibrium Green's function approach to high-temperature quantum transport in nanostructure devices. *J. App. Phys.*, 83:2574–2585, 1998.

[33] H. Tsuchiya and T. Miyoshi. Bipolar Quantum-Transport Modelling of Carrier Injection into a SCH-Quantum-Well-Laser. *IEEE Journal of Quantum Electronics*, 32:865–872, 1996.

[34] G.D. Mahan. Quantum Transport Equation for Electric and Magnetic Fields. *Phys. Reports*, 145:251–318, 1987.

[35] L. P. Kadanoff and G. Baym. *Quantum Statistical Mechanics : Green's Function Methods in Equilibrium and Non-Equilibrium Problems*. Benjamin, New York, 1962.

[36] P. Carruthers and F. Zachariasen. Quantum Collision theory with phase-space distributions. *Rev. Mod. Phys.*, 55:245–285, 1983.

[37] E. A. Renler. Use of the Wigner Representation in Scattering Problems. *Ann. Phys.*, 95:455–495, 1975.

[38] E. A. Renler. Composite Particle Cross Sections from the Density Operator. *Ann. Phys.*, 136:293–316, 1981.

[39] G. A. Baker. Formulation of Quantum Mechanics Based on the Quasi-Probability Distribution Induced in Phase Space. *Phys. Rev.*, 109:2198–2206, 1958.

[40] R. J. Glauber. Coherent and Incoherent States of the Radiation Field. *Phys. Rev.*, 131:2766–2788, 1963.

[41] A. M. Kiman amd N. C. Kluksdal, D. K. Ferry, and C. Ringhofer. *Wigner Function Modelling of the Resonant Tunneling Diode : in : Quantum Transport in Semiconductors, D.K. Ferry and C. Jacobion eds.* . Plenum Press, New York, 1991.

[42] H. C. Tso and N. J. M. Horing. Wigner-function formulation of nonlinear electron-hole transport in a quantum well and analysis of the linear transient and steady-state. *Phys. Rev. B.*, 44:11358–11380, 1991.

[43] O. Hess and T. Kuhn. Maxwell-Bloch equations for spatially inhomogeneous semiconductor lasers I. Theoretical formulation. *Phys. Rev. A.*, 54:3347–3359, 1996.

[44] W. W. Chow, S. W. Koch, and M. Sargent III. *Semiconductor-Laser Physics*. Springer, Berlin, 1994.

[45] M. Lindberg and S. W. Koch. Effective Bloch equations for semiconductors. *Phys. Rev. B*, 38:3342–3350, 1988.

[46] M. Silver and E. P. O'Reiller. Optimization of Long Wavelength InGaAsP Strained Quantum-Well Lasers. *IEEE Journal of Quantum Electronics*, 31:1193–1200, 1995.

[47] J. Bardeen. An improved calculation of the energies of metallic Li and Na. *J. Chem. Phys.*, 6:367–371, 1938.

[48] F. Seitz. *The Modern Theory of Solids*. McGraw-Hill, New York, 1940.

[49] J.M. Luttinger and W. Kohn. Motion of electrons and holes in perturbed periodic fields. *Phys. Rev.*, 97:869–883, 1955.

[50] C. G. Van der Walle. Band lineups and deformation potentials in the model-solid theory. *Phys. Rev. B*, 39:1871–1883, 1989.

[51] W. A. Harrison. Elementary theory of heterojunctions. *J. Vac. Sc. Tech.*, 14:1016–1021, 1977.

[52] J. J. Sakurai. *Modern Quantum Mechanics, S. F. Tuan ed.* Addison-Wesley, Reading, Massachusetts, second edition, 1994.

[53] M. Kucharczyk. Internal work.

[54] J. D. Jackson. *Classical Electrodynamics.* John Wiley and Sons, New York, 1975.

[55] C. Chen, P. Berini, D. Feng, and V. P. Tzolov. Efficient and Accurate Numerical Analysis of Multilayer PLanar Optical Waveguides. *Proceedings of SPIE*, 3795, 1999.

[56] S. Seki, K. Yokoyama, and P. Sotirelis. Theoretical Analysis of High-Temperature Charactersitics of 1.3 μm InP-Based Quantum-Well Lasers. *IEEE Journal of Selected Topics in Quantum Electronics*, 1:264–274, 1995.

[57] A. Trellakis, A. T. Galick, A. Pacelli, and U. Ravaioli. Iteration scheme for the solution of the two-dimensional Schrödinger-Poisson equations in quantum structures. *J. Appl. Phys.*, 81:7880–7884, 1997.

[58] P. A. Chen, C. Juang, and C. Y. Yang. Carrier-Induced Energy Shift in GaAs/AlGaAs Multiple Quantum Well Laser Diodes. *IEEE Journal of Quantum Electronics*, 29:2607–2618, 1993.

[59] E. Butkov. *Mathematical Physics.* Addison-Wesley, Reading, Massachusetts, 1968.

[60] C. F. Hsu amd P. S. Zory, C. H. Wu, and M. A. Emanuel. Coulomb Enhancement in InGaAs-GaAs Quantum-Well Lasers. *IEEE Journal of Selected Topics in Quantum Electronics*, 3:158–165, 1997.

[61] D. G. Howe J. Aikio. Direct semiconductor laser readout in optical data storage. *Proc. SPIE*, 4090:56–65, 2000.

[62] A. I. Akhtar, C.Z. Guo, and J. M. Xu. Effect of Well-Coupling on the Optical Gain of Multi-Quantum Well Lasers. *J. Appl. Phys.*, 73:4579–4585, 1993.

[63] M. S. Wartak and P. Weetman. On the design of Polarization Insensitive Semiconductor Optical Amplifier. *Microwave and Optical Tech. Lett.*

[64] C. R. Lutz, F. Agahi, and K. M. Lau. Resonant tunneling injection quantum-well lasers. *IEEE Photonics Technol. Lett.*, 7:596–598, 1995.

[65] L. Davis, H. C. Sun, H. Yoon, and P. K. Bhattacharya. Small-signal modulation and temperature dependence of the tunneling injection laser. *Appl. Phys. Lett.*, 64:3222–3224, 1994.

[66] M. S. Wartak, P. Weetman, T. Alajoki, J. Aikio, and V. Heikkinen. Extraction of rate-equation parameters from optical modal gain measurements for multiple quantum well semiconductor lasers. *Microwave and Optical Tech. Lett.*

[67] P. Weetman. Internal Work.

[68] L. V. Keldysh. Diagram Technique for nonequilibrium processes. *Soviet Physics JETP*, 20:1018–1026, 1965.

[69] R. A. Craig. Perturbation Expansion for Real-Time Green's Functions. *J. Math. Phys.*, 9:605–611, 1968.

[70] C. Y. Tsai, C. Y. Tsai, R. M. Spencer, Y. H. Lo, and L. F. Eastman. Nonlinear Gain Coefficients in Semiconductor Lasers: Effects of Carrier Heating. *IEEE Journal of Quantum Electronics*, 32:201–212, 1996.

[71] H. Tsuchiya, M. Ogawa, and T. Miyoshi. Simulation of Quantum Transport in Quantum Devices with Spatially Varying Effective Mass. *IEEE Trans. on Electron. Devices.*, 38:1246–1252, 1991.

[72] M. Sargent III. *Laser Physics.* Addison-Wesley, Reading, Massachusetts, 1974.

[73] W. Schäfer and J. Treusch. An approach to the nonequilibrium theory of highly excited semiconductors. *Z. Phys. B*, 63:407–426, 1986.

[74] C. Henry. Theory of Spontaneous Emission Noise in Open Resonators and its Application to Laser and Optical Amplifiers. *J. of Lightwave Tech.*, LT-4:288–297, 1986.

[75] B. Tromberg, H. Olesen, and X. Pan. Theory of linewidth for mutlielectrode laser diodes with spatially distributed noise sources. *IEEE Journal of Quantum Electronics*, 27:178–192, 1991.

[76] J. Kevorkian. *Partial Differential Equations: Analytical Solution Techniques (Texts in Applied Mathematics)*. Springer-Verlag, Berlin, second edition, 2000.

[77] H. Ghafouri-Shiraz and B. S. K. Lo. *Distributed Feedback Laser Diodes: Principles and Physical Modelling*. John Wiley and Son, New York, 1996.

[78] P. Meystre and M. Sargent III. *Elements of Quantum Optics*. Springer-Verlag, Berlin, 1991.

[79] A. Arnold. On absorbing boundary conditions for quantum transport equations. *Math. Modell. Anal*, 28:853–872, 1994.